IMPERIAL COLLEGE OF SCIENCE AND TECHNOLOGY

Petroleum Engineering Section

Department of Mineral Resources Engineering

High Velocity Gas Flow in Porous Media : Effects of Pore Structure and Liquid Saturation

by

Rashed Noman BSc, MSc, DIC

A thesis submitted for the degree of

Doctor of Philosophy

of the University of London

March, 1988

ABSTRACT

Darcy's law which describes fluid flow through porous media at low rates is inadequate at higher velocities due to the onset of inertial and turbulence effects. At high velocities the flow can be described by a quadratic equation containing a coefficient of inertial resistance which is dependent on the geometry of the porous medium. The present study is a theoretical and experimental investigation of fluid flow through porous media at high velocity. In particular, emphasis has been placed on understanding the important pore structural parameters which influence the flow at the microscopic scale.

Measurements of porosity, permeability and inertial coefficient, as well as of imbibition and drainage capillary pressure using mercury intrusion techniques have been carried out on over 40 sandstone core plugs. Pore size distributions were calculated from the capillary curves. Scanning electron microscopy was used to view the pore spaces in detail. Pore casts were made by injecting epoxy resin to visualize the pore systems and to estimate the aspect ratio and the coordination number for the samples. Thin sections were also investigated with an optical microscope. The results obtained using this integrated approach helped to explain the wide scatter observed in conventional inertial coefficient - permeability correlations. It is shown that the inertial effect is a function not only of porosity and permeability, but also of aspect ratio, coordination number, surface roughness and heterogeneities.

The presence of a wetting phase plays an important role in high velocity flow, eg in gas condensate reservoirs. The effect of a static liquid saturation on inertial coefficient has been investigated experimentally. A method for estimating the value of the coefficient at various saturation is given. The flow process has been visualized using coloured epoxy resin to enable a better understanding of the expected spatial distributon of the liquid phase.

Correlations have also been derived for estimating the inertial coefficient in high-rate gas wells from analysis of pressure transient data of over 100 gas wells. The correlations enable the value of the coefficients to be estimated from reservoir porosity, permeability and gas saturation. The correlations are compared with experimentally measured data using core plugs. They are found to be better than other published relationships in predicting observed performance.

CONTENTS

	Abstract	2
	Contents	3
	Acknowledgement	8
	List of Figures	9
	List of Tables	16
CHAPTER 1		
Introduction		17
1.1	Preamble	18
1.2	Scope of investigation	19
1.3	Arrangement of thesis	20
	References	21
CHAPTER 2		
Review of high velocity fluid flow in porous media		22
2.1	Introduction	23
2.2	Models of linear (Darcy) flow	23
	2.2.1 Kozeny-Carman model	25
	2.2.2 Critique of Kozeny model	27
2.3	Models of high-velocity flow	28
	2.3.1 Geometric models	28
	Flow inside conduits	28
	(a) Capillaric models	28
	(b) Hydraulic radius model	32
	Flow outside solid objects	34
	2.3.2 Continuum models	35
	2.3.3 Statistical models	36
2.4	Experiments on high velocity flow	38
2.5	Numerical studies	39
2.6	Effects of pressure and temperature	42
	References	42

CHAPTER 3

The role of inertia in high velocity flow 46

3.1 Physical description 47
3.1.1 Introduction 47
3.1.2 Analysis of forces 47
3.1.3 Streamline curvature 48
3.1.4 Expansion and contraction losses 50
3.1.5 Discussion 51
3.2 Mathematical description 53
3.2.1 Introduction 53
(a) Continuum concept 53
(b) Scales of observation 54
3.2.2 Microscopic equations of flow 55
3.2.3 Macroscopic equations of flow 57
3.2.4 Constitutive relations 59
3.2.5 A derivation of Forchheimer equation 61
3.2.6 Discussion 63
3.3 Conclusion 65
References 66

CHAPTER 4

Experimental measurements 73

4.1 Porosity measurement 74
4.1.1 Introduction 74
4.1.2 Sample preparation 75
4.1.3 Grain volume determination 75
4.1.4 Bulk volume determination 78
4.1.5 Discussion 79
4.2 Permeability measurement 80
4.2.1 Theory 80
4.2.2 Calculation 81
4.2.3 Discussion 82
4.2.4 Unsteady-state method 83
4.3 Inertial coefficient measurement 84
4.3.1 Theory 84

4.3.2 Calculation 85
4.3.3 Discussion 87
4.4 Capillary pressure measurement 88
4.4.1 Introduction 88
4.4.2 Porous diaphragm method 89
4.2.3 Mercury injection technique 90
4.4.4 Discussion 91
4.5 Results 92
References 92

CHAPTER 5
Transition from linear to nonlinear flow 101

5.1 Introduction 102
5.2 Regimes of flow 102
5.3 Quantitative relations 103
5.4 Reynolds number 106
5.4.1 Definition of term d 106
5.4.2 Definition of term v 108
5.4.3 An alternative approach 109
5.5 Experimental observations 112
5.6 Discussion 113
5.7 A numerical solution of the Forchheimer equation 117
5.7.1 Introduction 117
5.7.2 Numerical approach 117
5.7.3 Solution procedure 118
5.7.4 Discussion 120
References 122

CHAPTER 6
Effect of pore structure on high velocity flow 130

6.1 Introduction 131
6.2 Inertial effects and pore structure 131
6.2.1 Curvature of streamlines 131
6.2.2 Aspect ratio 133

6.2.3 Coordination number 134
6.2.4 Heterogeneities 135
6.2.5 Surface roughness 136
6.3 Experimental measurements 137
6.3.1 Capillary pressure 137
6.3.2 Recovery efficiency 138
6.3.3 Pore size distribution 139
6.4.3 Geological description 140
6.5 Comparative study 141
6.6 Conclusions 155
References 156

CHAPTER 7

Effect of liquid saturation on high velocity gas flow 207

7.1 Introduction 208
7.2 Experimental work 209
7.2.1 Flow measurements 209
7.2.2 Flow visualisation 210
7.3 Results 210
7.3.1 Dry cores 210
7.3.2 Saturated cores 211
7.4 Proposed correlation 212
7.5 Discussion 213
7.6 Conclusions 216
References 216

CHAPTER 8

Estimation of inertial coefficient in high rate gas wells 229

8.1 Introduction 230
8.2 Relation between β and k 230
8.2.1 Dimensional analysis 231
8.2.2 Kozeny - Carman relations 232
8.2.3 Empirical relations 232
8.3 Measurement of β from well tests 233

8.4 Data used 234
8.5 Prosposed correlations 235
8.6 Laboratory measurements 235
8.7 Discussion 236
8.8 Conclusion 238
References 239

CHAPTER 9
Summary and conclusions 256

9.1 The role of inertia 257
9.2 Transition from linear to nonlinear flow 258
9.3 Effects of pore structure 259
9.4 Effects of liquid saturation 259
9.5 Estimation of β in high rate gas wells 260
9.6 Suggestions for further work 261

APPENDIX
Equations of nonlinear flow 263
References 268

NOMENCLATURE 269

BIBLIOGRAPHY 273

ACKNOWLEDGEMENT

The author would like to express his sincere thanks and appreciation to Professor J.S. Archer for his supervision of this work and for his encouragement and help in numerous ways.

Thanks are also due to Dr R.A. Dawe and Professor C.G. Wall for their interest in this work and for some useful comments and suggestion.

I would like to acknowledge the financial support of British Gas plc (Exploration Dept.), the Society of Petroleum Engineers and North Sea Sun Oil Co. To British Gas I am also grateful for providing core samples and for the use of data from a number of gas wells which are reported here.

I am greatly indebted to Dr R. Pietlicki for the many hours of fruitful discussion, for his help and advice, and for being a source of encouragement.

Appreciation is due to Mr M. Bilsland for his advice and suggestions at the initial stages of this study and to Mr A. Jones (Geology Dept.) for some useful discussion on the preparation of thin sections.

I wish to express my gratitude to all my friends and colleagues in the department, and to those members of my family who have contributed to this work directly or indirectly, especially to my mother for her encouragement, support and understanding.

R. Noman
January, 1988

LIST OF FIGURES

Figure		*Page*
2.1	Relationship between the various models of single phase flow in porous media.	24
2.2	Blick's capillary orifice model of porous media.	31
2.3	Representation of some of the models of porous media used by the various authors for numerical computation.	41
3.1	Resolution of forces acting on a microscopic element of fluid during flow through a porous medium.	68
3.2	Pressure variation across a curved streamtube.	69
3.3	Diagram showing streamlines and secondary flow in a sinusoidal capillary model of a pore.	69
3.4	Schematic representation of the distortion of streamlines caused by the increasing flow rate, and the corresponding force balances on a volume element dV. Darcy's law would be valid only for case (a).	70
3.5	Four different scales of observation of sedimentary rocks.	71
3.6	Diagram showing a representative elementary volume (REV) and the relationship of the deviating vectors to their volume averaged value.	72
4.1	Schematic arrangement of the helium gas expansion porosimeter.	95
4.2	Mercury pycnometer for bulk volume measurement.	96
4.3	Hassler core holder and schematic arrangement for flow measurement.	97
4.4	A typical Klinkenberg plot with downward warp at high rate. Sample LE253.	98
4.5	A typical plot according to Forchheimer equation showing downward warp at low velocity. Sample LE253.	98
4.6	Soap-bubble meter for volumetric gas flow measurement.	96

4.7	Schematic arrangement of apparatus for capillary measurement using porous membrane technique.	99
4.8	Schematic arrangement of apparatus for capillary pressure measurement using mercury intrusion technique.	100
5.1	A log-log plot of the Ergun equation (ref. 9)	124
5.2	Graphical correlation of friction factor against Reynolds number (ref. 5)	124
5.3	Plots of pressure gradient against flow rate according to Darcy's law.	125
5.4	Modified pressure gradient - flow rate plot taking account of slippage correction.	126
5.5	Critical flow velocity at the onset of deviation from Darcy's law against permeability.	127
5.6	Critical flow velocity against a characteristic length of the media $\sqrt{(k/\phi)}$	127
5.7	Inverse relationship between the characteristic length $d = \beta k$ and permeability	128
5.8	Pressure gradient calculated using a numerical method. Broken lines were generated by changing the value of β by $\pm$ 10%.	129
6.1	Relationship between inertial coefficient and permeability.	158
6.2	Two capillaries of equal dimension but different radius of curvature.	159
6.3	Segments of pore networks representing similar k and ϕ but different β.	159
6.4	(a) Segment of pore network with asymmetric throats, (b) low flow rate, and (c) complex flow at higher rate.	160
6.5	Segment of pore network with tortuous channels.	160
6.6	Pore networks with coordination number of 3, 4, and 6.	161
6.7	Photomicrograph of sample LE253 showing heterogeneity in the form of thin laminations.	161
6.8	Laminar flow at a Y-junction.	162
6.9	Importance of surface roughness at increasing Reynolds number flow.	162

6.10	Three general types of dispersed clay in sandstone.	163
6.11	Typical features of a capillary pressure curve for calculation of the recovery efficiency.	163
6.12	(a) Idealized representation of a clean pore, and (b) reduction of pore space due to the growth of authigenic pore-lining clays.	164
6.13	Photomicrograph of sample LE718. Magnification x10.	165
6.14	Photomicrograph of sample M11004. Magnification x10.	165
6.15	(a) Capillary pressure curve. Sample LE718.	166
	(b) Capillary pressure curve. Sample M11004.	166
6.16	(a) Pore throat size distribution. Sample LE718.	167
	(b) Pore throat size distribution. Sample M11004.	167
6.17	Photomicrograph of sample AL79. Magnification x10.	168
6.18	Photomicrograph of sample M73002. Magnification x10.	168
6.19	(a) Capillary pressure curve. Sample AL79.	169
	(b) Capillary pressure curve. Sample M73002.	169
6.20	(a) Pore throat size distribution. Sample AL79.	170
	(b) Pore throat size distribution. Sample M73002.	170
6.21	Photomicrograph of sample AL29. Magnification x10.	171
6.22	Photomicrograph of sample AL40. Magnification x10.	171
6.23	(a) Capillary pressure curve. Sample AL29.	172
	(b) Capillary pressure curve. Sample AL40.	172
6.24	(a) Pore throat size distribution. Sample AL29.	173
	(b) Pore throat size distribution. Sample AL40.	173
6.25	Photomicrograph of sample RH101. Magnification x10.	174
6.26	Photomicrograph of sample AL111. Magnification x10.	174
6.27	(a) Capillary pressure curve. Sample RH101.	175
	(b) Capillary pressure curve. Sample AL111.	175
6.28	(a) Pore throat size distribution. Sample RH101.	176
	(b) Pore throat size distribution. Sample AL111.	176

6.29	Photomicrograph of sample RH103. Magnification x10.	177
6.30	Photomicrograph of sample MO63. Magnification x10.	177
6.31	(a) Capillary pressure curve. Sample RH103.	178
	(b) Capillary pressure curve. Sample MO63.	178
6.32	(a) Pore throat size distribution. Sample RH103.	179
	(b) Pore throat size distribution. Sample MO63.	179
6.33	Photomicrograph of sample M11003. Magnification x10.	180
6.34	Photomicrograph of sample M73004. Magnification x10.	180
6.35	(a) Capillary pressure curve. Sample M11003.	181
	(b) Capillary pressure curve. Sample M73004.	181
6.36	(a) Pore throat size distribution. Sample M11003.	182
	(b) Pore throat size distribution. Sample M73004.	182
6.37	Photomicrograph of sample M11011. Magnification x10.	183
6.38	Photomicrograph of sample M11008. Magnification x10.	183
6.39	(a) Capillary pressure curve. Sample M11011.	184
	(b) Capillary pressure curve. Sample M11018.	184
6.40	(a) Pore throat size distribution. Sample M11011.	185
	(b) Pore throat size distribution. Sample M11008.	185
6.41	Photomicrograph of sample M73006. Magnification x10.	186
6.42	Photomicrograph of sample RH97. Magnification x10.	186
6.43	(a) Capillary pressure curve. Sample M73006.	187
	(b) Capillary pressure curve. Sample RH97.	187
6.44	(a) Pore throat size distribution. Sample M73006.	188
	(b) Pore throat size distribution. Sample RH97.	188
6.45	Photomicrograph of sample M73005. Magnification x10.	189
6.46	Photomicrograph of sample M73009. Magnification x10.	189
6.47	(a) Capillary pressure curve. Sample M73005.	190
	(b) Capillary pressure curve. Sample M73009.	190
6.48	(a) Pore throat size distribution. Sample M73005.	191

	(b) Pore throat size distribution. Sample M73009.	191
6.49	Photomicrograph of sample M11007. Magnification x10.	192
6.50	Photomicrograph of sample LE249. Magnification x10.	192
6.51	(a) Capillary pressure curve. Sample M11007.	193
	(b) Capillary pressure curve. Sample LE249.	193
6.52	(a) Pore throat size distribution. Sample M11007.	194
	(b) Pore throat size distribution. Sample LE249.	194
6.53	Photomicrograph of sample M73001. Magnification x10.	195
6.54	Photomicrograph of sample AL118. Magnification x10.	195
6.55	(a) Capillary pressure curve. Sample M73001.	196
	(b) Capillary pressure curve. Sample AL118.	196
6.56	(a) Pore throat size distribution. Sample M73001.	197
	(b) Pore throat size distribution. Sample AL118.	197
6.57	Photomicrograph of sample RH94. Magnification x10.	198
6.58	Photomicrograph of sample M11002. Magnification x10.	198
6.59	(a) Capillary pressure curve. Sample RH94.	199
	(b) Capillary pressure curve. Sample M11002.	199
6.60	(a) Pore throat size distribution. Sample RH94.	200
	(b) Pore throat size distribution. Sample M11002.	200
6.61	Photomicrograph of sample M11001. Magnification x10.	201
6.62	Photomicrograph of sample M11009. Magnification x10.	201
6.63	(a) Capillary pressure curve. Sample M11001.	202
	(b) Capillary pressure curve. Sample M11009.	202
6.64	(a) Pore throat size distribution. Sample M11001.	203
	(b) Pore throat size distribution. Sample M11009.	203
6.65	Photomicrograph of sample M73003. Magnification x10.	204
6.66	Photomicrograph of sample LE253. Magnification x10.	204
6.67	(a) Capillary pressure curve. Sample M73003.	205
	(b) Capillary pressure curve. Sample LE253.	205

6.68	(a) Pore throat size distribution. Sample M73003.	206
	(b) Pore throat size distribution. Sample LE253.	206
7.1	Schematic diagram of the apparatus for flow measurement	218
7.2	An example of Klinkenberg plot	219
7.3	An example of Forchheimer plot	219
7.4	Effect of wetting phase saturation on gas permeability. Sample M11001.	220
7.5	Effect of wetting phase saturation on gas permeability. Sample M11003.	220
7.6	Effect of wetting phase saturation on gas permeability. Sample M11010.	221
7.7	Effect of wetting phase saturation on gas permeability. Sample M11011.	221
7.8	Effect of wetting phase saturation on inertial coefficient. Sample M11001.	222
7.9	Effect of wetting phase saturation on inertial coefficient. Sample M11003.	223
7.10	Effect of wetting phase saturation on inertial coefficient. Sample M11010.	223
7.11	Effect of wetting phase saturation on inertial coefficinet. Sample M11011.	224
7.12	Hysteresis in the inertial coefficient plot at saturations above the irriducible minimum. Lower portion represents increasing flow rate and the upper portion decreasing flow rate.	224
7.13	Photomicrograph showing the distribution of the wetting (blue) and nonwetting (red) phases in a sandstone rock sample.	225
7.14	Capillary pressure curves of sample (a) M11001, (b) M11003, (c) M11010 and (d) M11011.	227
7.15	Pore size distribution curves of sample (a) M11001, (b) M11003, (c) M11010 and (d) M11011.	228
8.1	Relationship between porosity and permeability for the sample set.	244
8.2	Permeability distribution of the sample set.	245
8.3	Porosity distribution of the sample set.	246
8.4	Gas saturation distribution of the sample set.	247
8.5	Correlation of β with permeability.	248

8.6	Plot according to Eq. (8.5-6)	249
8.7	Plot according to Eq. (8.5-3)	250
8.8	Correlation of β for experimental data.	251
8.9	Correlation between ϕ, β and k.	252
8.10	Correlation between reduced porosity, β and k.	253
8.11	Correlation between porosity and inertial coefficient.	254
8.12	Sketches of flow streamlines in a reservoir being produced by partially completed wells.	255

LIST OF TABLES

Table		*page*
4.1	Comparision of porosity measurements.	79
4.2	Comparision of permeability measured by two methods	87
4.3	Results of measurement.	94
5.1	Summary of various definitions of Reynolds number and friction factor used in the literature.	111
5.2	Flow rate at the onset of deviation from Darcy's law.	115
5.3	Reynolds number at critical velocities.	116
5.4	Data for numerical calculation	121
5.5	Sensitivity of β on calculated pressures	121
7.1	Core data	211
8.1	Field data	240
8.2	Regression equations	242
8.3	Laboratory data	243

Chapter 1

INTRODUCTION

1.1 PREAMBLE

The topic of flow of fluids through porous media is of importance in such diverse fields as petroleum engineering, chemical engineering, physiology, soil physics, subsurface hydrology, ceramics, surface and colloid physics, powder metallurgy as well as technologies associated with wood, paper, textiles, leather, cement, food and solid fuels to name but a few [1]. A systematic study of this subject seems to have started in 1856 with the now well known experiments [2] conducted by Henry Darcy on the flow of water through beds of sand. His primary intention was the determination of size of filters required for the purification of a given quantity of water. From the results of these experiments he proposed a relationship, now well known as the Darcy's law [3].

A few decades after Darcy's work, Osborne Reynolds conducted his classical experiments [4] on the flow of water through pipe-lines. His work was specifically aimed at gaining an understanding of the transition from laminar to turbulent modes of flow. Reynolds found that as the flow rate in a circular tube was increased, a linear relationship between the pressure gradient and flow rate did not hold. The resistance increased disproportionately due to eddy formation and was thought to be dependent on the kinetic energy per unit volume of the fluid, ie ρv^2. He therefore proposed the use of a quadratic equation for describing turbulent flow through pipelines, which may be written as

$$-\frac{\Delta P}{L} = a v + b \rho v^2 \qquad (1.1\text{-}1)$$

In the experiments that Darcy carried out, the fluid (water) was flowed through the sand bed at a very low rate and under the action of gravity alone. It is interesting to note that Darcy found [3] that at flow velocities greater than 10-11 cm/s the relationship he proposed was no longer found to be valid for his equipment. Some years after the report of Reynolds' work, it seems Forchheimer [5] was the first to suggest that a quadratic equation could also be used for describing flow through porous media at high rates where Darcy's law was no longer valid. Probably the earliest mention of the existence of nonlinear mode of flow in porous media is due to Krober in 1884 (see [6]). However, Forchheimer's work [5] is generally recognised as the start of a proper understanding of the nonlinear behaviour at high rates of flow. Forchheimer's proposition was based solely on experimental findings and no theoretical reasons were proposed to explain the observed deviation from Darcy's law. Since then, numerous investigations have been carried out to understand the limitations and applicability of Darcy's law. Early workers in this field presumed that at increasing flow rate turbulent eddies would form inside the pore spaces and thereby cause the deviation to occur. It is now acknowledged by most researchers that turbulence play an insignificant part in most situations of flow through porous media and it

is the inertial forces which are responsible. It seems that the first correct discussion of the deviation from Darcy's law as resulting from the fluid inertia, was by a Swedish engineer Lindquist in 1933 (see [7]). The equation Forchheimer proposed is normally expressed as

$$-\frac{\Delta P}{L} = \alpha \mu v + \beta \rho v^2 \qquad (1.1\text{-}2)$$

In this, the term α is known as the coefficient of viscous flow resistance, and β the coefficient of inertial flow resistance or inertial coefficient for short. Both these coefficients are assumed to be dependent only on the geometry of the porous medium and independent of the fluid properties. At very low rates of flow, where the viscous forces would dominate over the inertial forces, the second term in (1.1-2) would become negligibly small and the equation then becomes similar to Darcy's law with the coefficient α being the inverse of permeability, 1/k.

The equation proposed by Forchheimer forms the basis of almost all reported study on high rate flow through porous media, which is normally refered to in the petroleum engineering literature as "non-Darcy flow". This term does not convey an accurate description of the physical phenomena involved, since Darcy's law is found to fail for a number of other reasons as will be discussed later. The alternative term "high velocity flow" is prefered due to its clarity although the former term is far too entrenched in the literature to be ignored.

1.2 SCOPE OF INVESTIGATION

The main objectives of this work were as follows :

(a) In the past, all too often, analogy has been drawn between flow in porous media and flow in tubes or capillaries. In the latter case, flow changes from a linear to nonlinear mode due to the onset of turbulence. In the former, the situation is different due to the presence of a complicated three dimensional network of pore spaces. This study was undertaken to gain a better understanding of the basic reasons for which deviation from Darcy's law occur at increasing flow rate. In particular, it aimed to provide a physical and mathematical description of the role of inertia in the hydrodynamics of flow in porous media.

(b) The geometry of the pore spaces is believed to control flow patterns at the microscopic and hence the macroscopic scale. Most reported work however seems to consider the rock properties in bulk only, with porosity and permeability as the factors of significance. Further more, no published work could be found describing how flow in the non-Darcy regime is influenced by the pore structure. An attempt has been made to provide a discussion of the pertinent pore structural parameters which will control the overall flow.

(c) In the presence of a liquid phase, the coefficient of inertial resistance, β, for the gas phase can be expected to change from that when the sample is dry. Reports of investigations on micro-vugular carbonates are available. It has been assumed in the past that similar behaviour would also apply in consolidated reservoir rocks. Experiments have therefore been carried out to check the validity of this assumption. A method has also been developed for visualization of the wetting phase distribution during gas flow at high rates.

(d) A number of correlations are available for estimating the inertial coefficient, β, from bulk porosity and permeability of a rock sample. These correlations are however found to predict values of β containing unacceptably large errors. These correlations are often derived from a very limited set of data. An alternative method has been used in the present study. The values of β were calculated from gas well pressure transient data in over one hundred producing wells. Correlations were then formed using regression techniques for estimating the value of the inertial coefficients from bulk reservoir rock properties.

1.3 ARRANGEMENT OF THESIS

The next chapter contains a brief review of some of the important models which have been used for the theoretical derivation of both Darcy's law and Forchheimer's equation. The models reviewed are all based on specific geometric idealization of the porous media. The simplicity of these models have been their main advantages as well as their own disadvantages. Statistical models are outside the scope of this study and are not reviewed here in any detail.

In Chapter 3 a physical description of the role of inertia is provided. A theoretical derivation of the Forchheimer equation is also given which is based on the continuum approach. Implications of the results are discussed. In the following chapter, the important experimental methods used in this study are outlined. This includes measurements of porosity, permeability, inertial coefficient and capillary pressure. The detection of the transition of flow from a linear to nonlinear regime is discussed in Chapter 5. The important pore structural parameters which control the inertial coefficient are explained in the following chapter. Results of experimental investigations carried out using mercury porosimetry are discussed as well as observations of thin sections. Comparative examples are provided to highlight the differences in pore structures. In Chapter 7 the effect of static liquid saturations on the value of the inertial coefficient are reported. A method which has been developed for visualization of the wetting phase is discussed. A method for predicting the inertial coefficient from effective permeability of the rock samples is given. In the following chapter correlations are provided for estimating the value of inertial coefficient in high rate gas wells. This has been done using pressure transient and production data from over 100 gas wells. The final chapter provides a summary and suggestions for further work.

REFERENCES

1. Bear, J. : *Dynamics of Fluids in Porous Media,* Elsevier, New York (1972)
2. Darcy, H. : *Les Fontaines Publiques de la Ville de Dijon,* Victor Dalmont, Paris (1856)
3. Hubbert, M.K. : Darcy's law and the field equations for the flow of underground fluids, *Trans. AIME.,* (1956) **207**, 222-239.
4. Reynolds, O. : An experimental investigation of the circumstances which determine whether the motion of water shall be direct or sinuous and the law of resistance in parallel channels, *Phil. Trans. Roy. Soc.* (1883) A **174**, 935.
5. Forchheimer, P.: Wasserbewegung durch Boden, *Z. Ver. Duetsch. Ing.* (1901) **45**, 1782-88.
6. Bear, J., Zaslavsky, D. and Irmay, S. : *Physical Principles of Water Percolation and Seepage,* UNESCO Arid Zone Research Publication, Vol. XXIX, Paris (1965)
7. Scheidegger, A.E. : *The Physics of Flow Through Porous Media,* 3rd Ed., Toronto Univ. Press, Toronto (1974)

Chapter 2

REVIEW OF HIGH VELOCITY FLUID FLOW IN POROUS MEDIA

2.1 INTRODUCTION

The shapes, sizes and connections of pore spaces inside a porous medium are so complicated and variable that they currently defy any quantitative description. For any calculation to be possible, highly idealized models have to be used, where the pore connections are often assumed to be similar to capillary tubes or types of spaces associated with packing of spheres.

For the description of flow in porous media, there are perhaps three fairly distinct, although not mutually exclusive, approaches. The interrelationship of the various models are shown schematically in Fig.2.1.

(i) The first approach is the use of geometric modelling. In this, a particular geometric arrangement is postulated which hopefully bears some resemblence to the porous media, and yet would be sufficiently simple to allow the governing differential equation to be solved.

(ii) The second approach is to use stochastic models. Since a porous medium is generally not an ordered structure, the use of statistical models is quite appealing. A number of attempts have been made although with limited success.

(iii) The third approach, which lies somewhere between geometric models and statistical models, is the continuum approach. Here, volume averaged forms of the governing differential equations are developed which would be valid for any geometry. The results obtained for specific geometric models or any statistical models must be in agreement with the averaged equations.

All three approaches will lead to some unspecified coefficients which can be determined only through experiments. One of the primary objectives of theoretical work is to aid in the interpretation of experimental data. In this chapter some of the more popular models of flow in porous media are reviewed. First a model of low velocity (ie. Darcy) flow is discussed before the various models for high velocity flow which have been proposed in the literature are reviewed. General reviews of various models of porous media can be found in the texts of Bear [1], Scheidegger [2] and Dullien [3] as well as in a number of other papers [4,5].

2.2 MODELS OF LINEAR (DARCY) FLOW

Of the various models of flow in porous media, perhaps the most widely known and used is the one proposed by Kozeny [6]. This was later extended by Carman [7] and is now popularly

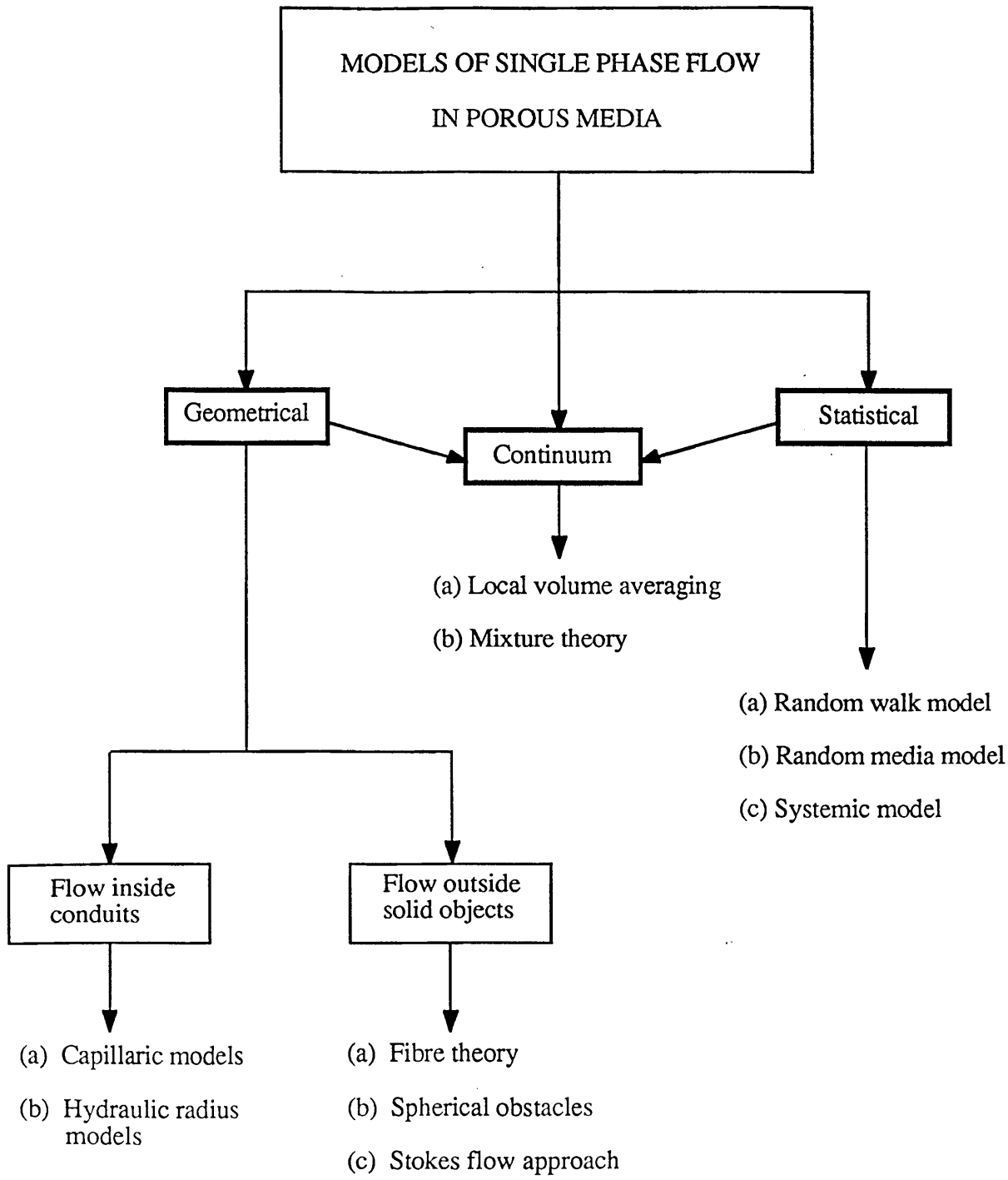


Figure 2.1 Relationship between the various models of single phase flow in porous media

known as the *Kozeny - Carman* model [8]. It will be useful to review this model since it has formed the basis of many subsequent models over the decades.

2.2.1 Kozeny - Carman model

The Kozeny equation relates the pressure drop and mean velocity for flow through a packing in terms of its porosity (voidage) and specific surface, as these quanitities are often known or can be measured. Alternatively, a knowledge of the pressure drop, velocity and porosity provide a convenient way of measuring the surface area of unconsolidated beds of particles.

The Kozeny model relies on use of the "hydraulic radius" concept, and assumes that the porous medium is equivalent to a bundle of capillary tubes. The exact shape of these capillaries may be complicated but they are all assumed to have a constant radius throughout their length. The cross - sectional area normal to flow is also assumed to be a constant.

Streamline flow through a circular channel is given by the Hagen-Poiseuille equation, which may be written as

$$u = -\frac{d^2}{32\,\mu}\frac{\Delta P}{L} \tag{2.2-1}$$

By analogy with this equation, streamline flow through the pores in a bed of particles may be expressed as

$$v_p = -\frac{d_e^2}{16K_o\mu}\frac{\Delta P}{L_e} \tag{2.2-2}$$

where, v_p = average pore (interstitial) velocity
d_e = some length equivalent of the pore channel
K_o = dimensionless "shape factor"
L_e = average flow path length

The pore or interstitial velocity has been related to the average seepage velocity by Dupuit [1]

$$v_p = v / \phi \tag{2.2-3}$$

This is known as the "Dupuit- Forchheimer assumption" and is true only for a randomly packed bed. A bed of spheres arranged in cubic packing, has for example $\phi = 0.476$, but the fractional free area can vary from 0.215 in the plane across the diameter to 1.0 between successive layers.

It was proposed by Carman [7] that (2.2-3) should be written as

$$v_p = \frac{v}{\phi}\frac{L_e}{L} \qquad (2.2\text{-}4)$$

The length ratio is thought to correct for the fact that fluid particles flowing with velocity v cover a path length L in the same time as fluid particles flowing with the velocity v_p cover an average effective path length L_e. Unfortunately, an exact value of L_e is virtually impossible to find in any natural porous media due to the complex pore geometries.

By analogy with well established practice in hydraulics, the mean hydraulic diameter is assumed to be four times the hydraulic radius, which is defined as

$$d_h = \frac{4\phi}{S} \qquad (2.2\text{-}5)$$

where S is the surface area presented to the fluid per unit volume of bed. This quantity is related to the "specific surface" S_o - the total particle surface/ the volume of particles - by the relation

$$S = S_o(1-\phi) \qquad (2.2\text{-}6)$$

Eqn.2.2-6 is true provided only a small fraction of surface area is lost due to overlapping of particles. Replacing d_e by d_h in (2.2-2) and substituting (2.2-4) we get

$$v = \frac{d_h^2\phi}{K_o\, 16\,\mu\,(L_e/L)^2}\left(-\frac{\Delta P}{L}\right) \qquad (2.2\text{-}7)$$

Replacing for d_h from Eqn.(2.2-5) and (2.2-6) we get the Kozeny - Carman relation for permeability

$$k = \frac{1}{K_o\, S_o^2\,(L_e/L)^2}\,\frac{\phi^3}{(1-\phi)^2} \qquad (2.2\text{-}8)$$

The term $(L_e/L)^2$ is usually called "tortuosity". The combined factor $K' = K_o(L_e/L)^2$ is generally known as the "Kozeny constant" and its value has been found to be about 5; the value of $(L_e/L)^2$ is around $2^{1/2}$ and that of K_o about 2.5. The value of K_o for non-circular capillaries can be expected to be different.

The diameter for spherical particles is related to its surface area by

$$d_p = 6/S_o \qquad (2.2\text{-}9)$$

Substituting Eqn.(2.2-9) and the value of Kozeny constant into Eqn.(2.2-8) we get the permeability of a bed of spherical particles to be

$$k = \frac{d_p^2}{180}\,\frac{\phi^3}{(1-\phi)^2} \qquad (2.2\text{-}10)$$

2.2.2 Critique of the Kozeny model

The Kozeny theory is based on the assumption that a porous medium can be represented by an assemblage of capillaries of various cross-sections, but of a definite length. To calculate the permeability of a medium, the momentum balance equations are solved simultaneously for all the capillaries passing through a cross-section normal to the flow. The theory therefore assumes that there is no tangential component of the fluid velocity. Any effect of expansion / contraction in the flow path is therefore completely ignored.

Due to the theory being based on parallel channels, it is unable to take account of any anisotropy in the porous medium [8]. It was pointed out that the Kozeny theory fails completely to describe structured media, eg 'stiff-fissured' clays. The structural fissures can contribute negligibly to porosity and specific surface, but dominate the permeability.

In an effort to substantiate his formula experimentally, Kozeny [6] found discrepancies between calculated and measured surface areas of -69 to +86 %. The question of validity of the Kozeny equation has been reviewed comprehensively by Scheidegger [2a,b]. It has been shown [9] that Kozeny's law breaks down for highly porous eg. fibrous media, and Walas (see [2]) found that modifications in the Kozeny equation were required for application to filtration. It was observed by Adamson [10] that the 'Kozeny constant' had to be adjusted a posteriori in all his experiments. It has also been observed that only if the flow channels are all equal and of uniform diameter is there a close correspondance between the average pore diameter and the volume - to - surface ratio [2a].

Other attempts have been made to substantiate the Kozeny equation, often by introducing various factors eg. tortuosity constant, lithological factor etc. Thus, Wyllie et al [11] placed a lot of emphasis on 'tortuosity' concepts and Brooks [12] claimed that their experimental results agree with the Kozeny equation even though they found large discrepencies between areas measured by the Kozeny equation and by a gas adsorption method.

In hydraulics, it is known that the hydraulic radius concept is a close approximation to reality only under turbulent flow conditions. The Kozeny-Carman model however is aimed at laminar (creeping) flow conditions, and as such the use of hydraulic radius concept is a significant drawback of the model. It has been mentioned by a number of researchers [2,7,13] that the Hagen-Poiseuille formula would not be valid for curved tubes. In curved tubes, the relation between pressure gradient and flow rate becomes nonlinear long before any turbulence can be observed. The curvature of channels is not taken into acount in the theories based on hydraulic radius concepts (eg Kozeny model). For tortuous tubes, the inertial forces do not vanish as they would for laminar flow in straight ones. The possibility that nonlinearity may occur even when

the flow rate as a whole is laminar is completely overlooked.

2.3 MODELS OF HIGH VELOCITY FLOW

Darcy's law represents a relationship between the filtration (seepage) velocity and the pressure (head) gradient. A plot of these two quantities is found to give a straight line passing through the origin. Any deviation from this linear relationship could therefore be termed as "non - Darcy flow". Kutilek [14] has proposed twelve possible ways in which this may happen. The present investigation is restricted to the non - Darcy phenomena which take place at high rates of flow. The term "high velocity flow" therefore seems more appropriate in this context as deviations from Darcy's law could take place for various other reasons.

2.3.1 Geometrical Models

For a comprehensive understanding of the physics of the phenomena involved in causing deviation from Darcy's law it is necessary to employ some theoretical model. Only by such means is it possible to understand the significance of the various coefficients involved in the heuristic equations, and to explain the dependence of these on various pore structural parameters. Virtually all the models used in the literature for describing flow in the Darcy regime have eventually been extended for the description of high velocity flow. Here just two geometric models, which are variations of the simple capillaric models, are reviewed.

2.3.1.1 Flow inside conduits

(a) Capillaric Models

The use of capillaries as an analogy for flow in porous media dates back to around the start of this century. Numerous models have been proposed though with limited success due to the inherent limitation in treating porous media as a bundle of capillary tubes. Scheidegger [2b] has given an excellent review of this type of model.

(i) **Scheidegger** [2a] used the basic capillary model used for deriving Darcy's law but instead of using the Hagen - Poiseuille equation for laminar flow, he used a 'turbulent' flow equation

$$\frac{dP}{dx} = c' (\rho v^2 / \delta) \qquad (2.3\text{-}1)$$

where v is the pore velocity, c' is some constant and δ the diameter of the tube. This equation would also hold for laminar, but non-linear flow.

The inherent weakness of this model is due to the neglect of any transition zone between the 'laminar' and 'turbulent' flow region. The model however has two significant advantages over simple capillary models in that (a) it takes account of the fact that flow may not be in one direction only. One third of the total number of capillaries are placed in any one of the 3 principal spatial directions, and (b) a distribution of capillary diameter sizes is taken into account.

The first modification is taken into account by including 1/3 in the permeability relationship derived from comparision of the Hagen-Poiseuille equation and the Darcy's law. This can be expressed as

$$k = \frac{\delta^2 \phi}{3 \times 32} \tag{2.3-2}$$

This equation however violates the Dupuit - Forchheimer assumption (2.2-3).

The second feature is introduced by taking a model where all capillaries permitting flow in a given direction are parallel to that direction, but vary in pore diameters. The pore size distribution of the model and that of the actual medium deduced from capillary pressure curves, are forced to be identical. The pore size distribution (PSD) is defined here by determining what fraction α of the total pore space has a pore diameter between d and d+dδ. The PSD defined in this way can be normalized and expressed as

$$\int_{\delta}^{\alpha} \alpha(\delta)\, d\delta = 1 \tag{2.3-3}$$

After appropriate substitution, Eq.(2.3-1) becomes

$$dP/dx = 9 \rho c' q^2 (\delta \phi^2) \tag{2.3-4}$$

By combining the Hagen-Poiseuille formula with the turbulent flow equation (2.3-1) it is possible [2a] to arrive at

$$p_2 - p_1 = -\int \frac{c \mu v}{\delta^2} ds + \int \frac{c' \rho v^2}{\delta} ds \tag{2.3-5}$$

The first term in Eq.(2.3-5) is for 'laminar' region and the second for 'turbulent' region. A distribution function $\alpha(\delta)$ is defined as

$$\alpha(\delta)\, d\delta = \frac{1}{4} \pi \delta^2 ds \Big/ \int_0^s \frac{1}{4} \pi \delta^2 ds \tag{2.3-6}$$

where s is the actual length of a capillary; x being the length of the medium itself. The tortuosity factor is therefore defined as

$$T = s/x = ds/dx \tag{2.3-7}$$

After further substitution and rearrangement, the pressure gradient can be [2a] expressed as

$$\text{grad } p = \left[-\frac{3\,c\,T^2}{\phi} \left(\int_{\delta r}^{\alpha} \frac{\alpha(\delta)\,d\delta}{\delta^6} \right) \left(\int \delta^2\,\alpha(\delta)\,d\delta \right)^2 \right] \mu\, q$$

$$+ \left[\frac{9\,c'\,T^3}{\phi^2} \left(\int_{0}^{\delta r} \frac{\alpha(\delta)\,d\delta}{\delta^7} \right) \left(\int \delta^2\,\alpha(\delta)\,d\delta \right)^3 \right] \rho\, q^2 \tag{2.3-8}$$

This expression corresponds to the Forchheimer relation

$$\text{grad } p = a\,\mu\, q + b\,\rho\, q^2 \tag{2.3-9}$$

where a and b are the viscous and inertial coefficients.

Evaluation of the two bracketed terms are rather difficult. The terms δr is also a function of q. Only if the integrals can be assumed to be independent of the value of δr can Eq.(2.3-8) be said to be equivalent to Forchheimer formula.

If the seepage velocity is expressed as

$$q = v\,\phi / 3 \tag{2.3-10}$$

then for a medium of ϕ = 20%, the critical Reynolds number, $(Re)_c$, would be about 120. This value is around 50 - 100 times higher than actual observations. This clearly shows that the non-linearity is not caused by the onset of turbulence, but is due to the inertia effects caused by the curvature of the flow channels. The critical Reynolds number will therefore be affected very significantly by the curvature of the flow channels. For two porous media with identical porosity and tortuosity, the critical Reynolds number will be different if the curvature of the stream tubes are different. This discussion suggests that only by bringing the curvature of flow channels into account will it be possible to suggest that the flow is identical in two media at identical Re. Otherwise, for identical Re the flow patterns and hence the frictional resistance would be quite different.

(ii) **Blick** [15]

A model proposed by Blick consisted of a bundle of parallel capillary tubes with orifice plates spaced along each tube, separated by a distance equal to the mean pore diameter (see Fig. 2.2). If the mean pore diameter is taken as δ, then the number of orifices per unit length would be equal to δ^{-1}. The flow was assumed to be one-dimensional. From momentum balance on the control volume, Blick obtained

$$-\frac{\partial p}{\partial x} = \frac{4\tau}{\delta} + \frac{C_d \rho v^2}{2\delta} + \frac{\partial (\rho v^2)}{\partial x} + \frac{\partial (\rho v)}{\partial t} - \rho F_b \qquad (2.3\text{-}11)$$

where v is the velocity, C_d the drag coefficient of orifice plates, F_b the body force per unit mass and τ the shear stress at the wall.

Assuming that the body force is the only due to gravity, the steady flow equation would then be

$$-\frac{\partial p}{\partial x} = \frac{4\tau}{\delta} + \frac{C_d \rho v^2}{2\delta} + \rho v \frac{\partial v}{\partial x} - \rho g \cos\theta \qquad (2.3\text{-}12)$$

where θ is the angle between the x-direction and the direction of gravitional force. The shear stress can be expressed as

$$\tau = C_f \frac{1}{2} \frac{v\mu}{\delta} \mathrm{Re} \qquad (2.3\text{-}13)$$

Substituting Eq.(2.3-13) into (2.3-12) and taking q = n v, it is possible [15] to arrive at (2.3-14) which is applicable for gas flow under isothermal conditions in the horizontal direction.

$$-\frac{\partial p}{\partial x} = \left(\frac{2 C_f \mathrm{Re}}{n \delta^2}\right) \mu q + \left(\frac{C_d}{2 \delta n^2}\right) \rho q^2 \qquad (2.3\text{-}14)$$

This equation is also analogous to the Forchheimer formula with the bracketed terms equal to the two coefficients a and b. The first term is for the head loss along the lengths of the capillary and the second produces local losses proportional to the second power of velocity. According to Eq.(2.3-14), permeability and the inertial coefficient are

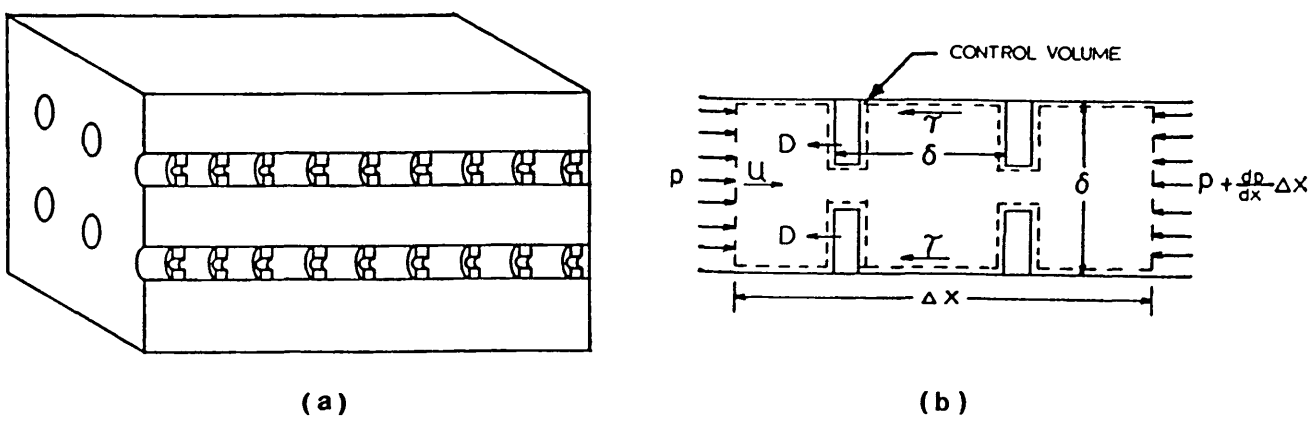


Fig. 2.2 (a) Capillary orifice model of Blick (1966), (b) cross-section of the model.

$$k = \frac{n\delta^2}{2 C_f Re} \quad , \qquad \beta = \frac{C_d}{2\delta n^2} \tag{2.3-15}$$

For laminar flow, the skin friction factor C_f is given by Hagen-Poiseuille equation as $C_f = 16/Re$. The permeability term in Eq.(2.3-15) then becomes $k = n\,d^2 / 32$.

The coefficient 1/32 is not particularly meaningful in so far as an actual porous medium is concerned. It would have to be replaced by some arbitrary coefficient which has to be determined experimentally. Eq.(2.3-14) could also be expressed as

$$-\frac{dp}{dx} = \left(\frac{32}{\rho g n D^2}\right) \mu q + \left(\frac{C_d}{2 D g n^2}\right) q^2 \tag{2.3-16}$$

where $D = 3(1-n)/n$ is the diameter of the capillary and

$$C_d = (1-h^2/D^2)\,(D^4/h^4 - 1)\,/\,C_o^2$$

where h is the diameter of the opening and C_0 the coefficient of the opening. This derivation has shown that the inertial coefficient is directly related to D, the characteristic dimension of the pore openings, and permeability (viscous coefficient) to D^2. The two coefficients can therefore be related to one another. This point will be discussed further in chapter 8.

(b) Hydraulic Radius Model (Kozeny theory)

The Kozeny theory and its various modifications are all based on flow in capillaries. The main advantage is that by using the 'hydraulic radius' concept, they are able to suggest more about the coefficients in non-linear equations. This idea was explored extensively by Ergun and coworkers [16,17].

Ergun started from an equation proposed originally by Reynolds for turbulent flow in tubes, Eq.(1.1-1). Reynolds had postulated that the resistance due to friction during fluid flow could be represented as the sum of a term proportional to the first power of the fluid velocity and a term which is the product of density and the second power of velocity. The factor a and b are dependent on the characteristics of the system. Ergun assumed that Reynolds' equation would also be valid for flow in porous media, if the filter (seepage) velocity q is used instead of v. This implies that the porous medium is assumed to be equivalent to a bundle of capillary tubes. The two terms in Eq.1 were presumed to represent viscous and inertial losses respectively. The viscous energy losses were thought to correspond to the Darcy equation. Using the hydraulic radius theory the Kozeny - Carman expression for this would be

$$a = 5\alpha \frac{(1-\phi)^2}{\phi^3} \mu S_o^2 \tag{2.3-17}$$

The kinetic energy losses would be identical to those in 'turbulent' flow mode in a cylindrical

capillary

$$b = \beta / 2\delta \qquad (2.3\text{-}18)$$

The diameter δ for a porous medium composed of cylindrical capillaries is related to porosity by the expression

$$\delta = \frac{4\phi}{S_o (1-\phi)} \qquad (2.3\text{-}19)$$

By using Eqns. 2.3-17, 18, 19 and the Dupuit-Forchheimer assumption Eq.(2.2-3) the pressure gradient for high rate flow can be [16] written as

$$\text{grad}\, p = \left[5\,\alpha \frac{(1-\phi)^2}{\phi^3} S_o^2 \right] \mu q + \left[\frac{\beta}{8} \frac{(1-\phi)}{\phi^3} S_o \right] \rho q^2 \qquad (2.3\text{-}20)$$

In this formulation α and β presumably depend on the critical Reynolds number for the system. Since any universally applicable critical value of Re cannot be determined, the coefficients α and β also cannot be evaluated universally. This presents a severe limitation on the theory, as those based on correlations of friction factor - Reynolds number relation (see Chapter 5).

A similar approach to Ergun was proposed by Cornell and Katz [18]. They however used the hydraulic radius instead of S_o and also introduced a tortuosity factor which they measured from electrical conductivity measurements. Everything was expressed in measurable quantities except the two coefficients α and β (called k_1 and k_2 by them).

An attempt has been made by Irmay [19] to derive a non-linear equation based on Kozeny-type expression. Irmay started from Navier-Stokes equation and using space averages, solved it retaining all the inertial terms. His approach is essentially similar to that of Ergun and eventually leads up to Eq.(2.3-20). By retaining the inertia terms however he gets an extra time dependent term

$$\text{grad}\, p = a v + b \rho v^2 + c \rho (\partial v / \partial t) \qquad (2.3\text{-}21)$$

This equation is similar to that proposed by Polubarinova-Kochina [20] who has shown that the final term is negligibly small except for a very brief period during the onset of motion.

The merit of Irmay's work has been to show that the kinetic energy losses are not necessarily due to turbulences but due to the inertial effects although the flow is in laminar mode. At very high Re, turbulence will set in and the coefficients a and b will take new values. The basic form of Eq.(2.3-21) is however expected to remain unchanged.

2.3.1.2 Flow Outside Solid Objects (Drag Theories)

In the drag theory approach, the walls of the pores are treated as obstacles to an otherwise straight flow of viscous fluid. The porous media is divided into a unit cell (eg. spheres). The drag of the fluid on the walls of the media is calculated from Navier-Stokes equation. The sum of all drags is then equal to the resistance of the medium (ie equal to μ/k in Darcy's law). Drag theory was initiated by Emersleben in 1924 and since then many variations of and improvements on it has appeared in the literature. A comprehensive discussion can be found in the text by Happel and Brenner [21].

The various models proposed which can be classified under drag theory can be divided into two convenient groups, depending on the geometric shapes of the obstacles. One approach has been to visualize the obstacles as fibres, and the other to visualize them as spheres. An alternative has been to calculate the resistance of arbitrary shaped objects and thereby generalize the basic idea of drag theory. This has been called 'Stokes flow approach' recognising the contribution of Stokes in calculation of resistance in steady-state flow of variously shaped objects.

(a) Fibre Theory Approach

In this type of model, the porous media is imagined to be composed of circular cylinders ('fibres') having a random distribution of diameters. The 'fibres' may be arranged so that one third of the total may be parallel to each spatial direction. The fibres are envisaged as being 'dragged' through the fluid and the total resistance, hence permeability, calculated.

The model assumes that the separation between fibres and the length of individual fibres are both large compared to the diameter of fibres ie. a high porosity media. The main criticism about this model is that each fibre is assumed to be unaffected by the presence of any adjacent fibres and so regarded as solitary in the fluid. Such an assumption may be acceptable for low Reynolds number flow, but at increasing flow velocity the eddies formed from a cylinder would reach a cylinder placed downstream. A detailed analysis of this problem - analytical or numerical, is a formidable task. Emersleben's original "fibre theory" has subsequently been extended for high velocity flow by many others (cf [2a, 21]).

(b) Spherical Obstacle Approach

Pioneering work in this area was carried out by Brinkman [22]. He was able to solve the Navier-Stokes equation for a swarm of particles by considering the forces acting on a volume element of fluid. In his solution, the inertia term was neglected since the density of the fluid was

assumed to be zero, and the fluid was also assumed to be incompressible. Brinkman's model has been improved considerably and discussed in detail by Happel & Brenner [21].

(c) Stokes Flow Approach

Here the Navier-Stokes equation is solved to calculate the resistance of arbitrary shaped objects in a steady-state stream of viscous fluid. The balance equations to be solved for steady flow of an incompressible fluid are

$$\mathbf{F} - 1/\rho \text{ grad } p - \mu/\rho \text{ curl curl } \mathbf{v} - \mathbf{v} \text{ grad } \mathbf{v} = 0 \qquad (2.3\text{-}22)$$

$$\text{div } \mathbf{v} = 0 \qquad (2.3\text{-}23)$$

Solution of this equation has been attempted by Stark [23] using numerical method. He obtained results corresponding to the solutions of Forchheimer's equation. Whitaker [24] has also indicated a method for solving the equation.

It is interesting to note that Philip [25] has given some solutions to the above equations without the inertia terms using a model of convergent - divergent pores. His results indicate that the notion that viscous flow in porous media takes place down a potential gradient on a microscopic scale should be abandoned. The velocity profile in such a model is quite different from that of Hagen - Poiseuille flow in a straight capillary.

2.3.2 Continuum Models

(a) Mixture theory

Two fairly distinct approaches have arisen, both of which use the fundamental principles of continuum mechanics. One approach used to obtain equations governing the flow of multiphase systems is often referred to as the theory of mixtures. Reviews of this method can be found in the literature [26]. In this method, the various phases are viewed as overlapping continua, existing simultaneously everywhere and occupying the whole space. Continuous field quantities are defined which account for the thermodynamic character of a phase due to its makeup as well as the interaction of the phases. Properties such as continuity are assumed to exist for most of the field quantities. Finally, balance laws for the various phases are derived in differential or integral form, which are an intuitive extension of classical single-phase relations.

(b) Local Volume Averaging

An alternative approach used to derive multiphase equations employs the technique of local volume averaging [1,24]. In this approach the system is visualized as being composed of interpenetrating continua, each occupying only a part of the space and separated by highly irregular interfaces. With each phases are associated the usual thermodynamic quantities which are continuous for that phase but discontinuous over the entire space. The classical balance laws of continuum mechanics along with appropriate interfacial and boundary conditions governing the state of the system are then derived. Since solution of these equations at the microscopic scale is virtually an impossible task, the scale at which the system is described is changed by averaging the equations over some local representative element of volume (REV). The volume averaged equations obtained are referred to as the macroscopic equations. Such equations obtained by the averaging technique have been applied to problems as diverse as flow through porous media, fluidized beds, flow of immiscible fluids, drying etc. In the next chapter this method is used for describing high velocity gas flow in porous media.

2.3.3 Statistical Models

The microscopic fluid momentum balance equation can be solved only if the geometry of the medium surrounding the fluid is known. Due to the complexity of a porous medium it is therefore not possible to derive an exact solution. There has therefore been a tendency to simplify the porous medium to the extent the balance equations become solvable. However this has lead to over- simplifications and the results are usually not found to be general enough ie. they do not hold for all types of porous media.

An alternative approach is to describe the process of flow in porous media using statistical methods which were originally used in solving problems of statistical mechanics, eg kinetic theory of gases, information theory, quantum mechanics etc. Three different approaches have been used for describing the flow process by stochastic models:

(a) Random - walk model : here the 'randomness' is ascribed to the fluid particles flowing in an homogeneous medium.

(b) Random - media model : here the flow is considered to be deterministic whereas the medium is taken to be composed of random channels.

(c) Systemic approach : no specific models are introduced, but only general relationships for expectation values of observables are employed.

The statistical approach was first attempted by Scheidegger [27] who drew an analogy between Brownian motion and a simple velocity - dispersion model of flow in porous media. The random-walk model was later extended by him [2a] to include the non-linear high flow region. For this, he considered the case of purely 'turbulent' flow through individual channels and took the ensemble average. He arrived at the equation:

$$\frac{\partial \rho}{\partial t} = \nabla^2 (D \rho) + \nabla . [m \sqrt{\rho}\ n \sqrt{\text{grad } p}\ ] \qquad (2.3\text{-}24)$$

where m is a constant dependent on the porous medium, n a unit vector in the direction of grad p and D a certain function that could be evaluated by taking further additional assumptions.

The above 'turbulent' flow equation is composed of two effects : one corresponding to the average turbulent flow through a set of small channels; and one due to dispersivity effects. It is interesting to note that the effect of dispersivity has been taken into account which is not the case for most of the non-linear equation. The equation has however not been tested with any rigour.

The systemic approach [2a] relies on the analogy between flow in porous medium and irreversible thermodynamics. The approach is based on Gibbs' kinetic theory of gases. The model has the advantage that any micro-dynamic assumptions are unnecessary. However it is unable to make any specific predictions regarding the factor of dispersion occuring in diffusivity equation.

The main acheivement of various statistical models of flow in porous media are that they can predict the phenomena of diffusion and dispersion better than any geometric models are able to. They have also been useful for the analysis of stability conditions in displacement processes and viscous fingering. A comprehensive review of the various statistical models of flow in porous media can be found in the text by Scheidegger [2a].

Fractals

The word "fractal" was coined by Mandlebrot [28] from the Latin of fractus - meaning irregular or fragmented. The origins of the fractal concept lie partly in probablity theory and partly in algebra (eg topology). Mandlebrot proposed that real objects in nature cannot be described simply as being one, two or three dimensional. Real surfaces are rarely, if ever, smooth. As such they will have fractional dimensions of $2 < D < 3$. The higher the value of D the more convoluted and irregular the surface will be, and hence more space filling. Graphite with a very smooth surface has $D = 2.07$ and carbonate rocks $D = 2.90$. Values of D for many other materials have been found by Anvir et al [29]. This group of workers used nitrogen and various polystyrene molecules to be adsorbed as monolayers covering the surfaces. The

decrease in the resulting apparant surface area for each type of adsorbate is related to the roughness of the surface under investigation. Gases of large molecules, for example, would be able to penetrate only through the widest pores whereas gases of smaller molecules can penetrate pore networks which are hidden from the larger molecular gases.

If n is the number of moles of adsorbate per gram of adsorbent which will cover some spheriodal particles of average radius R, then the fractional dimension, D, of the particles can be found from the equation

$$n \propto R^{D-3} \tag{2.3-25}$$

A log/log plot of this equation would give a straight line from which D could be found as the slope of the line. The great advantage in using fractals is the ease with which solid particles can be described by a number according to its surface roughness. This provides an added way of classifying porous media. For quantitative description of flow in porous media the use of fractals has yet to realise its potential. A review of some of the possible applications has been given by Williams & Dawe [30]. Current attempts are directed mostly to its use in the description of viscous fingering [31].

2.4 EXPERIMENTS ON HIGH VELOCITY FLOW

Experimental investigations of the deviation from Darcy's law at high flow rates have been carried out over many years. In order to characterise the domain of validity of Darcy's law, almost all workers make use of the Reynolds number, Re, which may be defined as

$$Re = \rho v \delta / \mu \tag{2.4-1}$$

where δ is a length scale characterising the porous media. This has often been taken as some average grain or pore diameter.

Most of the reported work expresses the results in terms of a friction factor versus Reynolds number plot, where the friction factor, f, is generally defined as

$$f = \frac{\delta}{\frac{1}{2}\rho v^2} \frac{\Delta P}{L} \tag{2.4-2}$$

There does not seem to be any convergence of opinion regarding the flow rate at which deviation fron Darcy's law will occur. Often this is referred to as the "critical" Reynolds number. Much discrepency can be observed in the reported works. This seems to be primarily due to an incorrect choice of δ, the characteristic length scale. Disagreement also exists regarding the proper definition of the friction factor term. These issues will be discussed further in Chapter 5.

Numerous experimental work on high velocity fluid flow in porous media has been conducted since the beginning of this century. Pioneering studies were carried out by Fancher & Lewis [32]. Other important work are those by Hickox [33], Bakhmeteff et al [34], Carman [7], Nissan [35], Fox [36], Plain et al [37], Schneenabeli [13], Dudgeon [38], Ward [39] and Wright [40]. Also of relevance to the present study are those by McFarland & Dranchuk [41], McDonald et al [42] and the recent works by Dybbs & Edwards [43] and Fand et al [44].

Hubbert [45] attempted to observe the "turbulent" eddies inside pores by injecting dyed water into glass bead pack assemblies. Later Wright [40] attempted to use hot wire anemometer and McFarland et al [41] used interference holograms to investigate the flow patterns in between glass spheres. Dybbs & Edwards [43] carried out measurements using laser doppler anemometry on a porous medium composed of glass cylinders arranged in layers oriented perpendicular to each other.

All of these investigators confirm that deviation from Darcy's law cannot be attributed to the phenomenon of turbulence alone. The deviation is found to be due to the inertial forces which are present, although they are negligibly small in comparision to viscous forces at low Reynolds number.

Besides the above mentioned works, a number of recent investigators have considered the implications of the non-Darcy effect in various practical problems. Cooke [46] has investigated non-Darcy gas flow through propped fractures using different grades of sands. Similar work has also been reported by Maloney et al [47] who also investigated the effect of partial liquid saturation and different stress conditions. Nguyen [48] conducted experimental study of non-Darcy flow through perforations. The pressure drop - flow rate data were presented as functions of the perforation geometry and gravel fill permeability. Buell et al [49] have investigated the use of Forchheimer's cubic and quadratic equations (see Appendix) for the design of gravel-packed gas wells and found the use of cubic term to be unnecessary.

2.5 NUMERICAL STUDIES

Numerical solution of the Navier-Stokes equation for quite complex geometries has been made possible by the advent of digital computers. Numerical approaches to the modelling of flow in porous media are a comparatively recent event, and to date only a few reported studies are available in the literature. To obtain solutions it was necessary to use highly idealized models of porous media, some of which are shown in Fig 2.3.

The first attempt at a numerical solution was probably that by Stark [23]. He retained the

inertia terms in the Navier-Stokes equation and solved for a model composed of square shaped grains as shown in Fig.2.3 (a) and (b). The calculations were performed only for a two dimensional domain. Different media were simulated by varying the porosity and the grain sizes. Although the idealized arrangement limits the usefulness of this study, it nevertheless provided some insight. In particular, Stark showed that the coefficients α and β are constants not only of the geometry of the media but are also influenced by the Reynolds number of the flow. However he showed that the permeability ($1/\alpha$) could be taken to be a constant of the media if the Re was less than 5 and β a constant if the Re was below 50. At Re of 100 his calculations showed that if α and β were assumed to be a constant it would result in an error in the pressure gradient of about 7%. His study therefore shows that the Forchheimer constant should not be extrapolated outside the range of data from which it was calculated.

Subsequent reported work includes those by Payatakes et al [50] and Azzam & Dullien [51]. The model of porous media used by the former group is in the form of a wavy channel as shown in Fig.2.3 (e). The latter group used a model of a straight periodically nonuniform capillary tube as shown in (d). Since the conduits used by both these groups were symmetrical, it was possible to bring the problem to two dimensions by the use of stream functions. The most recent study is that by Ralph [52] who used a model of a sinusoidal tube as shown in (c). It should be noted that analytical solutions for sinusoidally varying tubes have already been given by Elata et al [53] and Ralph's numerical solution does not throw any new light onto the physics of the phenomena.

Hannoura et al [54] have provided a review of non-Darcy flow in the design of dams and other related hydrological problems. Recently, Tariq [55] has investigated the flow of fluids at high velocity through perforations. For this purpose he has solved the non-linear Forchheimer equation using the Finite Element method for different perforation geometries.

The enormous potential of digital computers now makes it feasible to undertake calculations of even greater complexities. The study of Stark for example could be extended to models of cubes in three dimensions including more varied sizes of grains and arrangements in more complex fashion. In this manner the effect of various pore structural parameters on the inertial effects can be better understood.

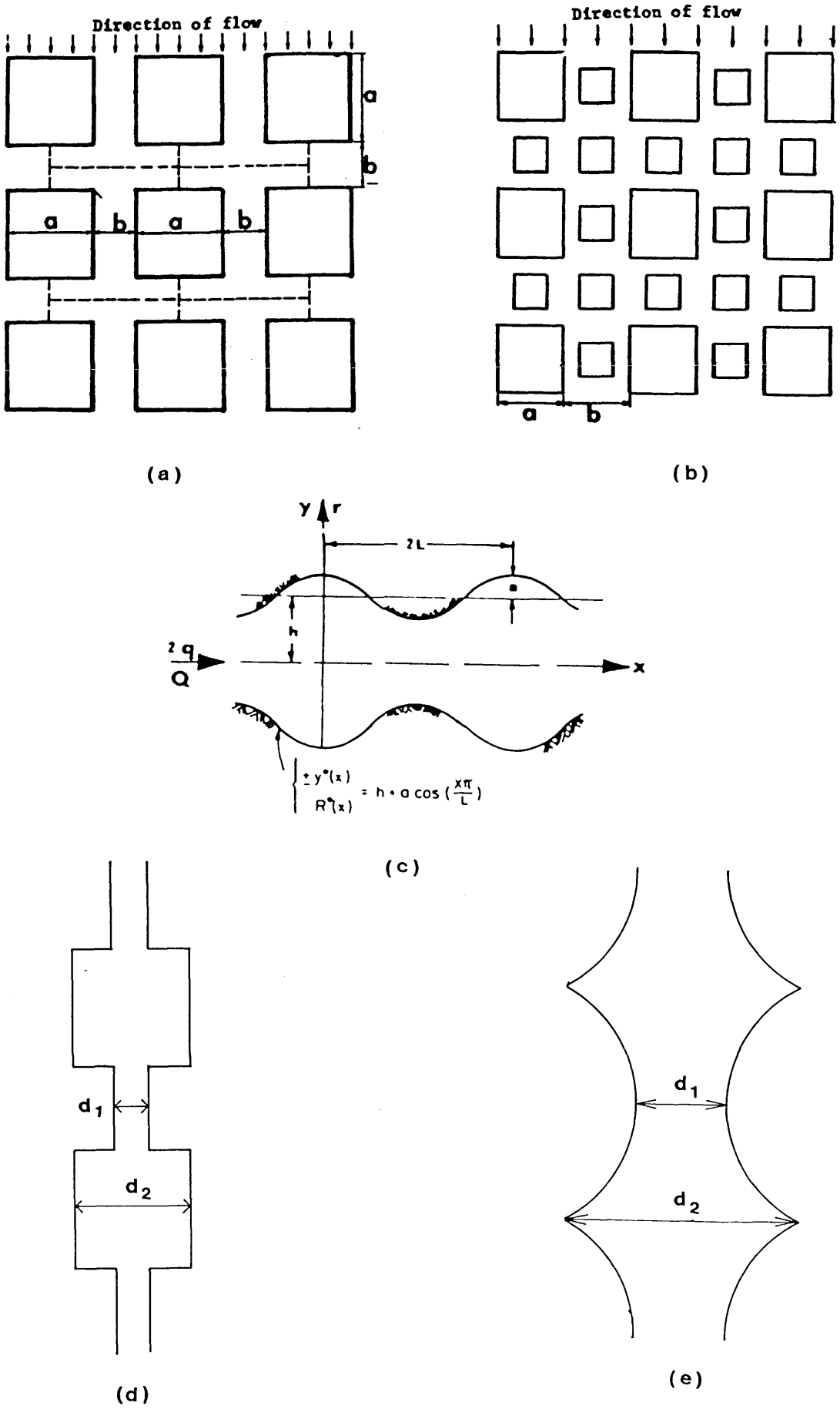


Fig. 2.3 Some of the models of porous media used by the various authors for numerical computation: (a) and (b) models of Stark 1972, (c) Ralph 1987, (d) Azzam and Dullien 1977 and (e) Payatakes et al 1973.

2.6 EFFECT OF PRESSURE AND TEMPERATURE

Since α and β in Forchheimer's equation are both dependent on the geometry of the porous medium, it is to be expected that changes in the temperature or pressure on the medium might change the structure of the medium and hence affect the value of both α and β. Numerous workers have attempted to measure the effect of pressure and temperature on α (eg [56]), however virtually nothing seems to have been done regarding β. The only reported work was carried out by Greenberg et al [57] who measured the value of β for temperatures between 15 and 60°C for a constant confining pressure. Their experimental measurements showed that inertial coefficient did not vary appreciably with temperature for any of their core samples.

The experimental findings of Greenberg et al are contrary to expectations since permeability is known to be affected by temperature and pressure changes due to changes in the pore structure. The value of β should also therefore be a function of these parameters since it is even more sensitive to pore structural changes. Further experimental work appears to be required in this area to verify the hypothesis.

It is interesting to note that Greenberg et al observed temperature gradients of the order of 5°C/in for high rate gas flow. This was possibly caused by Joule-Thomson expansion within the core. Some heating of the gas could also occur due to viscous dissipation. These particular phenomena may be important e.g. in gas condensate reservoir development. The gas flow near the wellbore may not be isothermal, and any significant drop in the temperature may then cause liquid dropout to occur due to retrograde condensation. Further theoretical and experimental work is therefore required to better understand the process and to provide a detailed energy balance.

REFERENCES

1. Bear, J.: *Dynamics of Fluids in Porous Media,* American Elsevier, New York (1972).
2. Scheidegger, A.E. : *The Physics of Flow through Porous Media,* Toronto Univ. Press, Toronto, (a) 3rd ed. (1974); (b) 2nd ed. (1960).
3. Dullien, F.A.L. : *Porous Media : Fluid Transport and Pore Structure,* Academic Press, London, (1978).
4. Wall, C.G. : Permeability - pore size distribution, *J. Inst. Petrol.*, Lond. (1965) **51**,195.
5. Marshall, T.J. : Permeability equations and their models, in *Symp. on Interactions between Fluids and Particles* (P.A. Rottenburg, ed.) Inst.Chem.Eng., Lond. (1962).
6. Kozeny, J. : Uber kapillare Leitung des Wasser im Boden, Sitzungsber. Akad. Wiss.,Wien (1927) **136**, 271 ; see also Wasserkr. U. Wasserw. (1927) **22**, 86.

7. Carman, P.C. : Fluid flow through a granular bed, *Trans. Inst. Chem. Eng.*, Lond. (1937) **15**, 150-156.
8. Carman, P.C. : *Flow of Gases through Porous Media,* Butterworths Scientific Publish., London (1956).
9. Childs, E.C. and Collis-George, N. : The permeability of porous materials, *Proc. Roy. Soc.* (1950) A**210**, 392.
10. Adamson, J.F. : Application of the Kozeny equation to consolidated porous media, *Nature* (1950) **166**, 314.
11. Wyllie, M.R.J. and Rose, W.D. : Application of the Kozeny equation to consolidated porous media, *Nature* (1950) **165**, 972.
12. Brooks, C.S. and Purcell, W.R. : Surface area measurements on sedimentary rocks, *Trans AIME* (1952) **195**, 289.
13. Scheneebeli, G. : Experiences sur la limite de validite de la loi de Darcy et l'apparition de la turbulence dans un ecoulement de filtration, *La Houille Blanche* (1955) **10**(2), pp.141-149
14. Kutilek, M. : Non-Darcian flow of water in soils - laminar region, Proc of 1st IAHR Symp. on Fundamentals of Transport Phenomena in Porous Media, IAHR Elsevier, Amsterdam (1972) p.327.
15. Blick, E.F.: Capillary orifice model for high speed flow through porous media, *Ind. Eng. Chem.* (1966) **5**(1), 90-94.
16. Ergun, S : Fluid flow through packed columns, *Chem. Eng. Prog.* (1952) **48**(2), 89-94.
17. Ergun,S. and Orning, A.A.: Fluid flow through randomly packed columns and fluidized beds, *Ind. Eng. Chem.* (1949) **41**(6), 1179-1184.
18. Cornell, D. and Katz, D.L. : Flow of gases through consolidated porous media, *Ind. Eng.Chem.* (1953) **45**, 2145.
19. Irmay S. : On the theoretical derivation of Darcy and Forchheimer formulas, *Trans. Am. Geophys. Un.* (1958) **39**(4), 702-707.
20. Polubarinova-Kochina, P. Ya. : *Theory of Groundwater Movement,* (English trans. by R.J.M. DeWiest) Princeton Univ Press., Princeton, N.J. (1962).
21. Happel, J. and Brenner, H. : *Low Reynolds Number Hydrodynamics,* Prentice-Hall, Englewood Cliffs, N.J. (1965).
22. Brinkman, H.C. : A calculation of the viscous force exerted by a flowing fluid on a dense swarm of particles, *Appl. Sci. Res.* (1947) **A1**, 27.
23. Stark, K.P. : A numerical study of the nonlinear laminar regime of flow in an idealised porous medium, 1st Int. IAHR Symp. on Fundamentals of Transport Phenomena in Porous Media, IAHR Elsevier, Amsterdam (1972) p.86
24. Whitaker, S. : Advances in the theory of fluid motion in porous media, *Ind. Eng. Chem.* (1969) **61**(12), 14.
25. Philip, J.R. : Fluid flow and transport in pores and porous media, *Symp. on Circulatory*

and Respiratory Mass Transport, Trans. Ciba Foundation, (Eds.: G.E.W. Wolstenhome and J. Knight), Churchill Ltd., London (1969) p.25.

26. Atkin, R.J. and Craine, R.E. : Continuum theories of mixtures : Basic theory and historical developements, *Q. J. Mech. Appl. Math.* (1976) **29**, 209.
27. Scheidegger, A.E. : Statistical hydrodynamics in porous media, *J. Appl. Phys.* (1954) **25**, 994-1001.
28. Mandelbrot, B.B. : *The Fractal Geometry of Nature,* Freeman, San Francisco (1982).
29. Anvir, D., Farin, D. and Pfeifer, P. : Surface geometric irregularity of particulate materials : the Fractal approach, *J. Coll. Interface Sci.* (1985) **103**(1), 112-123; see also Molecular Fractal surfaces, *Nature* (March 15, 1984) **308**, 261-263
30. Williams, J.K. and Dawe, R.A.: Fractals - an overview of potential applications to transport in porous media, *Transport in Porous Media* (1986) **1**, 201-209.
31. Nittmann, J., Daccord, G. and Stanley, H.E. : Fractal growth of viscous fingers : quantitative characterization of a fluid instability phenomena, *Nature* (March 1985) **314**, 141-144.
32. Fancher, G.H. and Lewis, J.A. : Flow of simple fluids through porous materials, *Ind. Eng.Chem.* (1933) **25**, 1139.
33. Hikox, G.H. : Flow through granular materials,*Trans. Amer. Geophys. Union* (1934) **15**, 567.
34. Bakhmeteff, B.A. and Feodoroff, N.V. : Flow through granular media, *J. Appl. Mech.* (1937) **4**A, 97.
35. Nissan, A.H. : Flow of liquids under critical conditions, *J. Inst. Pet.* (1942) **28**, 257.
36. Fox, J.W. : Onset of turbulent flow in certain arrays of particles, *Proc. Phys. Soc.* (1949) B**62**, 829-832.
37. Plain, G.J. and Morrison, H.L. : Critical Reynolds number and flow permeability, *Amer. J. Phys.* (1954) **22**, 143-146.
38. Dudgeon, C.R. : An experimental study of the flow of water through coarse granular media, *La Houille Blanche* (1966) **7**, 785-801.
39. Ward, J.C. : Turbulent flow in porous media, *J. Hydrau.*, Proc. ASCE, HY5 (1964) **90**, pp. 1-12.
40. Wright, D.E. : Nonlinear flow through granular media, *J. Hydrau.*, Proc. ASCE, HY4 (1968) **94**, 851-872.
41. McFarland, J.D.and Dranchuk, P.M. : Visulisation of the transition to turbulent flow in porous media, J. Can. Pet . Tech. (April 1976) 71-78.
42. Macdonald, I.F., El-Sayed, M.S., Mow, K. and Dullien, F.A.L.: Flow through porous media - the Ergun equation revisited, *Ind. Eng. Chem. Fund.* (1979) **18**, 199.
43. Dybbs, A. and Edwards, R.V. : A new look at porous media fluid mechanics - Darcy to turbulent, in *Fundamentals of Transport Phenomena in Porous Media,* (Eds.: J. Bear and M.Y. Corapcioglu) Martinus Nijhoff Publishers, NATO-ASI, Series E, No. 82,

(1984) 201 -56

44. Fand, R.M., Kim, B.Y.K., Lam, A.C.C. and Phan, R.T. : Resistance to the flow of fluids through simple and complex porous media whose matrices are composed of randomly packed spheres, *J. Fluids Eng.*, Trans ASME (Sept. 1987) **109**, 268-274.
45. Hubbert, M.K. : Darcy's law and the field equations for the flow of underground fluids, *Trans. AIME.* (1956) **207**, 222-239.
46. Cooke, C.E. : Conductivity of fracture proppants in multiple layers, *J. Pet. Tech.*, (Sept. 1973) p.1101-7.
47. Maloney, D.R., Gall, B.L. and Raible, C.J. : Non-Darcy gas flow through propped fractures : effect of partial saturation, gel damage and stress, Paper SPE 16899 presented at the 62nd Annual Conf. of the SPE, Dallas, Sept. 27-30, 1987.
48. Nguyen, T.V.: Experimental study of non-Darcy flow through perforations, Paper SPE 15473 presented at the 61st Annual Conf. of the SPE, New Orleans, Oct. 5-8, 1986.
49. Buell, R.S. and Crafton, J.W. : The application of the cubic and quadratic Forchheimer equations in the design of high-rate gravel-packed gas wells, Paper SPE 14448 presented at the 60th Annual Conf. of the SPE, Las Vegas, NV, Sept. 22-25, 1985.
50. Payatakes, A.C., Tien, C., and Turian,R.M. : A new model for granular porous media. Part II: Numerical solution of steady state incompressible Newtonian flow through periodically constricted tubes, *AIChE Jour.* (1973) **19**, 67.
51. Azzam, M.I.S. and Dullien, F.A.L. : Flow in tubes with periodic step changes in diameter : A numerical solution, *Chem. Eng. Sci.* (1977) **32**, 1445.
52. Ralph, M.E. : Steady flow structures and pressure drops in wavy-walled tubes, *J. Fluids Eng.*, Trans. ASME, (Sept. 1987) **109**, 255.
53. Elata, C. and Taskerman, U. : The viscous flow through channels and tubes with sinusoidal boundaries as a model for porous media, *Israel J. Tech.* (1976) **14**, 235.
54. Hannoura, A.A. and Barends, F.B.J. : Non-Darcy flow : state of the art, Proc. Euromech 143, Delft (1981) 37-51.
55. Tariq, S.M. : Evaluation of flow characteristics of perforations including nonlinear effects with the finite element method, *SPE Prod Engr. Jour.* (May 1987) 104-112.
56. Pulrabek, W.W. and Ibele, W.E. : The effect of temperature on the permeability of a porous material, *Int. J. Heat Mass Transfer*, (June 1987) 30, 1103-1109.
57. Greenberg, D.B. and Weger, E.: An investigation of the viscous and inertial coefficients for the flow of gases through porous sintered metals with high pressure gradients, *Chem. Eng. Sci.* (1960) **12**, 8-19.

Chapter 3

THE ROLE OF INERTIA IN HIGH VELOCITY FLOW THROUGH POROUS MEDIA

3.1 PHYSICAL DESCRIPTION

3.1.1 Introduction

A number of forces can arise during flow of fluids in porous media or in flow generally, which will control overall behaviour. The more important of these forces are:

(a) Forces due to differences of piezometric head between two points in the fluid - usually referred to as the 'pressure force',
(b) Forces arising due to the presence of viscosity,
(c) Forces acting from outside, eg. gravity, known as the body force,
(d) Forces due to surface tension, and
(e) Elastic forces, ie those due to fluid compressibility.

Any of these forces acting alone or in combination on fluid particles will have a resultant. According to Newton's Second law of motion, this resultant force F = m a, will cause an acceleration in the same direction as the applied force. If an additional force (- m a) was applied to the fluid particle in the same direction, the net force on the particle would be (F - m a), ie. the particle would have a zero acceleration. This hypothetical force (- m a), required to bring the acceleration of the particle to zero is termed [1] the *inertial force*. It therefore represents the reluctance of the fluid particle to be accelerated, and is not independent of the other forces. It is simply equal and opposite to the resultant of all the other forces. If all the forces acting on a fluid element were represented by a force polygon, then the inertia force could then be imagined as the side required to close the polygon.

3.1.2 Analysis of Forces

The forces acting on a differential volume element of fluid during its flow could be classified on the basis of the function that they perform. Using this approach [2,3] there is a driving force, F_d, and a resistive force, F_r, which would arise from frictional resistance due to the fluid viscosity. Using the D'Alembert principle we can introduce an inertia force, F_i, which according to Newton's second law would be equal to

$$F_i = -\rho . dV\, a \qquad (3.1\text{-}1)$$

This is basically the reactive force due to the reaction to acceleration. The various forces are shown schematically in Fig. 3.1. They may be written as :

$$F_d + F_r = -F_i \qquad (3.1\text{-}2)$$

This is essentially a statement of Newton's third law of motion, and could also be expressed as

$$F_d + F_r + F_i = 0 \qquad (3.1\text{-}3)$$

This equation states that the moving fluid element would be in a state of dynamic equilibrium under the action of these three forces. The driving force F_d is composed of the pressure force F_p and the body force F_b and may be thought of as being the independently variable force which supplies the necessary energy for fluid motion. Both F_r and F_i would then be the dependent variables, depending on the state of motion of the fluid, ie being zero when there is no motion.

The inertial force F_i does not contribute to the energy of the system, nor does it reduce it. The energy is reduced by the resistive force F_r which is basically the viscous dissipative force. From this argument it can be understood that F_d and F_r are the principal forces, and F_i is simply a superimposed modifying influence.

During flow through a porous medium, the fluid particles would move along a continuously curvilinear path at a varying speed, ie with a continuously varying acceleration. In the following section the acceleration term will be explained in more detail, as will the importance of streamline curvature.

3.1.3 Streamline Curvature

(a) The acceleration term

Before we can describe the inertial force properly we need to consider the acceleration term. The velocity of a fluid particle can be a function of position and time. The change of velocity could therefore be expressed as

$$\delta v = \frac{\partial v}{\partial t}\delta t + \frac{\partial v}{\partial x}\delta x \qquad (3.1\text{-}4)$$

In the limit dt --> 0, the acceleration would be

$$\frac{dv}{dt} = \frac{\partial v}{\partial t} + \frac{\partial v}{\partial x}\frac{dx}{dt} \qquad (3.1\text{-}5)$$

since dx / dt = v, Eq.(3.1-5) therefore becomes

$$\frac{dv}{dt} = \frac{\partial v}{\partial t} + v\frac{\partial v}{\partial x} \qquad (3.1\text{-}6)$$

For three dimensional flow, the equation can be expressed in vectorial notation as

$$\frac{Dv}{Dt} = \frac{\partial v}{\partial t} + v \cdot \nabla v \qquad (3.1\text{-}7)$$

We see that the fluid acceleration consists of two terms. The first term is the *local acceleration* and expresses the rate of change of velocity at a fixed point in space. The second term is the *convective acceleration* and it depends on the velocity gradient as well as the magnitude of the velocity. The rate of change of momentum per unit volume of the fluid (ie the inertial force) is therefore

$$\rho \frac{Dv}{Dt} = \rho \frac{\partial v}{\partial t} + \rho v \cdot \nabla v \qquad (3.1\text{-}8)$$

According to Newton's second law, the rate of change of momentum of a body (a fluid element) is equal to all the sum of forces imposed on it. The two force acting on a fluid element are the body force and the surface force; the latter is represented in terms of the pressure and viscous forces. The momentum balance equation - known as the Navier-Stokes equation - can then be written as:

$$\rho \left(\frac{\partial v}{\partial t} + v \cdot \nabla v \right) = -\nabla p + \rho g + \mu \nabla^2 v \qquad (3.1\text{-}9)$$

For compressible fluids however, it is necessary to consider $D(\rho v) / Dt$ instead of $\rho\, Dv / Dt$ in the above equations. Further discussion on the balance of momentum for compressible fluids can be found in various standard text [4,5]. It is useful to note that the left hand side of Eqn.(3.1-9) indicates that even for steady-flow the inertial force will not necessarily be zero, but will be dependent on the geometry of the boundaries surrounding the flow.

(b) Pressure Variation Across Curved Streamline

Although a streamline has no velocity component perpendicular to it, however it can have an acceleration component if there is any curvature. Therefore, whenever a particle moves in a curved path, it changes direction and so has an acceleration towards the centre of curvature of the path, whether or not the magnitude of the velocity is changing. If the radius of curvature is r, the particle accelerating toward the centre has a convective part v^2 / r and a temporal part $\partial v_n / \partial t$, where v_n represents the component of velocity towards the centre of curvature. For circular motion therefore, the acceleration is given by

$$a_n = \frac{v^2}{r} + \frac{\partial v_n}{\partial t} \qquad (3.1\text{-}10)$$

We consider two streamlines separated by a distance δr sufficiently close togather to be regarded as having the same radius of curvature r (see Fig.3.2). Between them we take a small cylindrical element of fluid of cross sectional area dA which will have a mass of $\rho\, \delta A\, \delta r$. The

pressure is p at radius r and p+ δp at radius r + δr. The net force on the element acting inwards along the streamline radius is [4] therefore

$$(p + \delta p)\,\delta A - p\,\delta A = \delta p\,\delta A \qquad (3.1\text{-}11)$$

This force would be equal to the product of the mass of the element and its centrifugal acceleration, a_n

$$\delta p\,\delta A = \rho\,\delta A\,\delta r\,.\,a_n = \rho\,\delta A\,\delta r\left(\frac{v^2}{r} + \frac{\partial v_n}{\partial t}\right) \qquad (3.1\text{-}12)$$

Dividing by δA δr and taking the limit as dr --> 0, gives

$$\frac{\partial p}{\partial r} = \rho\left(\frac{v^2}{r} + \frac{\partial v_n}{\partial t}\right) \qquad (3.1\text{-}13)$$

If the streamlines are not changing direction with time the second term on the right hand side of (3.1-13) becomes zero. The equation shows that as r --> α then ∂p / ∂r = 0, ie there will be no pressure variation if the streamlines tend to be parallel. It follows that as the radius of curvature becomes smaller the pressure variation will increase correspondingly.

During flow in porous media, the inertial forces are generally not parallel to the streamlines but are thought [3] to be randomly oriented. This would produce distortion in the streamlines, with the result that the streamlines get crowded where the curvature is sharp. The situation is shown schematically in Fig.3.4. As the fluid velocity is increased further, stagnant eddies would be expected to form within the pores where the streamlines pull away from the grain surfaces.This is particularly true where there is a sudden expansion of the pore throat. The situation could occur even though the flow as a whole is still in the laminar mode.

3.1.4 Expansion and Contraction Losses

The void space within any consolidated rocks consists of intricately branching three-dimensional network of flow channels with continuously varying cross-sections. Due to the curving flow paths, pressure gradients increase disproportionately with increasing flow rate as already discussed. The other important factor responsible for this disproportionate increase is the continuously changing cross-sectional area. This is a very important aspect which is not taken into consideration in capillaric models. A small element of fluid flowing steadily through a capillary will possess a constant linear velocity throughout. In a porous medium however, the magnitude and direction of the velocity of this fluid element will be changing continuously. Changes in the cross-sectional area of the flow path would therefore induce convective acceleration and deceleration of the fluid particles.

As the velocity is increased, the flowlines would not remain constant in length, but are thought [5] to increase the area for shear and tension stresses with consequent increase in the

viscous resistance. Flow separation would be expected to take place, with consequent eddy formation particularly at sudden enlargements of the flow channels. These losses can be explained in terms of the vortex formation that occurs when flow separation takes place. Energy must be supplied to maintain the vortex motion against the action of viscous forces.

The nature of flow separation occuring within a converging - diverging channel has already been studied [6] by solving the Stokes flow equation in a spherical space. A similar approach used later by Elata et al [7], who proposed a model of porous media as being composed of sinusoidal capillaries, also showed the presence of secondary flow occuring in such channels (see Fig.3.3).

These studies showed that significant differences exist between flow in parallel capillaries and those within a porous medium due to the converging-diverging nature of the passages. Some of the important differences found are:

(a) The maximum vorticty and shearing stress occur away from the pore wall, whereas in Poiseuille flow these quantities are at a maximum at the wall.
(b) The potential gradient is reversed in the outer regions of a pore, ie. near the walls.
(c) The velocity profiles deviate strongly from the parabolic profile predicted by Poiseuille's law. A point of inflexion is found which is related to the maxima of vorticity and shearing stress away from the pore wall.

The notion that viscous flow in porous media takes place down a gradient of potential may not therefore be applicable [6], at least on a microscopic scale. It is useful to bear in mind that the theoretical demonstration of secondary flow are based on the assumption that fluid behaves as a continuous media. However, in a porous media, where the dimensions of the channels are often of a similar order of magnitude as the mean free path of the fluid molecules, it is not known whether fluids would actually behave in a similar manner or not.

3.1.5 Discussion

The behaviour of fluid flow is controlled by the geometry of the confining boundary and by the velocity. During flow in porous media, the fluid passes through an intricately branching three dimensional network of channels and pores. Flow in porous media can therefore be quite different from that of flow in straight capillaries or tubes. In the latter, fluid particles move along a rectilinear path at constant velocity throughout,and therefore has no acceleration, unless the velocity becomes very large in which case the motion will become unstable and turbulence will set in. In the former however, the fluid particles move along a continuously curvilinear path at a varying speed, and hence with a continuously varying acceleration.

During uniform rectilinear flow in porous media, the integral of forces over a macroscopic volume due to inertia is zero, so that these can exercise no direct retarding effect upon the fluid motion. However they produce distortions which increases the terms [2] of the form $\partial^2 u / \partial y^2$ in the momentum balance equation (3.1-9), upon which the resistive forces depend. Since the forces due to inertia increase as the square of the velocity, this effect is non-linear with respect to v. For values of v for which the inertial forces are not negligible, the resistance to the flow must increase at a progressively greater rate as v is increased. It has been suggested [2] that the distortion of the flow lines by the inertial forces increases the velocity gradient, which in turn increases the frictional forces over what they would have been for the same rate of flow had the distortion not occured. Darcy's law is therefore valid for values of v small enough that the forces of inertia are negligible. This is shown schematically in Fig.3.4. The primary cause of the failure of Darcy's law is therefore due to the distortion that results in the flow lines when the velocity is great enough that the inertial force becomes significant.

Besides the curvilinear behaviour of the flow paths, it is also necessary to consider the expansion and contraction of the pores and channels. Due to the ever changing cross-sectional area of the channels, the fluid will undergo convective acceleration and deceleration during its flow. The losses due to expansion and contraction of the flow path are known to be dependent on the square of the velocity. It is important to realise that deviation from Darcy's law need not be caused by turbulence, which is the mechanism responsible for nonlinear flow in capillaries and tubes. The above discussion has shown that curvature of streamlines and the expansion / contraction losses are both nonlinear with respect to velocity. The linear relationship (Darcy's law) can therefore breakdown at increasing velocity even though the flow as a whole is still laminar.

Before closing this section, it is emphasised that flow in porous media cannot be understood fully by looking at the problem only from a fluid mechanics point of view, as has been done so far. For a complete understanding it is also necessary to consider the geometry and shape of the pore spaces in detail, since ultimately it is this that will control the overall macroscopic flow. The role of pore structure will be dealt with further in chapter 6.

3.2 MATHEMATICAL DESCRIPTION

3.2.1 Introduction

(a) Continuum Concept

For a detailed description of real material it is necessary that they be represented in terms of atoms and molecules. This may be thought of as a particulate model of materials. In reality therefore, mass is distributed discontinuously in space and is separated by relatively large voids. In the continuum model of materials however, mass is visualized to be distributed continuously through space. Any surfaces of discontinuity occuring are taken to represent phase interfaces or shock waves. For most practical problems it is not necessary to know the exact detail of molecular movements, since one is normally interested in the macroscopic properties such as density, viscosity, etc. It is by the use of continuum model that one can associate quantities like density with every point in space [8,9]. The continuum model is less realistic than the particulate model, but far simpler, and in any case, for most engineering purposes, the accuracy provided by the particulate model is unnecessary.

Using the basic theories of fluid mechanics, it is possible in principle to know the exact behaviour of flow in porous media even at the individual pore scale. For this to be possible it would however be necessary to know the exact shape of the boundaries confining the flow; this is a virtually impossible task, except for the very simple cases, for example if the medium was composed of straight capillaries, cylinders or spheres. It is not yet possible to describe mathematically the very complicated geometry of the solid surfaces that bound the flow domain within a porous matrix. Even if the geometry of the pore spaces were known exactly, it would be necessary to solve the momentum balance equations for many millions of individual pores for regions sufficiently large to be of any practical use. Besides there are as yet no means to verify whether such solutions are correct since this would require instruments for measuring the variables inside every pores.

In the continuum model of porous media, the media is visualized as being a structureless substance in which any point can be assigned kinematic and dynamic variables that are continuous functions of the spatial coordinates of the point and of time. The variables and the parameters of the continua, averaged over a sufficiently large volume will enable us to describe the flow phenomena within the domain of interest. Single phase flow in a porous medium may be imagined as a two phase flow system, solid particles being one phase. The phases are separated by interphase boundaries over which exchange of momentum, mass and other extensive quantities can take place. The continuum approach has been used frequently to solve

such diverse problems as multiphase flow in pipes, single and multiphase flow in porous media, fluidization, drying (combined heat and mass transfer), mixing and dispersion in porous media, etc.

(b) Scales of observation

By introducing the continuum model of porous media it becomes possible to move from individual pore scale to a more coarse, macroscopic scale where experimental measurements can be conducted. In the continuum description of porous media, when the microscopic scale is employed we shall be concerned with fluid elements that are of sizes smaller than the pores or grains, but large compared with the kinetic movements of molecules, eg Brownian motion. In contrast when the macroscopic scale is used it will be understood to be large compared with the grain or pore size so that microscopic irregularities of flow due to the geometry of the porous medium would not have to be considered, but only the statistical resultant. Such a scale is generally known as the Representative Elementary Volume (REV). The exact choice of the size which can be considered as macroscopic has been the subject of many investigations [10-14]. It appears that Hubbert [2] was the first to introduce the concept of averaging in porous media when he attempted to derive the Darcy's law from the Navier-Stokes equation. His approach was however intuitive and more rigorous solutions were provided later by others [8,10,14] using continuum mechanics.

In general, four different scales of observations can be associated with the description of porous media, as shown in Fig. 3.5. Just as an averaging procedure is required for moving from the micro to the macro scale, similarly other averaging laws will be required in moving from the macro to the mega and finally from the mega to the giga scale. The problem of scaling has assumed great importance in recent days [15-18] as it is realised that reservoir rocks are rarely, if ever, homogeneous. It is therefore essential to take account of the heterogeneities for realistic calculations to be performed. In reservoir simulation studies, for example, fluid flow equations are formulated on a macroscale, but are solved on a mega scale - the scale of large grid blocks. The averaging procedure from macro to megascopic scale is still a matter of active research. The present discussion will be restricted to the first two levels only, ie the micro and macroscopic scales.

In the present study, balance equations at a microscopic scale will be written for an arbitrary spatial point **r** which is at time t occupied by only one phase. For most engineering problems one is concerned with gross or average effect around a mathematical point which can be experimentally evaluated, ie with the macroscopic scale. The passage from microscopic to macroscopic scale is made possible through the application of an averaging procedure over the representative elementary volume (REV) which is the volume over which the state variables and

fluxes involved are averaged. By this averaging procedure single phase variables which are discontinious on the microscopic scale becomes continuous on the macroscopic scale. At each mathematical point properties associated with both phases can be assigned. Through the change of scale therefore, fields of variables differentiable both in space and time can be obtained for the fluid and the solid phase. A fictitious flow system of overlapping continua is established within which an interchange of various quantities takes place.

To move from the microscopic to the macroscopic scale it will be necessary to introduce medium coefficients (eg porosity, permeability, etc) which can only be evaluated experimentally. It is necessary to introduce such coefficients because of our inability to solve the flow problem at the micro scale. The main disadvantage of the continuum model is therefore that much of the micro- structural information is lost in moving from the micro to the macro scale by the process of averaging. The advantages gained by introducing such a conceptual model should not be ignored since they enable analysis of the flow problem in a more exact fashion. Also by employing such models it is possible to find out more about the empirical coefficients arising in experiments thereby providing help in planning and interpretation of experimental information.

In the following sections continuum approach is used to provide a description of the flow of a single phase incompressible fluid through porous media at high velocity. For this purpose the works of Cvetkovic [19], Stokes [20] and Hassanizadeh et al [21] have been referred to extensively. Various other approaches have also been used in the past for the description of high velocity flow in porous media [10,22-24].

3.2.2 Microscopic Equations of Flow

At any microscopic spatial point in the porous medium, either the solid or the fluid phase will exist at time t (Fig.3.6). The position vector of a spatial point of the interphase surface will be denoted by r^{fs} which may be assumed to belong to the solid phase.

The total volume of interest will be denoted by V, and will consist of the volumes occupied both by the solid V^s and by the fluid V^f. The boundaries of V^f, denoted by A^f, will consist of material surface adjacent to the solid phase denoted by A^{fs}, and a geometrical surface A^{ff} which is a part of the external boundary of V. Generally A^{ff} is not a material surface with respect to mass or any of the other extensive quantites such as momentum, energy, etc. Similarly the boundaries of the solid phase is denoted by A^s such that A^s is the sum of A^{ss} and A^{fs}.

At each microscopic point **r** and at time t, it will be assumed that the following balance equation will be valid [8].

Mass balance:

$$\frac{\partial \rho}{\partial t} + \nabla . (\rho \mathbf{v}) = 0 \tag{3.2-1}$$

Linear momentum balance:

$$\frac{\partial}{\partial t}(\rho \mathbf{v}) + \nabla . (\rho \mathbf{v}\mathbf{v}) = \nabla . \mathbf{t} + \rho \mathbf{f} \tag{3.2-2}$$

Angular momentum balance:

$$\mathbf{t} = \mathbf{t}^T \tag{3.2-3}$$

It is assumed that the fluid motion is laminar everywhere. This assumption implies the existence of a unique solution at time t for the fluid velocity and the fluid stress field within V^f.

We first consider a microscopic point **r** within the fluid at time t. The velocity vector can be expressed as

$$\mathbf{v} = \mathbf{v}(\mathbf{r}, t) = v_k(\mathbf{r}, t)\mathbf{i}^k = v(\mathbf{r}, t)\mathbf{e}(\mathbf{r}, t) \tag{3.2-4}$$

where **e** is a unit vector in the direction **v**, and v the magnitude of velocity vector **v**. On multiplying (3.2-4) by $\mathbf{i}^j$ we get

$$v_k \delta_{kj} = v\mathbf{e} . \mathbf{i}^j = v_j \tag{3.2-5}$$

The velocity vector can be written as

$$v_k = v \alpha_k \tag{3.2-6}$$

where

$$\alpha_k = \mathbf{e} . \mathbf{i}^k \tag{3.2-7}$$

The parameters α_k are therefore cosine of angles between the unit vectors **e** and $\mathbf{i}^k$ (see Fig. 3.7), so that

$$\alpha_k = \cos(\mathbf{e}, \mathbf{i}^k) = \cos \delta^k \tag{3.2-8}$$

The velocity vectors as given in Eq.(3.2-6) can therefore be expressed by four quantities which are functions of both space and time. It is important to note that α_k describes the geometry of flow pattern at the microscopic scale, which in turn is of course controlled by the pore structure of the media. If the microscopic streamlines are parallel then α_k = constant. This would correspond to a porous medium composed of straight parallel capillaries.

By substituting Eq. (3.2-6) and (3.2-1) into (3.2-2) we can express it in component form as

$$\rho \frac{\partial}{\partial t}(v \alpha_k) + \rho v \alpha_j (v \alpha_k)_{,j} = t_{jk,j} + \rho f_k \tag{3.2-9}$$

where $(,_j)$ represents the spatial derivative [9].

This can now be expanded further as

$$\rho \frac{\partial}{\partial t}(v \alpha_k) + \rho v v_{,j} \alpha_j \alpha_k + \rho v^2 \alpha_j \alpha_{k,j} = t_{jk,j} + \rho f_k \qquad (3.2\text{-}10)$$

The left hand side of this equation contains all the information required to describe the inertial forces acting on a microscopic fluid element. One of the term includes the square of velocity. The quantity $\alpha_j \alpha_{k,j}$ describes the curvature of the flow paths at a microscopic scale, as will be described in detail below. This quantity disappears if α_k is a constant.

3.2.3 Macroscopic Equations of Flow

To solve the above equations at a microscopic level it is necessary to be able to describe the boundaries (ie pore geometry) mathematically. This is a virtually impossible task. In any case our interest usually lies in a scale much larger than individual pores or grains. To move from microscopic to a macroscopic scale we use an averaging process over a Representative Elementary Volume (REV). Instead of using a spatial point **r** on a microscopic scale, we can now define a spatial point **x** as the centriod of the REV which will contain both phases simultaneously.

For any function $\langle\psi\rangle$, the volume averaged quantity can be expressed as :

$$\langle\psi\rangle \equiv \frac{1}{dV}\int_{dV} \psi\gamma \, dv = \frac{1}{dV}\int_{dV^f} \psi \, dv \qquad (3.2\text{-}11)$$

where γ is a distribution function which is defined [10] as

$$\gamma(\mathbf{r},t) = \begin{cases} 1 & \text{if } \mathbf{r} \text{ is within } dV^f \\ 0 & \text{if } \mathbf{r} \text{ is within } dV^s \end{cases} \qquad (3.2\text{-}12)$$

Using this definition, the porosity of a medium can written as

$$\phi \equiv \frac{dV^f}{dV} = \frac{1}{dV}\int_{dV} \gamma(\mathbf{r},t)\, dv = \phi(\mathbf{x},t) \qquad (3.2\text{-}13)$$

In a similar manner, an average mass density over an REV can be defined as

$$\bar{\rho} = \bar{\rho}(\mathbf{x},t) \equiv \frac{1}{dV}\int_{dV} \rho(\mathbf{r},t)\, \gamma(\mathbf{r},t)\, dv \qquad (3.2\text{-}14)$$

and the macroscopic velocity vector as

$$\bar{\mathbf{v}}(\mathbf{x},t) \equiv \frac{1}{\bar{\rho}\, dV}\int_{dV} \rho(\mathbf{r},t)\, \mathbf{v}(\mathbf{r},t)\, \gamma(\mathbf{r},t)\, dv \qquad (3.2\text{-}15)$$

The macroscopic velocity vector $\mathbf{v}(\mathbf{x},t)$ can be expressed in terms of its magnitude v, and a unit vector **e** pointed in the direction of v as was done for microscopic velocity in Eq.(3.2-4),

$$\bar{\mathbf{v}} = \bar{v}_k \, \mathbf{i}^k = \bar{v} \, \bar{\mathbf{e}} \tag{3.2-16}$$

After multiplying this equation by $\mathbf{i}^j$, we get

$$\bar{v}_k \, \delta_{kj} = \bar{v} \, \bar{\mathbf{e}} \, \mathbf{i}^k = \bar{v} \, \bar{\alpha}_j = \bar{v}_j \tag{3.2-17}$$

where the quantity α_k has been defined as

$$\bar{\alpha}_k \equiv \bar{\mathbf{e}} \cdot \mathbf{i}^k = \cos \bar{\delta}^k \tag{3.2-18}$$

By using Eq. (3.16) and (3.6) we can express the averaged velocity (3.14) as

$$\bar{v} \, \bar{\alpha}_k = \frac{1}{\bar{\rho} \, dV} \int_{dV} \rho \, v \, \alpha_k \, \gamma \, dv = \frac{1}{\bar{\rho} \, dV} \int_{dV^f} \rho \, v \, \alpha_k \, dv \tag{3.2-19}$$

The microscopic velocities at every point **r** may be quite different from the volume averaged macroscopic velocity at point **x**. We could interrelate the two by introducing a deviation velocity vector **v**, where

$$\hat{v}(\mathbf{r},t) \equiv v(\mathbf{r},t) - \bar{v}(\mathbf{x},t) \tag{3.2-19}$$

and similarly

$$\hat{\alpha}_k(\mathbf{r},t) \equiv \alpha_k(\mathbf{r},t) - \bar{\alpha}_k(\mathbf{x},t) \tag{3.2-20}$$

The values of v and α_k are both unique at **r** only for a specific macroscopic point **x** and for a given size of REV. Using the definitions of v and α as given above, one can express (3.2-9) as

$$\begin{aligned}
&\rho \frac{\partial \bar{v}_k}{\partial t} + \rho \, \bar{\alpha}_k \frac{\partial \bar{v}}{\partial t} + \rho \, \bar{v} \frac{\partial \hat{\alpha}_k}{\partial t} + \rho \, \bar{\alpha}_k \frac{\partial \hat{v}}{\partial t} + \hat{v} \, \rho \frac{\partial \bar{\alpha}_k}{\partial t} + \rho \frac{\partial}{\partial t}(\hat{v} \, \hat{\alpha}_k) \\
&+ \rho \, \bar{\alpha}_j \, \bar{v}^2 \, \hat{\alpha}_{k,j} + \rho \, \hat{\alpha}_j \, \bar{v}^2 \, \hat{\alpha}_{k,j} + \rho \, \bar{\alpha}_k \, \bar{\alpha}_j \, \hat{v}_{,j} \, \bar{v} + \rho \, \hat{\alpha}_k \, \bar{\alpha}_j \, \hat{v}_{,j} \, \bar{v} \\
&+ \rho \, \hat{\alpha}_k \, \hat{\alpha}_j \, \hat{v}_{,j} \, \bar{v} + 2 \rho \, \bar{\alpha}_j \, \hat{\alpha}_{k,j} \, \hat{v} \, \bar{v} + 2 \rho \, \hat{\alpha}_j \, \hat{\alpha}_{k,j} \, \hat{v} \, \bar{v} \\
&+ \rho \, \alpha_k \, \alpha_j \, \hat{v} \, \hat{v}_{,j} + \rho \, \alpha_j \, \hat{v}^2 \, \alpha_{k,j} = t_{jk,j} + \rho \, f_k
\end{aligned} \tag{3.2-21}$$

Since v is a function only of **x** and not **r**, therefore all terms multiplied by $v_{,j}$ were removed in deriving (3.2-21). This is the full linear momentum balance equation applicable for the microscopic scale.The left hand side of this equation includes all the inertial force terms which are expressed using the macroscopic quantities v and **e**.

By using the averaging procedure as defined by (3.2-12), we can express (3.2-21) in macroscopic form as

$$\bar{\rho}\frac{\partial \bar{v}_k}{\partial t} + \langle \rho \hat{\alpha}_k \rangle \frac{\partial \bar{v}}{\partial t} + \bar{v}\left\langle \rho \frac{\partial \hat{\alpha}_k}{\partial t} \right\rangle + \hat{\alpha}_k \left\langle \rho \frac{\partial \hat{v}}{\partial t} \right\rangle + \frac{\partial \bar{\alpha}_k}{\partial t} \langle \rho \hat{v} \rangle$$

$$+ \left\langle \rho \frac{\partial}{\partial t} (\hat{v}\, \hat{\alpha}_k) \right\rangle + \bar{v} \langle \rho \hat{\alpha}_{k,j} \rangle \bar{v}_j + \bar{v}^2 \langle \rho \hat{\alpha}_{k,j} \hat{\alpha}_j \rangle$$

$$+ \bar{\alpha}_k \langle \rho \hat{v}_{,j} \rangle \bar{v}_j + \langle \rho \hat{\alpha}_j \hat{v}_{,j} \rangle \bar{v}_k + \langle \rho \hat{\alpha}_k \hat{v}_{,j} \rangle \bar{v}_j$$

$$+ \langle \rho \hat{\alpha}_k \hat{\alpha}_j \hat{v}_{,j} \rangle \bar{v} + 2 \langle \rho \hat{\alpha}_{k,j} \hat{v} \rangle \bar{v}_j + \langle 2 \rho \hat{\alpha}_j \hat{\alpha}_{k,j} \hat{v} \rangle \bar{v}$$

$$+ \langle \rho \alpha_k \alpha_j \hat{v} \hat{v}_{,j} \rangle + \langle \rho \alpha_j \hat{\alpha}_{k,j} \hat{v}^2 \rangle$$

$$= \bar{t}_{jk,j} + \bar{\rho} T_k + \bar{\rho} \bar{f}_k \qquad (3.2\text{-}22)$$

This is the macroscopic version of the linear momentum balance equation and is applicable both for compressible and incompressible fluids. The equation is simplified if we consider the case of incompressible fluids (ie. ρ = constant). We can then write (3.2-22) as

$$\rho \phi \frac{\partial \bar{v}_k}{\partial t} + \langle \rho \hat{\alpha}_{k,j} \hat{\alpha}_j \rangle \bar{v}^2 + \langle \rho \hat{\alpha}_j \hat{v}_{,j} \rangle \bar{v}_k + \langle \rho \hat{\alpha}_k \hat{\alpha}_j \hat{v}_{,j} \rangle \bar{v}$$

$$+ \langle \rho \hat{\alpha}_{k,j} \hat{v} \rangle \bar{v}_j + \langle 2 \rho \hat{\alpha}_j \hat{\alpha}_{k,j} \hat{v} \rangle \bar{v} + \langle \rho \alpha_k \alpha_j \hat{v} \hat{v}_{,j} \rangle$$

$$+ \langle \rho \alpha_j \hat{\alpha}_{k,j} \hat{v}^2 \rangle + \bar{v}_j \bar{v}_k \rho \phi_{,j} = \bar{t}_{jk,j} + \rho \phi T_k + \rho \phi \bar{f}_k \qquad (3.2\text{–}23)$$

where ϕ is the porosity as defined in (3.2-13).

3.2.4 Constitutive Relation

A constitutive equation is the relationship between the stress component and the pressure and velocity gradients. This is normally introduced to reduce the number of unknowns in the equation of motion.

For flow in porous media, the macroscopic fluid stress tensor may be assumed (see eg Hassanizadeh et al [21]) to be of the form

$$\bar{t}_{kj} = -\phi \bar{p} \delta_{kj} + \bar{\lambda} \bar{d}_{jj} \delta_{kj} + 2 \bar{\mu} \bar{d}_{kj} \qquad (3.2\text{–}24)$$

where p is the macroscopic fluid pressure, **d** the rate of fluid deformation, and λ and μ are the macroscopic viscosity coefficients [9]. In Eq.(3.2-22) the macroscopic body force ρT_k arose

because of the presence of the solid phase in the REV which causes fluid resistance to occur. It has been shown by Hassanizadeh et al [21] that this body force is made up of two parts; a reversible and a dissipative part :

$$\bar{\rho}\, T_k = \phi_{,k}\, \bar{p} + R_{kj}\, \bar{v}_j \qquad (3.2\text{–}25)$$

The dissipative part of (3.2-24) arises due to the presence of fluid viscosity. These may be neglected in the present study since they are known to be much smaller than the dissipative part of (3.2-25), and also inertial forces will tend to dominate over the viscous forces at high flow rates.

The microscopic velocity may be related to the macroscopic velocity through a mapping

$$\mathbf{v}(\mathbf{r},t) = \Lambda(\mathbf{r},t) \,.\, \bar{\mathbf{v}}(\mathbf{x},t) \qquad (3.2\text{-}26)$$

The tensor quantity Λ has been shown [10] to be a constitutive (ie. depending only on the geometry of the pore spaces) although for high velocity flow it is expected [19] to be a function of macroscopic and microscopic velocities.

Using Eq. (3.2-6) and (3.2-16) and after multiplication of both sides of (3.2-26) by **e**, we can rewrite it in the form:

$$v = \bar{v}\, \Lambda_{kj}\, \bar{\alpha}_j\, \alpha_k \qquad (3.2\text{–}27)$$

On substituting (3.2-27) into (3.2-19) the equation becomes:

$$\hat{v} = (\Lambda_{kj}\, \bar{\alpha}_j\, \alpha_k - 1)\, \bar{v} \equiv \kappa\, \bar{v} \qquad (3.2\text{–}28)$$

where κ represents the terms within the brackets in (3.2-28) and is a scalar quantity. The microscopic deviation velocity has now been related to the averaged macroscopic velocity.

From the definitions of averaging it can be shown that:

$$\bar{\rho}\, \bar{v}_k = \langle \rho\, v_k \rangle \qquad (3.2\text{–}29)$$

We can therefore write (3.2-28) as:

$$\langle \rho\, v_k \rangle = \langle \rho\, \Lambda_{kj} \rangle \bar{v}_j = \bar{\rho}\, \delta_{kj}\, \bar{v}_j \qquad (3.2\text{–}30)$$

The scalar quantity κ can now be defined as:

$$\kappa \equiv \Lambda_{kj}\, \bar{\alpha}_j\, \alpha_k - 1 \equiv \kappa' - 1 \qquad (3.2\text{–}31)$$

From the conditions given in (3.2-22), the quantity κ must satisfy the relation -

$$\langle \rho\, \kappa\, \alpha_k \rangle = - \langle \rho\, \hat{\alpha}_k \rangle \qquad (3.2\text{–}32)$$

For a porous medium composed of straight parallel capillaries (ie. $\hat{\mathbf{e}} = 0$ and $\mathbf{e} = \bar{\mathbf{e}}$) we would have

$$\langle \rho \kappa \rangle = 0 \qquad (3.2\text{–}33)$$

Besides the condition given in (3.2-30) it is not possible to obtain any more information on the nine components of Λ. Also, any exact value of κ for the general case cannot be determined. An approximate value may be found if a specific geometric model (eg. interconnected random capillaries) was assumed. If the value of κ was considered to be a stochastic variable, then for a given model it would be possible to assume a specific distribution function of κ within dV^f.

3.2.5 A derivation of the Forchheimer equation

Only the case for incompressible fluid is shown here. Compressible fluids could also be treated in a similar manner although requiring slightly more manilpulation. For an incompressible fluid, (ie $\partial\rho/\partial t = \rho_{,j} = 0$), by using Eq.(3.2-28) we can write the macroscopic momentum balance equation (3.2-23) as

$$\phi\rho \frac{\partial \bar{v}_k}{\partial t} + \bar{v}\, \Pi'_{kj}\, \bar{v}_j = -\phi \bar{p}_{,k} + R_{kj}\, \bar{v}_j + \phi\rho \bar{f}_k \qquad (3.2\text{–}34)$$

where

$$\Pi'_{kj} \equiv \Pi_{kj} + \bar{\alpha}_k \phi_{,j}$$

$$\Pi_{kj} \equiv \{ \delta_{kj} \langle \hat{\alpha}_m \kappa_{,m} \rangle + \langle \hat{\alpha}_{k,j} \kappa \rangle + [\langle \hat{\alpha}_{k,m} \hat{\alpha}_m \rangle + \langle \hat{\alpha}_k \hat{\alpha}_m \kappa_{,m} \rangle + \langle \hat{\alpha}_m \hat{\alpha}_{k,m} \kappa \rangle + \langle \alpha_k \alpha_m \kappa \kappa_{,m} \rangle + \langle \alpha_m \hat{\alpha}_{k,m} \kappa^2 \rangle] \bar{\alpha}_j \} \rho \qquad (3.2\text{–}35)$$

Eq. (3.2-34) may now be rewritten in the form:

$$\phi\rho \frac{\partial \bar{v}_k}{\partial t} + \bar{v}\, \Pi'_{kj}\, \bar{v}_j + R'_{kj}\, \bar{v}_j = J_k \qquad (3.2\text{-}36)$$

where

$$R'_{kj} \equiv -R_{kj} \text{ and } J_k \equiv -\phi\, \bar{p}_{,k} + \bar{\rho}\, \bar{f}_k \qquad (3.2\text{–}37)$$

The Forchheimer equation can be derived as a special case of (3.2-36) if it can be assumed the the tensors **R** and Π are isotropic and invertible. If we neglect for the moment the local inertia term, ie the first term of (3.39) we can multiply it by the inverse of **R** ' to obtain -

$$(\bar{v}\, Q'_{kj} + \delta_{kj})\, \bar{v} = K'_{kj}\, J_j \qquad (3.2\text{-}38)$$

where

$$Q'_{kj} \equiv K'_{kn}\ \Pi'_{nj} \tag{3.2-39}$$

$$K'_{kj} \equiv \{R'_{kj}\}^{-1} \tag{3.2-40}$$

Assuming that **K'** can be represented as the product of an isotropic tensorial quantity (permeability) and the fluid viscosity μ, as

$$K'_{kj} = \frac{k'_{kj}}{\mu} \tag{3.2-41}$$

then (3.2-39) may be written as

$$Q'_{kj} = \frac{1}{\mu} k'_{kn}\ \Pi'_{nj} = \frac{1}{\mu} Q_{kj} \tag{3.2-42}$$

If it is also assumed that **Q** is isotropic, ie

$$Q_{kj} = \eta\ \delta_{kj} \tag{3.2.43}$$

we can write (3.2-38) in the form

$$\mu \left(\bar{v}\ \frac{\eta}{\mu} + 1 \right) \bar{v}_k = k'_{kj}\ J_j \tag{3.2-44}$$

Instead of the macroscopic velocity **v**, if we use specific discharge, defined as $\mathbf{q} = \phi\ \bar{\mathbf{v}}$, upon substitution (3.2-44) becomes

$$\mu \left(q\ \frac{\eta}{\phi\ \mu} + 1 \right) q_k = \phi\ k'_{kj}\ J_j \tag{3.2-45}$$

Since the porous medium has been assumed to be isotropic, (ie. tensor **k'** is isotropic), then

$$k'_{kj} = k'\ \delta_{kj} \tag{3.2-46}$$

For the one dimensional case Eq. (3.2-45) can be written as

$$J = a\,q + b\,q^2 \tag{3.2-47}$$

where

$$a = \frac{\mu}{\phi\ k'} \quad \text{and} \quad b = \frac{\eta}{\phi^2 k'} \tag{3.2-48}$$

If the local inertia term was included, we would get

$$J = a\,q + b\,q^2 + \rho\,\phi^2\ \frac{\partial q}{\partial t} \tag{3.2-49}$$

This relation is applicable for unsteady flow situations when local inertia is important. It is generally thought that the effect of local inertia term is very small and can be ignored. However, it has been reported [25] that in certain types of porous media, eg coarse granular media, the local inertia can be significant. It should be noted that the coefficient associated with this term is independent of microscopic flow only when ρ is a constant.

3.2.6 Discussion

Forces due to inertia become important as the macroscopic velocity increases. The inertial forces depend not only on the exact microscopic velocity field but also on the scalar density field for the general case. These two fields in turn depend on (a) the microscopic boundary conditions, ie. the geometry of the pore spaces, (b) macroscopic boundary conditions (over the given dA^{ff}) and (c) the material properties of the fluid.

From Eq. (3.2-23) it can be observed that the origin of inertial forces as observed at a macroscopic scale are due to the following three reasons:

(i) local changes of velocity at a microscopic scale

(ii) curvature of the microscopic streamlines

(iii) the difference in the magnitude of the macroscopic and microscopic velocities ie. $\hat{v} \neq 0$, $\kappa \neq 0$ and also $\nabla \hat{v} \neq 0$, $\nabla \kappa \neq 0$.

Eq. (3.2-36) relates the hydraulic gradient **J** with the macroscopic flow velocity **v**. From the definition of the coefficients Π' of this equation, it can be observed that the exact values can be calculated only if the microscopic velocity field $\mathbf{v} = \mathbf{v}(\mathbf{r}, t)$ is known exactly. This is the coefficient associated with the quadratic velocity term and it expresses the macroscopic inertial forces in terms of the microscopic flow pattern. It is composed of two parts: Π, which is a function of both the microscopic and macroscopic flows and $\bar{e}.\nabla\phi$, where $\nabla\phi$ depends on the spatial variation of the pore spaces.The coefficient Π' contains two terms (see Eq.3.2-35) without the scalar quantity κ, namely $\hat{e}.\nabla\phi$ and $< \hat{e}.\nabla\hat{e} > \bar{e}$. The latter term contains information only about the geometry of the microscopic flow. From the definition of $\hat{e}$ it can be shown that

$$\alpha_j \alpha_{k,j} = \alpha_j \hat{\alpha}_{k,j} = \bar{\alpha}_j \hat{\alpha}_{k,j} + \hat{\alpha}_j \hat{\alpha}_{k,j} \qquad (3.2\text{-}50)$$

It is also possible to show [19] that the curvature magnitude $|s|$ of a streamline curve in three dimensions can be expressed as

$$|s| = (\alpha_j \alpha_{k,j} \alpha_m \alpha_{k,m})^{\frac{1}{2}} \qquad (3.2\text{–}51)$$

A comparision with (3.2-35) reveals that a part of the coefficient Π' is directly related only to the microscopic streamline curvature within the field dV^f. The coefficient Π' is a tensor because the term $< \nabla\hat{e}\,\kappa >$ is a tensor, and also because in general the other five terms of (3.2-35) as well as the gradient $\bar{e}\,\nabla\phi$ will not have a resultant in the direction of $\bar{e}$. Since the configuration of dA^{fs} will be irregular, so it may be expected that all of these vectors will not be colinear with vector $\bar{e}$.

The magnitude of the individual terms of (3.2-35) is quite difficult to estimate and it is not

possible to know whether all the terms containing κ are small compared to the term $< \hat{\mathbf{e}}.\nabla\hat{\mathbf{e}} >$ which is a function only of the pore geometry. It is possible that the terms containing κ could make a significant contribution to the total value of Π', particularly since for a random configuration of the pore spaces the microscopic velocity can change considerably within the region dV^f.

When we consider the definition of the term Π', it is understood that the term is a function of time and space. Considering a macroscopically steady state and unidirectional flow through homogeneous and isotropic pore spaces (ie where $\Pi'_{kl} = \Pi_{kl}$, since $\nabla\phi = 0$), one may be inclined to think that Π is a constant and isotropic. For high velocity fluid flow however, where the flow is not uniform and unidirectional, eg the macroscopic streamlines are curved and possibly change in time, then even for a homogeneous and isotropic porous medium, the term Π will be a function of both space and time. It therefore seems that Π is not a constitutive coefficient, ie does not depend on the geometry of the pore spaces alone. This is because in general it depends on both $\mathbf{e}$ within a REV on the macroscopic flow curvature, and also on κ (ie on v through Λ, see Eq. 3.2-27 and 28). Variations of Π within the space domain may not be only due to possible heterogeneities in the pore geometry at microscopic scale, but also due to possible changes in the macroscopic flow field.

The Eq.(3.2-36) therefore relates the macroscopic dynamic field (pressure) to the macroscopic kinematic field (velocity) in a non-linear and anisotropic fashion. This equation may be considered as the constitutive equation for high velocity fluid flow through porous media. The relation contains two material type of coefficients Π' and $\mathbf{R}$. The coefficient $\mathbf{R}$ may be taken as independent of the macroscopic velocity field and is essentially the viscous resistance. The other coefficient Π' in general should be treated as being a function of the macroscopic velocity field eg. the macroscopic streamline curvature. This is in agreement with the conclusions reached by some [19,26] but directly contradicts most of the past work of others [27,28,29 etc.].

In the previous section, it has been shown that the non-Darcy flow equation (Forchheimer's equation) could be recovered from the macroscopic momentum balance equation assuming isotropy of the tensor quantities. Justification for introducing such assumptions is open to questions. The resistive force due to the presence of viscosity and the macroscopic stress originate in microscopic forces either over dA^{fs} or within dV^f. The macroscopic inertial forces are however different in nature. They have a kinematic origin and are therefore a direct function of the microscopic flow.

Before closure it should be mentioned that there exists a slightly different approach of describing the inertial effect during high rate flow. In this, the velocity term is kept intact which

is in contrast to the present approach where the velocity vector was split into its magnitude and direction (Eqn.3.2-6). This type of method has been used for deriving equations of single and multiphase flow at low as well as high velocities, by Whitaker [10], Slattery [23,24], Gray et al [13,14] and others. With their type of formulation, the final quadratic equation derived becomes much more complicated. It becomes virtually impossible to solve problems even for idealized cases, eg flow in straight parallel capillaries. Yet another approach to quantitative description of the inertial effect involves extension of the the mixture theory [22]. This approach has also been found to lead to similar kind of difficulties.

3.3 CONCLUSIONS

By employing the concept of a microscopic continuum it has been possible to derive the linear momentum balance equation for flow in a porous medium. Using an averaging procedure the microscopic equations were then extended for application to macroscopic volumes. For an incompressible fluid this is the Eq.(3.2-23).

If the dissipative part of the resistive tensor $\mathbf{T}'$ can be taken to be a linear function of the macroscopic fluid velocity, then Eq (3.2-36) may be considered as the generalized non-Darcy flow formula, applicable for high velocity flow. The Forchheimer equation (3.2-47) can then be derived from (3.2-36) as a special case by applying isotropy conditions. The equation provides us with a relationship between the dynamic quantity $\mathbf{J}$ and the kinematic quantity $\mathbf{v}$ by introducing a nonlinear and anisotropic inertial coefficient which may be regarded as a material constant.

The above discussion has shown that the macroscopic inertial forces arising in flow through porous media can be understood fully only if the microscopic flow phenomena is considered. By employing the averaging procedure we have been able to take into consideration at both micro and macroscopic levels the flow phenomena in detail. This has shown that the streamline curvature at the microscopic level play a vital role in the inertial effect which is felt at the macroscopic scale.

REFERENCES

1. Fung, F.C. : *A First Course in Continuum Mechanics,* Prentice Hall, Englewood Cliff, N.J. (1976).
2. Hubbert, M.K. : Darcy's law and the field equations of the flow of underground fluids, *Trans. AIME* (1956) **207**, 222-239.
3. Hubbert, M.K. : The theory of ground water flow, *J. Geol.* (1940) **48**, 785.
4. Whitaker, S. : *Introduction to Fluid Mechanics*, Prentice-Hall, Englewood Cliff, N.J. (1968)
5. Yih, C.S. : *Fluid Mechanics : A Concise Introduction to the Theory*, McGraw Hill, New York (1969).
6. Philip, J.R. : Fluid flow and transport in pores and porous media, Symp. on Circulatory and Respiratory Mass Transport, Trans. Ciba Foundation, (Eds.: G.E.W. Wolstenhome and J. Knight), Churchill Ltd., London (1969) pp.25.
7. Elata, C. and Taskerman, U. : The viscous flow through channels and tubes with sinusoidal boundaries as a model for porous media, *Israel J. Tech.* (1976) **14**, pp. 235-240.
8. Slattery, J.C. : *Momentum, Energy and Mass Transfer in Continua,* McGraw Hill Book Co., New York (1972)
9. Aris, R. : *Vectors, Tensors and the Basic Equations of Fluid Mechnacis*, Prentice-Hall, Englewood Cliffs, N.J. (1962).
10. Whitaker, S. : Advances in the theory of fluid motion in porous media, *Ind. Eng. Chem.*, (1969) **61**(12), 14-28.
11. Bear, J. : *Dynamics of Fluids in Porous Media*, Elsevier, New York (1972).
12. Bachmat, Y. : Spatial macroscopization of processes in heterogeneous systems, *Israel J. Tech.* (1972) **10**, 391.
13. Gray, W.G. and Lee, P.C.Y. : On the theorems of local volume averaging of multiphase systems, *Int. J. Multiphase Flow* (1977) **3**, 333-340.
14. Gray, W.G. and O'Neill, K. : On the general equations for flow in porous media and their reduction to Darcy's law, *Water Resour. Res.* (1976) **12**, 148-154.
15. Archer, J.S. : Reservoir volumetrics and recovery factors, in *Developements in Petroleum Engineering* (Eds.: R.A. Dawe and D.C. Wilson), Academic Press, London (1986) Chap. 2, p. 11-41.
16. Archer, J.S. : Reservoir definition and characterization for analysis and simulation, Proc. Eleventh World Petroleum Congress, J. Wiley & Sons, London (1984) Vol. 3, p.65.
17. Haldorsen, H.H. : Simulator parameter assignment and the problem of scale in reservoir engineering, in *Reservoir Characterization* (Eds.: L.W. Lake and H.B. Carroll), Academic Press, London (1986) pp.293-340.
18. Baudet, C., Charlaix, E., Clement, E., Gyron, E., Hulin, F.P. and Leroy, C. : Scaling

concepts in porous media, in *Scaling Phenomena in Disordered Systems,* (R. Pynn & A. Skjeltorp, Eds.) Plenum Press, N.Y. (1985) p.399-422.

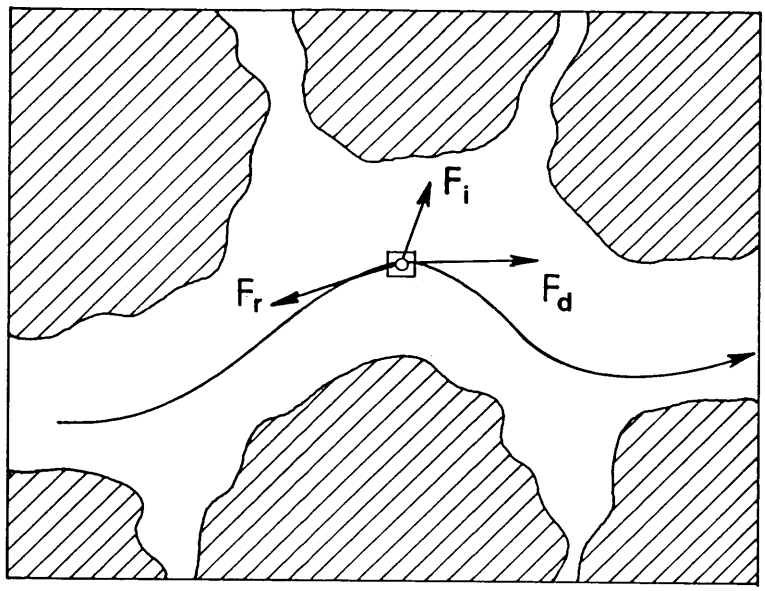
19. Cvetkovic, V.D.: A continuum approach to high velocity flow in a porous medium, *Transport in Porous Media* (1986) **1**, 63-97.
20. Stokes, J. : Field equations for flow through porous media and their relation to the microstructure, PhD thesis (unpublished), Dept. of Mechanics, Royal Institute of Technology, Stockholm (1983).

21(a) Hassanizadeh, M. and Gray, W.G. : General conservation equations for multiphase system, Part 1: Averaging procedure, *Adv. Water Resour* (1979) **2**, 131-144.

21(b) Hassanizadeh, M. and Gray, W.G. : General conservation equations for multiphase system, Part 2: Mass, momenta, energy and entropy equations, *Adv. Water Resour.* (1979) **2**, 191-203.

21(c) Hassanizadeh, M. and Gray, W.G. : General conservation equations for multiphase system, Part 3: Constitutive theory for porous media flow, *Adv. Water Resour.* (1980) **3**, 25-40

22. Bedford, A. and Ingram, J.D.: A continuum theory of fluid saturated porous media, *J. Appl. Mech.* (1971) **38**, 1-7.
23. Slattery, J.C.: Flow of visco-elastic fluids through porous media, *A.I.Ch.E.J.* (1967) **13**, pp. 1066.
24. Slattery, J.C. : Single-phase flow through porous media, *A.I.Ch.E.J.* (1969) **15**, 866.
25. Hannoura, A.A. and Barends, F.B.J. : Non-Darcy flow: State of the art, Proc. Euromech 143, Delft (1981) pp. 37-51.
26. Barak, A.Z. and Bear, J. : Flow at high Reynolds numbers through anistropic porous media, *Adv. Water Resour.* (1981) **4**, 54-66.
27. Irmay, S. : On the theoretical derivation of Darcys and Forchheimer formulas, *J. Geophys. Res.* (1958) **39**, 702-707.
28. Ahmed, N. and Sunada, D.K. : Nonlinear flow in porous media, *J. Hydrau. Div.* ASCE, (1969) **95**, 1847- 1857.
29. Bachmat, Y. : Basic transport coefficients as aquifer characteristics, IASH Symp. on Hydrology of Fractured Rocks, Dubrovnik (Oct. 1965) 63-75.
30. Whitaker, S. : The equations of motion in porous media, *Chem. Eng Sci.* (1973) **28**, pp. 139.



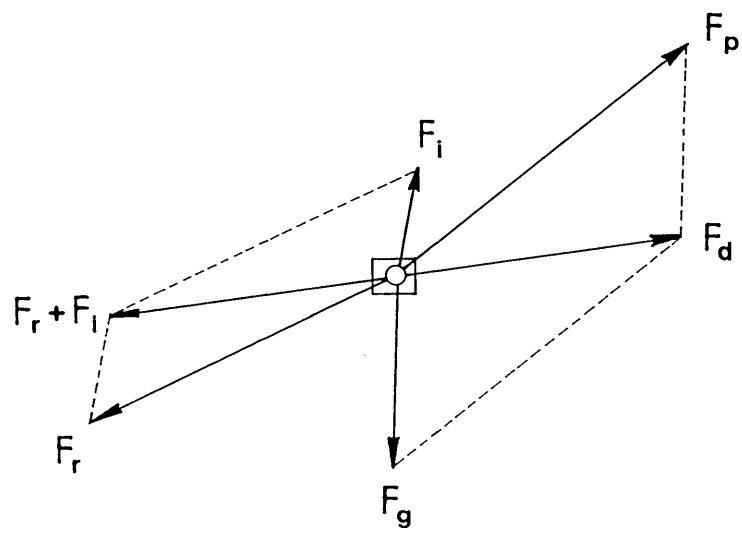


Fig. 3.1 Resolution of forces acting on a microscopic element of fluid during flow through a porous medium.

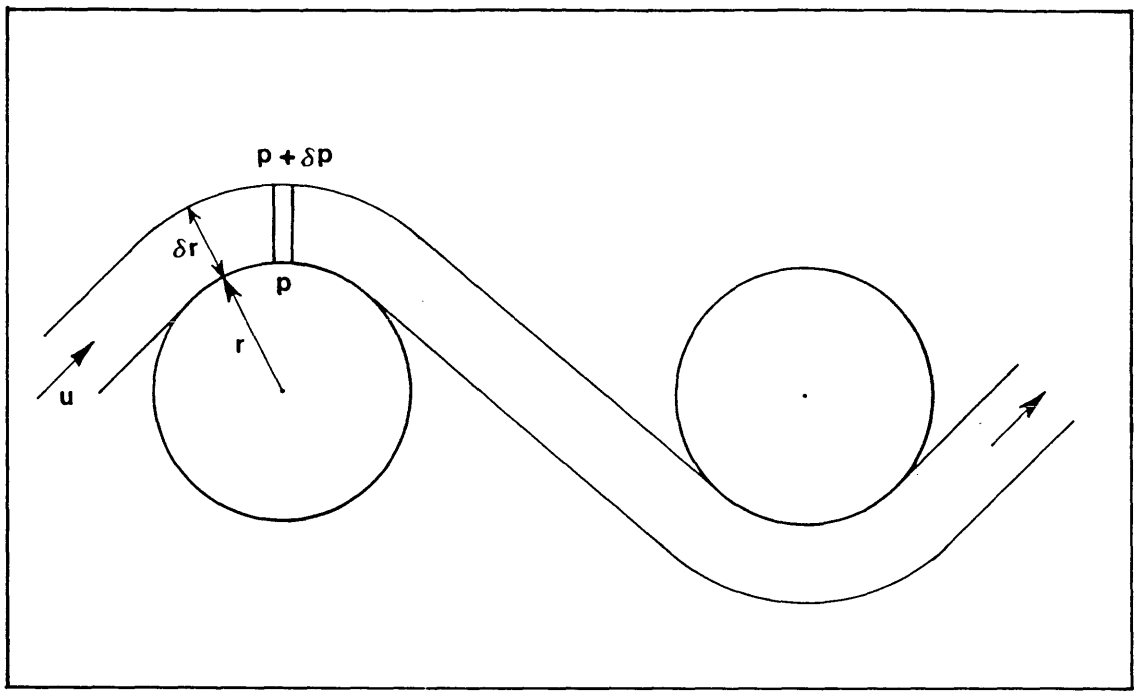


Fig. 3.2 Pressure variation across a curved streamtube.

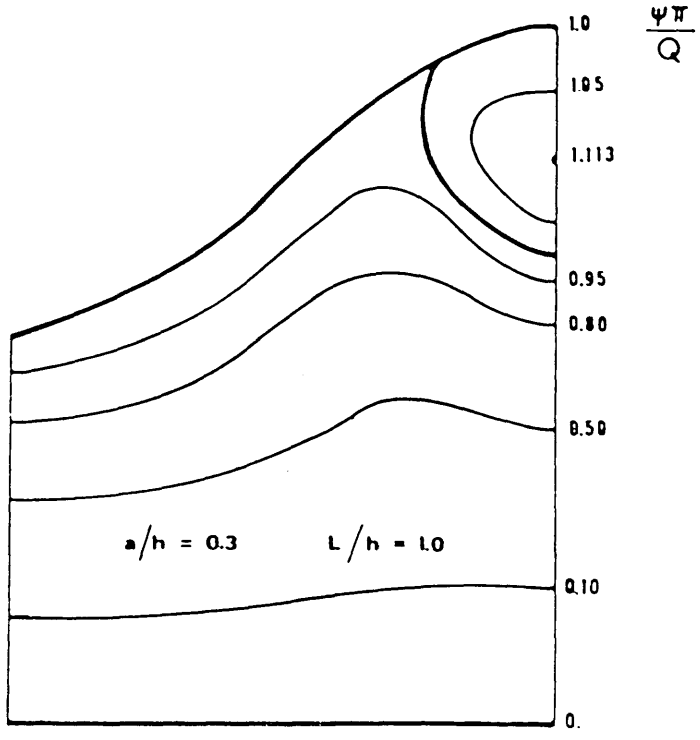


Fig 3.3 Diagram showing streamlines and secondary flow in a sinusoidal capillary model of a pore space (ref. 7).

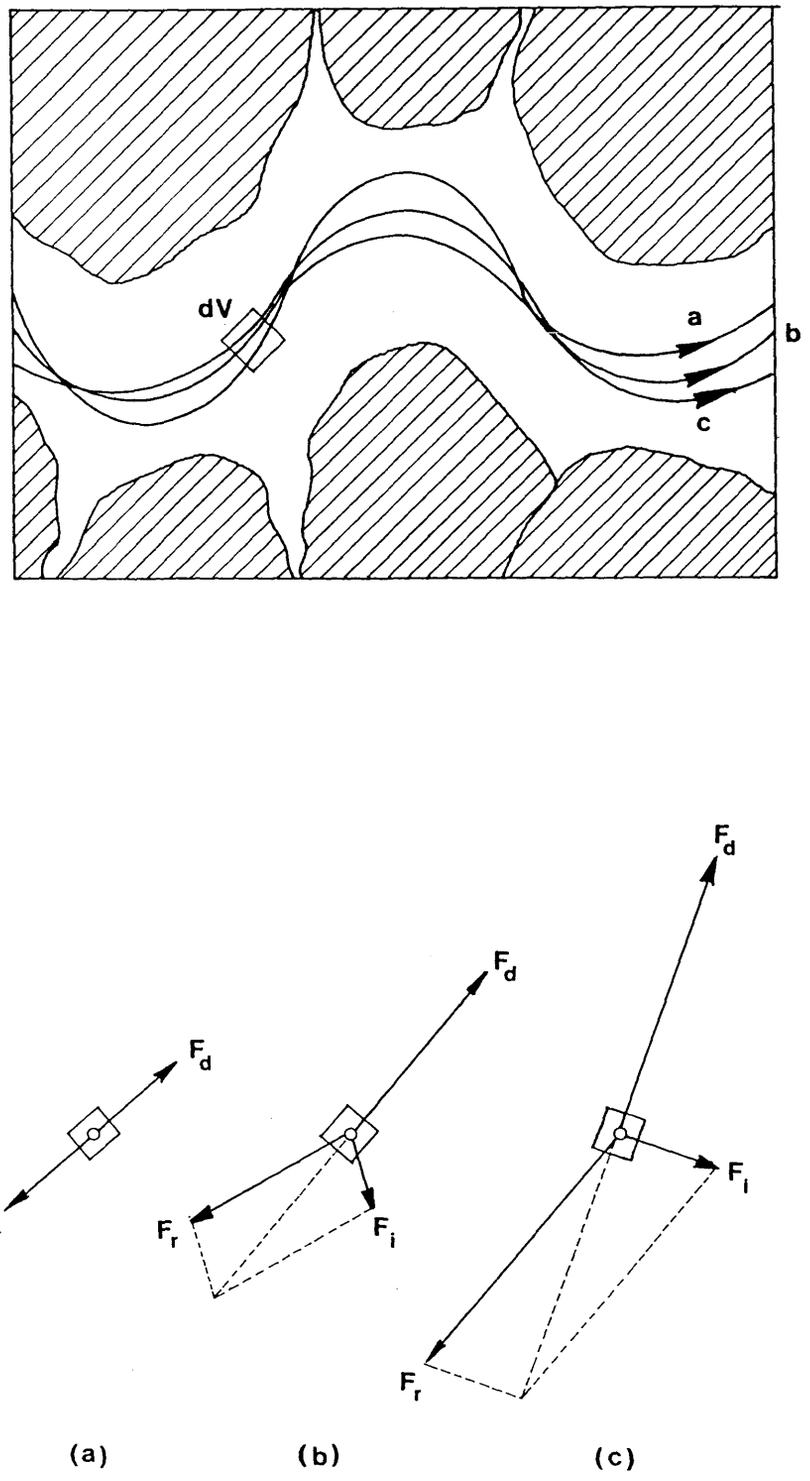


Fig. 3.4 Schematic representation of the distortion of streamlines caused by the increasing flow rate, and the corresponding force balances on a volume element dV. Darcy's law would be valid only for the first case

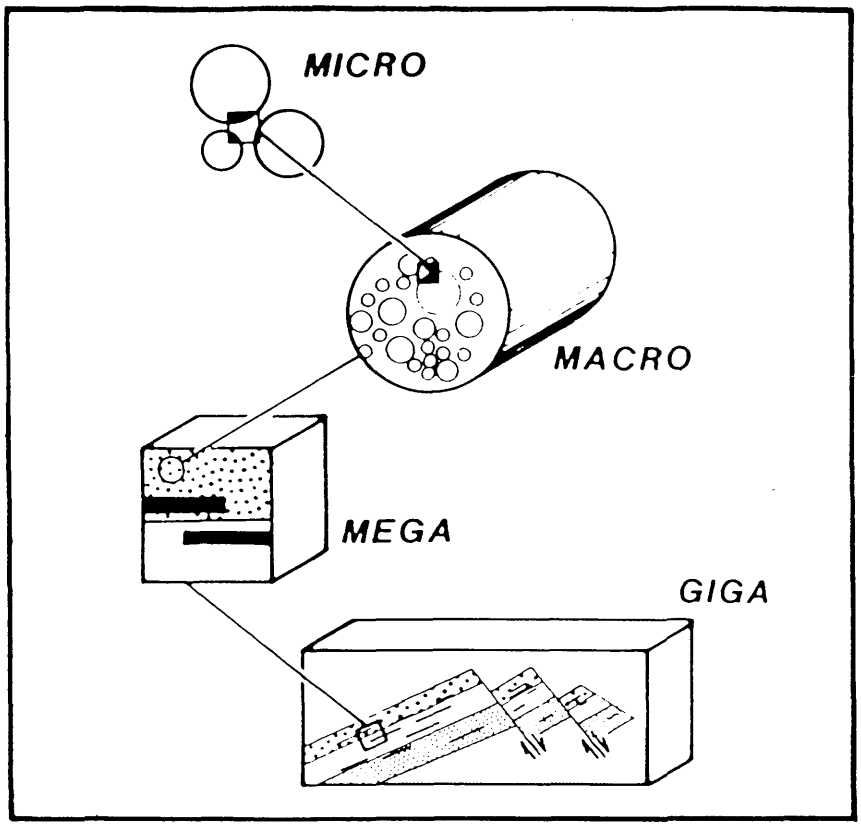


Fig. 3.5 Four different scales of observation of sedimentary rocks (ref.17)

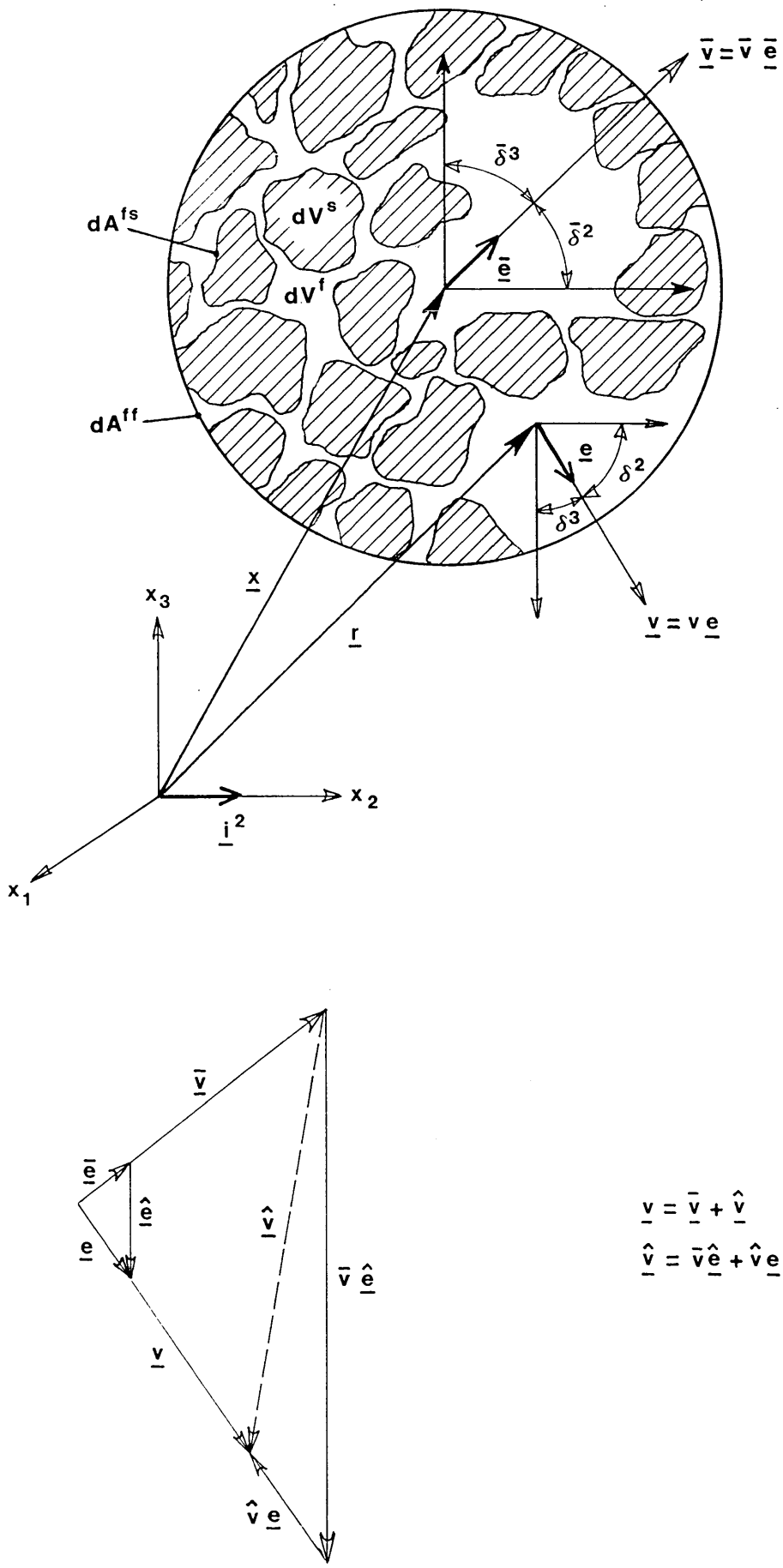


Fig. 3.6 Diagram showing a representative elementary volume (REV) and the relationship of the deviating vectors to their volume averaged values (modified after ref.19)

Chapter 4

EXPERIMENTAL MEASUREMENTS

This chapter outlines the methods employed to measure four important parameters of a rock sample, namely its porosity, permeability, inertial coefficient and capillary pressure. Errors and uncertainites associated with the measurement of these parameters will be discussed. General review of the various techniques employed for routine and special core analysis can be found in the literature [1-3].

4.1 POROSITY MEASUREMENT

4.1.1 Introduction

Porosity is defined as the ratio of pore volume to the bulk volume of a material. Porosity can either be total or effective. Total porosity is defined as the ratio of the volume of all the pores to the bulk volume whereas effective porosity is defined as the ratio of the interconnected pore volume to the bulk of the material.

Porosity in sands and sandstones varies primarily with grain size distribution and grain shape, packing arrangement, cementation and clay content. Environmental and depositional factors influence porosity as well as permeability. In a producing consolidated sandstone reservoir, increasing porosity is generally associated with increasing permeability. The relationship varies with formation and rock type, and reflects the variety of pore geometry present.

Existence of porosity in a sedimentary rock is the single most important property required for a hydrocarbon reservoir. Its accurate measurement is also therefore essential. A number of methods are available for the measurement of this parameter [1]. For the purpose of the present work a Boyle's law helium gas expansion porosimeter [4] was used. In this method helium gas is used since it has one of the smallest atoms found in nature and can therefore fill the pore spaces of any rock sample in the shortest possible time. The adsorption of this gas is also said to be minimal compared to air. The main advantages and disadvantages of this method [2] are as follows :

Advantages :

i) Accurate

ii) Fairly rapid for majority of the samples encountered, and

iii) Samples can be used for further testing.

Disadvantages :

i) Slow for low permeability rocks

ii) Preparation of sample is important

iii) Drying technique is critical especially if hydratable minerals are present.
iv) Measurement of bulk volume is critical in the determination of grain volume.
v) Adsorption of gas on the surface of the rock may give erroneously high value.

4.1.2 Sample preparation

Samples or plugs to be used for porosity and permeability tests have to be thoroughly extracted of oil and brine which may be present, and then properly dried. The Soxhlet refluxing solvent extractor [5] was used for this purpose. The solvent used depends on the nature of the problem but toluene was used and in some cases was followed by methanol. The refluxing operation was carried out for a period of 8 hours or longer until the colour of the distillate was found not to be changing, thus indicating that any residual oil or mud inside the core sample had been washed out.

The drying of the sample after the extraction is important especially when hydratable minerals are present. The drying procedure is important because the interstitial water needs to be removed with no alteration of the minerals. Ideally, humidity controlled ovens should be used to maintain the proper state of hydration. Since these were not available, the cores were oven-dried at about 45°C for 8 hours and then stored in a desiccator.

To determine porosity of a material it is necessary to measure at least two of the three following variables : bulk volume, grain volume and pore volume. All three could be measured to provide a cross check. The methods used for measurement of the first two quantites are described below.

4.1.3 Grain Volume Determination

Use is made of the Boyles law helium gas expansion porosimeter. The method basically relies on an isothermal expansion of gas following the ideal gas law PV = constant. A schematic arrangement of the apparatus is shown in Fig 4.1. One of the chamber is charged up to a pressure of P_1 and the other chamber, filled with dummy cores (steel cylinders) of approximately the same size as the actual core samples, is kept at atmospheric pressure. The gas in the first chamber is then expanded and the equilibrium pressure monitored. The procedure is repeated, this time with the real core plug in place of the dummy one. By comparision of the gas pressure obtained by expansion from the reference volume when the actual sample is present to that obtained in a duplicate determination with the dummy plugs, the volume of the solid framework of the sample may be calculated.

The actual procedure and calculation can be carried out in two different ways. The first

method was devised during the course of this work and the other method is as recommended by the manufacturers - Robertson Research [4]. Both the methods use the same principle but there are some differences in the actual measurement procedure. Both of these methods were used and were found to give almost identical results.

METHOD 1

Using Boyle's law,

$$P_1V_R + P_2V_B = P_3(V_A+V_B)$$

Since P_2 is at atmospheric pressure, the gauge pressure is zero. Hence

$$P_1V_R = P_3(V_A+V_B) \qquad (4.1\text{-}1)$$

The dummy plug is removed and the pressure in the reference chamber is brought back to P_1 and then allowed to expand.

$$P_1V_R = P_4(V_R+V_B+V_S) \qquad (4.1\text{-}2)$$

The procedure is repeated with the core plug in place.

$$P_1V_R = P_5(V_R+V_B+V_S-V_G) \qquad (4.1\text{-}3)$$

where :

P_1 = initial pressure at each step

P_2 = atmospheric pressure

P_3 = equilibrium pressure with the dummy plug in place

P_4 = equilibrium pressure with the chamber empty

P_5 = equilibrium pressure with the chamber containing core plug

V_R = reference volume

V_B = volume of the system

V_S = volume of the steel blanks (dummy cores)

V_G = grain volume

From Eqn.(4.1-1)

$$V_B = \frac{V_R(P_1 - P_3)}{P_3} \qquad (4.1\text{-}4)$$

From Eqn.(4.1-2)

$$V_B = \frac{V_R(P_1 - P_4)}{P_4} - V_S \qquad (4.1\text{-}5)$$

From Eqn.(4.1-3)

$$V_G = V_B + V_S - \frac{V_R(P_1 - P_5)}{P_5} \qquad (4.1\text{-}6)$$

Since (4.1-4) and (4.1-5) are the same, we get

$$V_R = \frac{P_3 P_4 V_S}{P_1 (P_3 - P_4)} \qquad (4.1\text{-}7)$$

Substituting (4.1-7) into (4.1-4) we get,

$$V_B = \frac{P_4 V_S (P_1 - P_3)}{P_1 (P_3 - P_4)} \qquad (4.1\text{-}8)$$

Finally substituting (4.1-7) and (4.1-8) into (4.1-6), we get

$$V_G = \frac{P_4 V_S (P_1 - P_3)}{P_1 (P_3 - P_4)} + V_S - \frac{P_3 P_4 V_S (P_1 - P_5)}{P_1 P_5 (P_3 - P_4)} \qquad (4.1\text{-}9)$$

Simplification of Eqn.(4.1-9) yields

$$V_G = \frac{P_3 V_S (P_5 - P_4)}{P_5 (P_3 - P_4)} \qquad (4.1\text{-}10)$$

In Eqn.(4.1-10) the value of V_S (volume of the dummy plugs) as well as all the pressures can be measured, hence the grain volume, V_G, determined.

METHOD 2

Using Boyle's law

$$P_1 V_R + P_2 V_1 = P_3 (V_R + V_1) \qquad (4.1\text{-}11)$$

where:

P_1 = reference pressure

V_R = reference volume

P_2 = pressure in the unknown volume

V_1 = unknown volume

P_3 = resultant equilibrium pressure

P_2 is at atmospheric pressure (0 psig).

Eqn.(4.1-11) therefore becomes

$$(P_1 + B) V_R + B V_1 = (P_3 + B) (V_R + V) \qquad (4.1\text{-}12)$$

where B is the barometric pressure. Also

$$P_3 V_1 = V_R (P_1 - P_3)$$

which can be rewritten as

$$V_1 = V_R [P_1/P_3 - 1] \qquad (4.1\text{-}13)$$

Similarly, upon expansion with the dummy pieces taken out, we get

$$V_2 = V_R [P_1/P_3 - 1] \qquad (4.1\text{-}14)$$

and with the core plug in place,

$$V_3 = V_R [P_1/P_3 - 1] \quad (4.1\text{-}15)$$

The ratio $[P_1/P_3 - 1]$ in Eqns. 4.1-13, 14 and 15 are denoted by R_1, R_2 and R_3 respectively. Then, the dummy pieces would be given by

$$V_2 - V_1 = \text{dummy volume} = V_R (R_2 - R_1)$$

Since the dummy volume is already known, then V_R can be found from

$$V_R = \frac{\text{vol. of dummy pieces}}{R_2 - R_1}$$

The grain volume V_g is given by $V_2 - V_3$. So that

$$V_g = V_R (R_2 - R_3) \quad (4.1\text{-}16)$$

Since all the parameters on the right hand side of Eqn.16 can be found experimentally, hence the grain volume can be calculated from this equation.

4.1.4 Bulk Volume Determination

Having determined the grain volume, it is necessary to measure either the bulk volume or the pore volume to be able to estimate the porosity. The pore volume could be determined, for example, by saturating the core in a non-reacting fluid and weighing. Here a method for the determination of bulk volume is described. For a perfectly cylindrical core plug with sharp edges, the dimensions could be measured directly with a caliper and the bulk volume calculated. However this is not possible for plugs with very rounded edges. The usual procedure in this sort of situations is to measure the bulk volume of the plug by volumetric displacement of mercury using an instrument called "pycnometer". The schematic arrangement of the apparatus is shown in Fig. 4.2.

The core plug is held submerged under mercury by pointed needles attached to the lid of the chamber. The mercury displaced by the volume of the core plug can be read off from the tube attached to the chamber. The tube has to be calibrated accurately by submerging pieces of steel blanks, the volumes of which are already known precisely.

It is known [6] that the largest error in porosity measurements occur in the bulk volume measurement which are affected by the way the samples are oriented in the pycnometer chamber. Some other problems associated with this form of bulk volume measurement are :

(i) There is a possibility of some mercury entering the sample, particularly if the sample has high permeability. The presence of this mercury in the sample will cause errors in any saturation measurement and will also create problems for any resistivity measurement. In order to avoid mercury penetrating it is necessary to keep the depth to which the sample is submerged to a minimum.

(ii) Due to the high surface tension, mercury does not spread smoothly over the surface of the core plug. Quite often air bubbles can be found between the plug and the wall of the container.

(iii) It is essential to have a fine capillary to be able to make accurate measurements. This however means that core plugs of very different sizes cannot be accomodated to give readings within the range of the scale. It is also quite difficult to take meaasurements from an inclined tube since the meniscus is usually not distinct.

(iv) It is assumed that there is no loss of mercury from the container during the calibration or subsequent measurements. This is not completely true since it is usually found that minute globules of mercury stick to the surface of the plugs and have to be brushed off. For a large number of measurements calibration may have to be performed more than once.

TABLE 4.1
Comparision of porosity measurements

	Porosity %	
Sample	Method 1	Method 2
LE249	15.26	15.09
LE253	7.43	7.43
LE718	6.83	6.84
LE728	11.39	11.38
RH94	12.18	12.17
RH97	16.91	16.93
RH100	8.70	8.68
RH101	5.92	5.82
RH103	10.00	9.92

4.1.5 Discussion

The two methods described above were both used to determine the porosity of some core samples. The results are shown in Table 4.1. The full set of experimental data are presented in Table 4.3. A small number of samples were chosen from the full set since they cover a wide range of porosity distribution. A comparision between the two methods show that they both give virtually the same result. In some cases they agree upto two decimal places, the largest difference being less than 2%. Method 1 is however slightly more difficult to perform experimentally since the initial

pressure P_1 has to be set at exactly the same value each time requiring fine adjustments of the pressure regulators. The second method makes use of the ratio of the pressures of the charged chamber before and after expansion. As such the exact value of the initial pressure is not so vital. The second method was therefore used for most of the measurements because of the simplicity of operation.

It should be noted that both method assumes that the expansion of gas takes place isothermally and that the whole system is at a thermal equilibrium. Corrections for expansion/contraction of the pipes, etc. could be incorporated but these are so small [3] that they were neglected.

Error analysis of the results has shown that porosity measurements could be carried out with a precision of $\pm$ 3 % .

4.2 PERMEABILITY MEASUREMENT

4.2.1 Theory

It was widely known that during flow of gas through a capillary the gas molecules suffer from "slippage' as the mean free-path of the molecules approach the dimensions of the flow conduit. This concept was later extended for porous media and is now popularly known as the 'Klinkenberg effect'. From considerations of gas flow through straight capillaries of radius r, Klinkenberg [7] showed that the permeability of gas could be expressed as

$$k_a = k_1 \left(1 + \frac{4 c \lambda}{r} \right) \qquad (4.2\text{-}1)$$

where

k_a = apparant permeability

c = a constant (= 1)

λ = mean free path of molecular motion, and

k_1 = is the permeability which would be obtained from flow of liquid not suffering from any molecular slippage.

Since λ, the mean free path, is inversely proportional to P and r is fixed for a medium, Eqn. (4.2-1) could be rewritten as

$$k_a = k_1 (1 + b / P_m) \qquad (4.2\text{-}2)$$

where P_m = mean pressure $\{ (P_1+P_2) / 2 \}$

b = a constant

It has been shown [8,9] that the constant b is related to the absolute permeability k_l. This is to be expected since the factor b is dependent on c / r where r represents a length parameter characterising the porous medium.

Eq.(4.2-2) shows that if the apparant gas permeability k_a is plotted against the inverse of mean pressure, a straight line can be obtained, the intercept of which will give the true permeability. The intercept is esentially an extrapolation of the apparant permeabilities to an infinite mean pressure. At very high pressures the permeability to gas is indeed found to be equal to the permeability to liquid. Klinkenberg effects are found to be particularly significant for cores of low permeability. The inverse relationship between apparent permeability and mean pressure predicted by Klinkenberg hold for small values of mean pressure. It is interesting to note that in his experiments, Klinkenberg did not exceed a pressure gradient of 0.05 atm, which is very small.

4.2.2 Calculation

Air was injected through the core plugs at a wide range of flow rate for measurements of permeability and the inertial coefficients. Both these parameters could be measured from the same set of measurement. The maximum flow rate possible was always restricted by the upstream pressure transducer which was capable of measuring only up to about 100 psi. This was however found to be adequate for most of the rock samples. A schematic arrangement of the core holder and ancilliary equipments are shown in Fig 4.3.

Calculation of permeability using the Klinkenberg method requires that the apparant gas permeability be calculated directly from Darcy's law, which may be written as

$$q = -\frac{k A}{\mu} \frac{dP}{dL} \qquad (4.2\text{-}3)$$

For flow of gases, since the volumetric flow rate q varies with pressure, it is therefore necessary to use and integrated form of Eq.(4.2-2), or alternatively an average value of q must be used. If the average pressure is used, the volume at mean pressure has to be converted to volume Q measured at 1 atmosphere :

$$Q = q \frac{P_1 + P_2}{2 P_b} \qquad (4.2\text{-}4)$$

where P_b is the base pressure (abs. atm.) and Q is in cc/sec.

Substituting Eq.4.2-4 into 3, we get

$$Q = \frac{k A}{2 \mu L P_b} (P_1^2 - P_2^2) \qquad (4.2\text{-}5)$$

or

$$k = \frac{2000\, Q\, L\, \mu\, P_b}{A\,(P_1^2 - P_2^2)} \quad \text{(md)} \qquad (4.2\text{-}6)$$

Eq.(4.2-6) was used for calculating the apparant permeabilities and then used in the Klinkenberg plots according to Eq.(4.2-2) for calculating the true permeability of the sample.

To perform a run, a clean core plug was placed in the Hassler core holder (Fig. 4.3) and an overburden (sleeve) pressure of 250psi imposed on it. The core plugs were stored in a desiccator for at least 48 hours prior to the start of the run.The ambient atmospheric pressure was recorded from a mercury barometer for use in Eq.(4.2-6) and for calibration of the pressure transducers. The flow valves were opened very gently and the upstream pressure increased until a flow rate of around 2-3 cc/min could be achieved. For very tight core samples it was often necessary to wait for some 3-4 minutes to ensure that a steady state had been reached. In all cases at least two pore volumes were flowed through the core to be certain that the pressure had stablised. The upstream pressure was increased at various increments, often until a maximum of 100psi - which was the upper limit of the transducer, and the flow rates monitored simultaneously.

4.2.3 Discussion

It is important to be aware of the interrelationship between slippage effects and inertial effects for experimental measurements. As a result of slippage, the apparant permeability becomes more than the true value, whereas inertial effect results it to be less. Slippage is reduced if the mean free path is decreased, which can be caused by increasing the gas density (ie by increasing the pressure). Thus, as the pressure gradient across the core becomes larger, slippage is reduced and inertial effect is increased. It is to be expected that there will be a range of flow rate (and pressure gradient) where molecular slippage and inertial effects will coexist. In this transitional range it is likely that in some pore spaces, slippage will be dominant, and in others the inertial effect, since there is a wide spectrum of pore sizes and shapes in a porous medium.

It is generally observed that at increasing flow rate, the curve in the Klinkenberg plots (see Fig 4.4) tend to dip downwards. This is because of the presence of turbulence / inertial effect which reduces the permeability at high rates [10]. To get a sufficiently wide spread of data points for drawing a straight line it was sometimes found to be necessary to impose some back pressure in the flow system using valves situated in the downstream side of the core holder.

From Eqn. 4.2-5 or 6 it is obvious that for Darcy's law to remain valid, a plot of QP_b / A against $(P_1^2 - P_2^2) / 2L$ would give a straight line passing through the origin. The slope of the line should be equal to k / μ from which the permeability could be calculated. In practice, deviation from a straight line is normally observed which reflects the change in the nature of flow from purely viscous to inertia dominated flow. Typical plots of ΔP^2 vs. Q are shown in Chapter 5 along with further discussion.

4.2.4 Unsteady-State Method

All the measurements reported in this thesis were obtained using the steady state method, ie the values of flow rate and pressure gradients were taken after they had stablised and no further changes could be observed with time. An alternative technique, known as the unsteady - state method, has gained popularity in recent years.

Construction and use of a number of different unsteady-state permeameters have been reported [11] since the early 1950's, but these required empirical correlations using cores of known permeability for preparation of calibration curves. Jones [12] was probably the first to construct an unsteady-state permeameter for routine core analysis which was capable of measuring the Klinkenberg permeability and the inertial coefficient directly from a single run.

The equipment for the unsteady-state method essentially consists of a tank of pressurised gas and a pressure transducer, both of which are connected to a Hassler core holder and are separated by a quick opening valve. To perform a run, the tank is charged to a high pressure and then the valve opened. The pressure is monitored as the gas flows through the core, rapidly at first and then slowly. The theory for analysing the decline in pressure with time has been given by Jones [12].

It has been claimed [13] that the unsteady state method is capable of reproducing the results obtained by the steady state method with an error of less than 5%. One advantage of this method is that only the pressure needs to be monitored, which can of course be done with greater convenience and accuracy than flow rate measurements. Another advantage in its favour is that the method is much faster than the conventional technique, this being quite important for low permeability rocks for which it is necessary to wait for many minutes before a steady state is reached. This method has therefore gained popularity for permeability measurements of tight gas sands [14,15].

4.3 INERTIAL COEFFICIENT MEASUREMENT

4.3.1 Theory

The coefficient of inertial resistance β is defined by the Forchheimer equation which may be expressed as

$$-\frac{dP}{dL} = \frac{\mu}{k} v + \beta \rho v^2 \qquad (4.3\text{-}1)$$

Here v is the Darcy velocity, ie volumetric flow rate / cross sectional area. For high velocity liquid flow, the coefficient β could be found from Eq.(4.3-1) directly if it is rearranged in the form :

$$-\frac{1}{\rho v}\frac{dP}{dL} = \frac{\mu}{\rho k} + \beta v \qquad (4.3\text{-}2)$$

A plot of the left hand side against velocity would yield a straight line with β as the gradient of the slope. During flow of a compressible fluid, eg gas, the fluid would expand in volume with decrease in pressure and would consequently accelerate along the direction of the pressure gradient. The mass flow rate, W, however remains constant along any cross section, and can therefore be used in place of velocity

$$W = \rho v A \qquad (4.3\text{-}3)$$

Upon substitution, Eq.(4.3-2) becomes

$$-\rho\frac{dP}{dL} = \frac{\rho \mu v}{k} + \beta \rho^2 v^2$$

$$= \frac{\mu W}{kA} + \beta (W/A)^2 \qquad (4.3\text{-}4)$$

Since ρ = MP/ ZRT, Eq.(4.3-4) can be written [16] in an integrated form as :

$$-\frac{M}{ZRT}\int_1^2 P\,dP = \left[\frac{\mu W}{kA} + \beta (W/A)^2\right]\int_1^2 dL \qquad (4.3\text{-}5)$$

Integration of this equation between the limits will give

$$\frac{M(P_1^2 - P_2^2)}{2ZRT\mu L(W/A)} = \frac{W}{A\mu}\beta + \frac{1}{k} \qquad (4.3\text{-}6)$$

where:

k = permeability, Darcy (cm^2)

M = molecular weight, gm/ gm-mole

Z = compressibility factor, (dimensionless)

R = gas constant, cm^3 atm / gm-mole K

T = temperature of measurement, °C

W = mass flow rate, gm / sec

A = cross sectional area, cm^2

P_1 = upstream pressure, atm

P_2 = downstream pressure, atm

L = length of core sample, cm

μ = viscosity of gas at mean pressure, cp

β = inertial coefficient, atm-sec^2 / gm

4.3.2 Calculations

Eq.(4.3-6) forms the basis of calculating the inertial coefficient β. If it is assumed that the flow is isothermal, and that for a small pressure drop the compressibility factor is constant, then a plot of the left hand side of Eq.(4.3-6) against $W/A\mu$ will result in a straight line having :

gradient $m = \beta$ (atm-sec^2/ gm)

intercept $c = 1/k$ (darcy $^{-1}$)

It should be noted that 1 atm-sec^2/gm = 1.01325×10^6 cm^{-1}, so that if β is expressed in terms of cm^{-1}, then

$\beta = m \times 1.013420 \times 10^6$ cm^{-1}

In field units, this becomes

$\beta = m \times 2.54 \times 12 \times 10^6$ ft^{-1}

and the intercept

$k = 1000 / c$ (md)

For the purpose of calculations, the mass flow rate W was calculated from the volumetric flow rate Q and the density ρ at mean pressure :

$$W = \rho Q \quad \text{gm/s} \tag{4.3-7}$$

The density ρ was determined from the ideal gas equation

$$\rho = \frac{(P_1 + P_2)\,M}{2\,Z\,R\,T} \quad gm/cc \qquad (4.3\text{-}8)$$

A typical plot according to Eq.(4.3-6) is shown in Fig. 4.5, where the downward warp at low flow rate is caused by the slippage effect.

Calculation of Viscosity of Air

The viscosity of air is strongly dependent on temperature and very weakly dependent on the pressure. As such the pressure effect can be neglected since the experimental measurements were all carried out at pressures not too far from atmospheric. The viscosity of air was calculated from a relation given by Steil et al [17] as follows

$$\mu = \frac{34.0 \times 10^{-5}}{\xi} T_r^{0.94} \qquad \text{for } T_r < 1.5$$

$$\mu = \frac{17.78 \times 10^{-5}}{\xi} (4.58\,T_r - 1.67)^{0.625} \qquad \text{for } T_r > 1.5$$

$$\xi = T_c^{0.167}\, M^{-0.5}\, P_c^{-0.667}$$

where :

ξ = viscosity parameter (defined above)

μ = dynamic viscosity (cp)

T_c = critical temperature (132 K)

P_c = critical pressure (37.207 atm)

M = molecular weight (28.97)

T_r = reduced temperature (T / T_c)

Gas Compressibility Factor

For most purposes a value of 1.0 would have been sufficient since the working pressures were not too high. However, for more accurate calculations, the following relations [18] were used :

For P > 4.935 atm

$Z = 0.9998 + 1.379 \times 10^{-5} (0.9869 - P)$

For P < 4.935 atm

$Z = 0.999 + 9.65 \times 10^{-6} (4.935 - P)$

Flow Metering

Accurate measurement of volumetric gas flow rate proved to be more difficult than had been anticipated. For very low flow rates, a soap bubble meter, as shown in Fig. 4.6., was used. It was possible to measure flow rates upto 200 cc/min. The tube had a narrow portion with which it was possible to measure flow down to 2 cc/min. For higher flow rates - upto about 800 cc/min, a larger bubble meter of similar design was used. For even higher flow rates, a wet drum meter had to be used. This was capable of measuring rates of upto 4 litres/min with an accuracy of ±0.1%. For flow rates higher than this it is necessary to use variable area meters (rotameters). This equipment has a far lower level of accuracy and its use was not found to be necessary.

4.3.2 Discussion

The permeability of a rock sample can be determined from gas flow data by two distinct methods : either by plotting the flow rate-pressure gradient data according to the Klinkenberg equation or alternatively by using the Forchheimer equation. In the former, permeability is found from the intercept and in the latter case, the inverse of the intercept. Results of some of the measurements are given in Table 4.2. It can be observed that permeability obtained from the Forchheimer plots are consistently larger, which cannot be attributed to experimental errors alone.

Table 4.2
Comparision of permeability measured by two methods

	Permeability (md)	
Sample	Klinkenberg	Forchheimer
LE249	99.5	120.5
LE253	0.41	0.61
LE718	0.04	0.05
LE728	0.26	0.39
RH94	2.21	2.55
RH97	17.0	19.34
RH99	5.9	7.0
RH101	0.14	0.16
RH103	0.23	0.26

One explanation provided by Dranchuk et al [19] is that most of the data points in the inertial coefficient plots are apparently influenced by slippage effect. By introducing the Klinkenberg equation into the Forchheimer equation they corrected for the slippage. The equation they derived is

$$\frac{(1 + b/P_m)\ (P_1^2 - P_2^2)\ M}{2\,Z\,R\,T\,\mu\,L\,(W/A)} = \frac{W}{A\,\mu}\,(1 + b/P_m) + \frac{1}{k} \qquad (4.3\text{-}9)$$

Permeability calculated using this equation was found by them to be in close agreement with those found using the Klinkenberg method. The equation they derived were however heuristic in nature and no theoretical reasons are as yet available to explain the differences in permeability calculated by the two methods.

Error analysis of the results has shown that permeability and inertial coefficient measurements could both be carried out with a precision of ± 5 %.

4.4 CAPILLARY PRESSURE MEASUREMENTS

4.4.1 Introduction

The essential concept of capillary pressure for fluids within a porous media has been defined and discussed in detail by Leverett and others [20,21]. Details of the use and application of this concept to reservoir engineering are also available in the literature [9].

The capillary pressure - saturation relationship is known to be dependent on the following:

(a) The size and distribution of the pores

(b) The fluids and solids present (wettability)

(c) Saturation history

(d) Gravitional effect

Although gravitational effect is fairly small in most experimental situations, it can nevertheless exert some influence [22].

There are four basic methods available for experimental determination of capillary characteristics of rock samples. These are:

(a) Porous diaphragm method

(b) Mercury injection method

(c) Centrifuge method

(d) Dynamic capillary pressure method

Only the first two methods were used during the course of the present investigation, and are

described below. The third method relies on centrifugal forces to displace the wetting phase. The centrifugal force - measured from the revolutions per unit time of the sample holder - is converted to capillary pressure. The method has been discussed in detail by Hassler et al [23]. The final technique - dynamic capillary pressure method, was apparently first used by Brown [24]. In this, two fluids are injected simultaneously through a core sample and the upstream as well as the downstream pressures are monitored for both phases. The capillary pressure is then taken to be the difference in pressure between the two phases. Comparision between the dynamic and other static methods have shown [24] that the two methods give virtually similar results.

4.4.2 Porous Diaphragm Method

The essential part of equipment for this method consist of a permeable membrane of uniform pore-size distribution containing pores such that the displacing fluid would not be able to penetrate the diaphragm when the pressures applied to the displacing phase are below some selected maximum pressure of investigation. The porous membrane is placed in a high pressure chamber. A schematic arrangement of the apparatus is shown in Fig 4.7.

The maximum pressure obtainable by this method depends on the size distribution of the porous membrane. For maximum accuracy, porous plates are manufactured such that they perform best within a range of pressures. If the pressure limit is exceeded then the breakthrough of the displacing fluid occurs. During measurements of oil-air capillary pressure curves, it was found that gas was produced continiously even at pressures below the maximum for the given membrane. This is most likely due to diffusion - rather than convection - taking place through the membrane.

The porous membrane is saturated with the fluid to be displaced - oil in this particular case. The core samples are placed on the membrane with fine diatomaceous powders placed in-between to establish good capillary contact. A thin tissue paper (Kleenex) was placed underneath the core samples to ensure that the powders do not cling on to the core when it is lifted out of the membrane for saturation measurements. Pressure of the nonwetting phase is then increased to displace the wetting phase in a stepwise manner. The core is allowed to approach a state of static equilibrium at each pressure step.

Before the core plug was placed in the capillary pressure cell, it had to be saturated completely by placing the sample in a vessel and evacuating the vessel to a vacuum of about $1x10^{-2}$ torr and then introducing the liquid. The arrangement for such an apparatus has been described by Pirson [6].

The liquid used in this experiment was a refined oil - Isopar, produced by Esso Petroleum Co. The properties of this fluid are as follows:

Chemical composition:

C_{11}	5 % w/w
C_{12}	75
C_{13}	15
Napthenes	5

Density: 0.7696 g/cc

Viscosity:

(a) using Ostwald viscometer	1.49 cp @ 21 C
(b) using Stress Rheometer	1.7 cp @ 20 C

Surface tension: 22.5 mN/m @ 20 C

4.4.3 Mercury Injection Technique

In this method, the core sample is placed in a chamber and evacuated under vacuum. Mercury is then forced into the core in a stepwise fashion, with sufficient time given for equilibrium to be reached at each pressure increment. Since mercury is a nonwetting fluid, the volume of mercury injected at each pressure step determines the nonwetting phase saturation.

The above procedure was continued until the injection pressure reaches a predetermined value. The maximum pressure that the equipment could tolerate was 80 bars. The reverse procedure was carried out after the maximum pressure has been reached to measure the withdrawl capillary pressure. It was not possible to fill the core completely with mercury as this requires a very high pressure to penetrate the smallest of pores.

A schematic arrangement of the apparatus is shown in Fig 4.8. The basic features of this equipment are similar to those used originally by Purcell [25]. A sighting glass tube capable of withstanding pressures upto 80 bar was attached to the top of the pressure chamber. This glass tube allows observation of any trapped gas to be made during the mercury injection process. Ideally, when a good vacuum is achieved, there should be no trapped gas inside the pressure chamber. In most runs, due to the limitation of the pump, a vacuum of 10^{-2} mbar could be achieved. This was found to be adequate since any gas bubble observed at the top of the glass tube usually disappeared upon increasing the mercury pressure by about 1 or 2 psig. A good

vacuum is essential to the success of this experiment and for this purpose the vacuum pump had to be run continuously for 4 to 8 hours and longer for very low permeability core sample. The equipment was initially calibrated using a steel "dummy" plug of known volume to account for the system compressibility, eg. compression of mercury, expansion of tubes and fittings. The equipment was also found to be sensitive to temperature changes and was therefore kept in an air conditioned laboratory to minimise temperature fluctuations.

4.4.4 Discussion

A complete determination of capillary pressure curves using the porous membrane technique was found to take up to 40 days or longer with about a week at each pressure step. Low permeability cores were found to take longer time to reach equilibrium. The long time required is thought to be due to the vanishing pressure differentials which causes flow as the core approaches equilibrium at each imposed pressure. At low saturations, the effective permeability to the displaced phase is reduced which also contributes to the slow approach to equilibrium. The main difficulty of this method is to be able to correctly predict the time at which the fluid in the core sample should reach capillary equilibrium with the displacing fluid.

An advantage of the mercury injection technique is that very high capillary pressures can be measured since the limitation of the properties of the diaphragm is removed. The main advantage claimed in favour of this method is a significant reduction in the time required to reach equilibrium. Some have even claimed [25] that equilibrium times could be as low as a few minutes. During the course of the present work, pressures were monitored for a particular sample at a given pressure step for up to 48 hours. It was found that the pressure declined almost exponentially with time and even after 48 hours there was a detectable drop in pressure with time. Claims of a reduction in the equilibrium time therefore seems to be suspect and require further investigation.

Comparision between the mercury injection and the porous membrane methods have been carried out by Rose et al [26]. They found that the mercury injection technique gives essentially the same result provided the differences in the surface tension and contact angles are taken into account. Others however have found significant discrepancy between the results obtained by these two methods. The main disadvantage of this method therefore is the differences in the wetting properties of mercury compared to reservoir fluids. Due to the very high interfacial tension of mercury, most of the fine clay structure inside pores can be expected to be destroyed during the injection process. This method is therefore not as accurate as the other method for pore structural measurements. The other disadvantage of this method is that the core sample will contain residual mercury upon reduction of pressure and is therefore not usable for any further analysis.

Leverett [20] proposed a relation, commonly called the "J - function", which can be used to correlate the physical properties of the porous media and its fluids with its capillary pressure. The Leverett's J - function has been found to be unsatisfactory [9] in correlating data taken from rocks of different lithology. A new generalized model has been proposed by Bentsen et al [27] for describing the drainage capillary pressure. This has however been tested successfully only on artificially consolidated cores.

4.5 RESULTS

The results of measurement of permeability, porosity, inertial coefficient and recovery efficiency are summarised in Table 4.3. Method for calculating the recovery effciency and its use in the interpretation of pore structure are discussed later in Chapter 6.

REFERENCES

1. Monicard, R.P. : *Properties of Reservoir Rocks : Core Analysis*, Edition Technip, Paris, (1980)
2. Core Laboratories: *Fundamentals of Core Analysis*, Published by Core Analysis Laboratories Inc., Dallas, Texas.
3. Keelan, D.K. : A critical review of core analysis techniques, *J. Can. Pet. Tech.*, April (1972) pp. 42-55.
4. Lombos, L. : Robertson Research Helium Gas Expansion Volume Meter - Operational Instruction Manual, supplied to Imperial College (1983)
5. Pirson, S.J. : *Oil Reservoir Engineering*, McGraw Hill Book, New York (1958) p.33.
6. Taylor, R.P. and Wardlaw, N.C. : Increased precision of porosity measurements using a modified Ruska Universal Porometer, *J. Can. Pet. Tech.* (April 1975) 33-37.
7. Klinkenberg, L.J.: Permeability of porous media to liquids and gases, *Drill & Prod. Prac.*, API, (1941) pp.200.
8. Heid, J.G., McMahon, J.J., Nielsen, R.F. and Yuster, S.T. : Study of permeability of rocks to homogeneous fluids, *Drill. Prod. Prac.*, API (1950) 230-246.
9. Amyx, J.W., Bass, D.M. and Whiting, R.L. : *Petroleum Reservoir Engineering - Physical Properties*, McGraw Hill Book Co., New York (1960).
10. Dranchuk, P.M. and Sadiq, S.: The interpretation of permeability measurements, *J. Can. Pet.Tech.* (July 1965) 130.
11. Wallick, G.C. and Aronofsky, J.S. : Effect of gas slip on unsteady flow of gas through porous media : Experimental verification, *Trans. AIME,* (1954) **201**, 322-324.
12. Jones, S.C. : A rapid accurate unsteady-state Klinkenberg permeameter, *Soc. Pet. Eng. Jour.*, (Oct. 1972) 383-397.

13. Freeman, D.L. and Bush, D.C. : Low-permeability laboratory measurements by non-steady state and conventional methods, *Soc. Pet. Eng. J.*, (Dec. 1983) 928-936.
14. Walls, J.D.; Nur, A.M.; Bourbie, T. : Effects of pressure and partial water saturation on gas permeability in tight sands : Experimental results, *J. Pet. Tech.*, (April 1982) 930-936.
15. Walls, J.D. and Amafule, J.O. : Capillary pressure and permeability relationships in tight gas sands, Paper SPE 13879, presented at the SPE/DOE Low Permeability Gas Reservoir Symp., Denver, Co., May 19-22, 1985.
16. Katz, D.L. et al : *Handbook of Natural Gas Engineering,* McGraw Hill Book Co., New York (1959).
17. Stiel, L.I. and Thodos, G. : The viscosity of nonpolar gases at normal pressure, *AIChE Jour.*, (1961) 7(4), 611-615.
18. Perry, J.H. and Chilton, T.H. (Eds) : *Chemical Engineers Handbook,* 5th Ed., McGraw Hill Book Co., N.Y. (1973).
19. Dranchuk, P.M. and Kolada, L.J. : Interpretation of steady linear visco-inertial gas flow data, *J. Can. Pet. Tech.* (Jan. 1968) 36-40.
20. Leverett, M.C.: Capillary behaviour in porous solids, *Trans AIME* (1941) **142,** 152-169.
21. Morrow, N. : Physics and thermodynamics of capillary action in porous media, *Ind. Eng. Chem.* (1970) **62** (6), 33.
22. Szabo, M.T. : The role of gravity in capillary pressure measurements, *Soc. Pet. Eng. J.* (April 1972), 85-88.
23. Hassler, G.L. and Brunner, E. : Measurement of capillary pressures in small core samples, *Trans AIME,* (1945) **160**, 114-123.
24. Brown, H.W. : Capillary pressure investigations, *Trans. AIME* (1951) **192**, 67-74.
25. Purcell, W.R.: Capillary pressures - their measurement using mercury and the calculation of permeability therefrom, *Trans. AIME* (1949) **186**, 39-48.
26. Rose, W. and Bruce, W.A. : Evaluation of capillary characters in petroleum reservoir rocks, *Trans AIME* (1949) **186**, 127-142.
27. Bentsen, R.G. and Anli, J.: A new displacement capillary pressure model, *J. Can. Pet. Tech.* (July 1976) 75-79.

TABLE 4.3

Experimental Results

Sample	k (md)	ϕ (%)	β (cm^{-1})	Recovery efficiency (%)
M73001	0.064	12.31	1.39 E12 *	84.6
M73002	0.10	11.50	0.57 E12	75.0
M73003	0.46	10.01	2.84 E10	81.1
M73004	0.52	11.0	2.38 E10	75.3
M73005	33.0	21.0	1.70 E7	79.8
M73006	15.2	20.50	3.84 E7	69.6
M73007	10.5	20.9	6.59 E7	63.1
M73008	13.0	23.9	3.54 E7	63.7
M73009	32.5	25.6	8.63 E6	68.2
M73012	28.4	19.6	2.09 E7	61.2
M73013	20.8	19.0	2.67 E7	70.9
AL23	0.16	10.05	3.90 E10	41.6
AL29	0.17	10.04	1.35 E10	39.7
AL40	0.17	9.94	3.25 E10	37.8
AL79	0.11	10.26	1.01 E11	40.3
AL111	0.14	13.5	8.10 E10	32.9
AL118	0.05	12.31	3.35 E11	47.1
MO63	0.21	9.34	1.22 E10	50.7
RH94	2.21	12.17	5.68 E8	43.6
RH97	17.01	16.92	6.63 E7	32.2
RH99	5.9	14.9	2.42 E8	39.5
RH101	0.14	5.87	2.60 E11	57.5
RH103	0.23	9.96	3.71 E10	60.5
LE249	99.5	15.17	2.51 E7	80.2
LE253	0.41	7.43	2.63 E10	45.3
LE718	0.041	6.83	1.03 E12	47.9
LE728	0.26	11.39	3.74 E10	41.3
M11001	59.0	20.76	1.21 E7	75.9
M11002	2.1	13.82	3.81 E8	73.6
M11003	0.52	10.02	4.07 E9	77.5
M11004	0.038	8.19	3.0 E12	82.6
M11005	0.7	10.19	4.07 E9	85.5
M11006	4.03	9.9	3.24 E8	-
M11007	84.0	20.58	3.89 E6	67.8
M11008	1.24	12.74	1.93 E9	80.0
M11009	66.0	19.7	5.71 E6	69.7
M11010	206	20.9	1.16 E6	65.2
M11011	1.18	11.6	1.62 E10	76.9

* E12 = x 10^{12}

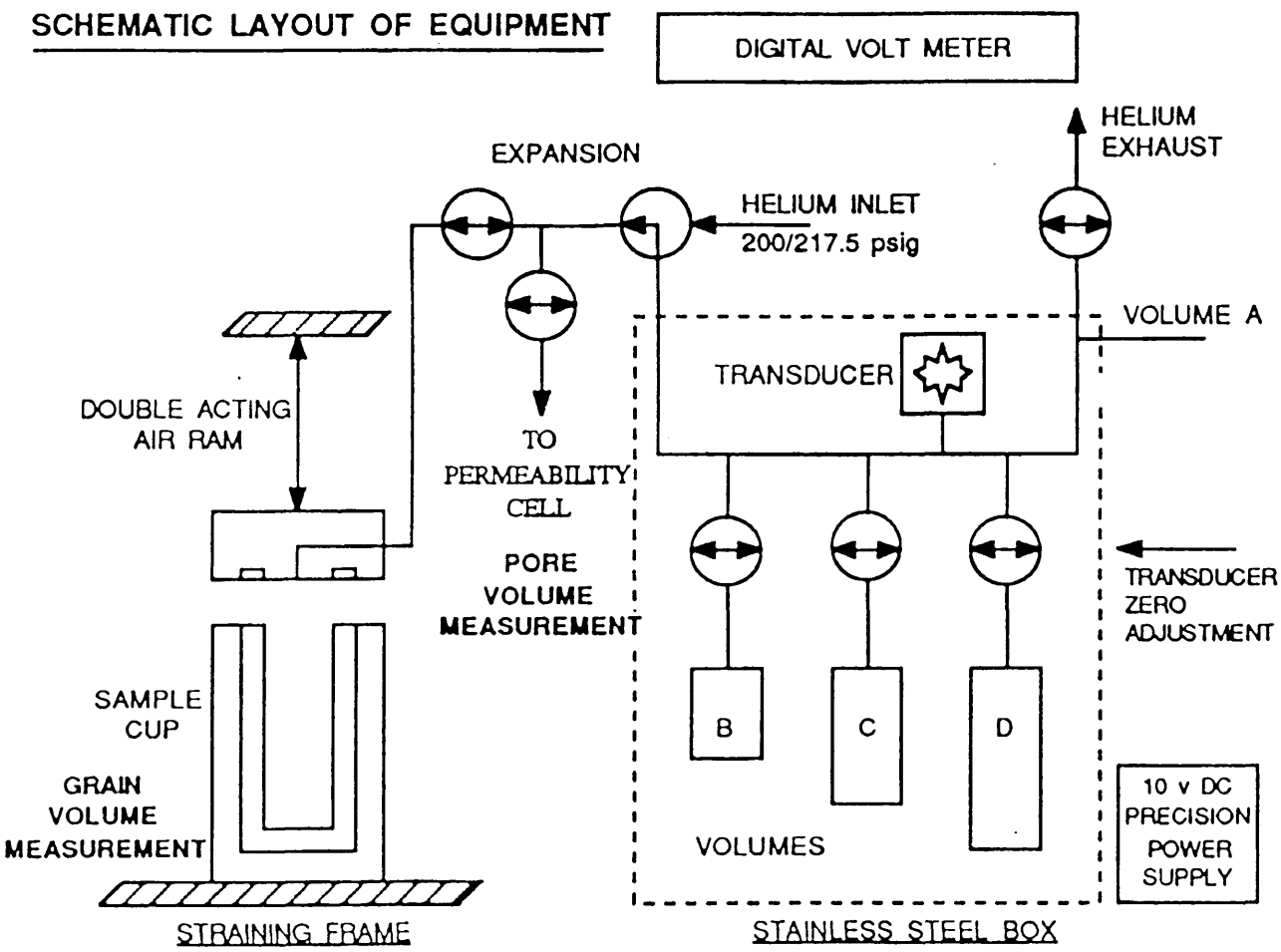


Fig 4.1 Schematic arrangement of the helium gas expansion porosimeter.

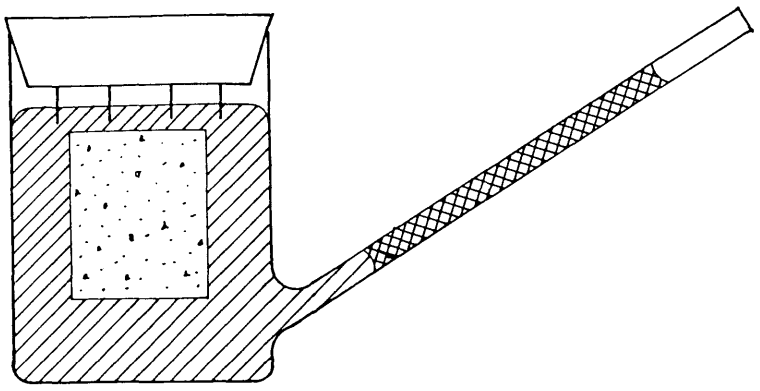


Fig. 4.2 Mercury pycnometer for bulk volume measurement.

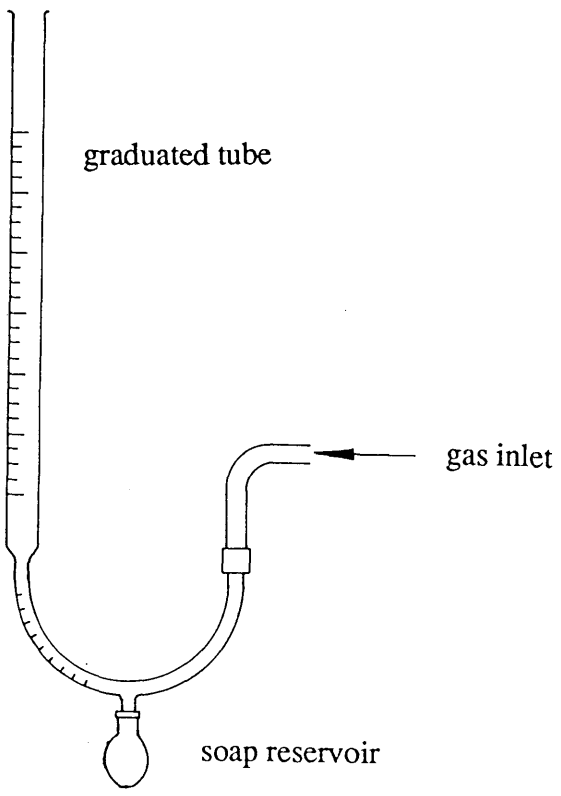


Fig. 4.6 Soap-bubble meter for volumetric gas flow measurement.

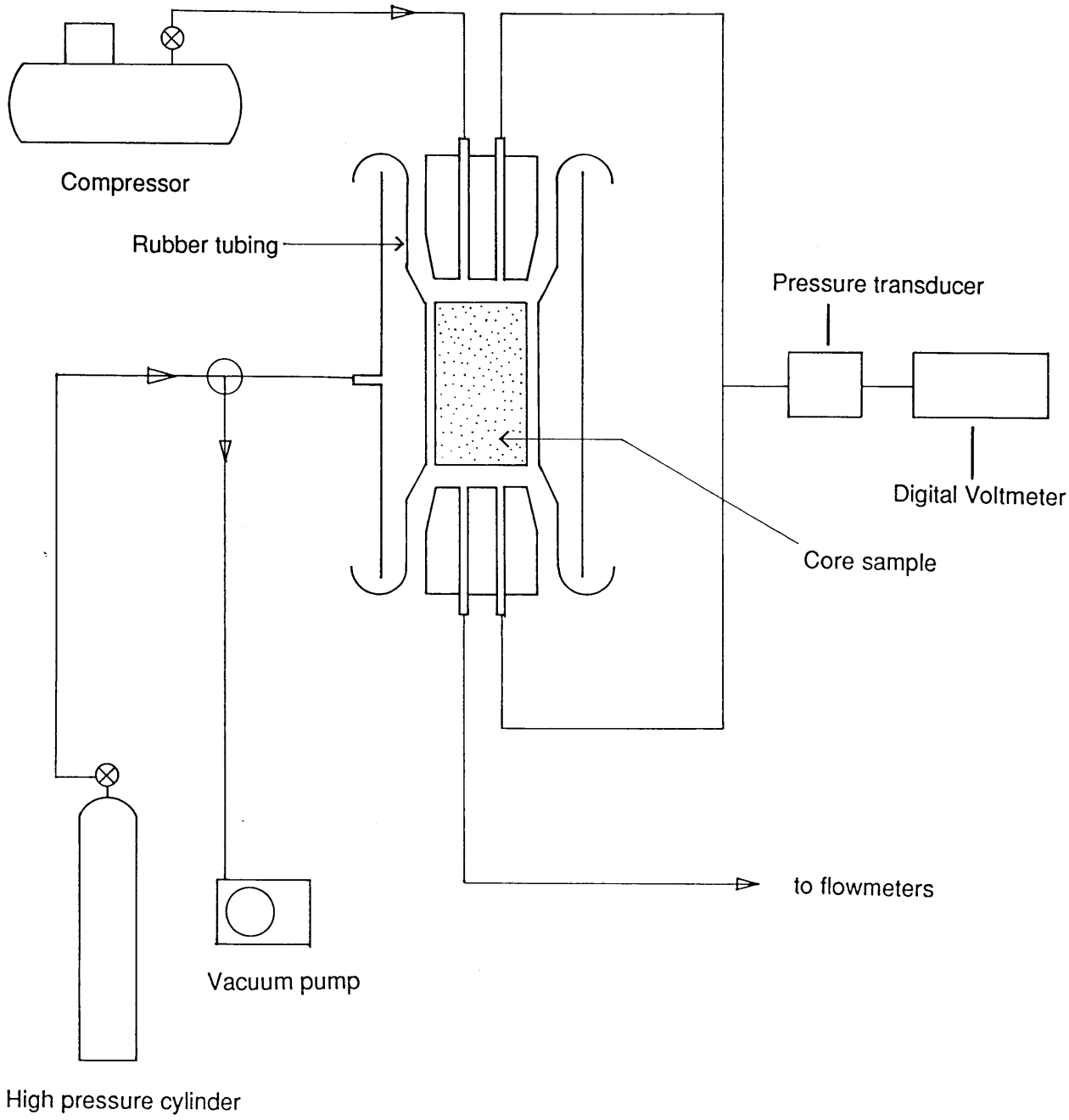


Fig 4.3 Schematic arrangement of the Hassler cell assembly for flow measurement.

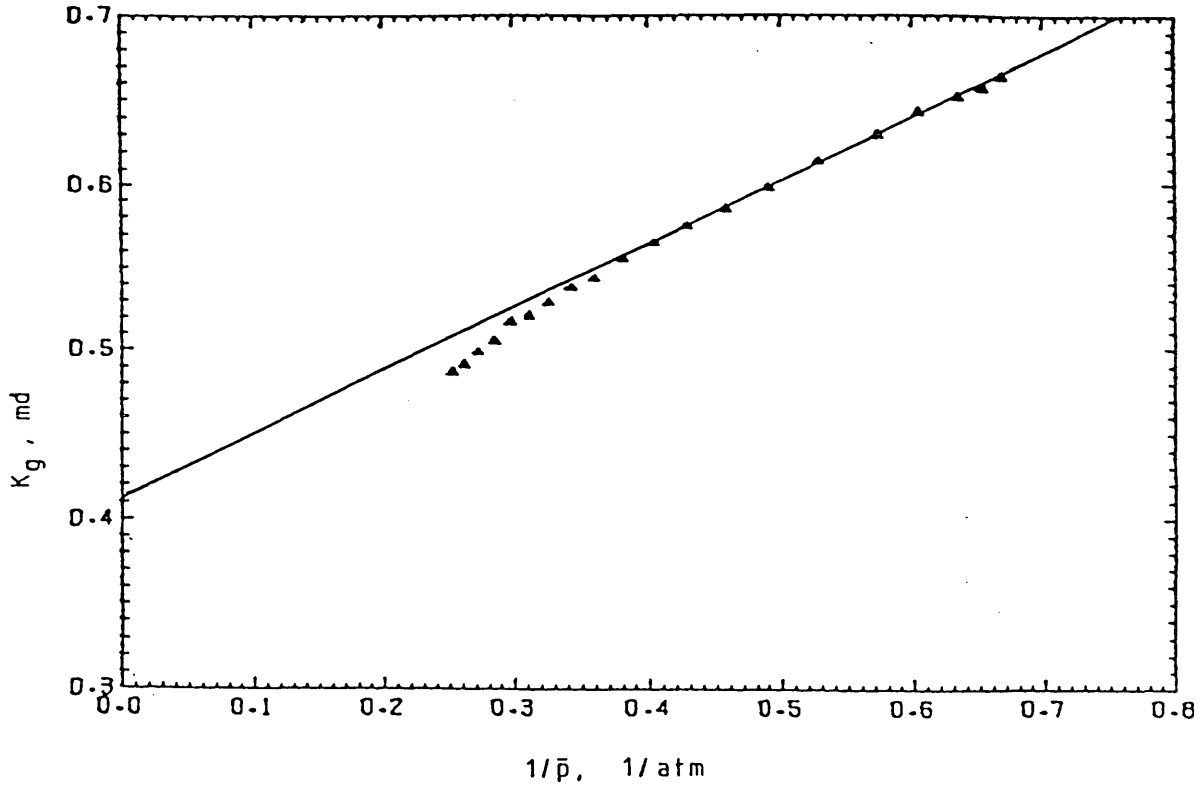


Fig. 4.4 A typical Klinkenberg plot with downward warp at high rates. Sample LE253.

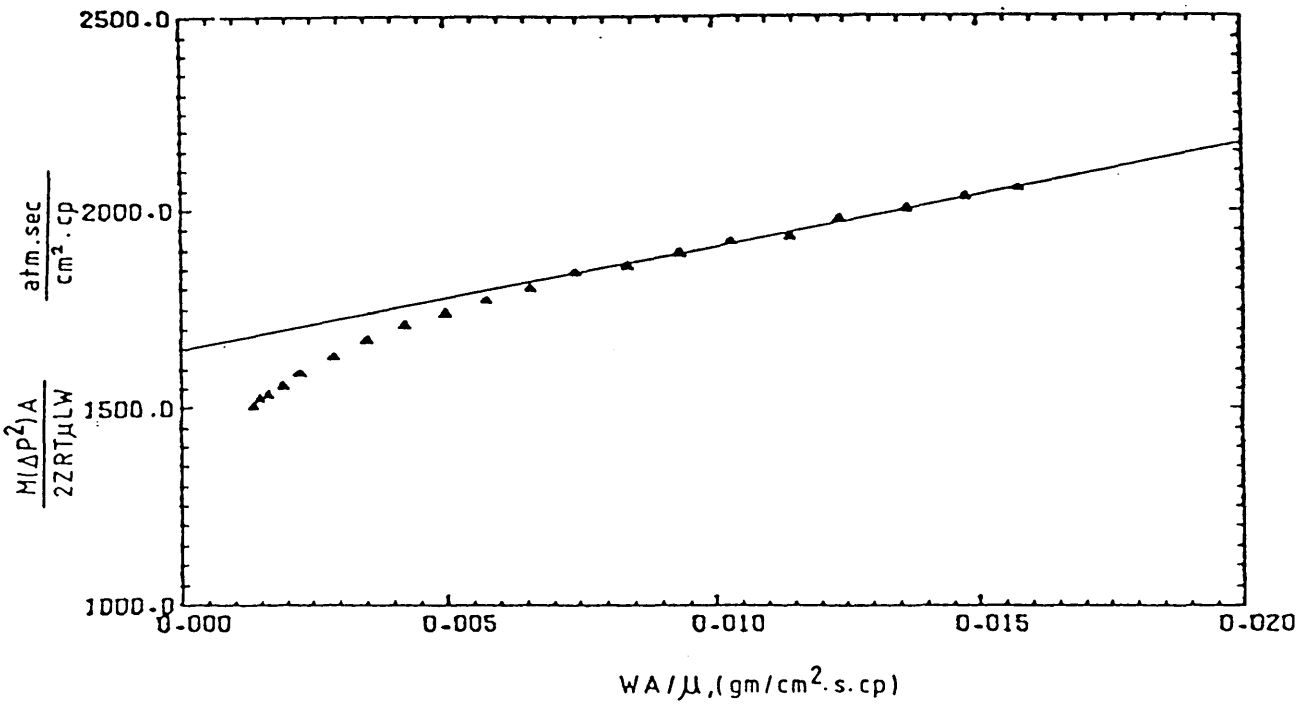


Fig. 4.5 A typical plot according to Forchheimer equation showing downward warp

Sample LE253.

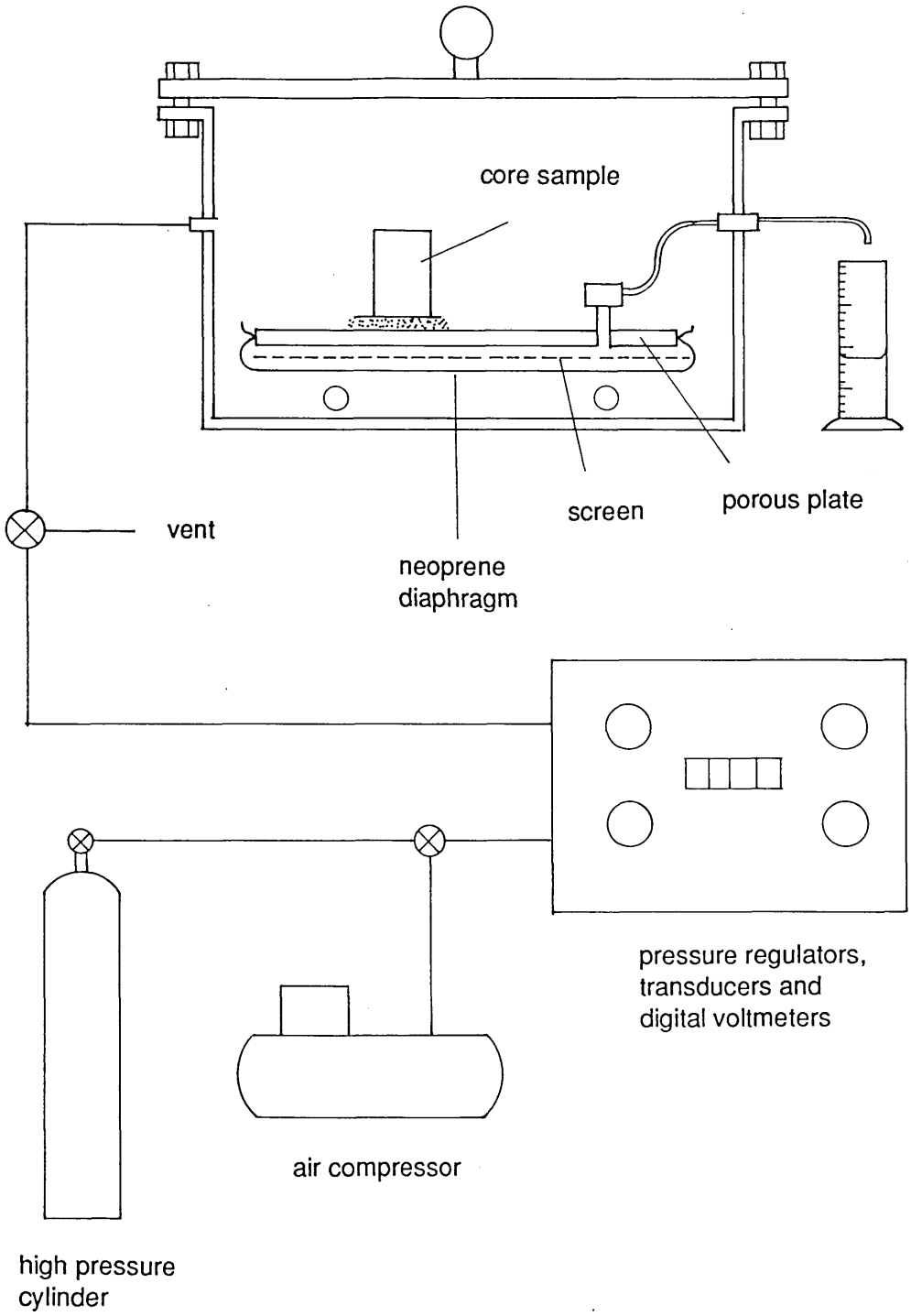


Fig. 4.7 Schematic arrangement of apparatus for the measurement capillary pressure using the porous membrane method.

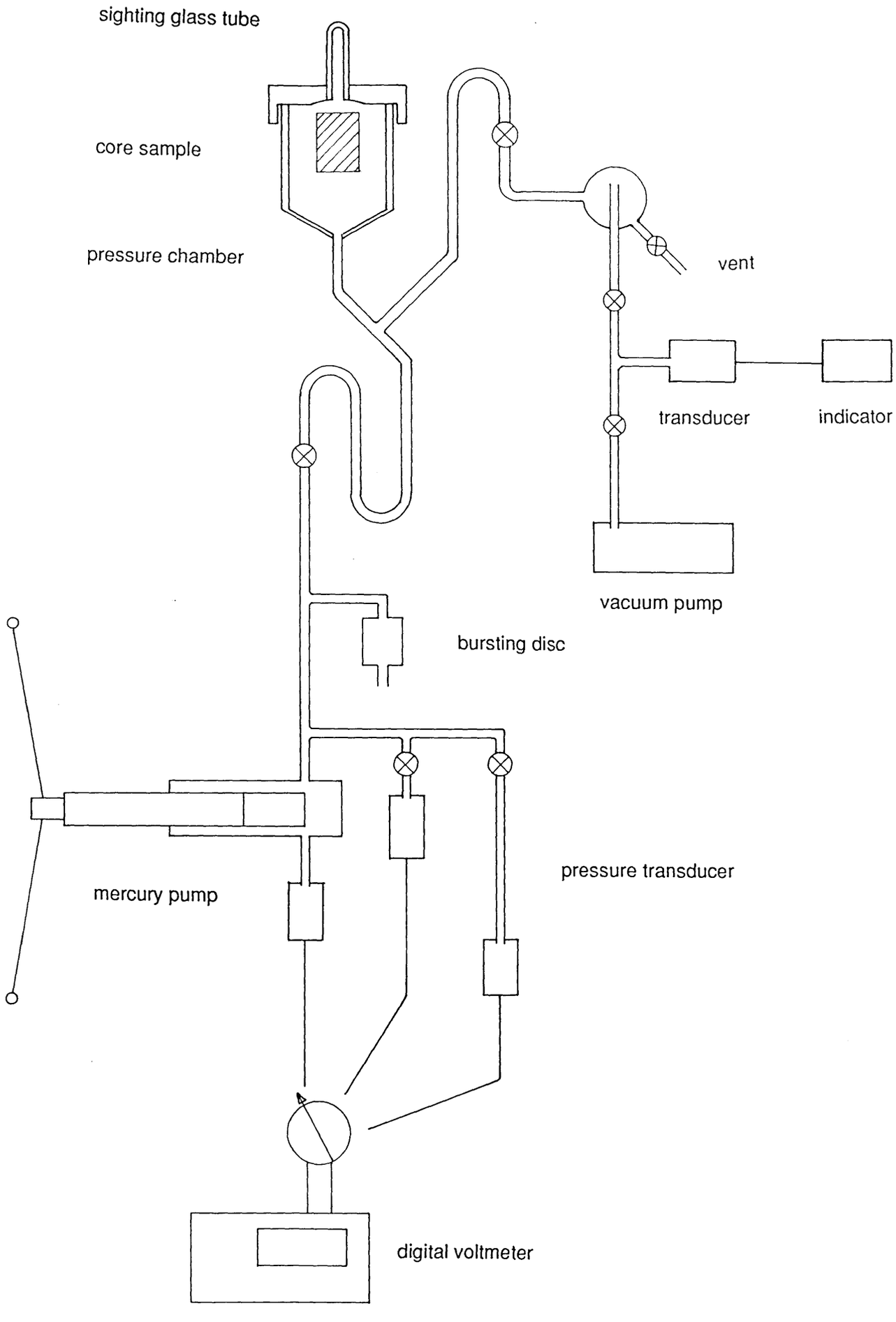


Fig. 4.8 Schematic arrangement of the mercury porosimeter.

Chapter 5

TRANSITION FROM LINEAR TO NON-LINEAR FLOW

5.1 INTRODUCTION

Some of the differences between flow in capillaries and that in porous media have already been outlined in chapters 2 and 3. In a capillary the flow changes from laminar to turbulent mode at a critical value depending on the Reynolds number ($Re = \rho vd/\mu$) of the flow. The critical number is generally accepted to be around 2000. It would of course be useful to find such a critical Reynolds number for flow in porous media, eg in the interpretation of experimental flow data or to estimate the region where non-Darcy effects would be significant in gas wells. Unfortunately, there does not seem to be any simple method for predicting this value.

In this chapter the various regimes of flow in porous media are described and attempts are made to predict the transition rates. In particular, the present study will focus on the transition from viscous (linear) to inertial dominated (non-linear) flow. Results of some experimental measurements of flow rate - pressure gradient data will also be discussed.

5.2 REGIMES OF FLOW

Due to the wide distribution of pore sizes and shapes in any naturally occurring porous medium it is possible for two or more different modes of flow to coexist simultaneously. The difficulty of describing the transition rates between two modes of flow is therefore obvious. It is nevertheless possible to divide flow in porous media into a number of broad categories. This is not a matter of semantics alone, since a different mathematical expression may be required for the best description of each mode of flow. The various common types of flow are :

(a) diffusional flow (Knudsen equation)
(b) molecular slip flow (Klinkenberg equation)
(c) viscous flow (Darcy's law)
(d) visco-inertial flow (a transition region)
(e) inertial dominated flow (Forchheimer equation)
(f) inertial / turbulence transitional region
(g) turbulent flow (a cubic equation)

There are of course many other types of flow in porous media which will not be discussed here. A discussion of some of these have been given by Kutilek [1] who has shown that there exists at least 12 possible situations where Darcy's law would be inapplicable. It has been pointed out [2] that below a certain value of Re, the Darcy's law does not hold. The existence of this pre-Darcy flow regime is attributed to non-Newtonian behaviour of many fluids and also the fact that the streaming potential generated by the flow, especially in fine grained porous media, can produce small countercurrents along the pore walls in a direction opposite to the bulk flow.

One aspect of the pre-Darcy regime is that a finite value of pressure gradient exists below which the velocity is zero.

Experimental observations using laser anemometry on porous media consisting of glass bead packs has shown [3] that in the Darcy regime, where the flow is dominated by viscous forces, the exact nature of the flow is determined by the local geometry of pore spaces. This type of flow was found to be valid for Re < 1, the value of Re being based on average pore size and the average pore velocity. At Re = 1, boundary layers were found to develop near the solid boundaries of the pore. A transition region was found at Re between 1 and 10 where the flow changed from purely viscous to inertial dominated. Here the boundary layers became more pronounced and an "inertial core" appeared. The development of these "core" flow outside the boundary layers was found to be the cause for a nonlinear relationship between the pressure gradient and the flow rate.This steady nonlinear flow relationship persisted to a Re of 200. Flow in the range 200 < Re < 350 was of an unsteady laminar type, which was characterized by laminar wake oscillations in the region 200 < Re < 300 and was followed by the formation of vortices in the range 300 < Re < 350. Thereafter, at Re > 350, a highly unsteady and chaotic flow pattern ensued which qualitatively resembled turbulent flow.

It is important to remember that this reported study was conducted on porous media consisting of smooth glass spheres and cylinders arranged in a regular packing. The exact values of Re for media with different pore structures may be quite different or even nonexistent. The general trend of flow regimes as described above would however be expected to hold for many types of porous media.

5.3 QUANTITATIVE RELATIONS

The Hagen-Poiseuille equation for laminar flow in a capillary is given by

$$v = \frac{R^2}{8\mu}\left(-\frac{\Delta P}{L}\right) \tag{5.3-1}$$

The capillary radius can be written in terms of a 'hydraulic radius' R_h as

$$v_p = \frac{R_h^2}{2\mu}\left(-\frac{\Delta P}{L}\right) \tag{5.3-2}$$

where v_p is the pore velocity. It should be noted that the hydraulic radius $R_h = R / 2$. For spherical particles, the diameter is related to its surface area by

$$D_p = 6 / S_o \tag{5.3-3}$$

The surface area is related to the specific surface by

$$S = S_o (1 - \phi) \tag{5.3-4}$$

where S_0 is the specific surface area based on the solids volume. Further, the hydraulic radius is related to S by

$$R_h = \phi / S \tag{5.3-5}$$

The superficial velocity v_0 is related to the pore velocity by the Dupuit - Forchheimer relation

$$v_0 = v_p \cdot \phi \tag{5.3-6}$$

Combining Eqns. 5.3-3, 4 and 5 and substituting into (5.3-2) we get

$$v_o = \frac{D_p^2}{2\,(36\,\mu)} \frac{\phi^3}{(1-\phi)^2} \left(-\frac{\Delta P}{L}\right) \tag{5.3-7}$$

Experimental data suggests [4] that the coefficient 2 in (5.3-7) should be replaced by 25/6. We then get

$$v_o = \frac{D_p^2}{150\,\mu} \frac{\phi^3}{(1-\phi)^2} \left(-\frac{\Delta P}{L}\right) \tag{5.3-8}$$

This is the *Blake - Kozeny* equation and is supposed to be valid for the flow region given by

$(D_p G_0 / \mu) / (1-\phi) < 10$, where $G_0 = \rho v_0$

Fluids flowing in a packed bed will exert a force on the solid surfaces. This force can be [4] split into two parts : (a) a force F_s that is exerted by the fluid even at a stationary situation, and (b) an additional force F_k associated with the kinetic energy of the fluid. The force F_k may be expressed as the product of a characteristic area A, a characteristic kinetic energy per unit volume K and a dimensionless "friction factor", f

$$F_k = A\,K\,f \tag{5.3-9}$$

This equation defines the value of f and is known only if the values of A and K are specified. For flow in a conduit this may be written as

$$F_k = (2\,\pi\,R\,L)\,(1/2\,\rho\,v^2)\,f \tag{5.3-10}$$

The force F_k can be expressed in terms of pressure difference along the length as

$$\begin{aligned} F_k &= [(p_o - p_L) + \rho\,g\,(h_o - h_L)]\,\pi\,R^2 \\ &= (P_o - P_L)\,\pi\,R^2 \end{aligned} \tag{5.3-11}$$

From Eqns. 5.3-10 and 11, f can be expressed as

$$f = \frac{1}{4}\left(\frac{D}{L}\right)\left(\frac{P_o - P_L}{\frac{1}{2}\rho\,v^2}\right) \tag{5.3-12}$$

The quantity f as expressed above is known as the *Fanning Friction Factor.* The bed friction factor for Blake-Kozeny equation can be found from comparision with Eq.(5.3-12) to be

$$f = \left(\frac{(1-\phi)^2}{\phi^3}\right) \frac{75}{D_p G_o / \mu} \tag{5.3-13}$$

For highly turbulent flow the friction factor can be expected to be a function only of surface

roughness as in pipeline flow.

Using the following substitutions : $v = v_o / \phi$; $D = 4 R_h$; $R_h = \phi / S$; $S = S_o(1- \phi)$ and $D_p = 6/S$, from Eq.(5.3-12) we get

$$\frac{P_o - P_L}{L} = 6 f_o \cdot \frac{1}{D_p} \cdot \frac{1}{2} \rho v_o^2 \cdot \frac{1 - \phi}{\phi^3} \tag{5.3-14}$$

From experiments, $6f_o$ is found to be about 3.50, so that

$$\frac{P_o - P_L}{L} = 3.5 \frac{1}{D_p} \cdot \frac{1}{2} \rho v_o^2 \cdot \frac{1 - \phi}{\phi^3} \tag{5.3-15}$$

This is the *Burke-Plummer* relation and is found [4] to be valid for

$$\frac{D_p G_o / \mu}{1 - \phi} > 1000$$

Comparision of Eq.(5.3-15) with (5.3-12) shows that friction factor is a function only of porosity

$$f = 0.875 \frac{1 - \phi}{\phi^3} \tag{5.3-16}$$

The Burke-Plummer relation is valid for "turbulent" flow, and the Blake-Kozeny equation for a laminar regime. A quadratic equation can be formed by the addition of these two, to form a relation which would be valid for the whole range of flow rates

$$\frac{P_o - P_L}{L} = \frac{150}{D_p^2} \frac{(1- \phi)^2}{\phi^3} \mu v_o + \frac{1.75}{D_p} \frac{(1- \phi)}{\phi^3} \rho v_o^2 \tag{5.3-17}$$

This equation is analogous to the Forchheimer relation with the coefficients α and β defined in terms of porosity and grain sizes.

Eq.(5.3-17) could be written in terms of dimensionless groups as

$$\left(\frac{(P_o - P_L)}{G_o^2} \rho \right) \left(\frac{D_p}{L} \right) \left(\frac{\phi^3}{1 - \phi} \right) = 150 \frac{(1 - \phi)}{D_p G_o / \mu} + 1.75 \tag{5.3-18}$$

This is the *Ergun equation* [5]. The density of the fluid is found as the arithmetic average of the end pressures. The equation is sketched in Fig 5.1, and a comparision with experimental data shows it to be fairly good. Various other equations can also be found in the literature for estimating the pressure drop in packed beds and consolidated media (see Appendix).

It should be noted that for consolidated media, the friction factor is not a unique function of surface roughness. As such a unique curve would be difficult to obtain.

5.4 REYNOLDS NUMBER

Numerous experimental and theoretical investigations have been reported in the literature in an attempt to predict the limits of the different flow regimes. Most reported work make use of the Reynolds number ($Re = \rho v d / \mu$) as a criterion for the "critical" transition rates. Unlike flow in pipes however, during flow through a porous media, there does not seem to exist any such critical value. The general consensus is that the transition from one mode of flow to the next is a smooth one. We therefore need to address three important questions regarding the use of Reynolds number for a porous media. These are: (a) is the use of Reynolds number valid for determining the onset of deviation from Darcy's law, (b) what is the correct definition of the term d for a porous media, and (c) what is the correct definition of the term v for a porous media.

The second and the third points will be discussed under separate headings below. Regarding the first point suffice it to say that there is a very wide divergence of view as to the exact value of the Re at the onset of deviation. Some [6,7] have claimed that the deviation starts at $Re = 1.0$ while others [8-10] have found a value close to $Re = 0.1$. These values have all been derived from plots of Friction Factor versus Reynolds number. The wide discrepency is certainly due to the different ways in which the Friction Factor and the Reynolds number have been defined by the various authors. Here we shall not dwell on the question of how best to define the Friction Factor.

Table 5.1 is a summary of some of the important publications in this area and shows the numerous ways the Friction Factor and the Reynolds number has been defined. The end of inertial regime (ie. start of turbulence) has been reported to occur at Re between 10 to 2000.

5.4.1 Definition of the term d

For flow through pipes which are circular in shape, the characteristic length representing the tube is taken to be its diameter. For pipes of any other shape (eg square, ellipsoidal etc) the general procedure is to find the length by dividing the cross sectional area available for flow by the perimeter wetted by the fluid.

Using these concepts of pipeline flow various workers have attempted to define a characteristic length which would be applicable for a porous media. Brownell & Katz [11] for example, claimed that there exist a complete analogy between flow in porous media and that in pipeline flow. It was however realised by many others [7,12] that the characteristic length should represent the pore diameters. However due to convenience it became popular to use the

grain diameter as the representative length. The usual procedure for unconsolidated media was to pass the sand through a successively finer mesh of seives and to find some kind of a mean by knowing the diameters of the seives and the weight fraction that it will pass. For consolidated media the same procedure was used by firstly breaking it into small peices and finally crushing it very finely using a mortar. Fancher et al [7] then defined the characteristic length as:

$$D = \sqrt[3]{\frac{\Sigma n d^3}{\Sigma n}} \qquad (5.4\text{-}1)$$

where n, the number of grains for any average diameter opening d was calculated by assuming that the sand grains were spherical and of average density 2.65.

Elenbaas & Katz [13] and Brownell & Katz [11] found the characteristic length from the formula:

$$D = \sqrt{\frac{\Sigma (M/d)}{\Sigma (M/d^3)}} \qquad (5.4\text{-}2)$$

where d is the average size of a weight fraction taken as the arithmetic average of the screen openings that pass the particles and retain the particles; and M the weight fraction of a given particle size.

Later Tek [6] used the formula:

$$D = \sqrt{\frac{\Sigma n d^3}{\Sigma n}} \qquad (5.4\text{-}3)$$

Regarding the characteristic length of a porous media, Muskat [12] wrote that "the difficulty lies essentially in the inherent ambiguity in the definition of the quantity d entering in the Reynolds number". For beds of packed materials, other definitions have also been proposed [4]

From simple dimensional analysis, Collins [14] has shown that the characteristic length can be represented by $\sqrt{(k / \phi)}$ and Ward [8] has shown that it can be represented by $\sqrt{k}$. Their derivations are based on some simplifying assumptions which are not sound. Calculation using these characteristic lengths are often found to give values that are physically unrealistic.

Green & Duwez [15] were probably the first to tackle this issue from a completely different viewpoint. Observing that the first term in the Forchheimer's formula represents the viscous forces and the second term the inertial forces, and that the Reynolds number is in fact the ratio of the latter to the former, they defined the Reynolds number as:

$$Re = \frac{\beta \rho v}{\alpha \mu} \qquad (5.4\text{-}4)$$

Thus the characteristic length scale is therefore defined as β / α involving both the inertial and viscous resistance coefficients. A similar formulation was also arrived at by Ahmed et al [9] from analysis of the Navier-Stokes equation. This definition of the characteristic length has been used fairly widely [16,10 etc.]. Although this definition is based on sound arguments, experimental measurements show that it decreases with increasing permeability of the media, which is contrary to expectation (see Section 5.6).

5.4.2 Definition of the term v

For fluids flowing through a pipe, the superficial velocity v is found by simply dividing the total volumertic flow rate by the cross sectional area. This then gives the average macroscopic velocity which can be used in the Reynolds number. Similarly for flow through a porous media, the flow rate divided by the cross section will also give the superficial velocity. The flow however does not actually take place across the whole cross-sectional area, but only through the pores. It has therefore been suggested [14] that the velocity should be found from $v = Q / A \phi$. By introducing the porosity, the area available for flow is reduced and hence the velocity considerably increased. The velocity found in this manner is the average microscopic (pore) velocity. It was noted by Fancher et al [7] that this is the velocity of interest for use in Reynolds number. However they have not used it in their calculation due to inconvenience and mentions that either method can give only an approximation to the actual mean velocity through a pore. The difference however is quite significant and it has been observed by Nemenyi (see [12]) that the velocities in the pores of a medium are higher by a factor of 4 to 8 than the macroscopic velocity. Wright [17] has also attempted to measure velocities using a hot wire anemometer and noted that micro-velocities can be 5-6 times higher than the macro-velocities.

In the literature relating to flow through consolidated media, it is seen that the majority of researchers have used the superficial (macro) velocity in the Reynolds number. Quantitative relationships between pressure drop and flow rate for packed columns (eg Ergun equation) clearly show that the porosity term enters the Reynolds number. Wright [17] has shown that the pore velocity is related to the macro-velocity through $v_p = v_m / \phi$. Further, the relationship between the pore dimension and the grain dimension could be expressed by the relation

$$d_p = \frac{d_g \phi}{1 - \phi} \tag{5.4-5}$$

Using the pore dimension, the Reynolds number can be expressed by

$$Re_p = \frac{v_p d_p \rho}{\mu} \tag{5.4-6}$$

or

$$Re_p = \frac{v_m d_g \rho}{\mu (1-\phi)} \qquad (5.4\text{-}7)$$

where $v_m = Q / A$.

Alternatively, based on the grain dimension, it can be shown that

$$Re_g = \frac{v_m d_g \rho}{\mu \phi} \qquad (5.4\text{-}8)$$

Stewart et al [18] have used a 'pseudo' Reynolds number to determine the transition fom laminar flow. From one of the figures in their paper the deviation from laminar flow could be seen to have occured at a flow rate of less than 0.4 cc/s for a core sample of permeability 25 md.

From a review of the published work, it seems that the best way for defining the Reynolds number would be

$$Re = \frac{\rho v d}{\mu} = \frac{\rho Q d}{\mu A \phi} \qquad (5.4\text{-}9)$$

where $d = \beta / \alpha = \beta k$

although, as mentioned earlier, experimental measurements reveal that the above definition of d may not be physically plausible.

5.4.3 An alternative approach

An alternative method of deriving the friction factor charts is to use the integrated form of the Forchheimer equation, which can be written as

$$\frac{M(P_1^2 - P_2^2) k}{2 Z R T \mu L U_m} = 1 + \frac{\beta U_m k}{\mu} \qquad (5.4\text{-}10)$$

where $U_m = W / A$ = mass velocity.

The density of gas at mean pressure is given by the relation

$$\rho = \frac{(P_1 - P_2)\, M}{2 Z R T} \qquad (5.4\text{-}11)$$

Substituting Eq.5.4-11 into 10 we get

$$\frac{\rho (-\Delta P)}{\beta L U_m^2} = 1 + \frac{1}{\beta k U_m / \mu} \qquad (5.4\text{-}12)$$

where $\Delta P = (P_2 - P_1)$.

The second term on the right hand side has the form of a Reynolds number which is characteristic of flow through porous media, while the left hand side represents [19] a so-called Darcy number, Da.

$$Re = \frac{\beta U_m k}{\mu} = \frac{\beta k \rho v}{\mu} = \frac{D \rho v}{\mu} \qquad (5.4\text{-}13)$$

where the quantity $D = \beta k$ is the equivalent of some length dimension of the porous matrix, and the Darcy number, Da, is

$$-Da = \frac{M(P_1^2 - P_2^2) k}{2 Z R T \mu L U_m}$$

$$= \frac{\rho (-\Delta P) k}{\mu L U_m} \qquad (5.4\text{-}14)$$

Eq.(5.4-12) could also be rewritten in terms of two non-dimensional numbers

$$-\frac{Da}{Re} = 1 + \frac{1}{Re} \qquad (5.4\text{-}15)$$

The quantity -Da / Re represents a friction factor f so that Eq.(5.4-15) becomes

$$f = 1 + \frac{1}{Re} \qquad (5.4\text{-}16)$$

where

$$f = \frac{\rho (-\Delta P)}{\beta L U_m^2} \quad \text{and} \quad Re = \frac{\beta k U_m}{\mu} \qquad (5.4\text{-}17)$$

A logarithmic plot of friction factor against Reynolds number for consolidated porous media has been given be Cornell & Katz [16] which is shown in Fig. 5.2. It can be seen that if Re is defined as in Eq.(5.4-17) then a single curve is adequate to fit the entire set of data. Also, for small values of Re (small mass velocity), $1 / Re >> 1$, so that

$f = 1/Re$ (Darcy flow)

or $\log f = -\log Re$

For Darcy flow where inertial effects are insignificant, slope of the graph is -1. Departure from the unit slope would signify the Re when inertial effects can no longer be neglected.

TABLE 5.1

Various definitions of Reynolds number and friction factor used in the literature

Author	Media	Fluid	Permeability Porosity	Diameter in Reynolds No.	Friction factor	Inertial region Re	Comments
Fancher & Lewis (1933)	consolidated & unconsolidated	water	12 - 38 %	$\sqrt{\frac{\Sigma n\, d^2}{\Sigma n}}$	$\frac{g\, d\, (\Delta P)}{2 \rho L u^2}$	1.0 - 1000	different f.f. curves for different types of consolidated media
Green & Duwez (1951)	Sintered metals	gas	26 - 46 %	βk	$\frac{\Delta(P)^2\, g\, M}{LZRT\beta G^2}$	0.1 - 50	samples used were iron, stainless steel, porex plugs etc.
Ergun (1952)	glass beads, coal, coke, etc.	gas	not available	particle diameter D_p	$\frac{\phi^3}{1-\phi}\frac{g D_p}{\rho u^2}\frac{\Delta P}{L}$	5 - 4000	plots make use of micro - velocity in the Re, defined as $(\rho u D_p) / \mu(1-\phi)$
Cornell & Katz (1953)	consolidated rocks	gas	1.0 - 508 md 8.0 - 22.8 %	βk	$\frac{64\,(1/\beta)\,\rho\,\Delta P}{L\,G^2}$	0.1 - 20	introduced 'tortuosity' constant into the definition of Re and friction factor
Tek (1957)	consolidated sands	air & water	139 - 3400 md 12 - 29 %	$\sqrt{\frac{\Sigma n\, d^3}{\Sigma n}}$	$\frac{d\,(\Delta P)}{2 \rho u^2 L}$	> 1.0	also finds different curves for various types of media.
Greenberg & Weger (1960)	sintered metals	gas	35 - 2500 md	βk	$\frac{\Delta(P^2)\, M}{2LZRT\mu G}$	0.6 - 60	also measured effect of temperature on the β factor
Ward (1964)	glass beads & unconsolidated	water	58 - 1.8 x 10^5 D	$\sqrt{k}$	$\frac{\sqrt{k}\,\Delta P}{\rho u^2 L}$	0.2 - 100	media used : glass beads, activated charcoal, gravel, resin
Blick (1966)	metals, unconsolidated sands	gas	28 - 48 %	average pore diameter δ	$\frac{\Delta(P)^2 M\, \delta\phi^2}{2LG^2ZRT}$	1 - 2000	plot based on data mostly from other workers
Ahmed & Sunada (1969)	unconsolidated sands, glass beads	water	82 md - 230 D	βk	$\frac{\Delta(P)^2\, M}{2LZRT\beta G^2}$	0.05 - 10	data collected from 8 different sources
McFarland & Dranchuk (1976)	glass beads	water	.9 - 3.6 x 10^5 D 39 - 48 %	$\beta . D_p$	1 + 1/Re	0.1 - 10	used a birefringence visualization method to observe transition to turbulence
Fand et al (1987)	glass beads	water	34 - 36 %	particle diameter d	-	5 - 80	plotted pressure gradient directly against Reynolds number

5.5 EXPERIMENTAL OBSERVATIONS

An alternative to using the Reynolds number is to use the Darcys law directly to determine the flow rate for the onset of deviation. Since the absolute permeability is a constant, and (μ Z) is approximately constant for the low pressures used in most experiments, then a plot of the pressure drop against flow rate should yield a straight line passing through the origin. The deviation from this line will indicate the departure from Darcys law. The flow rate at which this departure occurs would then be expected to be a unique value depending on the pore structure of the media, for the particular fluid used. A typical pressure drop - flow rate plot is shown in Fig 5.3. The plot confirms our expection and the departure from the straight line is observed as the flow rate increases. In comparing the flow rate at which departure occurs with the Klinkenberg plots it was found that the departure occurs much earlier than expected. It should be noted that Darcys law as expressed in Eq.(4.2-5) cannot be used directly since the 'permeability' is actually not the absolute value but an apparant value affected by slippage at low pressures. It is possible to account for this slippage [21] by substituting the Klinkenberg equation into the Darcy's equation, which then becomes

$$Q_o = \frac{k A}{2 \mu Z P_o L} (1 + b / P_m) (P_1^2 - P_2^2) \qquad (5.5\text{-}1)$$

The permeability in the above equation is now the absolute value and would be a constant. According to this modified Darcy's law, a plot of $(1+b / P_m) (\Delta P^2)$ against the flow rate would yield a straight line passing through the origin. This was indeed found to be the case as shown in Fig 5.4. Departure from the straight line was also found to occur at a much higher flow rate this time, suggesting that slippage and inertial effect can co-exist within a certain range of flow rate and mean pressure. The delay in the departure from the straight line was generally found to be much higher for lower permeability plugs - sometimes by upto 20 times higher. For a core plug of permeability about 100md (sample LE249), inclusion of the slippage correction term in Eq.(5.5-1) changed the critical flow rate by only about 5%. This seems to be reasonable since slippage is more prominent in low permeability rocks. The Klinkenberg slippage "correction factor", b, were calculated from the gradients of the Klinkenberg plots according to Eq. (4.2-2).

Using this type of plot the onset of deviation from Darcys law was found for a number of the core plugs and they are reported in Table 5.2. The flow rates at the onset of deviation from Darcy's law - the "critical" flow rate - have been found to be related to the permeability of the rock sample. A plot of the flow rates versus permeability is shown in Fig 5.5. The scatter in the data show that in addition to permeability there are also other pore structural parameters controlling the onset of deviation. The plot suggests that the critical flow velocity is a unique

value for the medium and for the particular fluid used. A better correlation is achieved (see Fig. 5.6) when the critical flow velocities are plotted against $\sqrt{(k / \phi)}$ since this parameter provides a better characterisation of the pore structure.

5.6 DISCUSSION

If the deviation from Darcy's law is assumed to take place at a Reynolds number of one (as is often done in the literature), then the critical flow rate for deviation from Darcy's law can be predicted directly from the definition of Reynolds number :

$$Q = A \phi \mu / \rho d$$

where

$$d = \beta k$$

The predicted and the observed flow rates are given in Table 5.3. The calculated critical flow velocities are generally found to be much larger than the experimentally observed values - sometimes by as much as two order of magnitude. The difference between the observed and the calculated values generally increase as the permeability of the sample decrease. This suggests that for rocks of moderate permeability (10-100 md) the critical Reynolds number could be around 1. For rocks of lower permeability (1-10 md) the critical Re could be around 0.1 and for rocks with permeability in the range 0.1- 1md, the critical Re is around 0.05. As permeability decreases, the pore structure also tend to become more complicated, eg. due to the growth of authigenic clays. This will therefore help to bring the nonlinear mode of flow much earlier than for high permeability cores.

At a given scale of observation it is reasonable to expect that as the permeability of a rock increases so its mean pore size will also increase and so the length parameter, d ($= \beta / \alpha$), in Reynolds number as defined by Green & Duwez [15] will also become larger. Values of d were calculated for a number of samples and plotted against their permeability to check this hypothesis (see Fig 5.7). The data has a wide scatter but the trend is obvious. The plot in fact shows that the characteristic length, d, decreases with increasing permeability, which is contrary to expectation. This therefore brings into question the validity of using the definition proposed by Green et al. The above discussion shows that there is no simple or unique way of defining a suitable length parameter which will characterise a porous medium and could be used in the Reynolds number. It seem that the best way of finding the transitional flow rate is to plot the flow data according to Eq.(5.5-1).

There is plenty of evidence in the literature to suggest that the Reynolds number is strongly influenced by the pore structure of the media. Fancher et al [7] studied the deviation from Darcy's law at high rates by a series of systematic experiments and found that for unconsolidated sands, a plot of the Fanning Friction factor vs. Reynolds number can be used to

draw a single line for all the data points. However for consolidated media, a definite line was observed for each media. They explained that this was due to the smallness of d in a consolidated media, and also due to the amount and arrangement of cementing materials and the degree of angularity of sand grains. Of these they found from experiments that the amount and arrangement of cementing materials was the most significant.

McFarland and Dranchuk [10] have carried out experiments using glass bead packs to observe the transition from laminar to fully turbulent flow. They used packs with bead diameters of 0.25 and 0.5 inches and the packings were of cubic and orthorhombic type. Their results show that the Reynolds number for the transition to turbulence changes 10 folds if the packing arrangement is changed and by 20 folds if the diameter is also changed. This work therefore leads us to conclude that the Reynolds number is indeed a function of the pore structure.

Blick [4] has also carried out some experimental work and suggests that the slight discrepency between his proposed theory and his experimental observations is due to the way in which mean pore diameter is defined and measured. He suggests that incorporation of pore size distribution data from capillary pressure curves might be the path to an improved description. Others [22,23] have had to use various pore 'shape factors' for describing flow through porous media. It is however not possible to measure these shape factors by any direct means.

TABLE 5.2

Flow rate data

Sample	k (md)	ϕ (%)	β k (μm)	$\sqrt{k/\phi}$ (md)	Flow rate (cc/s)	Modified (cc/s)	Velocity (cm/s)
M11001	59.0	20.76	71.23	16.86	3.5	17.0	3.41
M11002	2.18	13.82	1080.	3.97	0.35	3.2	0.64
M11005	0.98	10.19	4210.	3.10	0.15	1.0	0.20
M11008	1.23	12.74	972.	3.11	0.3	0.6	0.12
LE253	0.41	7.43	106.6	2.35	0.16	0.65	0.13
LE718	0.041	6.83	382.6	0.77	0.042	0.065	0.013
LE728	0.26	11.39	722.3	1.51	0.14	0.35	0.07
RH94	2.21	12.17	125.4	4.26	0.19	1.4	0.28
RH97	17	16.92	112.7	10.02	1.10	5.0	1.0
RH99	5.9	14.90	142.8	6.29	0.80	3.5	0.70
RH101	0.14	5.87	3642.4	1.54	0.03	0.07	0.014
RH103	0.23	9.96	852.7	1.52	0.052	0.40	0.08
M73001	0.064	12.31	9010	0.71	0.01	0.10	0.02
M73002	0.10	11.50	5880	0.94	0.015	0.11	0.02
M73003	0.46	10.01	1320	2.14	0.025	0.30	0.06
M73004	0.51	11.0	1240	2.16	0.03	0.65	0.13
M73005	33.0	21.0	56.7	12.54	0.55	10.0	2.0
M73006	15.2	20.5	58.9	8.61	0.35	9.0	1.8
M73007	10.5	20.9	69.9	7.09	0.25	4.0	0.8
M73008	13.0	23.9	46.5	7.37	0.5	8.5	1.7
M73009	32.5	25.6	28.4	11.27	0.95	15.0	3.0
M73012	28.4	19.6	59.9	12.04	0.90	8.5	1.7
M73013	20.8	19.01	56.2	10.46	0.45	8.0	1.6

TABLE 5.3
Reynolds number at critical velocities

Sample	permeability (md)	Critical Velocities (cm/s) observed	calculated @ Re = 1	Re
M11001	59.0	3.41	8.57	0.40
M11002	2.18	0.64	0.56	1.14
M11005	0.98	0.20	0.14	1.43
M11008	1.23	0.12	0.63	0.19
LE253	0.41	0.13	5.73	0.023
LE718	0.041	0.013	1.60	.0081
LE728	0.26	0.07	0.85	0.083
RH94	2.21	0.28	4.87	0.057
RH97	17.0	1.0	5.42	0.18
RH99	5.9	0.70	4.28	0.16
RH101	0.14	0.014	0.17	0.083
RH103	0.23	0.08	0.72	0.11
M73001	0.064	0.02	0.068	0.29
M73002	0.012	0.02	0.10	0.19
M73003	0.46	0.06	0.46	0.13
M73004	0.515	0.13	0.49	0.26
M73005	33.0	2.0	10.77	0.19
M73006	15.2	1.8	10.37	0.17
M73007	10.5	0.8	8.74	0.091
M73008	13.0	1.7	13.13	0.13
M73009	32.5	3.0	21.50	0.14
M73012	28.4	1.7	10.19	0.17
M73013	13.0	1.6	10.87	0.15

5.7 A NUMERICAL SOLUTION OF FORCHHEIMER EQUATION

5.7.1 Introduction

The Forchheimer equation is the most widely used relationship for describing high velocity flow in porous media. It may be expressed as

$$-\frac{dP}{dx} = \frac{\mu v}{k} + \beta \rho v^2 \qquad (5.7\text{-}1)$$

For gas flow however, this relation is not strictly true due to compressibility of the fluid. It is therefore necessary to use mass flow rate W instead of volumetric flow rate v. After appropiate substitution, (see section 4.3) integration of the Forchheimer equation will give :

$$\frac{M(P_1^2 - P_2^2)}{2Z R T \mu L (W/A)} = \frac{W}{A\mu}\beta + \frac{1}{k} \qquad (5.7\text{-}2)$$

The above equation is generally used to obtain the inertial coefficient by plotting the left hand side of Eq.(5.7-2) against (W / Aμ). This yields a straight line with β as the gradient, and k as the inverse of the intercept.

The main disadvantage in using Eq.(5.7-2) is that it is necessary to carry out a series of accurate measurements at increasingly high rate of flow to enable proper fit of a straight line. Accurate measurement of high flow rate can become very difficult. Using the numerical approach described below it is possible either to obtain the value of β from only one set of pressure drop - flow rate measurement or if the value of β is already known, to calculate the pressure profile accurately.

5.7.2 Numerical Approach

The conservation of mass may be expressed as

$$\rho \frac{\partial v}{\partial t} - \nabla(\rho v) = 0 \qquad (5.7\text{-}3)$$

For a steady, one dimensional flow this becomes

$$-\frac{d}{dx}(\rho v) = 0 \qquad (5.7\text{-}4)$$

To solve the Forchheimer equation numerically, we first rearrange (5.7-1) as follows:

$$-\frac{dP}{dx} = v\left[\mu/k + \beta \rho v\right] \qquad (5.7\text{-}5)$$

or

$$v = - \frac{k}{\mu + \beta \rho k v} \frac{dP}{dx} \tag{5.7-6}$$

where v is the volumetric flow rate across the cross section per unit time, ie. a velocity term. Substituting Eq.5.7-6 into 4 we get

$$\frac{d}{dx} \left[\frac{\rho k}{\mu + \beta \rho k v} \frac{dP}{dx} \right] = 0 \tag{5.7-7}$$

or

$$\frac{d}{dx} \left(C \frac{dP}{dx} \right) = 0 \tag{5.7-8}$$

where C is the transmissibility term [27], defined as

$$C = \frac{\rho k}{\mu + \beta \rho k v} \tag{5.7-9}$$

The above equation (5.7-8) is non-linear since the term C depends on pressure and cannot be solved analytically. The equation can however be linearised and solved numerically if it is assumed that C remains constant for a small increment of dP. The equation can then be written as

$$C \frac{d^2 P}{d x^2} = 0 \tag{5.7-10}$$

The above equation can now be solved using finite difference method as discussed below.

5.7.3 Solution Procedure

The pressure equation given above (5.7-10) can be discretised using a finite difference scheme. The equation can be written as

$$\left[C_i \frac{(P_{i-1} - P_i)}{\Delta x} - C_{i+1} \frac{(P_i - P_{i+1})}{\Delta x} \right] \frac{1}{\Delta x} = 0 \tag{5.7-11}$$

The coefficient C_i is evaluated at a pressure which is the arithmetic average of P_i and P_{i+1}. Ignoring the Δx terms in Eq.(5.7-11) and rearranging, we can express it simply as

$$C_i P_{i-1} - (C_i + C_{i+1}) P_i + C_{i+1} P_{i+1} = 0 \tag{5.7-12}$$

This is then the final version of the finite difference form of the original equation which has to be solved with the appropiate boundary conditions. To start the calculation, the pressure profile is assumed to be linear. The iterations are continued until the downstream end point pressure P_n for two consecutive iterations are found to be less than 10^{-6}.

Boundary Conditions

The solution of a second order differential equation requires at least two boundary conditions to be specified [28,29]. A number of solutions to the problem can be obtained depending on the boundary conditions. Here three cases are given:

(i) If the pressures at the two extreme boundaries are specified for the one dimensional flow, the solution of Eq.(5.7-10) poses no difficulty at all when expressed in the form of Eq.(5.7-12). This equation would then give n equations for n unknowns. The tridiagonal matrix thus formed can be solved by any of the traditional methods (eg. Thomas algorithm). The pressure profile at a particular flow rate for a core plug with a known value of inertial coefficient is shown in Fig.5.6.

(ii) The problem can also be solved if only the upstream pressure is specified. The object would then be to predict the downstream pressure for a given value of inertial coefficient at a particular flow rate.

Besides the upstream pressure, it is necessary to specify another boundary condition. This can be given in the form of a first derivative of the pressure, ie. the Forchheimer equation itself. In finite difference form this can be written as :

$$\frac{(P_{i-1} - P_{i+1})}{2\Delta x} = \frac{\mu v}{k} + \beta \rho v^2 \qquad (5.7\text{-}13)$$

where P_{i+1} is an imaginary pressure, the value of which can be calculated from

$$P_{i+1} = P_{i-1} - 2\Delta x B \qquad (5.7\text{-}14)$$

where

$$B = \frac{\mu v}{k} + \beta \rho v^2 \qquad (5.7\text{-}15)$$

The value of β is evaluated at either of the end points.

An example with this type of boundary condition is shown an Fig 5.2. The predicted downstream pressure is within 1% of the value observed experimentally.

(iii) If the value of the inertial coefficient is unknown and only the upstream pressure and the gradient is given, then the problem is essentially similar to he one above. In this case an approximate value of the inertial coefficient is first obtained using an empirical correlation. The pressure at the downstream end is then calculated by the method outlined in (ii) above. If this pressure is found to be different from the measured pressure then the value of the inertial coefficient is changed and the downstream pressure recalculated. This process is repeated by changing the value of the inertial coefficient in small increments until the calculated downstream pressure matches the experimentally observed value.

5.7.4 Discussion

The validity of the method outlined above was checked by comparision with results obtained experimentally on a core sample with known properties. The relevant data are given in Table 5.3. The results are shown in Table 5.5 and also on Figure 5.8.

The straight line in Fig 5.8 is the pressure drop as would be expected from Darcy's law, ie pressure dropping linearly with distance for a constant flow rate. The iterations were started by using this linear profile. The final pressure profile obtained is almost parabolic in shape. This is to be expected from the non-linear nature of gas flow at high velocity.

As mentioned above in (ii), the gradient can be specified at either of the ends. It was found that if the gradient was specified at the upstream end, the downstream pressure then had an error of 3%, whereas if it was specified at the downstream end then the error was reduced to only 1%.

Runs were also performed to look at the sensitivity of β on the predicted downstream pressure. Results of these are given in Table 5.7 and also shown in Fig.5.8 with broken lines for the 10% change of β.

TABLE 5.4
Data for Numerical Calculation

SAMPLE M73012

Permeability	=	31.75	md
Porosity	=	19.60	%
Beta	=	20.60	cm^{-1}
Length	=	4.6	cm
Area	=	4.99	cm^2
Flow rate	=	33.11	cm^3/s
Velocity	=	6.64	cm/s
P (upstream)	=	6.89	atm (101.22 psi)
P (downstream)	=	1.80	atm (26.48 psi)

TABLE 5.5
Sensitivity of β on calculated pressures

Boundary position	Beta (cm^{-1})	Change (%)	Predicted pressure (atm)	Difference (%)
Downstream	20.60	-	1.79	-0.73
Upstream	20.60	-	1.75	-2.84
Downstream	22.66	+10	1.50	-16.79
"	18.54	-10	2.04	+13.32
"	25.75	+25	0.99	-44.81
"	15.45	-25	2.37	+31.76

REFERENCES

1. Kutilek, M.: Non-Darcian flow of water in soils - laminar region, Proc. of the 1st IAHR Symp. on *Fundamentals of Transport Phenomena in Porous Media,* IAHR Elsevier, Amsterdam (1972) p.327.
2. Bear, J. : *Dynamics of Fluids in Porous Media,* American Elsevier, N.Y. (1972).
3. Dybbs, A. and Edwards, R.V. : A new look at porous media fluid mechanics -Darcy to turbulent, in *Fundamentals of Transport in Porous Media,* (Eds.: J. Bear and M.Y. Corapcioglu), Martinus Nijhoff, NATO-ASI, Series E, No.82, (1984) pp.201-256.
4. Bird, R.B., Stewart, W.E. and Lightfoot, E.B.: *Transport Phenomena,* J. Wiley & Sons, New York, 1960, Section 6.4.
5. Ergun, S. : Fluid flow through packed columns,*Chem. Eng. Prog.* (1952) **48**, 93.
6. Tek, M.R. : Developement of a generalised Darcy equation, *Trans. AIME* (1957) **207**, pp.376.
7. Fancher, G.H. and Lewis, J.A.: Flow of simple fluids through porous materials, *Ind. Eng. Chem.* (1933), **25**(10), 1139.
8. Ward, J.C. : Turbulent flow in porous media, *J. Hydrau.* Div., Proc ASCE (Sept 1964), 1-12.
9. Ahmed, N. and Sunada, D.K.: Non-linear flow in porous media, *J. Hydrau.* Div., Proc ASCE, (1969) **95**, 1847.
10. McFarland, J.D. and Dranchuk, P.M. : Visualisation of the transition to turbulent flow in porous media, *J. Can. Pet. Tech.* (April 1976), 71-78.
11. Brownell, L.E. and Katz, D.L.: Flow of fluids through porous media, *Chem. Eng. Prog.* (1947) **43**, 537.
12. Muskat, M. : *The Flow of Homogeneous Fluids through Porous Media,* McGraw Hill Book Co., New York, (1937).
13. Elenbaas, J.R. and Katz D.L.: A radial turbulent flow formula, *Trans. AIME* (1947) **174**, 25-40.
14. Collins, R.E.: *Flow of Fluids through Porous Media,* Reinhold Publishing Co., New York (1961) p52.
15. Green, L. and Duwez, P.J.: Fluid flow through porous metals, *J. Appl. Mech.* (1951) **18**, pp. 39.
16. Cornell, D. and Katz, D.L.: Flow of gases through consolidated porous media, *Ind. Eng. Chem.* (1953) **45**, 2145.
17. Wright, D.E. : Nonlinear flow through granular media, *J. Hydrau.* Div., Proc ASCE (July 1968), 851-872.
18. Stewart, C.R. and Owens, W.W. : A laboratory study of laminar and turbulent flow in heterogeneous porosity limestone, *Trans. AIME,* (1958) **213**, 121.

19. Stutzman, L.F. and Thodos, G. : Adaptation of friction factors to flow of fluids through consolidated formations, *Trans. AIME* (1956) **207**, 352-355.
20. Geertsma, J., Croes, G.A. and Schwartz, N. : Theory of dimensionally scaled models of petroleum reservoirs, *Trans. AIME* , (1956) **206**, 178.
21. Dranchuk, P.M. and Kolada, L.J. : Interpretation of steady linear visco-inertial gas flow data, *J. Can. Pet. Tech.* (Jan. 1968) 36-40.
22. Klinkenberg, L.J. : The permeability of porous media to liquids and gases, *Drill. Prod. Prac.*, A.P.I. (1941) p.200.
23. Blick, E.F.: Capillary orifice model for high speed flow through porous media, *Ind. Eng. Chem.*, (1966) **5**, 90-94.
24. Irmay, S.: On the theoretical derivation of Darcy and Forchheimer formulas, *Trans. Amer. Geophys. Union* (1958), **39**(4), 702-707.
25. Houpert, A.: On the flow of gases in porous media, *Revue l'Inst Francaise Petrole* (1959) **14**, 1468.
26. Tek, M.R., Coats, K.H. and Katz, D.L. : The effect of turbulence on the flow of natural gas through porous reservoirs, *J. Pet. Tech.* (1962), 799-806.
27. Tariq, S.M. : Evaluation of flow characteristics of perforations including nonlinear effects with the finite element method, *SPE Prod. Engr. J.*, (May 1987) 104-112.
28. Aziz, K. and Settari, A. : *Petroleum Reservoir Simulation,* Applied Science Publishers, London (1979).
29. Carnahan, B., Luther, H.A. and Wilkes, J.O. : *Applied Numerical Methods,* J. Wiley & Sons Ltd, New York, (1969)

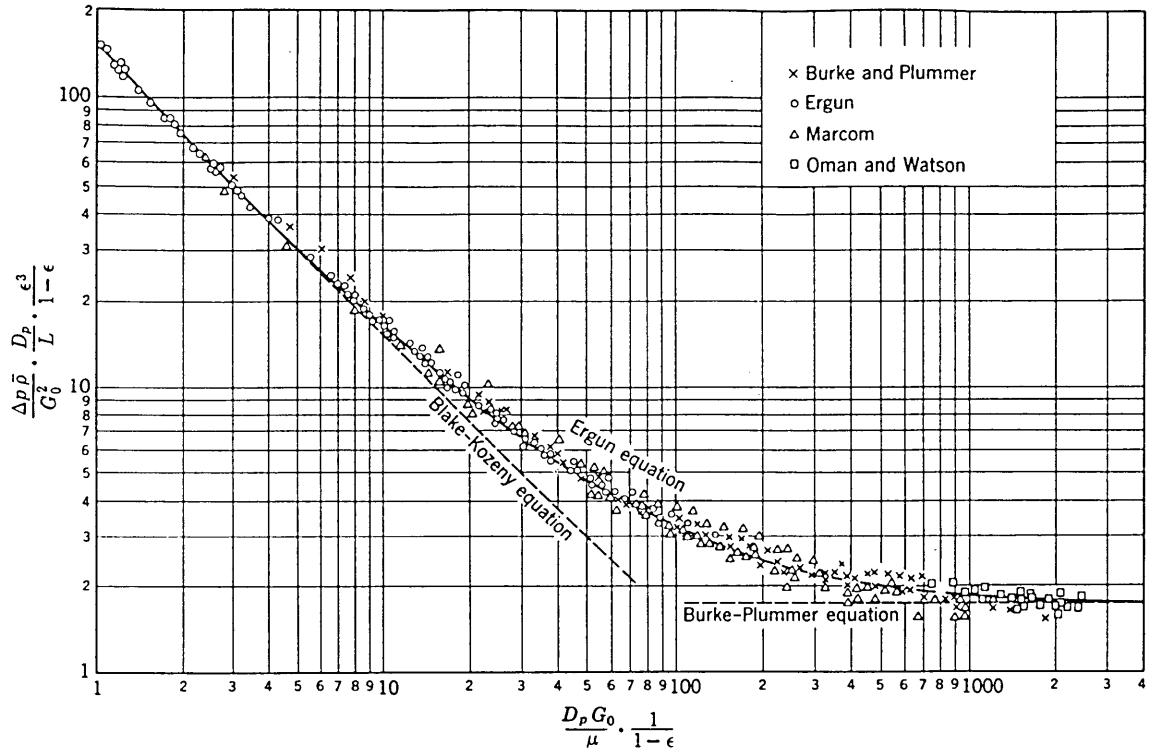


Fig. 5.1 A log-log plot of the Ergun equation (ref. 5)

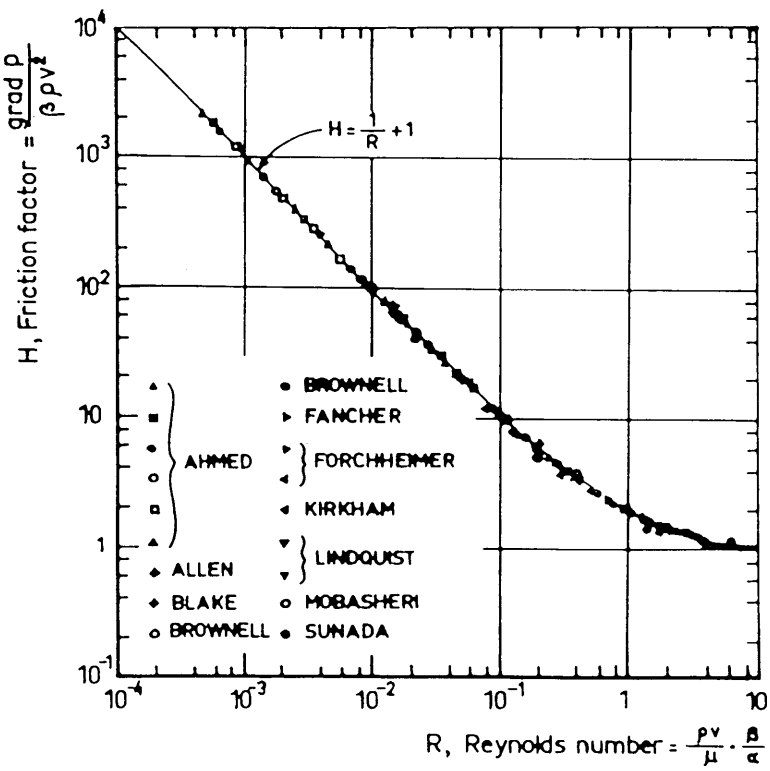
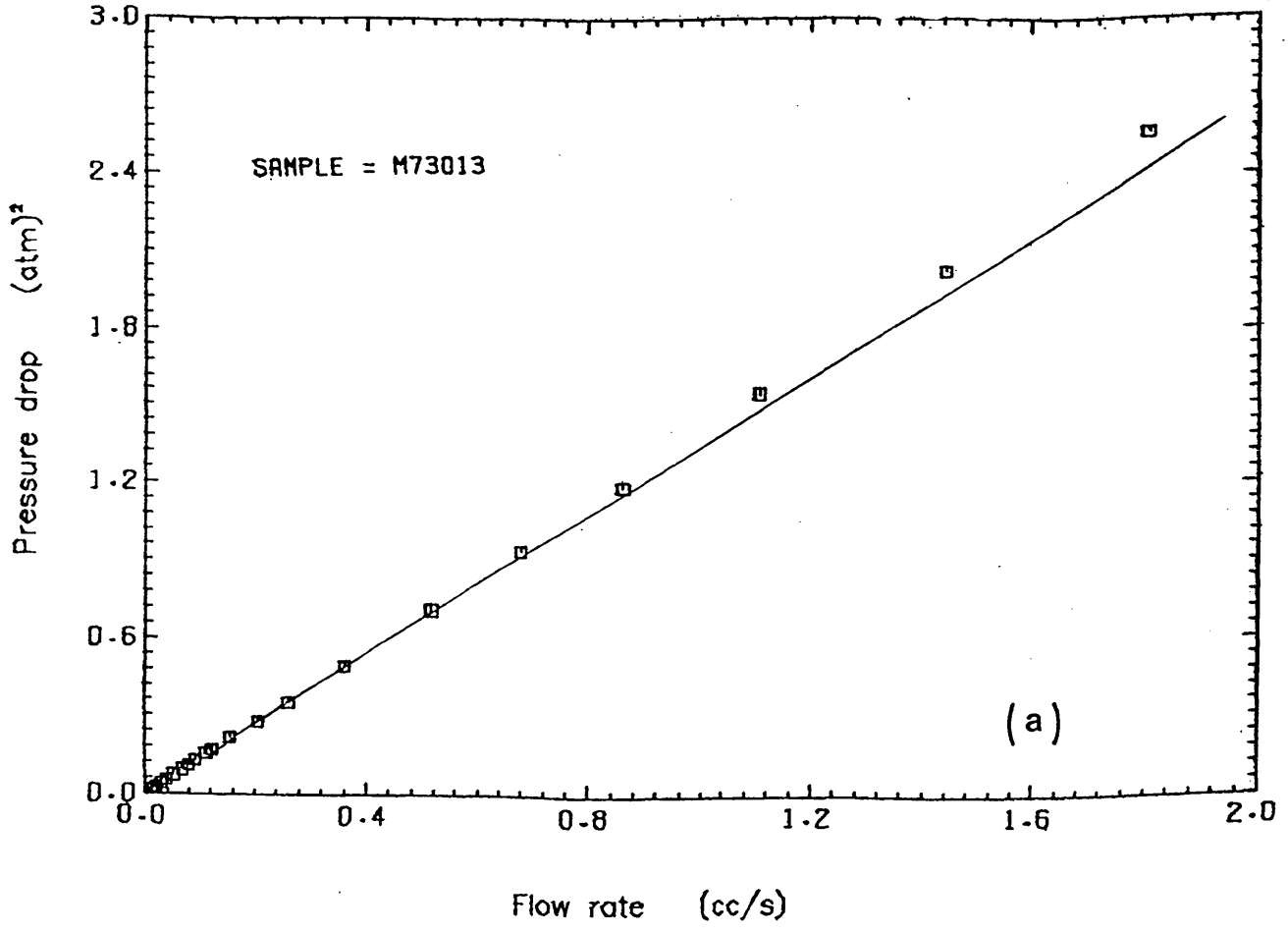


Fig. 5.2 Graphical correlation of friction factor against Reynolds number (ref.9)



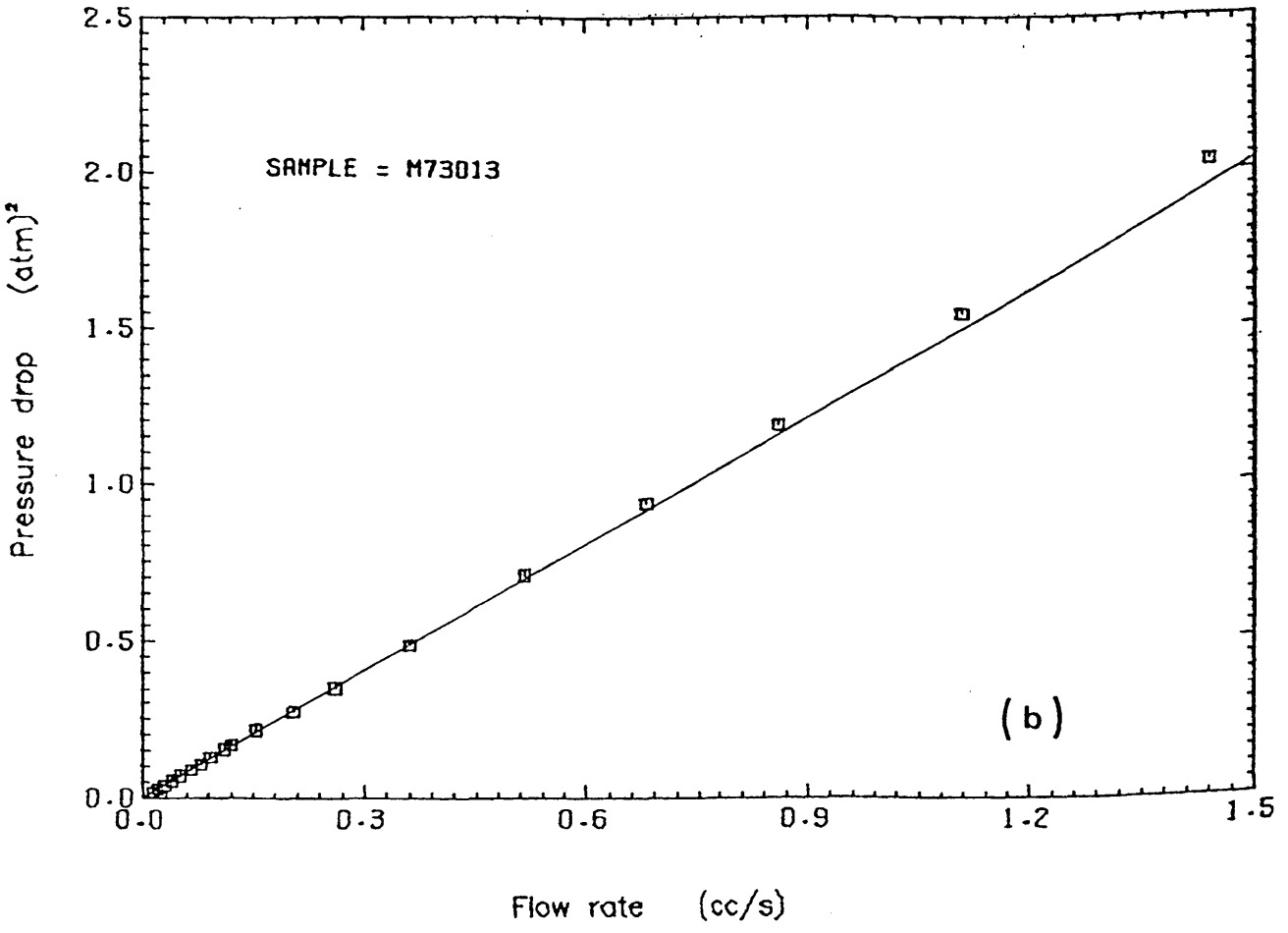
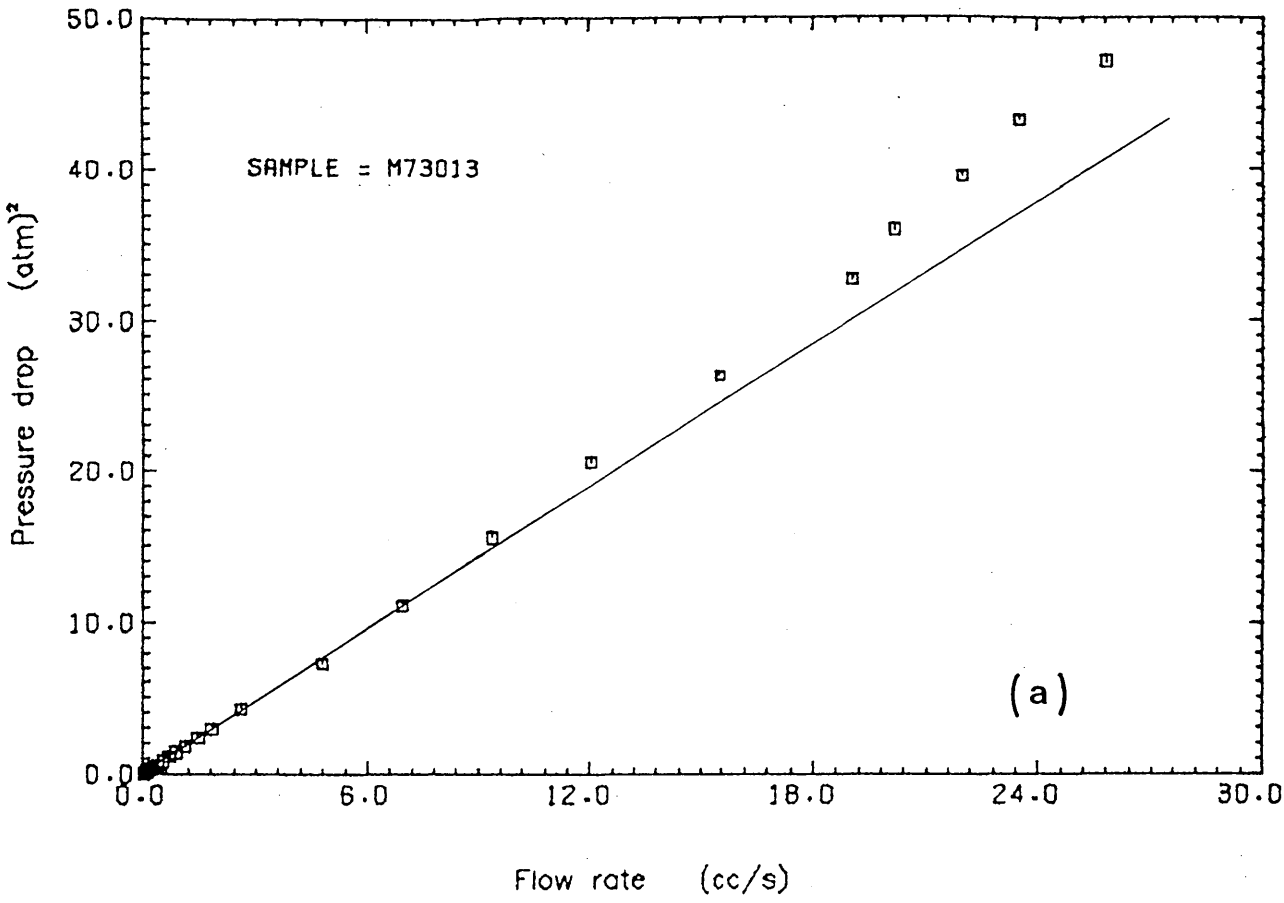


Fig 5.3 (a) Pressure drop squared (P_1^2-P_2^2) against volumetric flow rate. Sample M73013. (b) Enlarged view of the previous plot to show the critical flow rate.



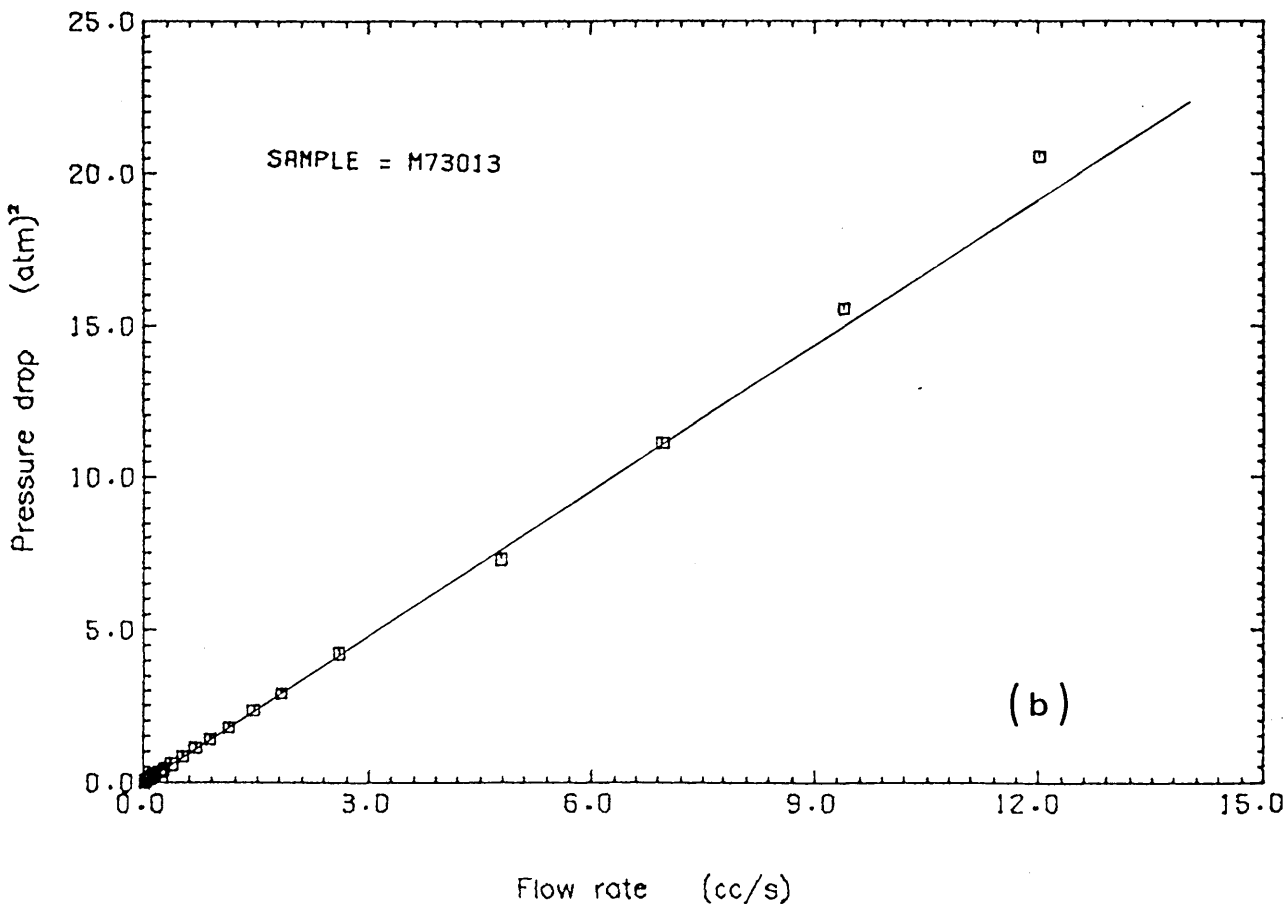


Fig 5.4 (a) Pressure drop modified to take account of slippage (see Eqn 5.5-1) against volumetric flow rate. Sample M73013. (b) Enlarged view of the previous plot.

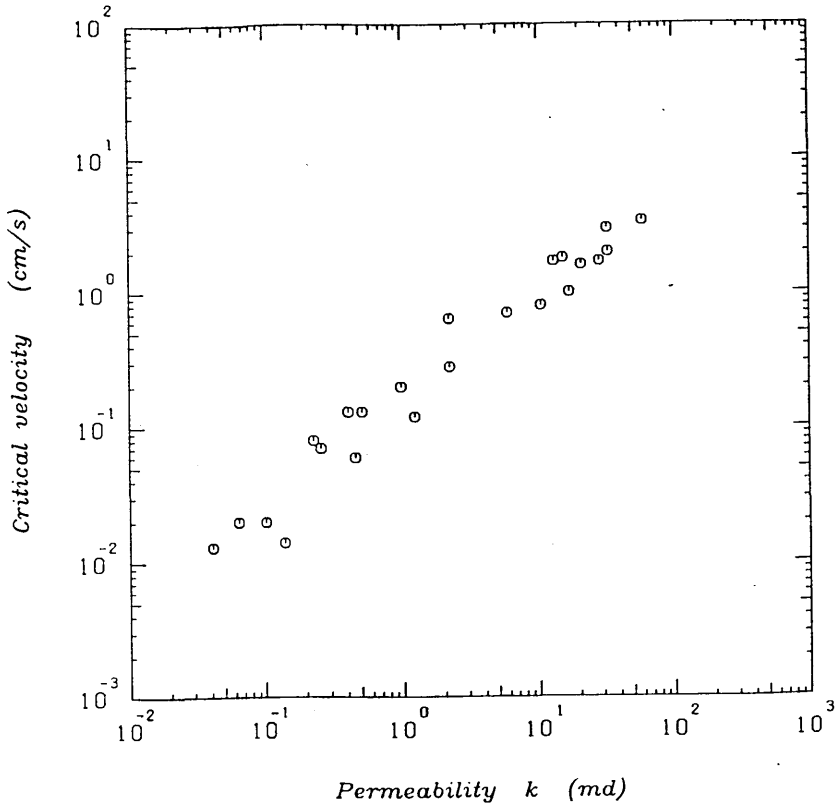


Fig 5.5 Critical flow velocity at the onset of deviation from Darcy's law against permeability.

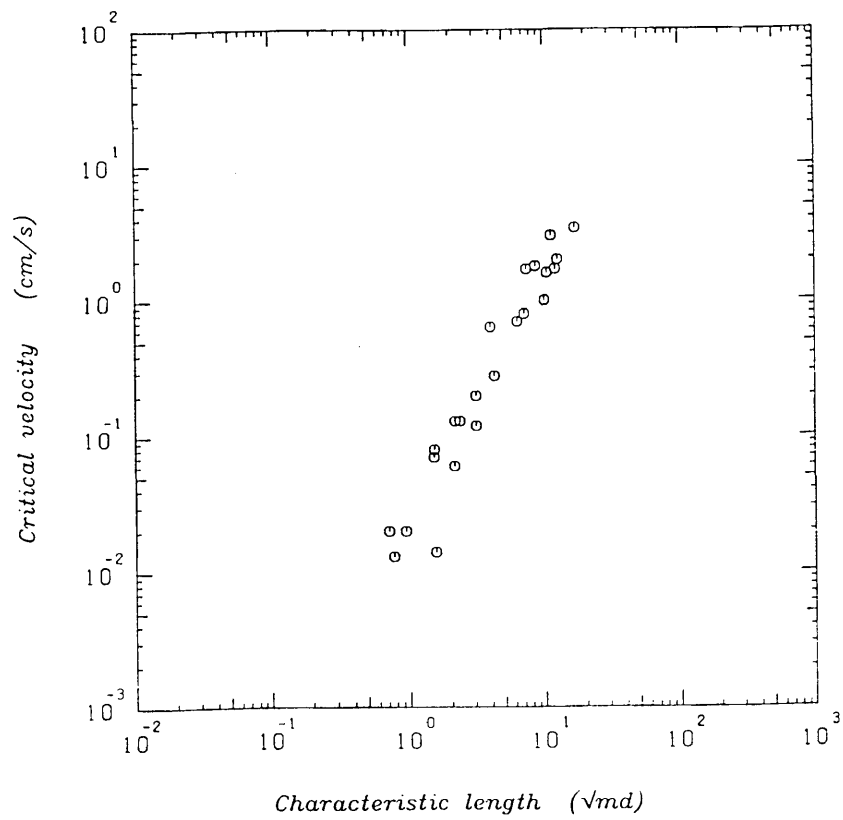


Fig 5.6 Critical flow velocity at the onset of deviation from Darcy's law against a characteristic length of the media $\sqrt{k / \phi}$.

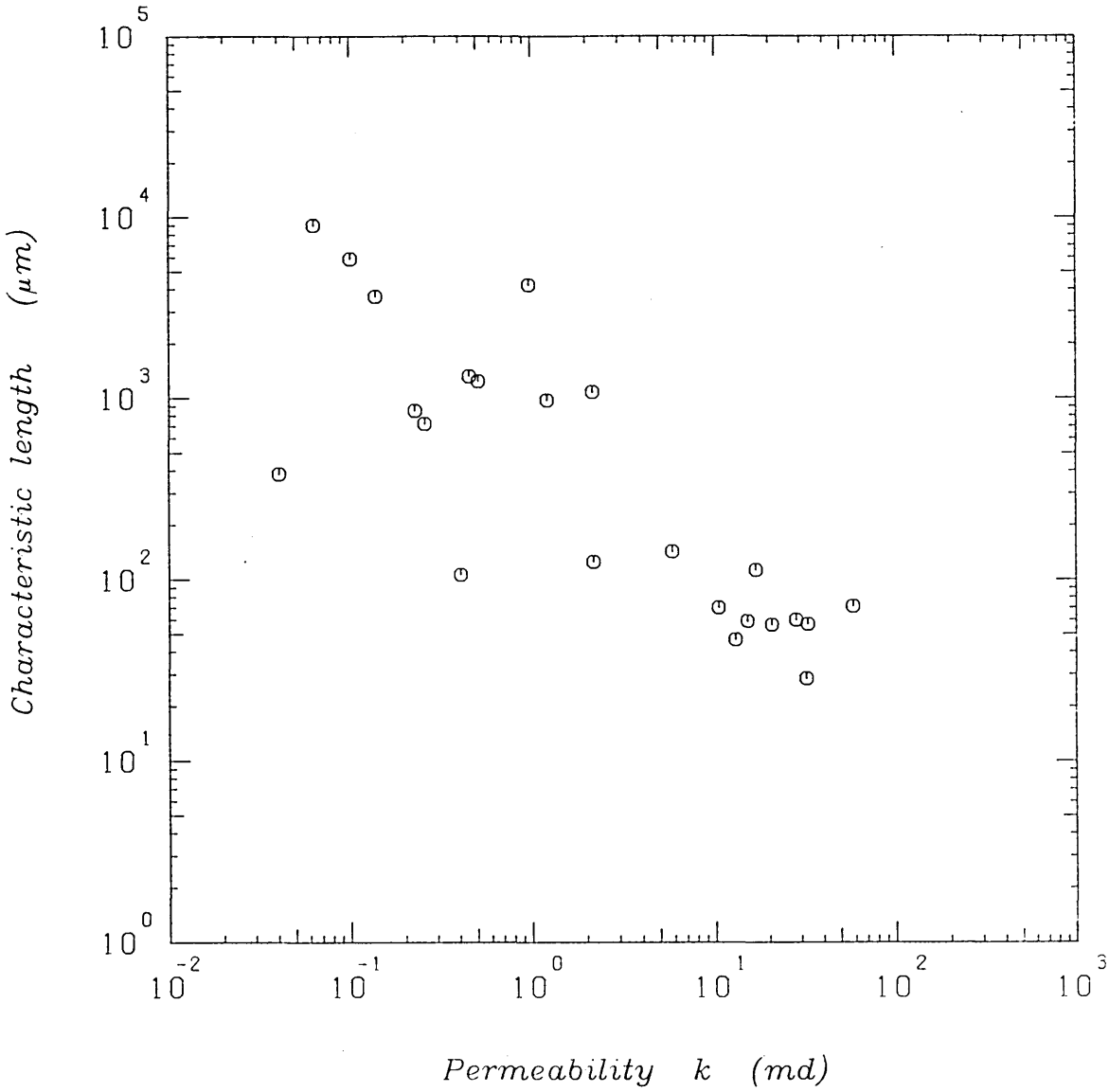


Fig 5.7 Inverse relationship between the characteristic length d = β k and permeability.

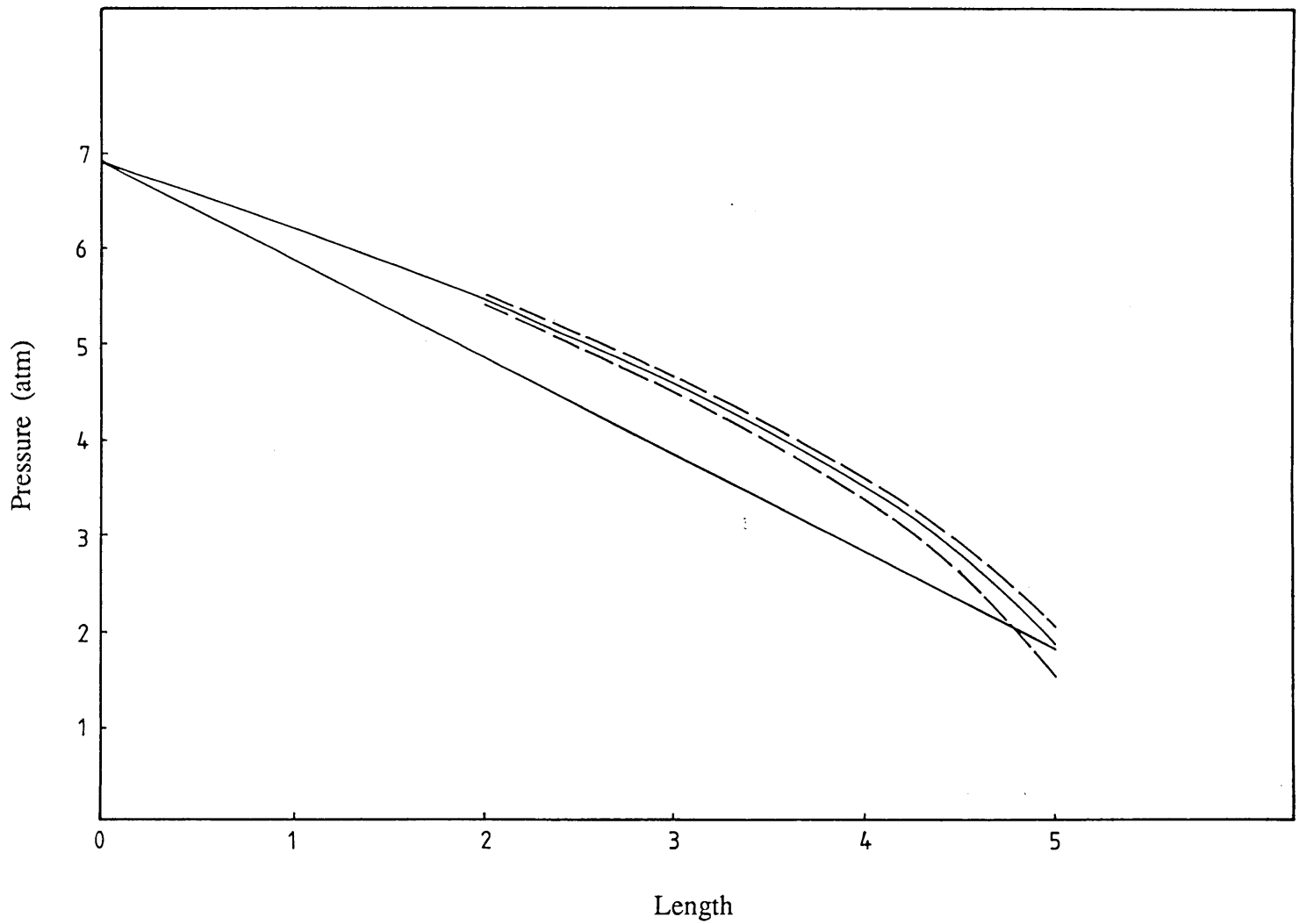


Fig. 5.8 Pressure gradient calculated using a numerical method. Broken lines were generated by changing the value of β by ± 10%.

Chapter 6

THE EFFECT OF PORE STRUCTURE ON HIGH VELOCITY GAS FLOW

6.1 INTRODUCTION

A number of correlations are available in the literature for predicting the value of inertial coefficient from porosity and permeability of the rock samples. However these correlations - often found from only a limited set of experimental data, are found in general to be inaccurate in representing the inertial coefficient. A plot of inertial coefficient against permeability shows a wide scatter (Fig 6.1). It can be observed that two different rock samples may have similar permeability but values of inertial coefficient may vary by up to one order of magnitude. The resistance to flow in both these samples at very low flow rates are obvioulsly similar but as the flow rate is increased the pressure gradient becomes quite different.

The limited accuracy of these correlations is due to the fact that only the bulk rock properties were considered [1,2] in the past. It is however beginning to be accepted that the differences in the bulk fluid flow behaviour between two rock samples can be explained only by looking at their pore structures in detail [3,4]. The present work was therefore carried out in an attempt to investigate the significant pore structural parameters which will control the non-Darcy flow at a microscopic scale.

6.2 INERTIAL EFFECT AND PORE STRUCTURE

In this section we shall explain the significance of pore structure on the value of the inertial coefficient is explained by first considering some idealized models of pore spaces and then by provision of some examples of real porous media. The importance of expansion/ contraction losses as well as streamline curvature on the inertial forces has already been discussed in Chapter 3. The discussion was however based on a fluid dynamics point of view. In this section the importance of pore structures is considered since it is the geometry of the pore spaces that will control the pattern of flow at a microscopic scale and ultimately the macroscopic scale.

6.2.1 Curvature of Streamlines

Inertial forces are present during any flow of fluids, even when the flow as a whole is steady and not changing direction. During flow through a straight pipeline at low rate, ie at low Reynolds number, the viscous forces are dominant and so the inertia term is usually ignored in the momentum balance equation. For flow through a porous medium the presence of a solid matrix ensures that fluid streamlines are never straight. The slightest degree of curvature in the path-line introduces acceleration of the fluid particles, hence inertia forces can become significant in the flow through porous media even at fairly low rates. Experimental measurements have shown [5] that in unconsolidated media the Darcy equation begins to fail at a

Reynolds number of about 1 and no turbulence was observed below Reynolds number of around 600.

Whenever fluid particles move in a curved path there will be a force acting radially on the fluid to provide an acceleration. Consider a capillary tube with radius of curvature r (Fig 6.2) carrying fluid with a velocity v. The equation of motion written in cylindrical coordinates [6] shows that centrifugal forces acting on unit volume is given is given by $\rho v_\theta^2 / r$. This is the effective force operating in the r-direction caused by the fluid motion in the θ - direction. A further term $\rho v_r v_\theta / r$ will also arise in the equation of motion, called the Coriolis force. This is an effective force in the θ-direction when there is fluid motion in both r and θ directions, which is applicable for changing cross-sectional area.

It can be seen that both centrifugal and Coriolis forces are dependent on the square of velocity and inversely related to the radius of curvature. The forces therefore become more prominent with a decrease in the radius, and the inertial coefficient would therefore be expected to be related to the grain size in a porous medium by

$$\beta \propto 1/r \tag{6.2-1}$$

It has been shown [5] that the permeability of an unconsolidated porous medium is related to the grain sizes by

$$k = N r^2 \tag{6.2-2}$$

where N is a dimensionless constant dependent on pore geometry. From the above relations we can conclude that the inertial coefficient would be related to the permeability of the medium by

$$\beta \propto 1/\sqrt{k} \tag{6.2–3}$$

The inverse relationship, derived using an intuitive argument here, is indeed found to be true from experimental measurements (Fig 6.1). The power of -0.5 on permeability (Eqn.6.2-3) however does not strictly hold due to the far greater complexity of a consolidated medium [3].

Increasing flow rate in a curved tube will also cause pressure variation in the radial direction. Flow separation can then take place both on the inner and outer side of the tube causing an adverse pressure gradient, unless the curvature of the bend is very large comrpared to the internal radius of the tube. Losses can also arise from secondary flow. This secondary flow produces a double spiral motion which increases the local velocity, and so losses due to friction are increased.

6.2.2 Aspect ratio

Fluids will always undergo excess pressure losses whenever there is a sudden change in the cross-section of the flow stream. It can easily be shown [6] that the pressure difference caused by sudden enlargement in a tube or capillary can be written, in terms of downstream velocity, v, as:

$$P_2 - P_1 = \rho v^2 \left[\left(\frac{d_2}{d_1} \right)^2 - 1 \right] \qquad (6.2\text{-}4)$$

where d_2 is the diameter of the enlarged section and d_1 the diameter of the narrower section. The ratio of the two diameters (d_2 / d_1) is usually known as the *aspect ratio*.

It should be noted that (a) the pressure actually rises in moving downstream and (b) pressure drop depends on the square of the flow rate and the ratio of diameters, ie the aspect ratio. It can also be shown that energy loss, E, due to the sudden expansion is given by:

$$E = \frac{1}{2} v^2 \left[\left(\frac{d_2}{d_1} \right)^2 - 1 \right]^2 \qquad (6.2\text{-}5)$$

Clearly, both Eqns. (6.2-4) and (6.2-5) are highly dependent on the aspect ratio; the energy loss being dependent on its fourth power. Similar terms could also be written for sudden contractions in the flow path.

Using a network of pores (see Fig 6.3) it can be shown that the porosity and permeability could be kept constant but at increasingly high flow rates the pressure gradient in the two system would be different due to differences in the aspect ratio.

It is useful to note that during non-Darcy flow, the pressure gradient is dependent on two length scales - diameter of both the wider and the narrow sections. During slow viscous (Darcy) flow, the pressure gradient and hence permeability, is controlled by the narrower sections only. This can be seen from the Poiseuille's law, which is applicable for low Re flow through a capillary, and may be written as :

$$\frac{\Delta P}{L} = \frac{8 \mu Q}{\pi r^4} \qquad (6.2\text{-}6)$$

The equation shows that the overall pressure gradient is related inversely to r^4. The gradient in the wider sections can therefore be neglected in comparision to that of the narrower ones since $1/(r_1)^4 >> 1/(r_2)^4$. This is thought to be one of the main reason why inertial coefficient is much more sensitive to pore structures than permeability. For increasing flow rate however the case is more complicated.

The Eqns. 6.2-4 and 5 have been arrived at using a number of simplifying assumptions. For a more rigorous analysis the full momentum balance equation would have to be solved numerically. This has already been attempted by, among others, Dullien and coworkers [7] for a straight periodically nonuniform capillary tube. Their work demonstrated that for low flow rates, Darcy's law could predict the pressure drop adequately and the quadratic term could be ignored. For higher rates of flow, the Forchheimer relation represented all their experimental data accurately. It was also found that the inertial term rapidly increased with an increase in the pore-to-throat size ratio. The excess viscous dissipation was however found to be related very weakly to the length of pores and throats. A variation of this method has been given by Stark (see chapter 2).

With increasing flow rate the total flow path length inside a pore which is connected through an asymmetric throat will become more complex and longer. This will cause changes in the direction of the streamlines causing extra pressure losses (see Fig 6.4). The flow equations could be solved numerically for this arrangement of pores and throats, although no attempts seem to have been made. An alternative arrangement is shown in Fig 6.5 which would be a more realistic representation of porous media - although perhaps more difficult to solve numerically. Fluid flowing through such an arrangement of pore spaces will encounter (a) losses due to expansion / contraction effect as well as (b) losses due to streamline curvature.

6.2.3 Coordination number

The coordination number for a porous media is usually defined as the average number of throats that connect with each pore. Various studies reported in the literature suggest that the average coordination number for sandstone rocks can vary from as low as 2 up to 15 or more.

It is well known [8-10] that in rocks with large coordination numbers, the recovery of non-wetting phase is high since higher coordination number favours displacement. It has been suggested that rocks of low permeability have low coordination number giving rise to high residual non-wetting phase saturation.

The significance of coordination number in relation to non-Darcy flow is still unclear since a

number of other competing factors also become important at the same time. Pore networks with coordination numbers of 3, 4 and 6 are shown in Fig 6.6. It may seem that in a porous network with high coordination number, paths oriented parallel to the direction of flow are more frequent. Thus it may be supposed that a high coordination number would lead to a low value of the inertial coefficient. The situation is however complicated by the fact that in a rock with a high coordination number the fluid may undergo more losses due to changes in the direction of the streamlines as well as more frequent expansion / contraction losses. The control on the overall pressure gradient by these different parameters could be found through a more detailed study requiring the momentum balance equation to be solved numerically for a large network of pores with known dimensions. As far as we know this has not yet been attempted.

6.2.4 Heterogeneities

Observation of thin sections of core in many of the samples show the presence of small cluster areas of well cemented grains, effectively without any porosity at all. Such micro-heterogeneity is caused by local variations in sorting energy and is related to depositional enviornments and to subsequent diagenetic processes particularly cementation and selective leaching of unstable minerals. Often these small scale heterogeneities and thin laminations cannot be recognised by visual inspection of the core sample alone. Observations of thin sections using an optical microscope is therefore essential. Much of the porosity in ancient sedimentary rocks, such as those found in the North Sea area, are of the secondary type [11]. The primary porosity in these cases has generally been lost through various physical and chemical changes during and after burial.

The influence of heterogeneity on residual non-wetting phase saturation during a displacement process is well documented in the literature [4,7-10,12,13]. Archer et al [14] found small-scale local heterogeneities to be significant in the calculation of relative permeabilities from waterflood experiment. Dawe and coworkers [15] have investigated the effect of heterogeneities on flow of chemical slugs through layered porous media. Recently Jones [16] has attempted to explain the importance of heterogeneities on the measurement of inertial coefficients. It should be emphasised that Jones' study was reported after the first report of the present work [3].

Random micro-heterogeneities as well as non-random ones (eg. laminations) have been found to exert a strong influence on non-Darcy flow in porous media . It has been found that a rock may have a value of β far lower than expected for its permeability. In the present study, a closer inspection of the sample under the microscope revealed in many cases the presence of a thin, more permeable lamination, the presence of which lowered the inertial coefficient

(Fig.6.7). Any orientation of laminations, vugs and micro-heterogeneities is also vitally important.

Another interesting situation in capillary or pipe flow arises when single phase flow bifurcates as at a Y-junction, as shown in Fig 6.8. If the diameter of the two arms are different then the throughput in the narrower channel will decrease disproportionately with increasing flow rate. This can be observed from the Hagen-Poiseuille relation (Eq.6.2-6). The pressure drop can be seen to be inversely related to the fourth power of the radius, so that the slightest difference between the two diameters will exaggerate flow differences. In a large network of interconnected pores it is therefore possible that the flow path length will change with increasing rate.

6.2.5 Surface roughness

The importance of surface roughness is well known for pipeline flow [6,17]. For laminar flow the presence of any roughness is generally ignored, but it becomes important during turbulent flow. This is because at low flow rates there is a laminar sub-layer which is thick enough to cover the surface irregularities. However at increasing flow rates, the thickness of the sub-layer decreases and the protrusions become prominent (see Fig 6.9). Thus, a surface which is 'smooth' at low flow rates may at a higher rate become 'rough'. Energy is dissipated by the production of eddies created by these protrusions. The kinetic energy loss is proportional to the square of the fluid velocity thereby contributing to the nonlinearity in flow.

It has been found that the absolute value of roughness, eg the height of the individual protrusions, are less significant than the 'relative roughness', that is the height of the protrusion in relation to some characteristic dimension of the tube - usually taken as the diameter. Various other features of roughness, such as the geometry of protrusions, their spacings and 'waviness' of the surface, ie the presence of tranverse ridges on a larger scale are all known to contribute to extra friction losses. None of these parameters however have been properly quantified so that it is necessary to resort to empirical correlations for calculation purposes.

Recently attempts have been made [18,19] to try to quantify the effects of surface roughness on flow through porous media. Experiments were conducted by Crawford et al [18] with packs of glass beads of 5mm diameter, the "roughness" of which were increased by coating them even finer beads of 100μm diameter. The results obtained from their experiments are of qualitative value only and cannot be expected to hold for consolidated rocks which have a very different pore structure. The results however clearly show that the viscous coefficient (α) increases substantially due to the surface roughness: displaying a 169 % increase for the roughest spheres

compared to the value for the smooth spheres. The main reason for this increase is thought to be due to the fact that although the mean diameters of the spheres change very little by the addition of the roughness elements, the surface area however increases substantially. The results also show that surface roughness can significantly affect the inertial dominated regime of flow.

In consolidated porous rocks, the presence of authigenic pore filling clays (see Fig 6.10) have been found to reduce significantly the permeability of rocks [20,21]. The morphology and distribution, rather than the quantity seems to be the controlling factor. Surface roughness is considerably increased by the presence of pore lining materials such as chlorite and smectite which are usually present in a honeycomb matrix form.

During the formation of secondary pores by the dissolution of unstable minerals, the process is often found to be incomplete with remnants of the precursor grain left behind. This can increase the surface roughness of the pores considerably, thereby causing extra pressure losses at higher flow rates.

6.3 EXPERIMENTAL MEASUREMENTS

Experimental measurements and visual observations were carried out on some 40 core samples collected from 5 producing hydrocarbon reservoirs of the North Sea area. A summary of the results are given in Table 4.1. The techniques employed to measure porosity, permeability and inertial coefficient for the rock samples have already been discussed in Chapter 4. Some other aspects of experimental measurements and their interpretation are discussed below.

6.3.1 Capillary pressure

The injection and withdrawl capillary pressures were obtained for all the samples using the mercury intrusion technique as described in Chapter 4. Using linear regression technique, it was possible to fit smooth curves to most of the capillary pressure data (eg. Fig. 6.15 (b)). Polynomials of upto order 3 were used for this purpose. In some cases, where the injection curve had a very large change of gradient, it was not possible to fit a close fitting curve using the linear regression method. More sophisticated curve fitting methods were not used as it was thought to be unnecessary. Instead, in these cases, data points were simply joined together by straight lines in sequence.

The shape of capillary pressure curves provide a direct indication of the internal pore structure of a rock sample, particularly sizes and sorting of pores, the amount of narrow throats

and large vuggy pores, etc. Interpretation of capillary curves have been dealt with extensively by Wardlaw and coworkers [22,8-10] amongst others. Some of the important features of a capillary pressure curve to note are as follows : threshold pressure increases as pore throat sizes decreases and recovery efficiency (RE) decreases as aspect (pore/throat) ratio increases (see Section 6.3.2). Gradient of the central region increases as pore sorting decreases [23] and length of the flat portion (plateau) of the injection curve is related to the volume of recesses associated with the larger pores. Generally RE increases as pore-to-throat coordination number increases. A high RE indicates that the throat volumes are large in relation to pore volumes. Withdrawal of the injected mercury generally tend to be incomplete for samples that are vuggy or have large connecting throats and pores in addition to finer conduits. Samples of this kind tend to have injection curves without a well defined plateau.

By using a model of parallel capillaries of various sizes, Purcell [24] was able to show that the pemeability of a porous medium can be obtained from its capillary pressure. He was able to obtain the permeability by graphically integrating the plot of mercury saturation verses reciprocal capillary pressure squared. It has also been observed [25] that a log-log plot of capillary pressure data approximates a hyperbola. It is then possible, empirically, to relate the hyperbolic functions to the permeability of the rock. Improvements to this method were proposed later by others [26,27]. An attempt was also made [26] to relate permeability to pore volume, pore throat size and the throat size distribution.

6.3.2 Recovery efficiency

The recovery efficiency (RE) has also been calculated for all the samples (see Table 4.1) as it provides an indication of the aspect ratio and the coordination number. The recovery efficiency is defined [9] as the ratio of the volume of mercury recovered from the sample at the minimum pressure to the volume that was injected before the pressure was reduced (see Fig 6.11) :

$$RE = \frac{S - S_r}{S} \times 100 \qquad (6.3\text{-}1)$$

where S is the total volume of mercury which invaded the pore system at the maximum pressure imposed. S_r represents the volume of mercury retained in the pores when the pressure was reduced from the maximum to the minimum, both S and S_r being expressed as a percentage of the total pore volume. It should be noted that S does not represent the "irriducible saturation", since a further increase of pressure would actually increase the non-wetting phase saturation.

Recovery efficiency is affected both by the properties of the fluid as well as by the pore

geometries. The important fluid properties such as - viscosities, interfacial tensions, fluid densities, wettability, hysteresis of wettability and also velocity of displacement could all have an effect on the recovery efficiency. In the presence of a strongly nonwetting phase (mercury) the following pore structural parameters are thought to have an influence on the recovery efficiency : (a) pore -to - throat size (aspect) ratio, (b) throat-to-pore coordination number, (c) type and degree of heterogeneities and (d) surface roughness.

As already mentioned in the previous section, recovery efficiency (RE) increases as the coordination number increases. Large aspect ratio reduces RE since it causes "snap-off" to occur more easily in the non-wetting phase [28]. Presence of nonrandom heterogeneities also reduces the recovery efficiency. In fact it has been demonstrated [12] that high irreducible wetting phase saturation are caused mainly by the presence of such nonrandom heterogeneities.

Samples of low porosity have low RE probably because the coordination number of the system is low and perhaps because of a tendency for aspect ratio to increase with decreasing porosity. This is illustrated in Fig 6.12. It has also been shown that [8] a significant correlation exist between RE and porosity but none between RE and permeability.

6.3.3 Pore size distribution

The pore size distributions (PSD) were calculated directly from the capillary pressure curves, following the method first proposed by Ritter et al [29] and used later by Burdine et al [30]. The throat size for a given pressure was calculated from the Washburn equation :

$$P_c = 2\sigma \cos\theta / r \qquad (6.3\text{-}2)$$

In all calculations the surface tension of mercury was taken to be 480 dynes/cm and the contact angle 180°. The distribution function D(r) was calculated by taking small increments of the capillary curve dP_c/dS and substituting in the following equation:

$$D(r) = \frac{P_c}{r}\frac{dS}{dP_c} \qquad (6.3\text{-}3)$$

The above method assumes that mercury is forced into smaller and smaller pores as the pressure is increased. This is not completely true due to the presence of "ink bottle" pores, that is large pores which may be accessed only through other smaller pores. Necessary corrections for this effect are available in the literature [31]. Such corrections however seem to be

unnecessary in the present context since the distribution curves are being used only for comparative and qualitative description of reservoir rocks.

As mentioned in Section 6.3.1, it was possible to fit polynomials to most of capillary curves. In these cases, the polynomials were divided into 50 increments and the value of dP_c / dS calculated. The pore throat size distribution curves generated in this manner were smooth (eg Fig. 6.16) For the other capillary curves where it was not possible to fit a polynomial, the size distributions were calculated by taking the gradient directly from two neighbouring data points. The PSD curves therefore looks quite jagged although the general trend can be visualized easily.

6.3.4 Geological Description

The samples tested were all from producing hydrocarbon reservoirs of the North Sea area, except for MO63 which was from a well drilled in the Irish Sea. Much has already been published [32,33] about the geology of these two areas. Only the relevant aspects are therefore summarised here.

The samples with the initial 'M' are from a producing northern North Sea field. The reservoir sandstone rock is of the Upper Jurrasic age and was laid down as a submarine turbidite fan. The source for the hydrocarbon is thought to be the Upper Jurrasic Kimmeridgian shale. The seal is Lower Cretaceous shale. The trap is formed by tilted fault blocks, truncated by unconformities.

The samples with the initials 'RH', 'LE' and 'AL' are from the southern North Sea area. The reservoir rock is the Lower Permian Rotliegendes sandstone which was formed from aeolian sand-dunes. The seal in these cases are the Upper Zechstein evaporites, and the traps are block - faulted horsts. Gas source in these field are thought to be the Upper Carboniferous coal measures.

Detailed geology of the sample MO63 is not available although it is thought to be from the Bunter sandstone of the Permo-Triassic age. Futher discussion on the geology of this area can be found in Ref.33 (Chapters 3 & 4) and elsewhere.

6.4 COMPARATIVE STUDY

In this section a number of examples of inertial coefficient measurements are shown to contrast the effects of pore structure. The full set of experimental results are given in Table 4.1. Here, samples having very similar porosity and permeability are paired togather to highlight the effect of various pore structural parameters on inertial coefficient.

EXAMPLE 1

Sample	k (md)	ϕ (%)	β (ft^{-1})	RE (%)
LE718	0.041	6.83	3.13×10^{13}	47.89
M11004	0.038	8.19	9.11×10^{13}	82.56

LE718 : The sample (Fig 6.13) contains a lot of random micro-scale heterogeneities, possibly calcite cemented. There are large areas where the porosity has disappeared due to the cementation process. The grains are very poorly sorted but well rounded. A thin lamination with slightly larger grains is seen to be passing through the samples. The pores are all primary in origin with virtually no matrix or clays in this region and the grains well sorted and well rounded.

M11004 : The sample (Fig 6.14) contains more interconnected network of pores and also has a higher aspect ratio. Some larger vuggy pores are visible. The grains are well sorted but very angular. The porosity is almost all secondary in origin. The pores are not 'clean'; there is a lot of pore lining clays as well as remnents of precursor grains left behind, quite jagged in some cases.Some of the pores contain pore-filling illitic clays. The sample is quite homogeneous.

Comparision : The two samples have almost the same permeability and porosity and yet the inertial coefficient of M11004 is three times higher than the other. A comparision between the two samples (see Fig 6.15-16) reveals significant differences. Sample M11004 has a far higher recovery efficiency (RE) due to its high connectivity whereas the low RE for the former is due to its micro-heterogeneity. The pore size distribution (PSD) curve shows the pore throats in LE718 to be slightly larger. However the low value of β is primarily due to the presence of the lamina of high permeability.

EXAMPLE 2

Sample	k (md)	ϕ (%)	β (ft^{-1})	RE (%)
AL79	0.11	10.26	3.09×10^{12}	40.30
M73002	0.102	11.50	17.40×10^{12}	75.00

AL79 : The sample (Fig 6.17) is texturally mature containing little or no clays. The grains and pores are quite well sorted. All primary porosity seems to have been lost due to cementation caused by silica overgrowth. Pores are therefore secondary in origin and reasonably 'clean', without much clay growth. Small clusters of areas can be seen with virtually no pore spaces.

M73002 : The grains are well sorted but subangular and the sample (Fig 6.18) contains a lot of clay and matrix (around 5%). Few large vuggy pores are visible but mostly pores are smaller in size. There are a lot of pores with pore lining and pore filling clays. Some of the unleached precursor grains can also be seen. The sample has a high aspect ratio.

Comparision : The two samples (see Fig 6.19-20) again have markedly different values of inertial coefficient although their porosity and permeability are very similar The primary reason for the high value of β in M73002 is the high aspect ratio as well as highly connective flow paths. Furthermore, the pores being 'unclean' helps to increase the tortuosity. The higher connectivity is reflected in the high value of RE.

EXAMPLE 3

Sample	k (md)	ϕ (%)	β (ft^{-1})	RE (%)
AL29	0.17	10.04	0.41×10^{12}	39.73
AL40	0.17	9.94	0.99×10^{12}	37.84

AL29 and **AL40** : The two samples (Fig 6.21-22) are from the same formation but cored at different depths. As such, the lithology is very similar. The primary porosity has been lost due to silica overgrowth. In both cases small clusters of areas could be observed with no porosity due to this cementation process. Both samples are texturally mature with very little clays between grain contacts although most pores contain some illite/smectite type of clays and in some cases remnants of precursor grains. The only significant visible difference is that the sample AL40 contains pores which are larger and more vuggy in nature, ie has larger aspect ratio.

Comparision : This example is quite interesting since both samples (see Fig 6.23-24) are from the same formation and similar lithology. Furthermore both of these samples have almost the same porosity, permeability and capillary behaviour. However sample AL40 has slightly larger pore throats which is reflected in the lower threshold capillary pressure and also in PSD curve. The larger pore-to-throat ratio is reflected in the capillary curve having a wider and less steep plateau and also in the slightly lower recovery efficiency. Clearly the higher value of β in this sample is due to the high pore-to-thraot ratio compared to AL29.

EXAMPLE 4

Sample	k (md)	ϕ (%)	β (ft^{-1})	RE (%)
RH101	0.14	5.87	7.93×10^{12}	57.53
AL111	0.14	13.50	2.47×10^{12}	32.89

RH101 : The sample (Fig 6.25) contains well sorted and rounded grains. The pores are secondary in origin but are not easily visible. They are very fine, sheet-like and tortuous, but well connected. Most of the pores have been filled up by authigenic vermicular kaolinite, easily detected from its morphology. The sample also contains a lot of carbon rich shales seen as dark patches.

AL111 : The sample (Fig 6.26) is similar in texture to the ones mentioned above in the AL series. The pores are all secondary in origin with wide distribution of sizes. Some small patches of pore filling clays can be seen. The sample has a very high pore-to-throat ratio; some large vuggy pores are also present.

Comparision : The wide range of sizes in sample AL111 can be observed in the PSD curve (see Fig 6.27-28) and also is reflected in the wider and less steep plateau of the capillary curve. The recovery efficiency is also low. Porosity of sample RH101 is almost half the other. The higher value of β is clearly due to the much more complex and highly connected network of pores leading to an increase in the tortuosity of the pathway. It is important to note that the high pore-to-throat ratio in AL111 did not increase the value of β as much as in the other sample. From this and the previous examples it seems that the connectivity (tortuosity) is more significant than the aspect ratio.

EXAMPLE 5

Sample	k (md)	ϕ (%)	β (ft^{-1})	RE (%)
RH103	0.23	9.96	1.13×10^{12}	60.53
MO63	0.21	9.36	3.71×10^{11}	50.70

RH103 : The sample (Fig. 6.29) is texturally mature with plenty of silica overgrowth. Porosity is almost all secondary in origin, the pores having been created by the leaching out of unstable minerals and shale particles. Most of the pores are lined with carbon-rich shale probably being the remnant of precursor grains. In many pores infact large portions of the precursor grains are still remaining. Subsequent growth of vermicular kaolinite can also be clearly observed in most pores, in some cases completely filling the pore space. Growth of fine strands - possibly illite, can also be observed in some pores. A few pores are however fairly clean and quite large. The pores are generally not well connected.

MO63 : The grains in this sample (Fig. 6.30) are moderately rounded and well sorted although the sample is immature containing around 10 - 15% clay and matrix material. The pores are however quite clean and are very well connected. The grain and pores are generally much smaller in size than in RH103. The bedding plane can be observed from the orientation of the grains.

Comparision : The capillary pressure curves for both the samples (Fig. 6.31-32) are very similar in shape. Recovery efficiency for RH103 is higher. Pore size distribution curves show that RH103 has a larger number of pores of around 1.2 μm size and the sample also has a wider plateau in the capillary curve indicating the high aspect ratio. The larger aspect ratio, combined with large amounts of pore filling clays, which help to increase the intra-pore tortuosity, seems to be the reponsible mechanism for the higher value of β in sample RH103.

EXAMPLE 6

Sample	k (md)	ϕ (%)	β (ft^{-1})	RE (%)
M11003	0.520	10.02	1.24×10^{11}	77.46
M73004	0.515	11.0	7.26×10^{11}	75.30

M11003 : The sample (Fig. 6.33) is texturally immature containing nearly 10% clay and matrix. The grains are poorly sorted and angular in shape. The bedding plane can be detected from the arrangement of the grains and shale particles. The pores are generally quite fine, sheet-like and very well connected. A few large pores, dispersed throughout, can be observed. Most of the pores are secondary in origin.

M73004 : The sample (Fig. 6.34) is texturally submature, containing more than 5% clay matrix and shales. The grains are moderately sorted and subangular. The pores are virtually all secondary in origin.Some of the pores are quite fine but others are fairly large. Most of the pores contain authegenic clay as well as remnants of precursor grains which have been partially leached. From the morphology, the clays are thought to be of illite/smectite type, although further SEM analysis would be required for certainity.

Comparision : Values of porosity, permeability and RE are all very close. The two samples are from the same formation although from different wells and have been cored at different depths. The lithology is therefor the same. There is strong similarity in the shape of the capillary curves (Fig. 6.35-36), both containing double curves in the injection cycle which is fairly common for samples containing a lot of pores of secondary origin. In M73004 however, the "hump" is far more prominent. The PSD curve indicates that this sample contains a large amount of pores of size 1.5 - 2.5 μm. Observation of the thin section also reveal that this sample contains pores with large aspect ratio. The larger aspect ratio seems to be the parameter responsible for causing the value of β in M73004 to be nearly 6 times higher than the other sample.

EXAMPLE 7

Sample	k (md)	ϕ (%)	β (ft^{-1})	RE (%)
M11011	1.18	11.60	4.94×10^{11}	76.92
M11008	1.24	12.74	5.89×10^{10}	80.00

M11011 : The sample (Fig. 6.37) is very heterogeneous, containing laminae of fine grains mixed with a lot of carbon rich shale particles and clay matrix. The laminae are usually around 0.5-1.0 mm thick and present at intervals of around 5-6 mm apart. In these laminae the pores are very fine and sheet like and would probably contribute very little to the overall flow. In between the laminae, there are regions of higher porosity, with high aspect ratio. The sample is texturally immature, very poorly sorted and contains grains which are very angular.

M11008 : The heterogeneities in this sample (Fig. 6.38) are less pronounced than in the previous sample. Even in the laminae of finer grains, there are abundant pores. The sample is also immature, containing nearly 10% clay matrix. The grains are better sorted than M11001 although still quite poorly, and generally subangular. Like the previous sample, porosity is almost all of the secondary type.

Comparision : The samples are both from the same formation being a few feet apart vertically. The lithology is similar. The capillary pressure curves are also similar in shape (Fig. 6.39-40), both containing the double curves in the injection part, although in M11011 this is much more prominent. There is also a sharp peak of the PSD curve at pore radius of around 2 μm. The distribution of pore sizes in M11008 is much smoother. The "hump" in M11011 corresponds to the slightly larger aspect ratio. The higher degree of heterogeneity combined with larger aspect ratio seems to be the cause responsible for the large increase in β in sample M11011.

EXAMPLE 8

Sample	k (md)	ϕ (%)	β (ft^{-1})	RE (%)
M73006	15.2	20.5	1.17×10^9	69.62
RH97	17.0	16.92	2.02×10^9	32.18

M73006 : The sample (Fig. 6.41) is immature and contains more than 5% clay matrix. The grains are poorly sorted and angular in shape. Porosity is almost all of the secondary type. The pores are very well connected (high coordination number) and generally have a low aspect number. There are however a few pores of larger dimension created by the leaching out of unstable minerals. The sample contains no visible heterogeneities.

RH97 : The sample (Fig. 6.42) is supermature, containing grains which are well sorted, well rounded with high sphericity. Sample contains very little clay, matrix or cement and as such is quite friable. Porosity is virtually all primary in origin. The pores and grains are quite large. The permeability of this sample would probably have been higher had it not been for the presence of some heterogeneities. The lower recovery efficiency is also due to this cause.

Comparision : Although the permeability in RH97 is slightly higher, the RE (Fig. 6.43-44) is very much lower (almost half). Heterogeneites in RH97 are not visible with the naked eye. Under the optical microscope it can be seen as regions having slightly smaller and more compacted grains. The heterogeneities in this sample seems to be the dominant feature, causing low RE and much higher value of β (almost double). The capillary pressure curve has a fairly complicated shape - a high threshold pressure, followed by a plateau and then a second curve. The second curve is most like caused by the presence of the heterogeneites.

EXAMPLE 9

Sample	k (md)	ϕ (%)	β (ft^{-1})	RE (%)
M73005	33.0	21.0	5.19×10^8	79.76
M73009	32.5	25.6	2.63×10^8	68.23

M73005 and **M73009** : The samples (Fig. 6.45-46) are from the same formation and plugs have been cored less than a foot apart. The lithology is therefor very similar. Both samples are immature containing around 5 - 10% clay matrix. The grains are poorly sorted and angular in shape. Most of the pores are secondary in origin and contains authegenic clays - most likely of the illite / smectite type. Some of the pores are completely filled with this clay.

The aspect ratio of pores in sample M73005 seems smaller. This sample also contain some small clusters of areas with very little porosity - probably caused by overgrowth of silica cement. There are other smaller areas where the aspect ratio can be seen to be much higher. No such heterogeneites could be observed in the other sample.

Comparision : The slightly larger aspect ratio of sample M73009 observed using the microscope is confirmed by the shape of the capillary curve (Fig. 6.47-48) having a high threshold pressure and a wider plateau. The recovery efficiency is also lower. The absence of any distinct threshold pressure or plateau in the capillary curve of sample M73005 is indicative of the poor pore size sorting. The presence of micro-heterogeneites is the most likely cause of increasing the value of β by two two folds. The recovery efficiency in this sample is also better confirming the presence of pores with lower aspect ratio. At first sight, the value of β would have been expected to be higher in sample M73009 due to the higher aspect ratio pores. The presence of micro-heterogeneites in M73005 however seems to be a more dominating cause for the higher value of β in this case.

EXAMPLE 10

Sample	k (md)	ϕ (%)	β (ft^{-1})	RE (%)
M11007	84.0	20.58	1.19×10^8	67.82
LE249	99.5	15.17	7.66×10^8	80.22

M11007 : The grains are moderately sorted and angular. The sample (Fig. 6.49) is submature containing around 5% clay matrix. No heterogeneites could be observed with the naked eye or under the microscope. The pores are very well connected and can be expected to have a high aspect ratio. Most of the pores are lined with clays - mostly chlorite which can be detected from the morphology and the green / brown colour. Many of the pores also contain pore-filling clays.

LE249 : The sample (Fig. 6.50) contains heterogeneites in the form of laminations which could be observed in the core plug. Under the microscope, a layer could be observed containing excellent reservoir sands. Here the grains are well sorted, well rounded and contains virtually no clay matrix and very little cement. Sand grains have been coated with iron oxide after deposition giving it a red / brown colour. In the narrow laminations, the grains and pores are much smaller and less sorted. There is cinsiderable amount of clay matrix (around 10%) and shale particles. The grains are subrounded and elongated in shape. These regions would be expected to have fairly low permeability.

Comparision : Sample M11007 has a high aspect ratio which is reflected in the plateau of the capillary pressure curve (Fig. 6.51-52) as well as in the recovery efficiency. There is no distinct threshold pressure in sample LE249. The wide distribution pore sizes is the cause for the absence of any plateau. The sample LE249 is dominated by the presence of two laminae of lower permeability. The permeability of the middle (cleaner) section is probably far higher than the bulk value. The presence of the low permeability lamina seems to be the only reason for causing the calue of b to be nearly 6 times higher compared to the other sample.

EXAMPLE 11

Sample	k (md)	ϕ (%)	β (ft^{-1})	RE (%)
M73001	0.064	12.31	1.39×10^{12}	84.62
AL118	0.050	12.31	3.35×10^{13}	47.06

M73001 : The sample (Fig. 6.53) is immature containing around 5% clay matrix. The grains are poorly sorted and subangular. There has been considerable amount of silica overgrowth and growth of authegenic clay - mostly pore filling. The clays are probably of the illite / smectite type although further SEM analysis would be required to confirm this.

AL118 : The sample (Fig. 6.54) is mature, containing very little clays or matrix. The grain boundaries are not clearly visible due to silica overgrowth causing large clusters of areas without any porosity. The pores are all secondary in origin and fairly clean although some contain pore filling clays and precursor grain remnants. The sample has fairly low connectivity and high aspect ratio. The pores are generally very angular in shape due to the silica overgrowth in the grains.

Comparision : The very high aspect ratio in AL118 can be observed from the long plateau in the capillary curve (Fig. 6.55-56). There is also a high threshold pressure. The low recovery efficiency is symptomatic of the high aspect ratio. The sample M73001 contains a double curve in the injection cycle with high RE due to the low aspect ratio. The connectivity is better than in AL118. Although the permeabilkty of M73001 is higher by a few percent, however the value of β is nearly 3 times higher, which is contrary to excpection. The primary cause seems to be the presence of large amounts of pore -filling clays which would be expected to provide higher resistance at increasing flow rate.

EXAMPLE 12

Sample	k (md)	ϕ (%)	β (ft^{-1})	RE (%)
RH94	2.21	12.17	5.68×10^8	43.59
M11002	2.10	13.82	3.81×10^8	73.60

RH94 : The grains are moderately sorted and well rounded. The sample (Fig. 6.57) is submature and do not contain much clay matrix or cement. The pores are generally quite clean and are primary in origin. Authegenic clay growth has been minimal. The pore sizes and shapes are very varied. A few pores have been have partially leached out giving it a very jagged shape. The sample is friable due to the lack of cements. Aspect ratio in this sample is generally high.

M11002 : The sample (Fig. 6.58) is immature containing around 10% clay matrix and shales. The grains are very poorly sorted and ranges from angular to subrounded. Most of the pores are secondary and contain a lot of clays. They are however very well interconnected and has low aspect ratio.

Comparision : Permeability of RH94 is slightly higher even though the value of β is almost twice as large. The capillary pressure of the sample shows the wide distribution of pore sizes and shapes (Fig. 6.59-60). This most likely contributes to the low RE and high β. The high aspect ratio would also be responsible for both these causes. Sample M11002 at first sight may be expected to have the higher value of β due to the clays in the pore spaces. However its low aspect ratio seems to beresponsible for the lower value of β.

EXAMPLE 13

Sample	k (md)	ϕ (%)	β (ft^{-1})	RE (%)
M11001	59.0	20.76	1.21×10^7	75.91
M11009	66.0	19.70	5.71×10^6	69.66

M11001 and **M11009** : The samples (Fig. 6.61-62) are both from the same formation and have been cored a few feet apart. The lithology is the same. The samples are both texturally immature, containing 5 - 10% clay and matrix. The grains are poorly sorted and angular in shape. Pores are mostly secondary in origin. Considerable amounts of authigenic clay is present in most pores and in some cases are pore-filling.

Sample M11009 contains a considerable amount of heterogeneities. Nearly a third of the sample consists of grains which are much finer and very poorly sorted. This area also contains nearly 25% clay matrix and shales, and the pores are very fine and sheet-like. Shape of the PSD curve indicates the presence of pores of 8 - 10 μm sizes. This is probably due to the presence of the higher permeability region.

Comparision : Shape of the capillary pressure curves (Fig. 6.63-64) are very similar for the two samples since they are from the same formation and have the same lithology. Sample M11009 however contains a lot of heterogeneities with nearly one third containing much finer grains and pores which would be expected to make negligible contribution to the overall flow. The permeability of the rest of the core sample would therefor have to be much higher than than the bulk to compensate. The presence of this heterogeneity is the most likely cause of the value of β to be lower than for the other sample.

EXAMPLE 14

Sample	k (md)	ϕ (%)	β (ft^{-1})	RE (%)
M73003	0.46	10.01	2.83×10^{10}	81.08
LE253	0.41	7.43	2.63×10^{10}	45.33

M73003 : Like the other samples in the M73 series, this sample (Fig. 6.65) is also texturally immature containing around 10% clay matrix. There are no visible heterogeneites. The grains are poorly sorted and angular. Few pores are clean but generally contain pore-lining and pore-filling clays mostly of the illite/smectite type. Some pores also contain what appears to be remnants of precursor grains. The pores are fairly well connected and have low aspect ratio.

LE253 : The sample (Fig. 6.66) is dominated by heterogeneites which are fairly visible with the naked eye. In the more permeable layers, the sands are super mature, containing virtually no clay matrix or cement. This causes the rock to be very friable. Here the grains are well sorted and very rounded with high sphericity. In the less permeable layers however, the grains are much smaller in size, very poorly sorted and angular. These layers contain around 30% clay matrix and shales and the pore spaces are not easily visible. The contribution to the total flow in these regions can be expected to be negligible.

Comparision : The two samples (Fig. 6.67-68) have very similar values of k and β. This example was chosen to highlight the fact that even though the values of k and β may be similar in two samples, closer inspection may reveal that the pore structures may be quite different in the two cases. Sample LE253 contain laminae with very high and low permeability layers. The higher permeability layers would probably have permeabilities around two order of magnitude higher than the bulk value. Had it not been for the presence of these, the permeability would certainly have been far lower and β much higher.

Observation of the β-k plot shows that β increases more rapidly in lower permeability rocks than in samples with higher permeability. This is most likely due to the increase in pore-to-throat (aspect) ratio found in rocks with decreasing permeability. The situation can be understood from Fig 6.12. The figure show two idealised pore spaces of identical dimensions, one clean and the other lined with clays. The aspect ratio in (b) will be greater than in (a), ie $d_4 / d_3 > d_2 / d_1$. Furthermore, the presence of increased amounts of pore lining and bridging clays makes the flow paths more tortuous thereby increasing the value of β considerably.

The presence of authigenic clay poses a problem in experimental measurement of inertial coefficient due to their breakdown or movement of fines at high flow rates. The question of clay breakdown and their transport is being tackled by others [34,35] and so will not be dealt with here. The problem is however not unique to core analysis, as similar situations may also arise near gas wells producing at high rates. For all the samples reported in this study, observation with scanning microscope did not reveal any significant amount of clays which could make the results imprecise. Besides, the results were all found to be repeatable within experimental errors.

6.5 CONCLUSIONS

This study has shown that the inertial coefficient, β, is related inversely to the permeability of rock samples and is also dependent on the other pore structure parameters. A plot of β against permeability gives a wide scatter. Explanation for this can be found by considering the pore structure in detail. Some of the important factors, besides porosity and permeability, which were found to influence the inertial coefficient are as follows :

(a) High coordination number leads to a more complicated network of pores. Fluid flowing in such a rock encounters a more tortuous path with more expansion and contractions. The β values are generally found to be higher in these rocks.

(b) The inertial effect is strongly influenced by the pore-to-throat ratio. Higher pore-to-throat ratio leads to an increase in the inertial coefficient.

(c) The presence and orientation of small scale heterogeneity - random micro-scale or laminations, usually help to lower the value of β. The presence of any laminae with high permeability is likely to be a primary cause in the lowering of the inertial coefficient.

(d) The internal geometry of pores is found to be important. The presence of clays, authigenic or detrital, pore lining of pore bridging, increases the 'roughness' and thereby significantly increases the inertial coefficient.

REFERENCES

1. Katz, D.L. et al : *Handbook of Natural Gas Engineering,* McGraw-Hill Book Co., New York (1959)
2. Firoozabadi, A. and Katz, D.L. : An analysis of high velocity gas fow through porous media, *J.Pet.Tech.* (Feb. 1979), 211
3. Noman, R., and Archer, J.S. : The effect of pore structure on non-Darcy gas flow in some low permeability reservoir rocks, Paper SPE/DOE 16400 presented at the Joint SPE/DOE Low Permeability Reservoir Symposium, Denver, Co., May 18-19, 1987.
4. Morgan, J.T. and Gordan, D.T. : Influence of pore geometry on water-oil relative permeability, *J. Pet. Tech.* (Oct. 1970) p.1199.
5. Hubbert, M.K. : Darcy's law and the field equations of the flow of underground fluids, *Trans AIME* (1956) **207**, 222-239.
6. Bird, R.B., Stewart, W.E. and Lightfoot, E.N. : *Transport Phenomena,* J. Wiley & Sons Inc., New York (1960).
7. Dullien, F.A.L. : *Porous Media - Fluid Transport and Pore Structure,* Academic Press, New York (1979).
8. Wardlaw, N.C. and Cassan, J.P. : Estimation of recovery efficiency by visual observation of pore systems in reservior rocks, *Bull. Can. Pet. Geo.* (Dec. 1978) **26**, 572-585.
9. Wardlaw, N.C. and Cassan, J.P.: Oil recovery efficiency and the rock-pore properties of some sandstone reservoirs, *Bull. Can. Pet. Geo.* (June 1979) **27**, 117-138
10. Wardlaw, N.C. and Taylor, R.P. : Mercury capillary pressure curves and the interpretation of pore structure and capillary behavior in reservoir rocks, *Bull. Can. Pet. Geo.* (June 1976) **24**, 225-262.
11. Schmidt, V., McDonald, D.A. and Platt, R.L. : Pore geometry and reservoir aspect of secondary porosity in sandstones, *Bull. Can. Pet. Geo.* (1977) **25**, 106.
12. Morrow, N.R. : Small scale heterogeneities in porous sedimentary rocks, *Amer. Assoc. Pet. Geo. Bull.* (March 1972) **55**, 514-522.
13. Pickell, J.J., Swanson, B.F. and Hickman, W.B. : Applicaton of air-mercury and oil-air capillary pressure data in the study of pore structure and fluid distribution, *Soc. Pet. Eng. Jour.* (March 1966) 55-61.
14. Archer, J.S. and Wong, S.W. : Use of reservoir simulator to interpret laboratory waterflood data, *Soc. Petrol. Eng. J.,* (Dec. 1973) 343-347.
15. Wright, R.J., Wheat, M.R. and Dawe, R.A. : Slug size and mobility requirements for chemically enhanced oil recovery within heterogeneous reservoirs, *S.P.E. Reservoir Eng. J.,* (Feb. 1987) 92-102.
16. Jones, S.C. : Using the inertial coefficient, β, to characterize heterogeneity in reservoir rocks, Paper SPE 16949 presented at the 62nd Annual Conf. of the SPE, Dallas, TX,

Sept. 27-30, 1987.

17. Whitaker, S. : *Introduction to Fluid Mechanics,* Prentice Hall, Englewood Cliffs, NJ, (1968).
18. Crawford, C.W. and Plumb, O.A. : The influence of surface roughness on resistance to flow through packed beds, *J. Fluids Eng.,* Trans ASME (Sept. 1986) **108**, 343-347.
19. Brown, S.R. : Fluid flow through rock joints : the effect of surface roughness, *Jour. Geophys. Res.* (Feb. 1987) **92** (B2) 1337-1347.
20. Neasham, J.W. : The morphology of dispersed clay in sandstone reservoirs and its effect on sandstone shaliness, pore space and fluid flow properties, Paper SPE 6858 presented at the 52nd Annual Fall Meeting of the SPE, Colorado, Oct. 9-12, 1977.
21. Pallat, N., Wilson, J. and McHardy, W.J. : The relationship between permeability and morphology of diagenetic illite in reservoir rocks, J. Pet. Tech. (Dec 1984) p.2225.
22. Wardlaw, N.C. and McKellar, R. : Mercury porosimetry and the interpretation of pore geometry in sedimentary rocks and artificial models, *Powder Tech* (1981) **29**, 127.
23. Archer, J.S. and Wall, C.G. : *Petroleum Engineering - Principles and Practice,* Graham & Trotman, London (1986)
24. Purcell, W.R. : Capillary pressure - their measurement using mercury and the calculation of permeability therefrom, *Trans AIME* (1949) **186**, 39-48.
25. Thomeer, J.H.M. : Introduction of a pore geometrical factor defined by the capillary pressure curve, *Trans. AIME* (1960) **219**, 354-358.
26. Thomeer, J.H.M. : Air permeability as a function of three pore-network parameters, *J. Pet. Tech.* (April 1983) 809-814.
27. Swanson, B.F. : A simple correlation between permeabilities and mercury capillary pressures, *J. Pet. Tech.* (Dec. 1981) 2498-2504.
28. Roof, J.G. : Snap-off of oil droplet in water wet pores, *Soc. Pet. Eng. J .* (1970) **10**, 85.
29. Ritter, L.C. and Drake, R.L. : Pore size distribution in porous materials, *Ind. Eng. Chem.* (1945) **17**, 782.
30. Burdine, N.T., Gournay, L.S. and Reichertz, P.P. : Pore size distribution of petroleum reservoir rocks, *Trans. AIME* (1950) **189**, 195-204.
31. Meyer, H.I. : Pore distribution in porous media, *J. Appl. Phys.* (1953) **24**(5), 510-512.
32. Selley, R.C. : The habitat of North Sea oil, *Proc. Geol. Assoc.,* London (1975) **87**(4), pp.359-387.
33. Woodland, A.W. (Ed.) : *Petroleum and the Continental Shelf of the Northwest Europe,* Vol.1 Geology, Applied Science Publish., London (1975)
34. Lever, A. and Dawe, R.A. : Water sensitivity and migration of fines in the Hopeman sandstone, *J. Pet. Geol.* (Jan. 1984) 7, 97-108.
35. Muecke, T.W. : Formation fines and factors controlling their movement in porous media, *J. Pet. Tech.* (Feb. 1979) p.144.

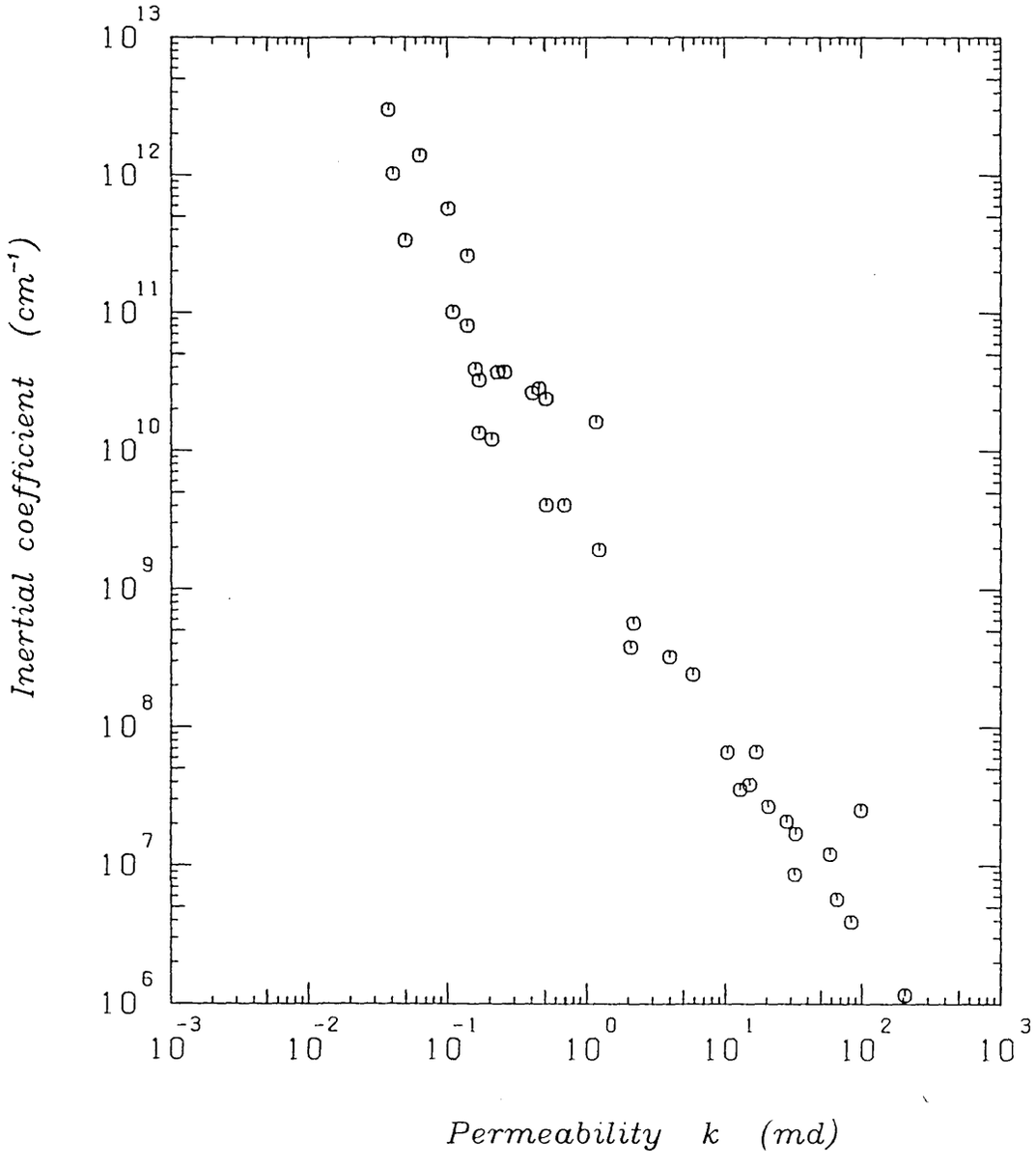


Fig. 6.1 Relationship between inertial coefficient and permeability for the sample set.

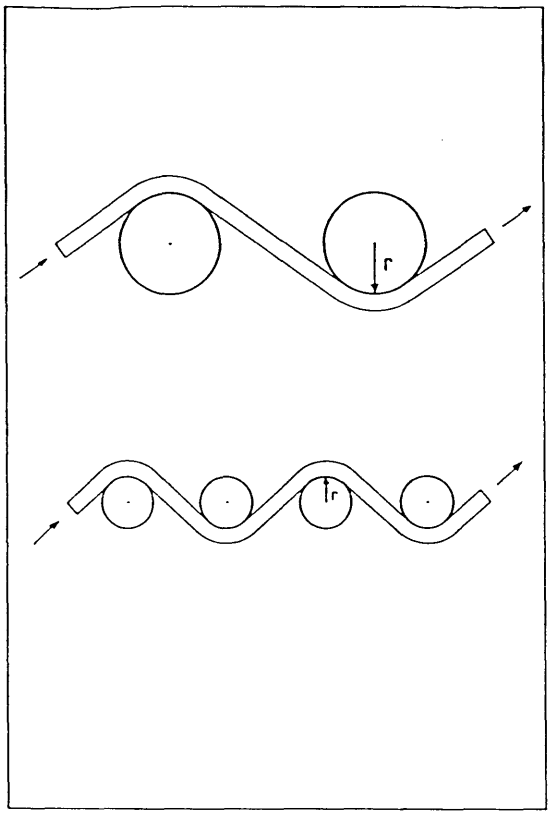


Fig. 6.2 Two capillaries of equal dimension but different radius of curvature.

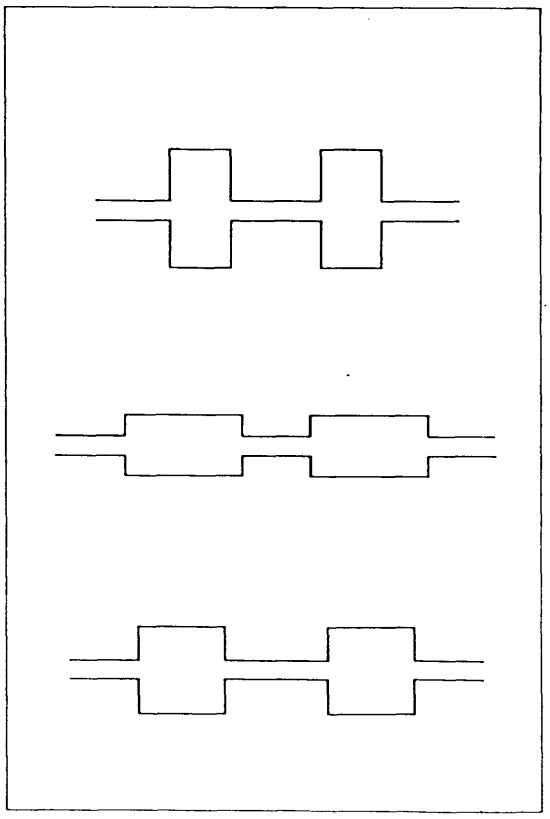


Fig. 6.3 Segment of pore networks representing similar k and ϕ but having different values of β.

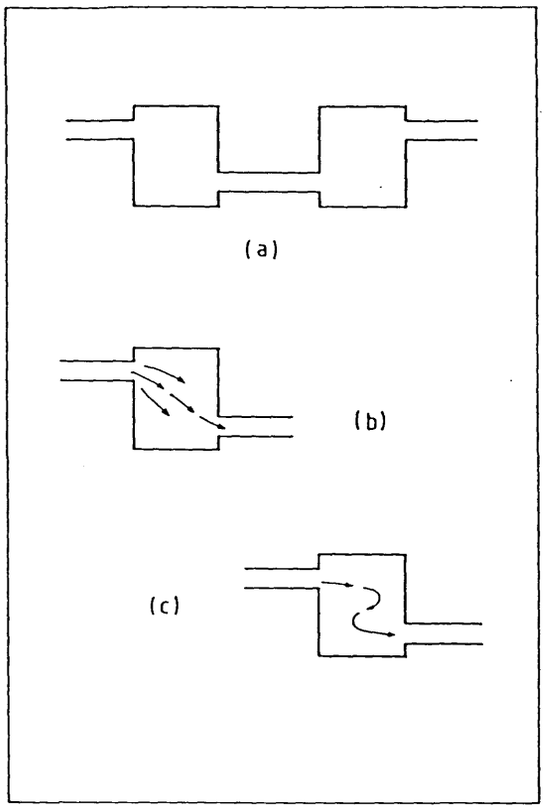


Fig. 6.4 (a) Segment of pore network with asymmetric throats, (b) low rate flow, and (c) complex flow at higher rates.

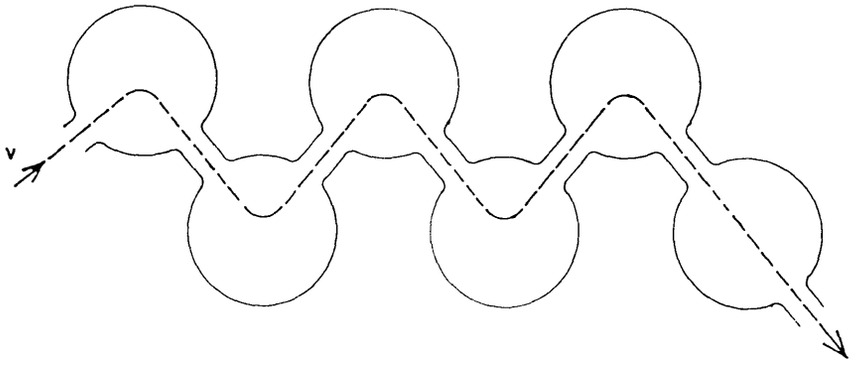


Fig. 6.5 Segment of pore network with tortuous channels.

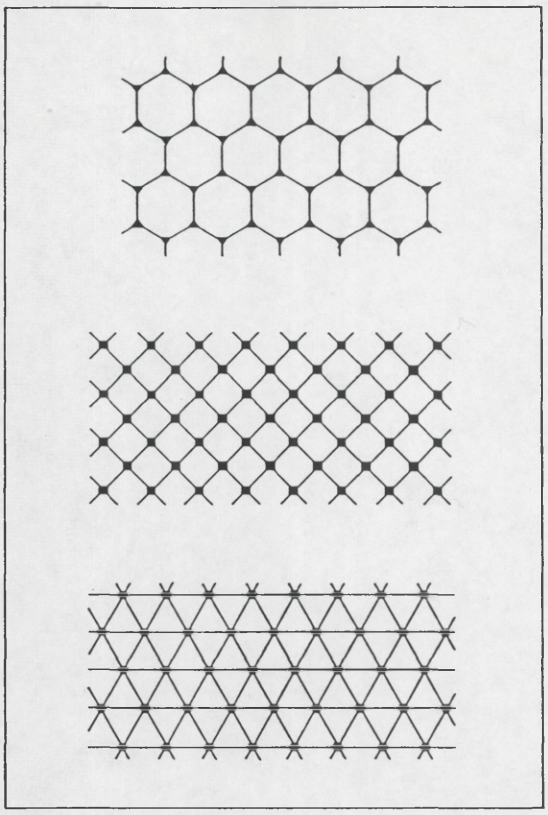


Fig. 6.6 Pore network with coordination number of 3, 4 and 6.

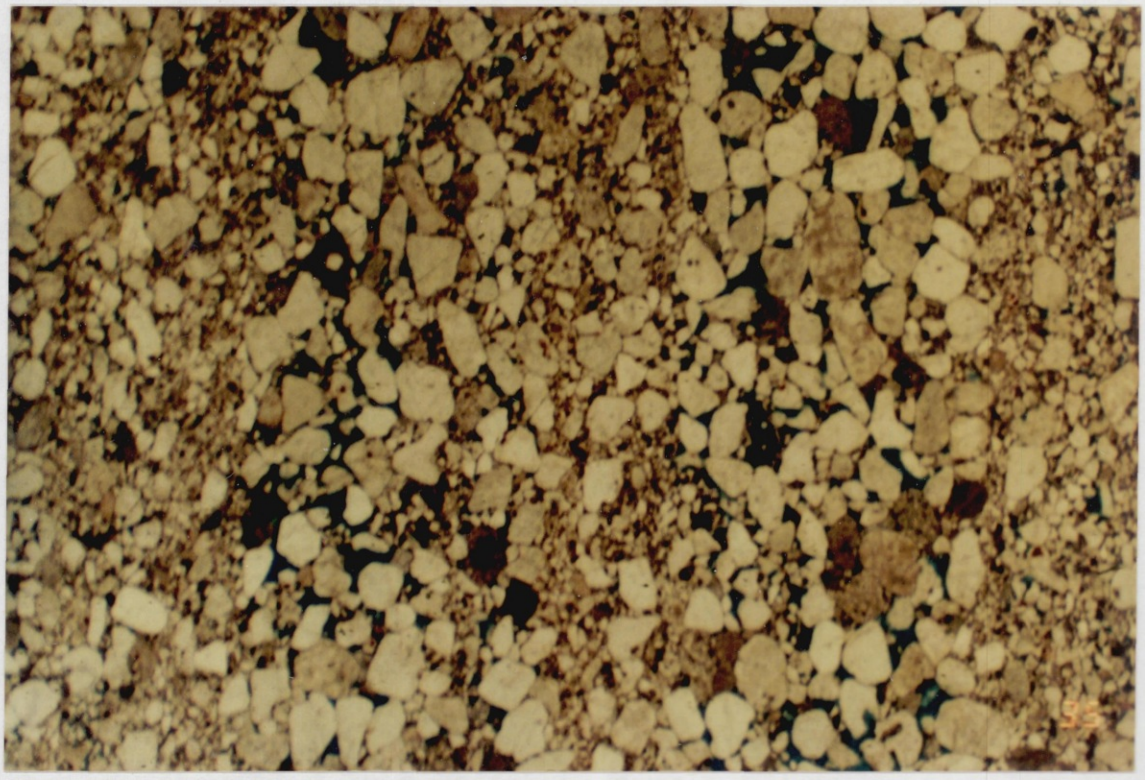


Fig. 6.7 Photomicrograph of sample LE253 showing heterogeneities in the form of thin laminations.

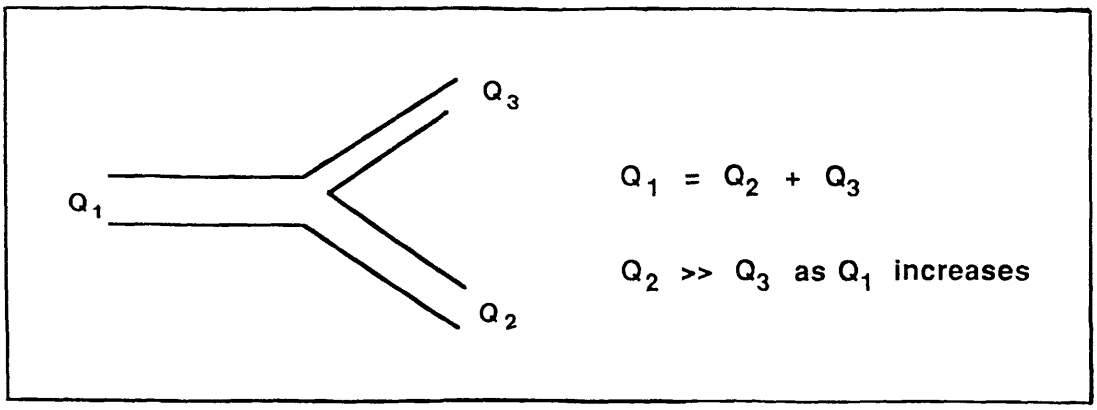


Fig. 6.8 Laminar flow at a Y-junction. Q_2 will increase disproportionately in comparision to Q_3 as Q_1 increases.

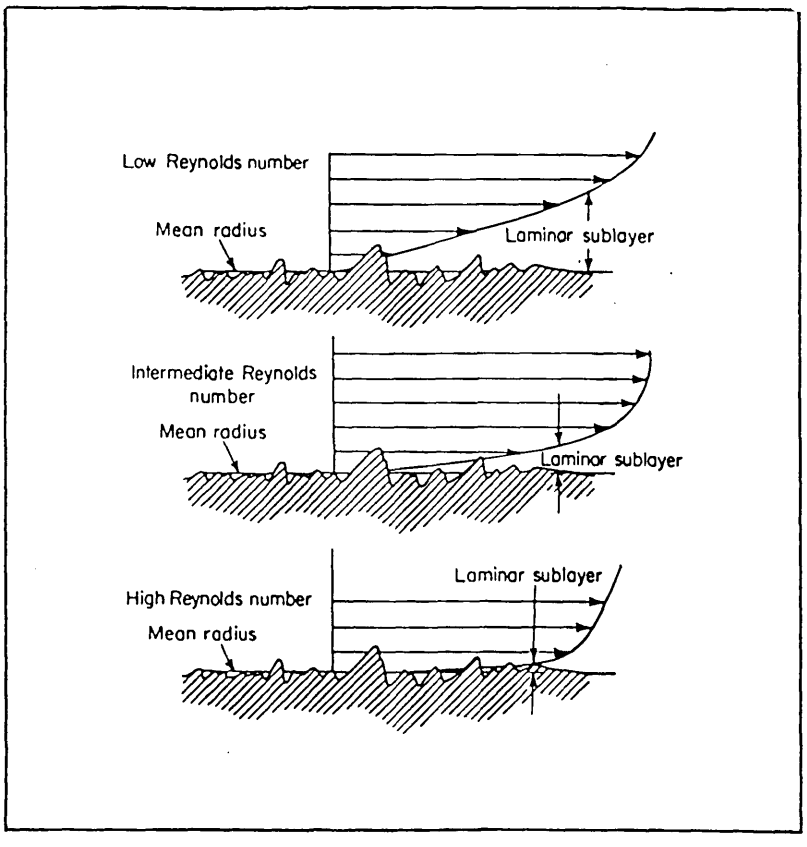


Fig. 6.9 Importance of surface roughness at increasing Reynolds number flow (after Whitaker 1968).

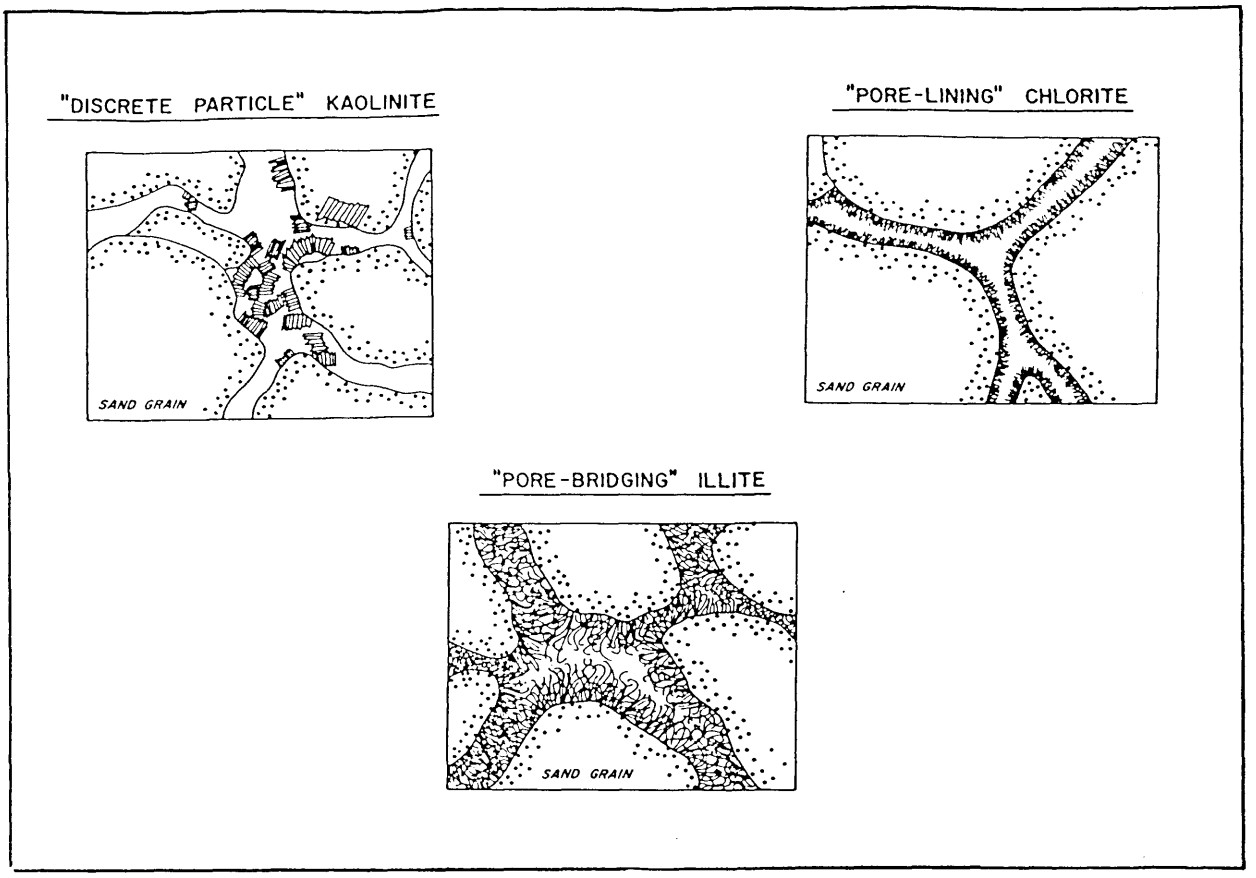


Fig. 6.10 Three general types of dispersed clay in sandstone (after Neasham 1977).

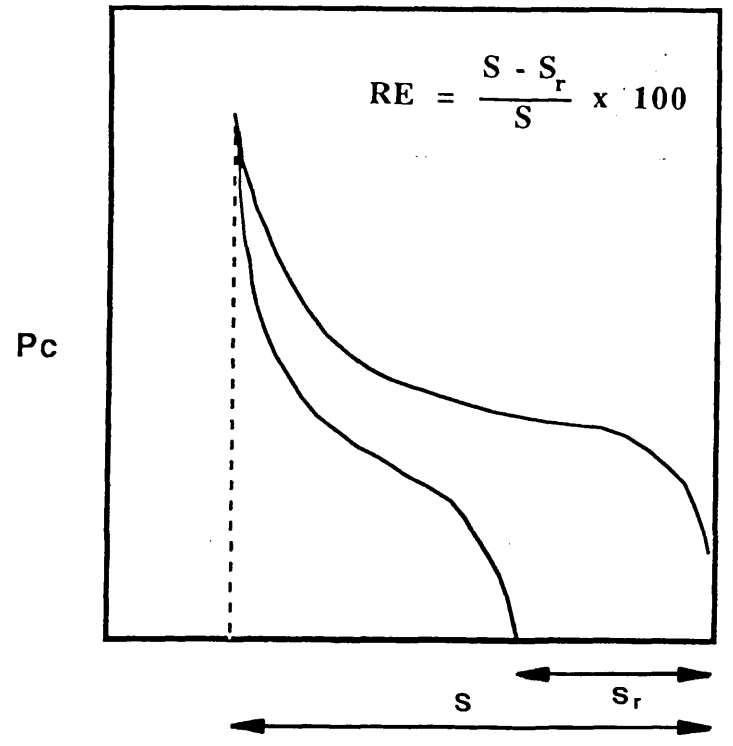


Fig. 6.11 Typical features of a capillary pressure curve for calculation of the Recovery Efficiency (RE).

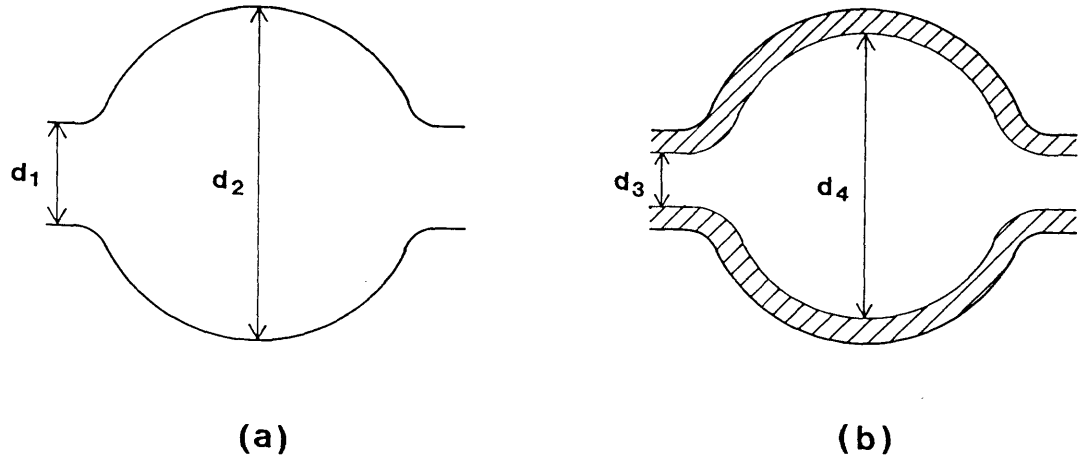


Fig. 6.12 (a) Idealized representation of a clean pore, and (b) reduction of pore space due to the growth of authigenic pore-lining clays. The aspect ratio d_4/d_3 is greater than d_2/d_1.

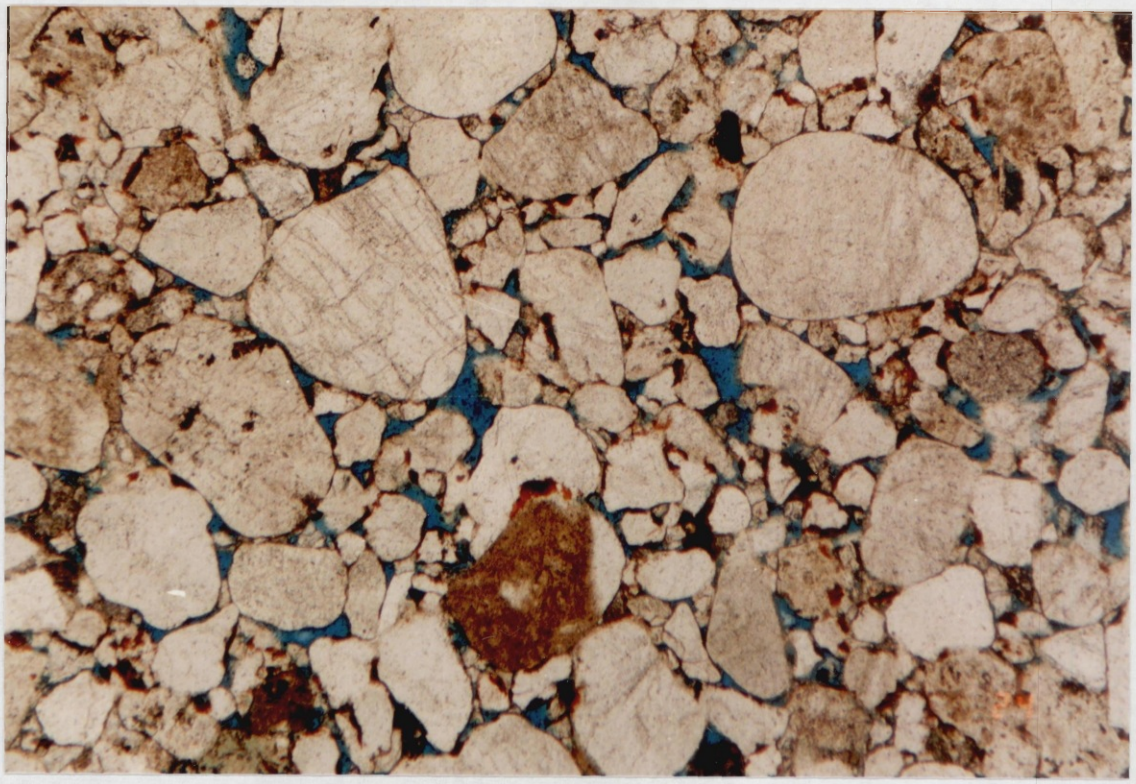


Fig. 6.13 Photomicrograph of sample LE718. Magnification x10.

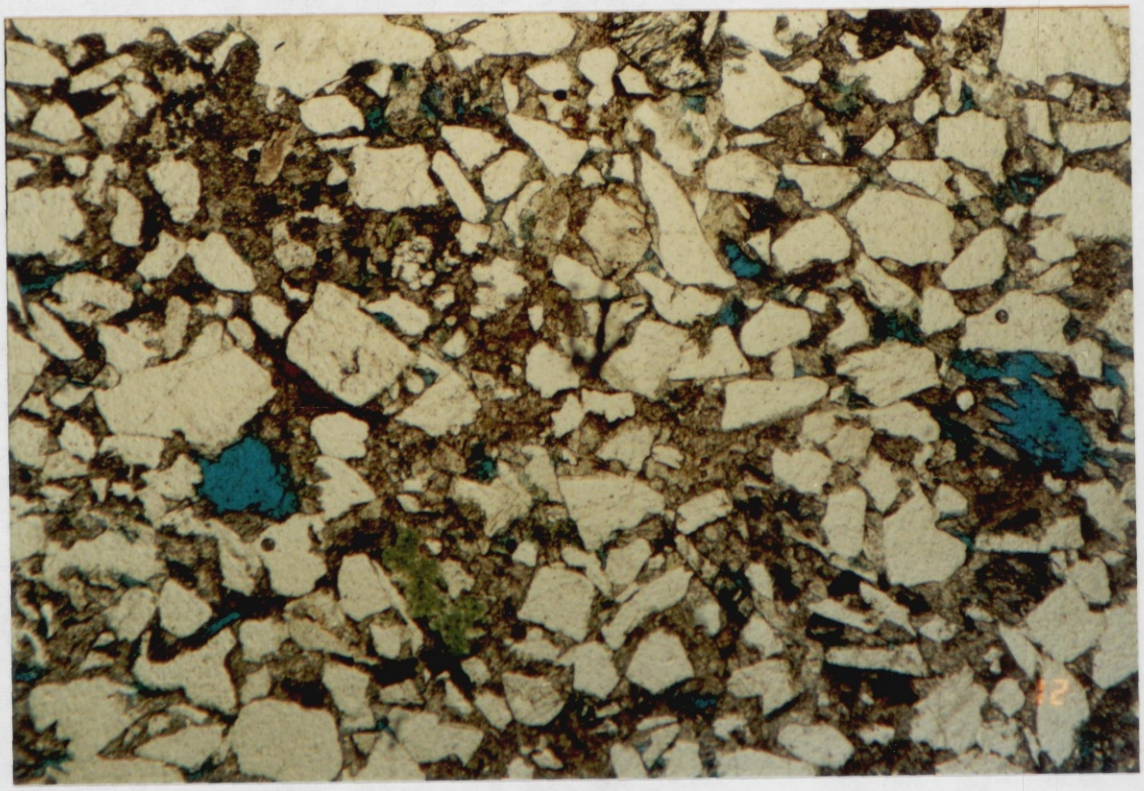
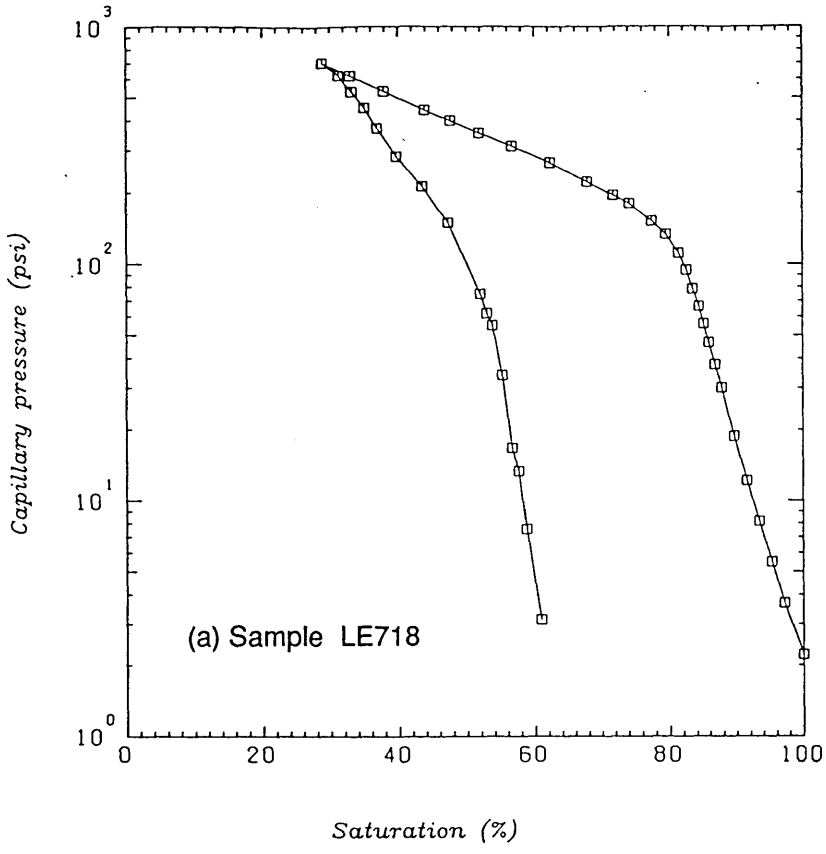


Fig. 6.14 Photomicrograph of sample M11004. Magnification x10.



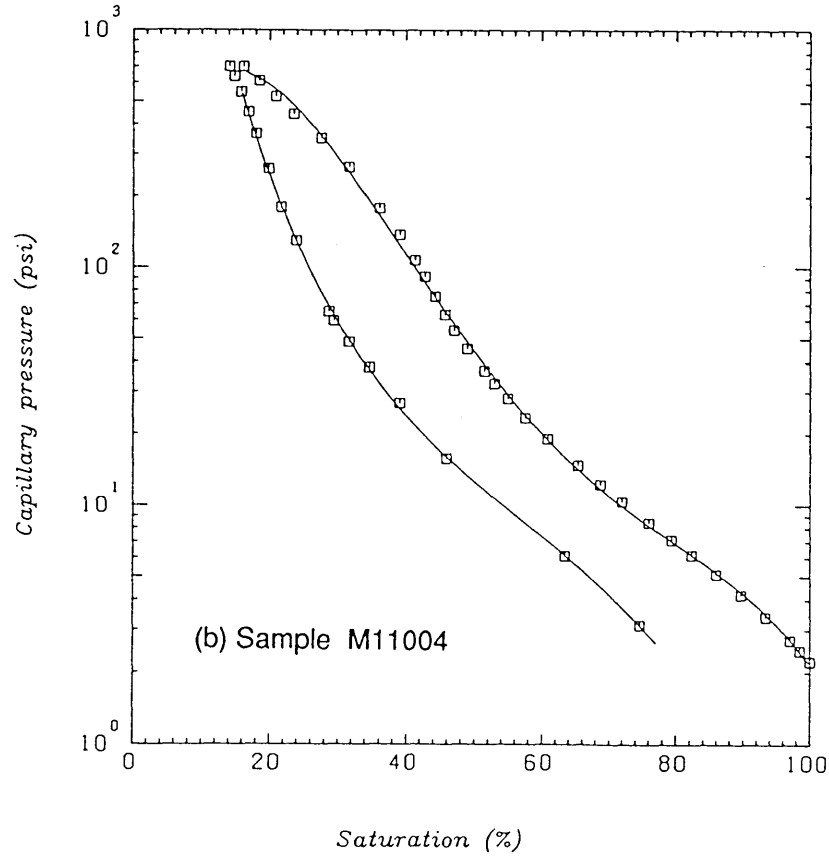
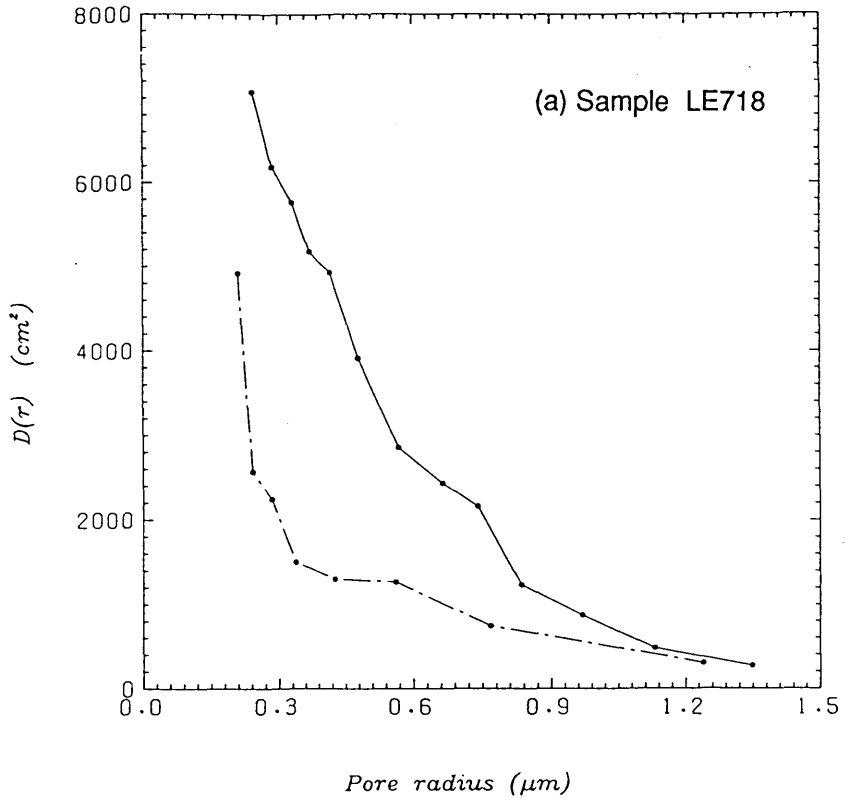


Fig. 6.15 Capillary pressure curves.



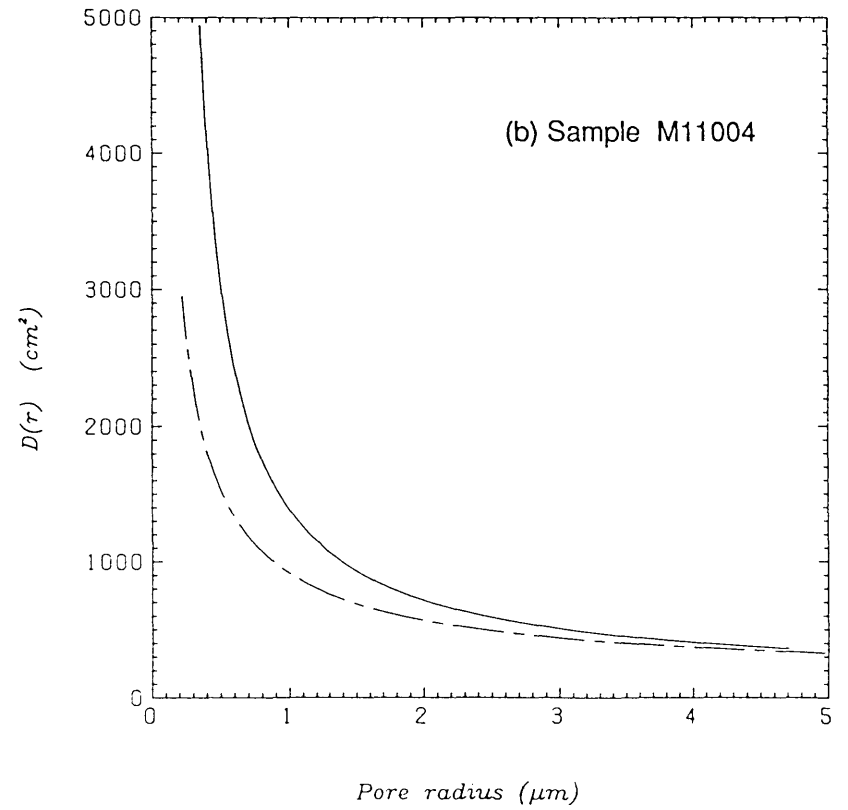


Fig. 6.16 Pore throat size distributions.

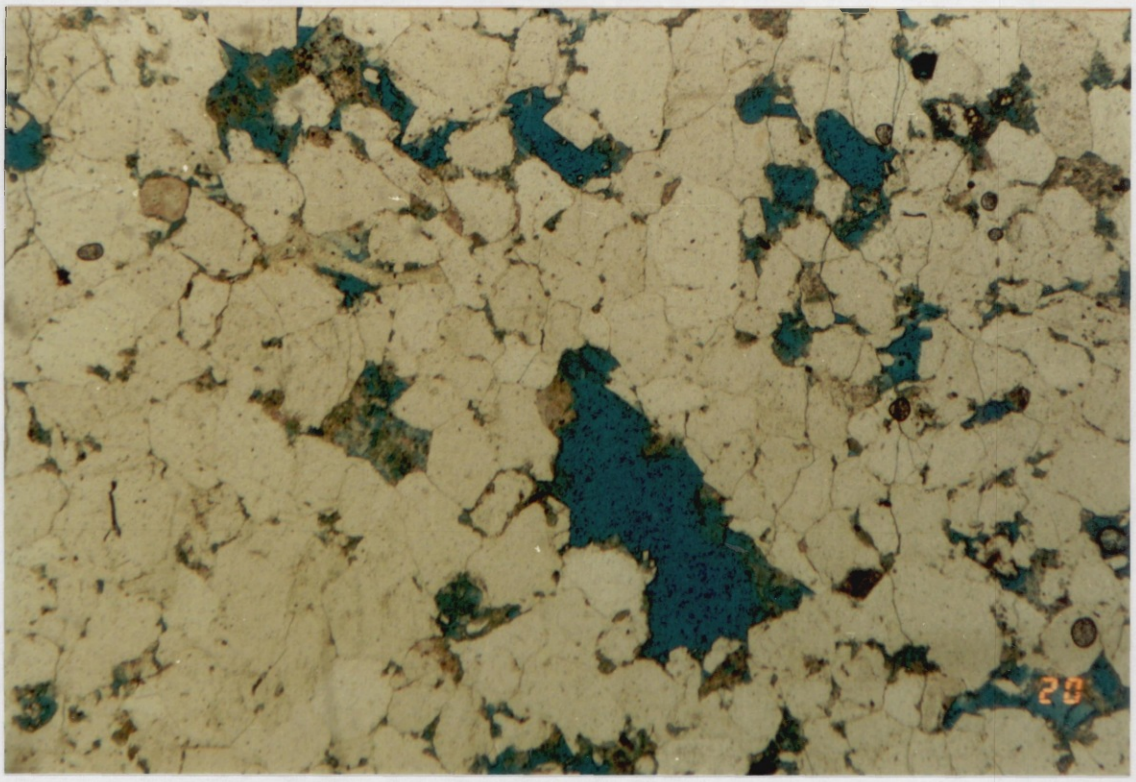


Fig. 6.17 Photomicrograph of sample AL79. Magnification x10.

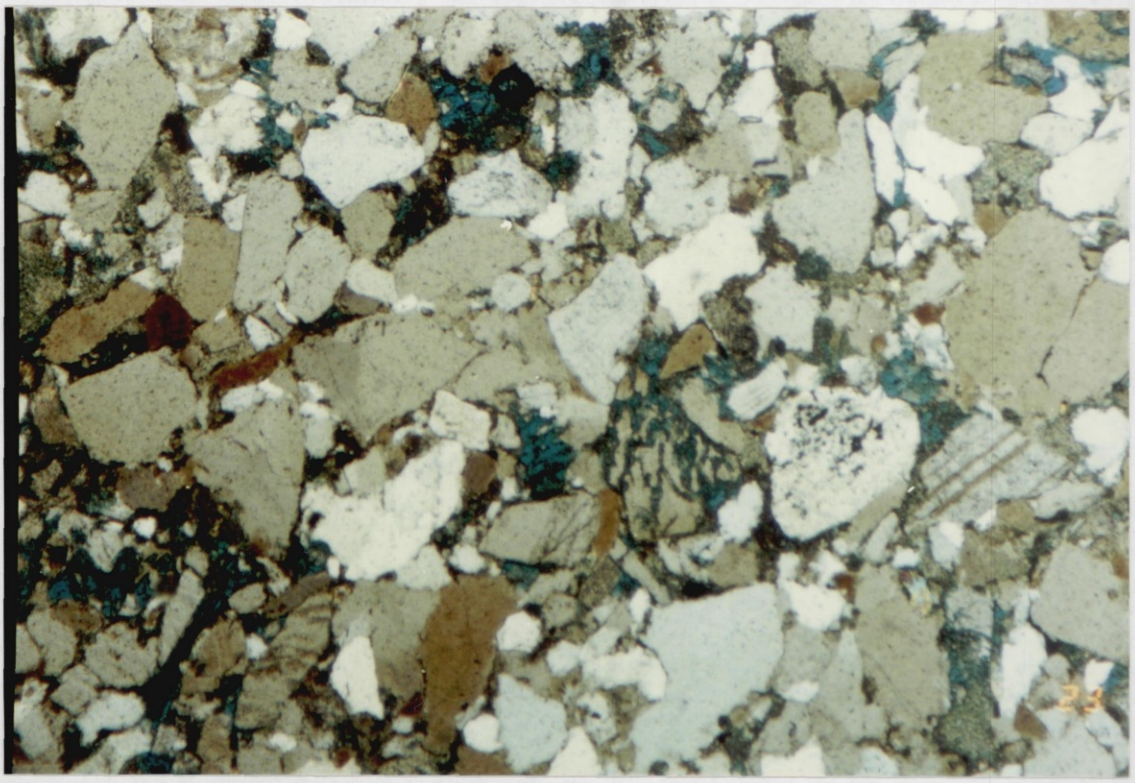
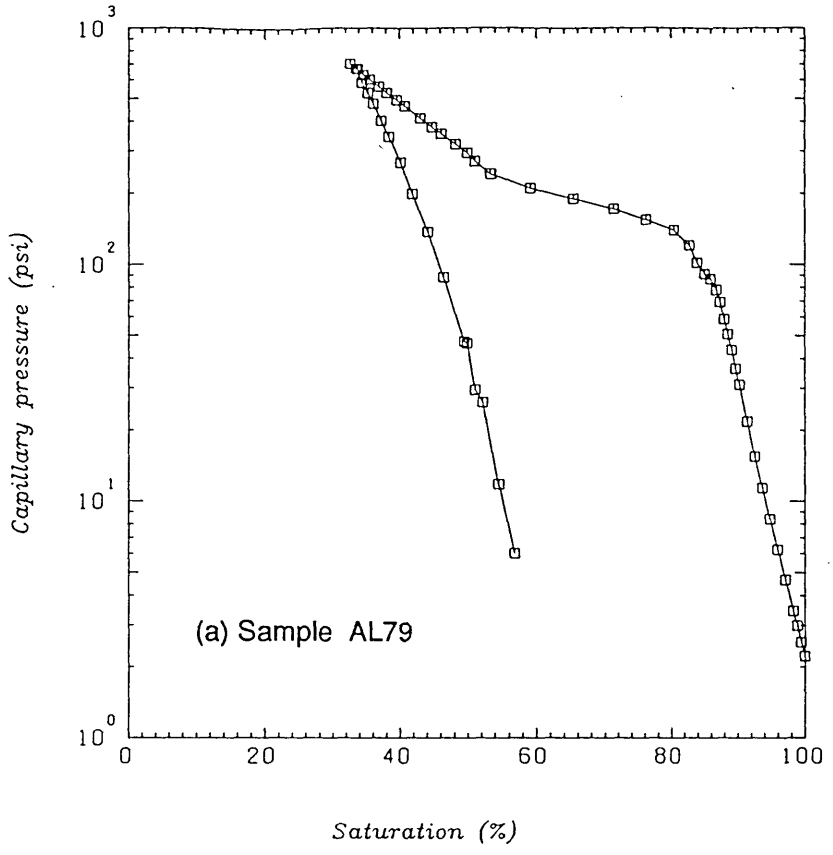


Fig. 6.18 Photomicrograph of sample M73002. Magnification x10.



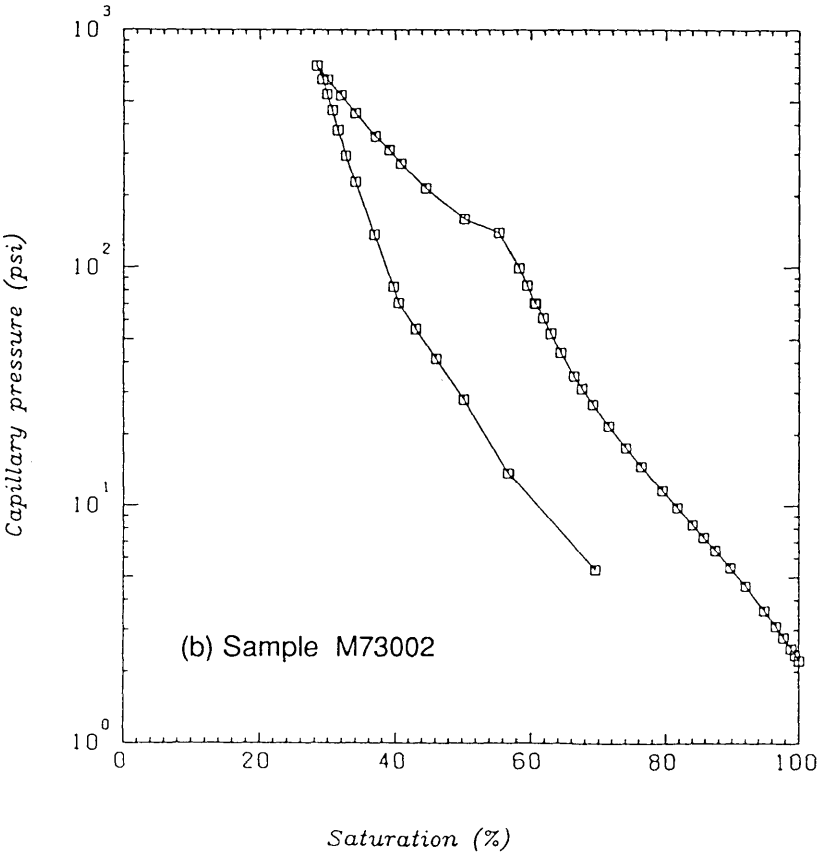
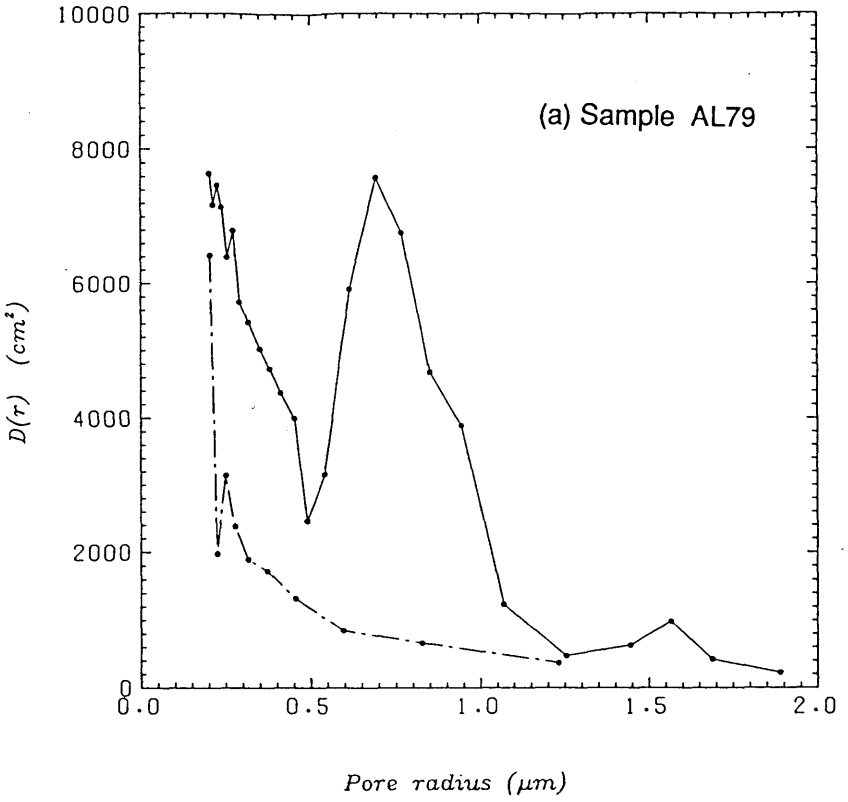


Fig. 6.19 Capillary pressure curves.



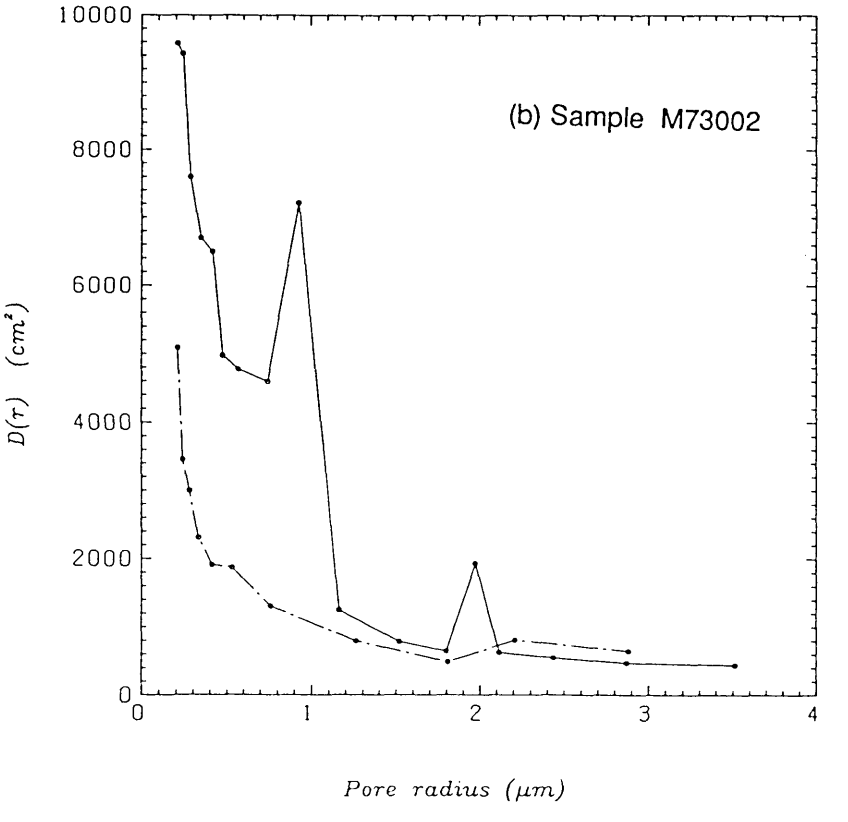


Fig. 6.20 Pore throat size distribution curves.

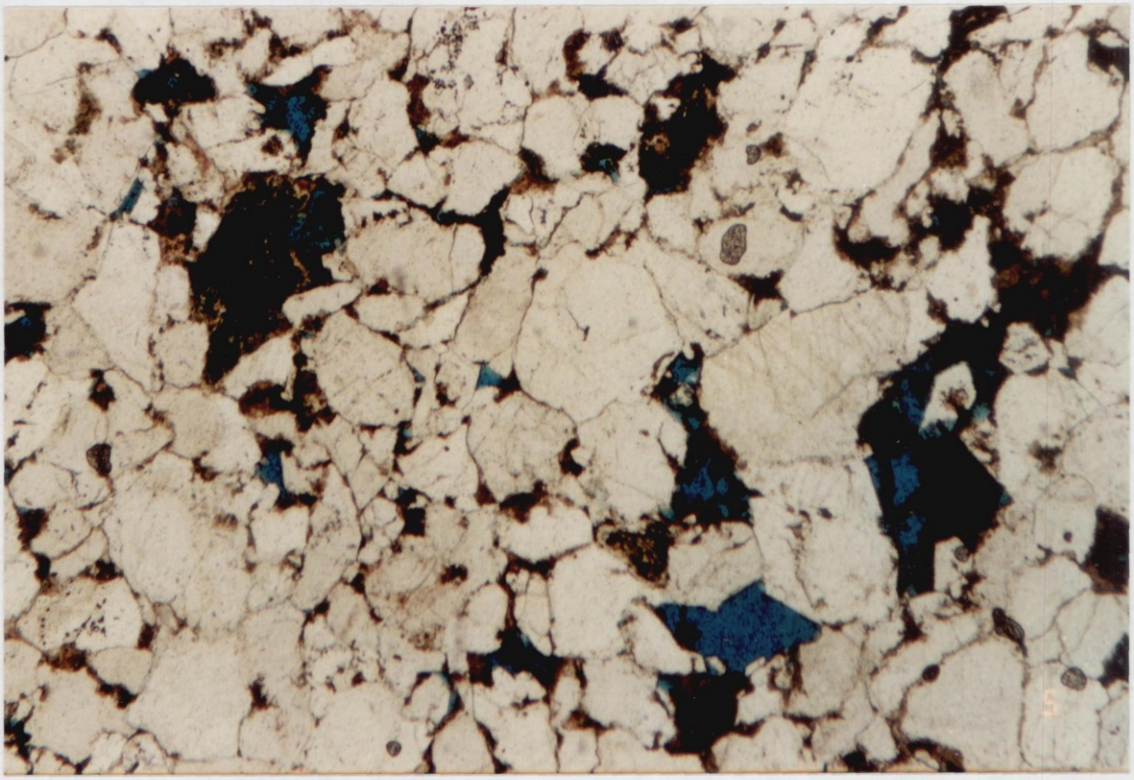


Fig. 6.21 Photomicrograph of sample AL29. Magnification x10.

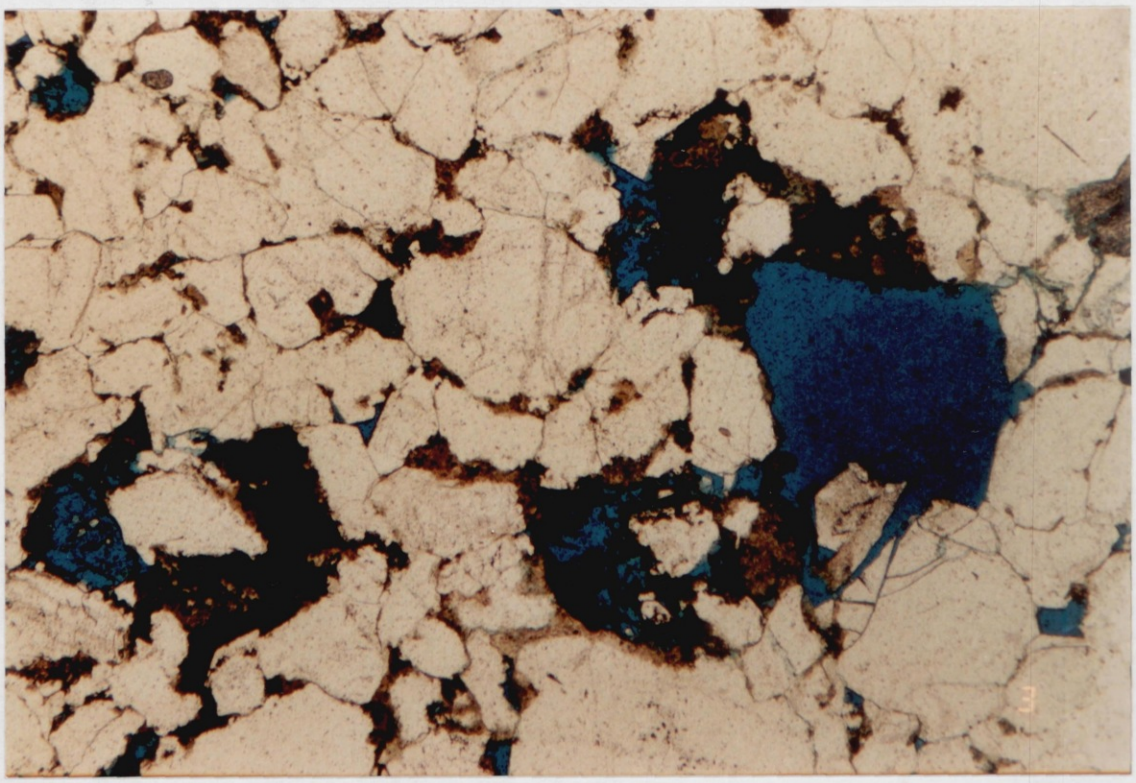
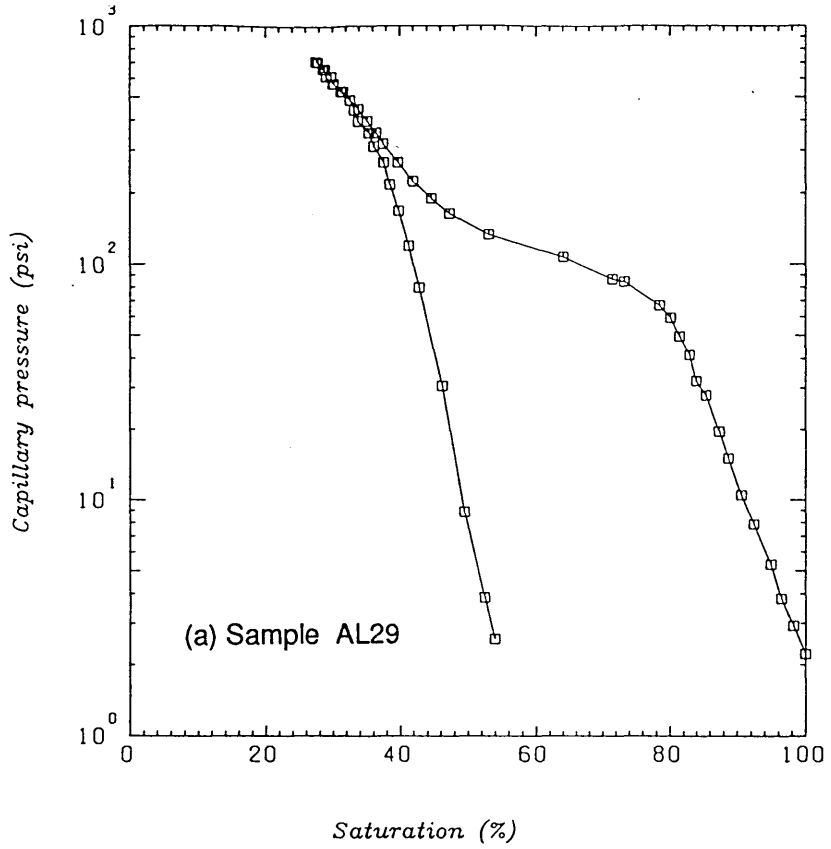


Fig. 6.22 Photomicrograph of sample AL40. Magnification x10.



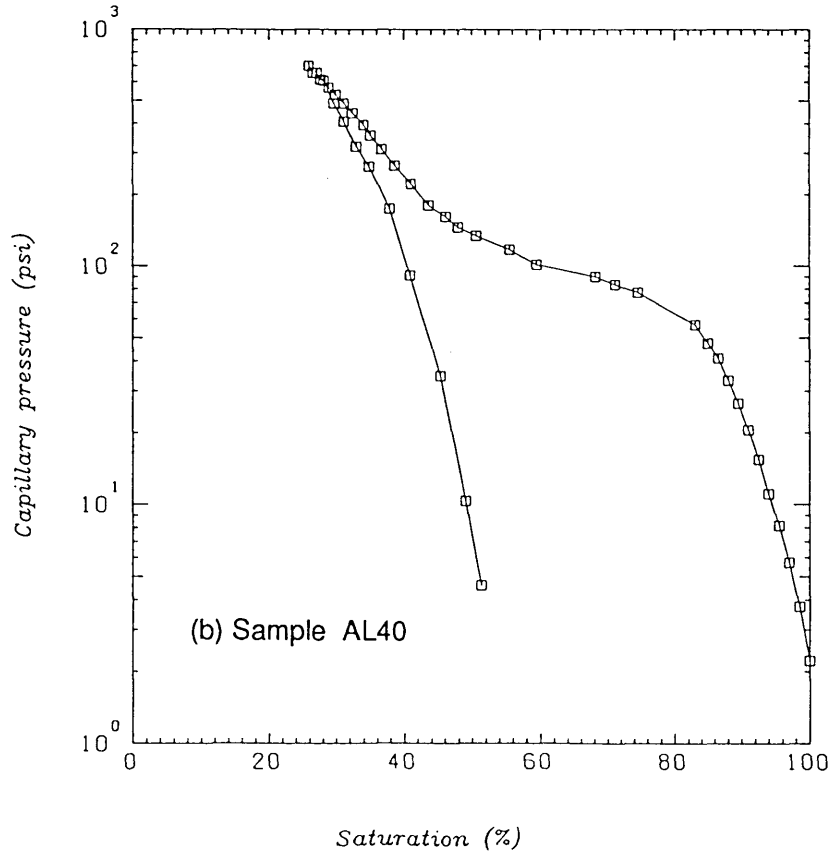
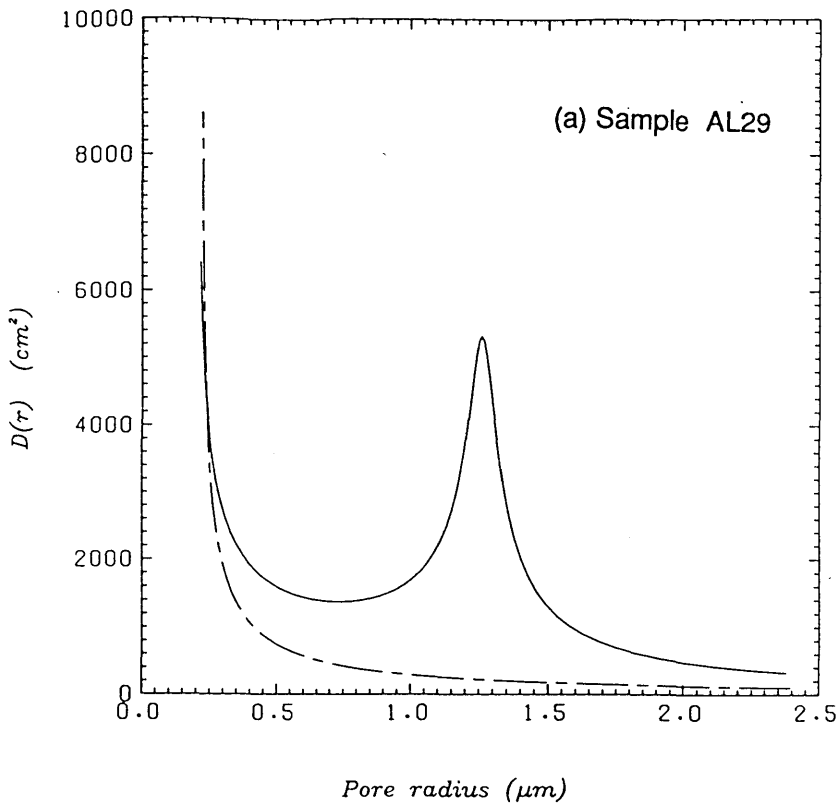


Fig. 6.23 Capillary pressure curves.



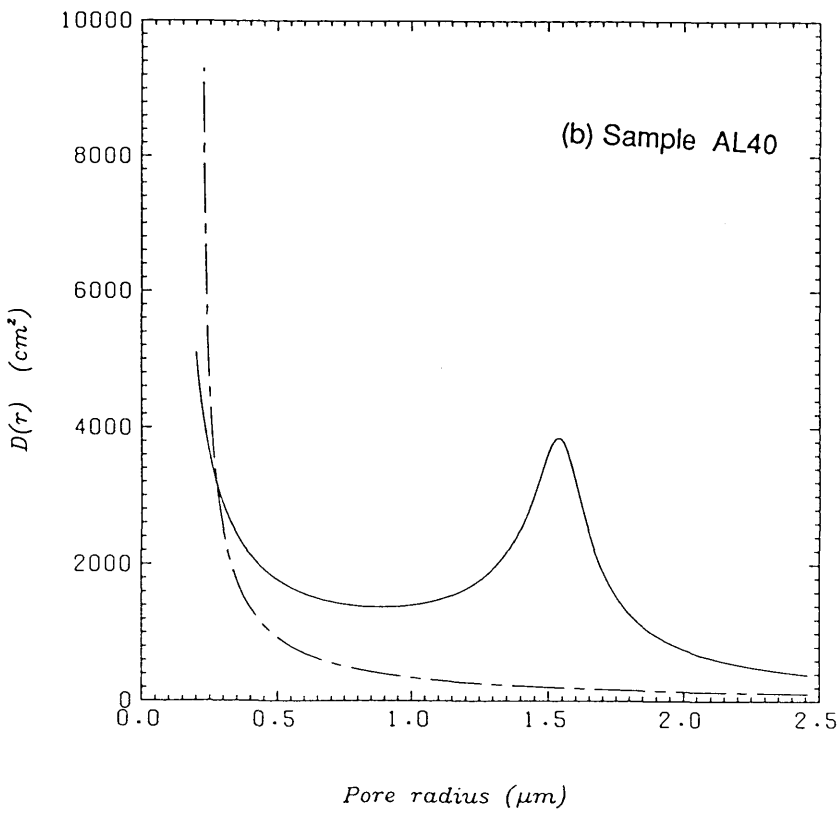


Fig. 6.24 Pore throat size distribution curves.

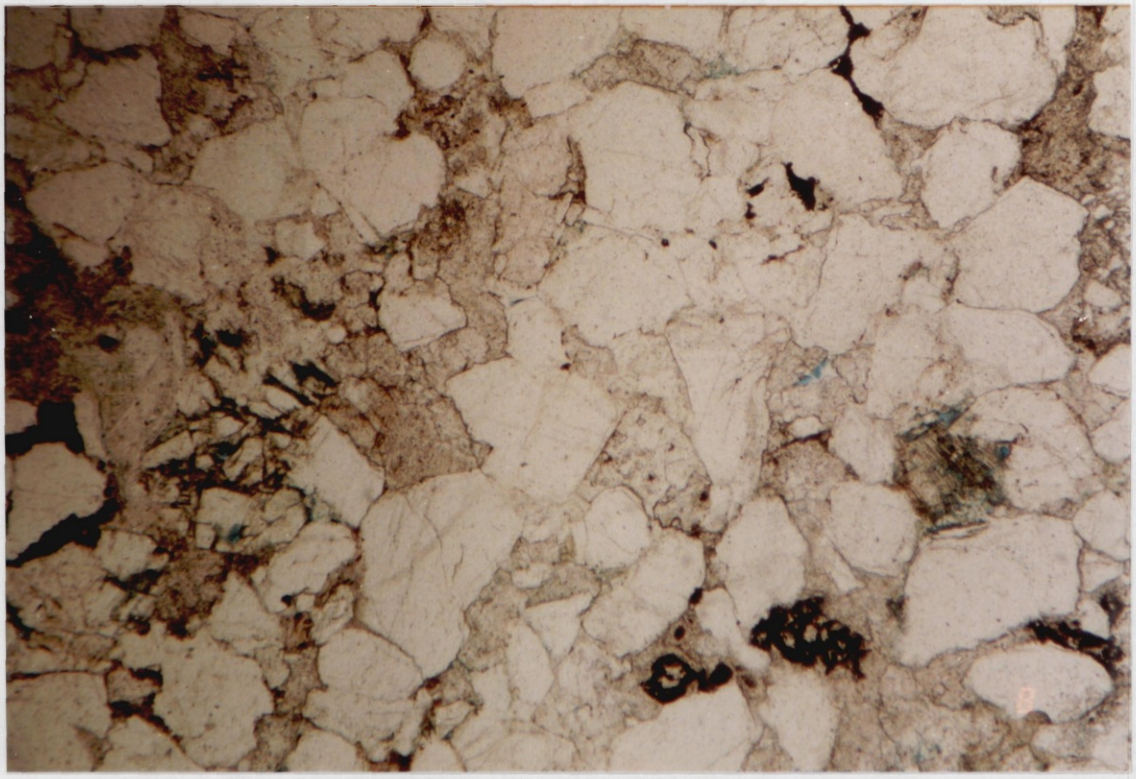


Fig. 6.25 Photomicrograph of sample RH101. Magnification x10.

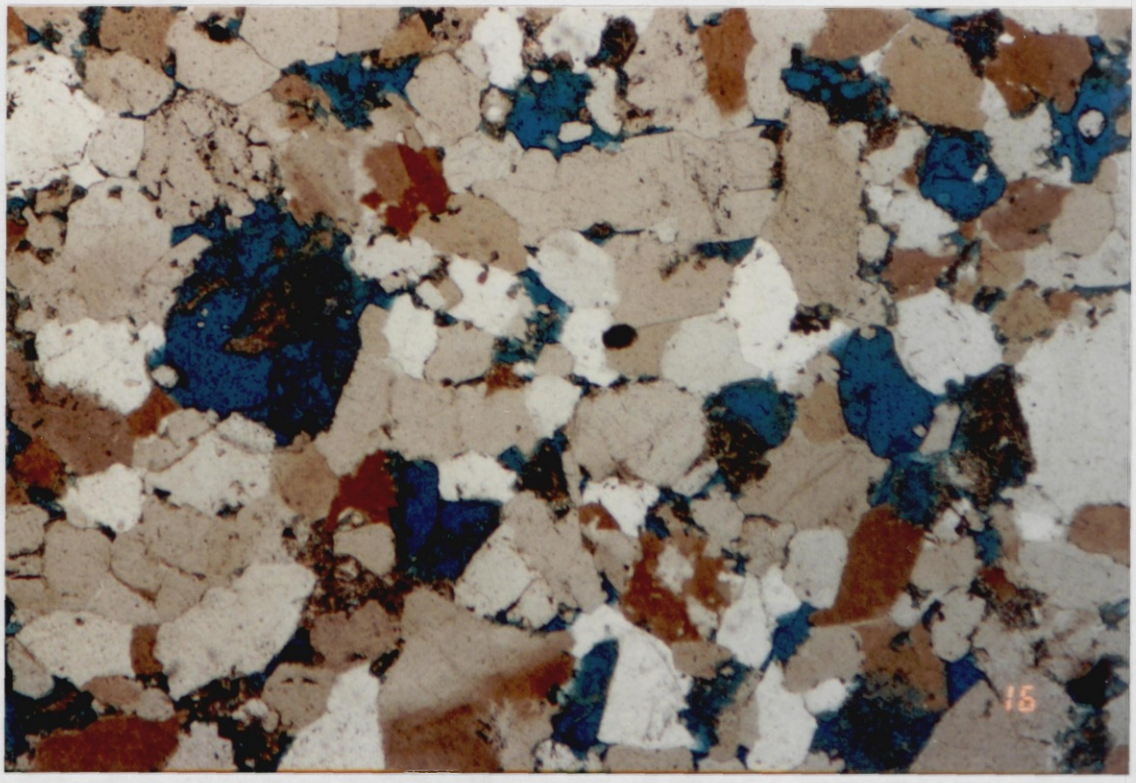
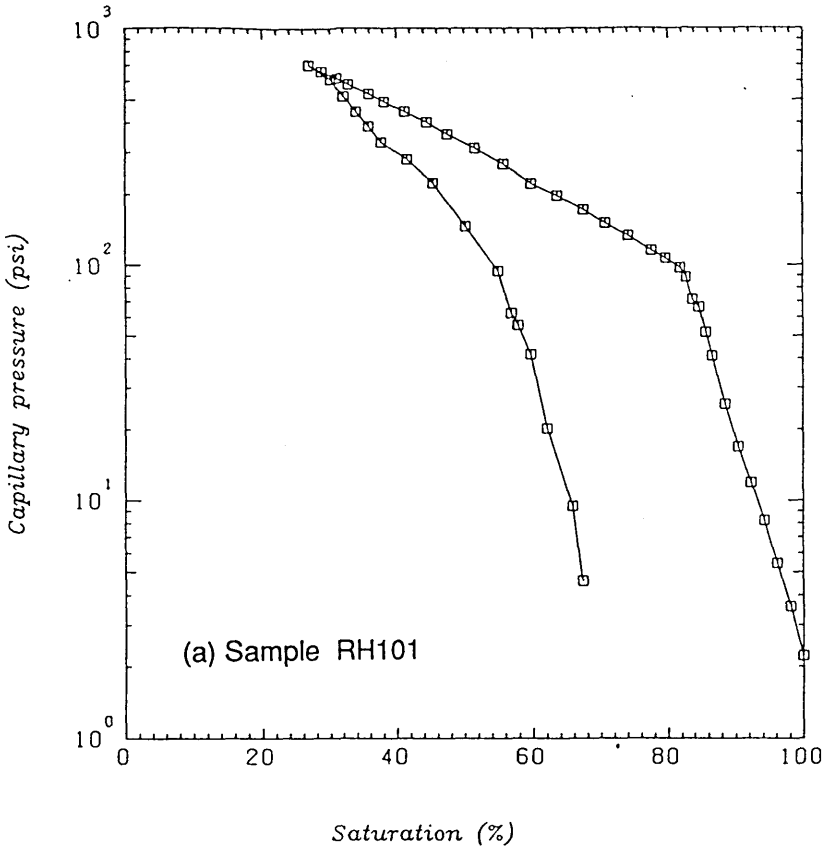


Fig. 6.26 Photomicrograph of sample AL111. Magnification x10.



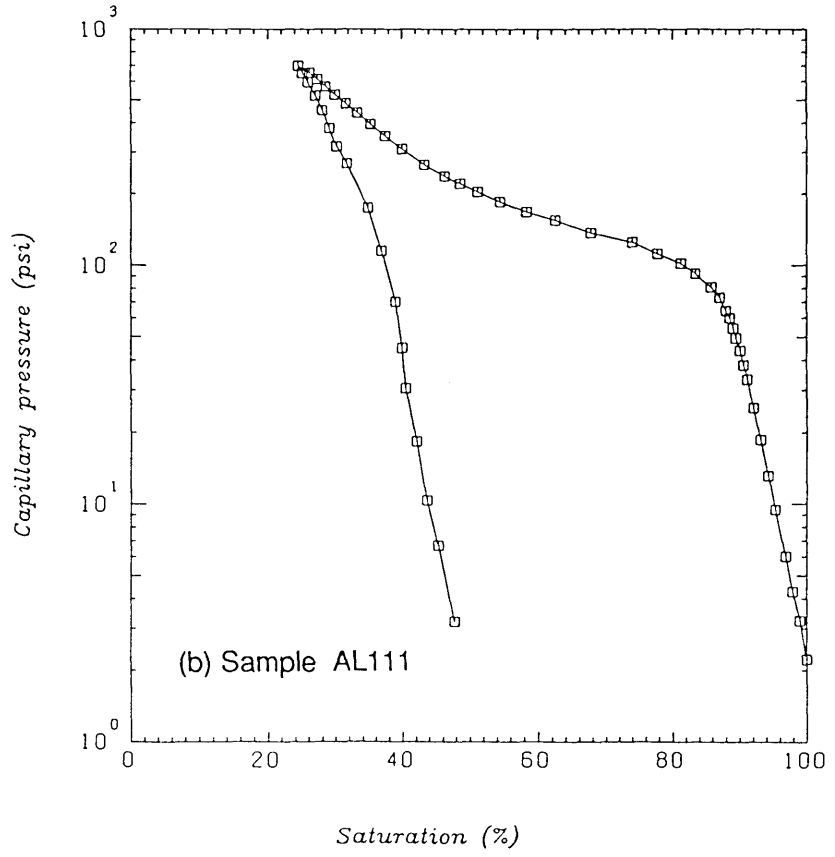
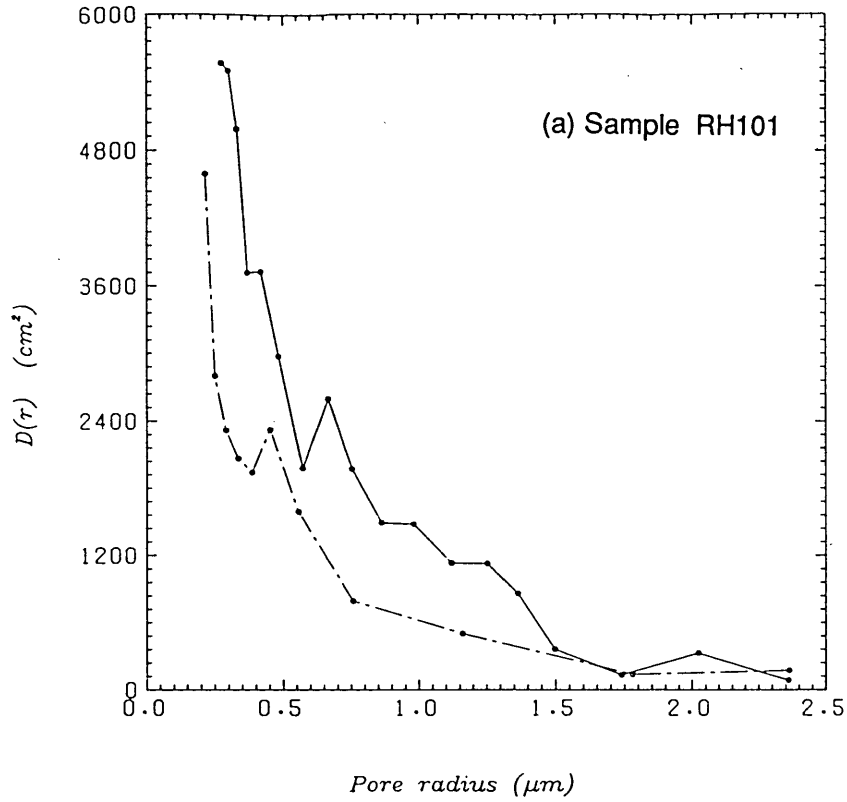


Fig. 6.27 Capillary pressure curves.



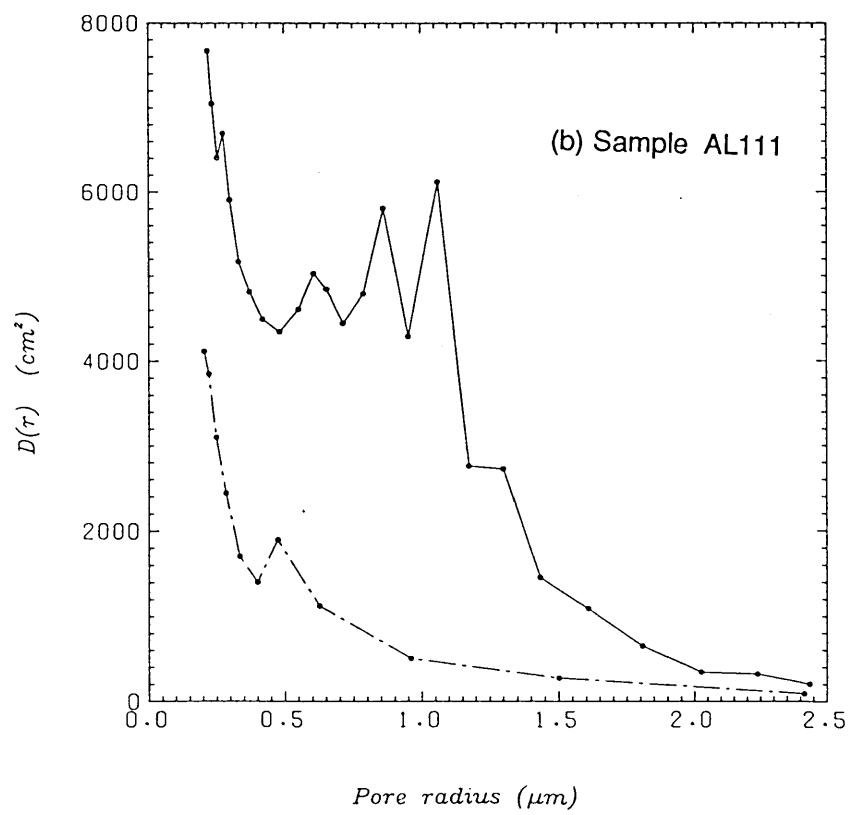


Fig. 6.28 Pore throat size distribution curves.

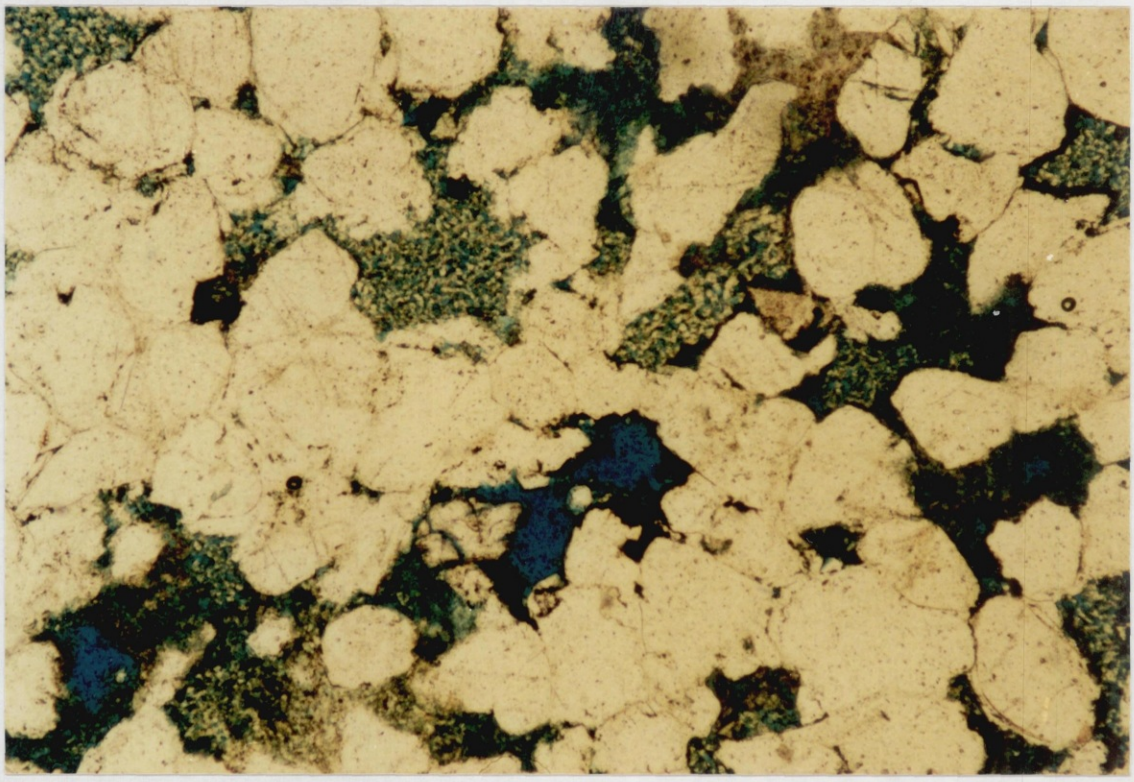


Fig. 6.29 Photomicrograph of sample RH103. Magnification x10.

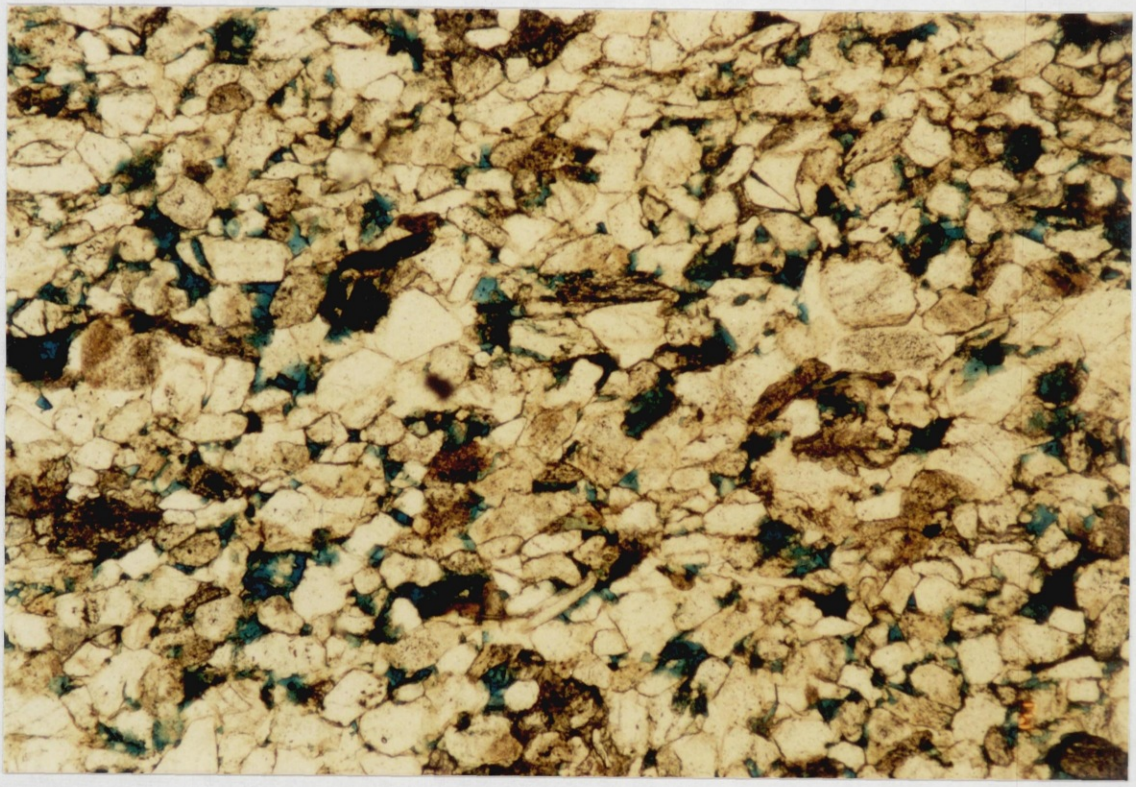
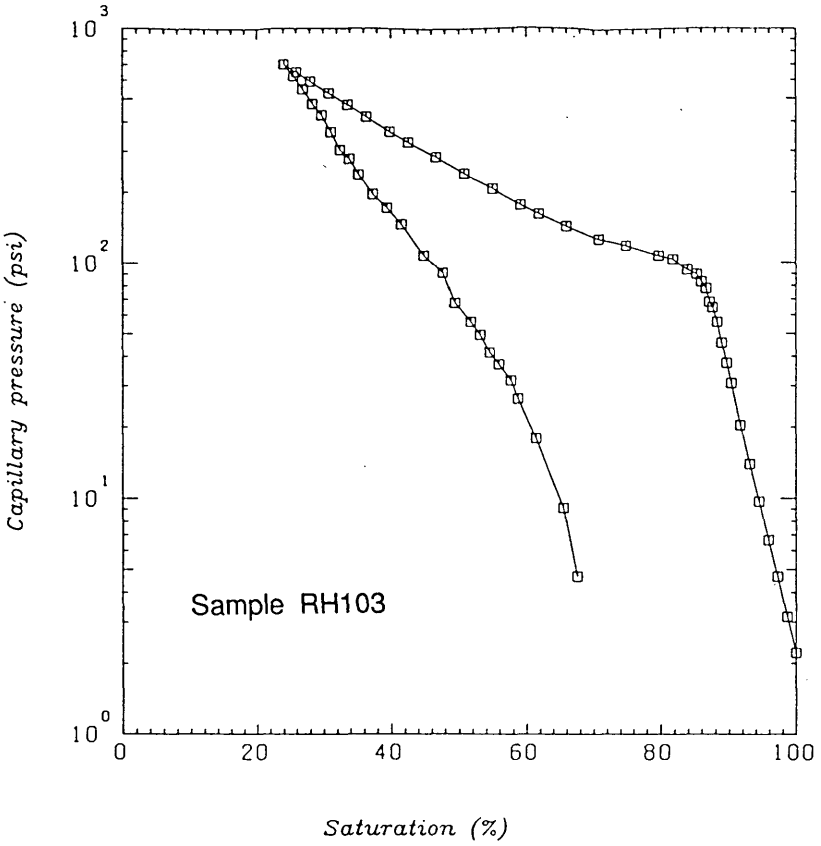


Fig. 6.30 Photomicrograph of sample MO63. Magnification x10.



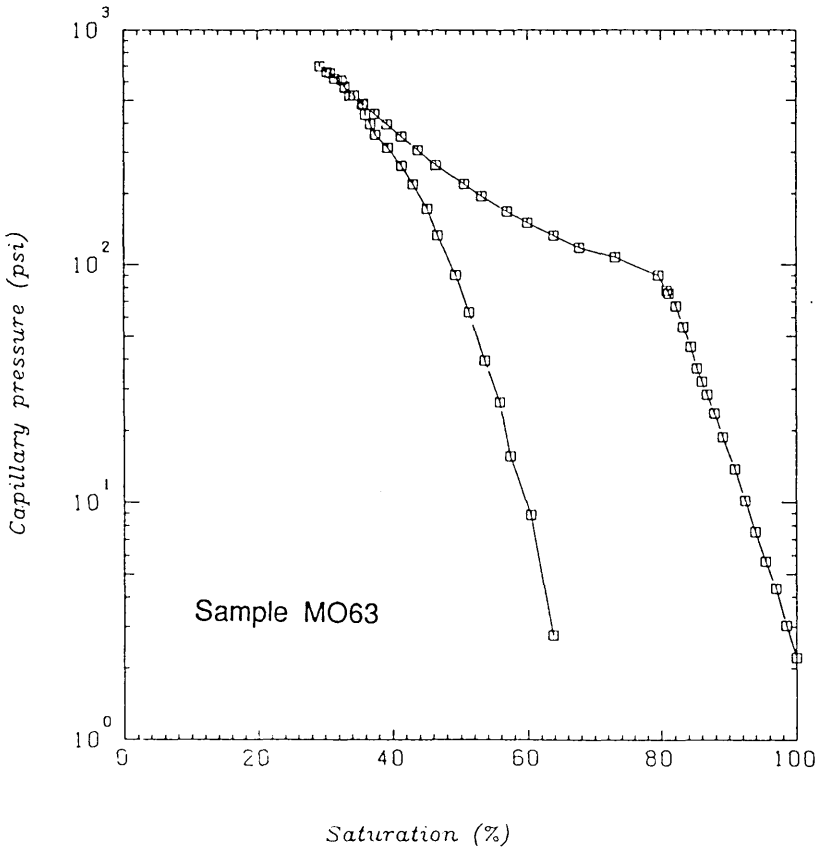
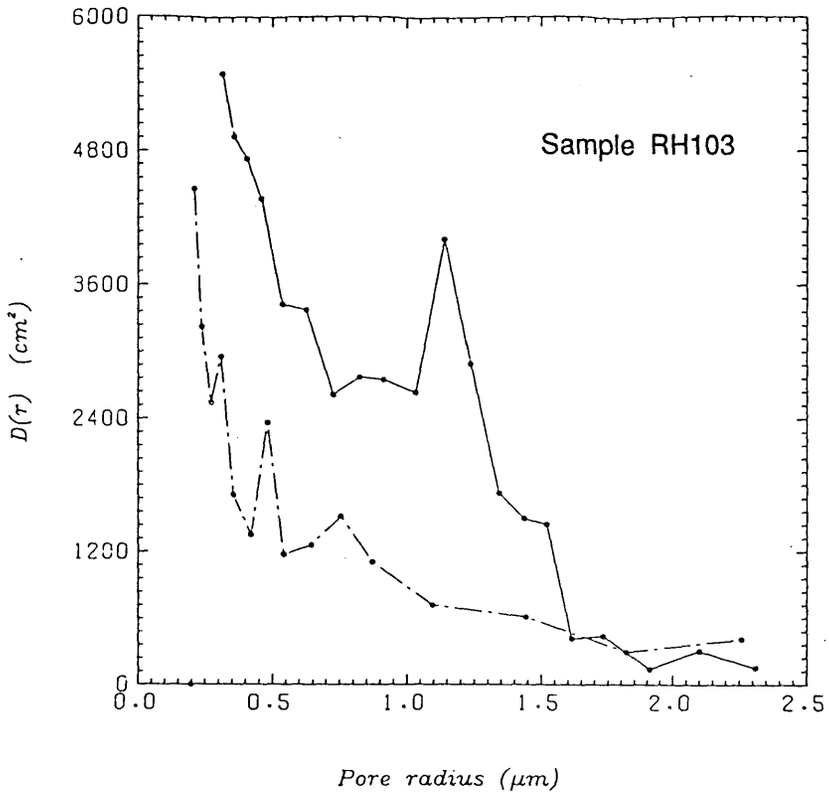


Fig. 6. 31 Capillary pressure curves.



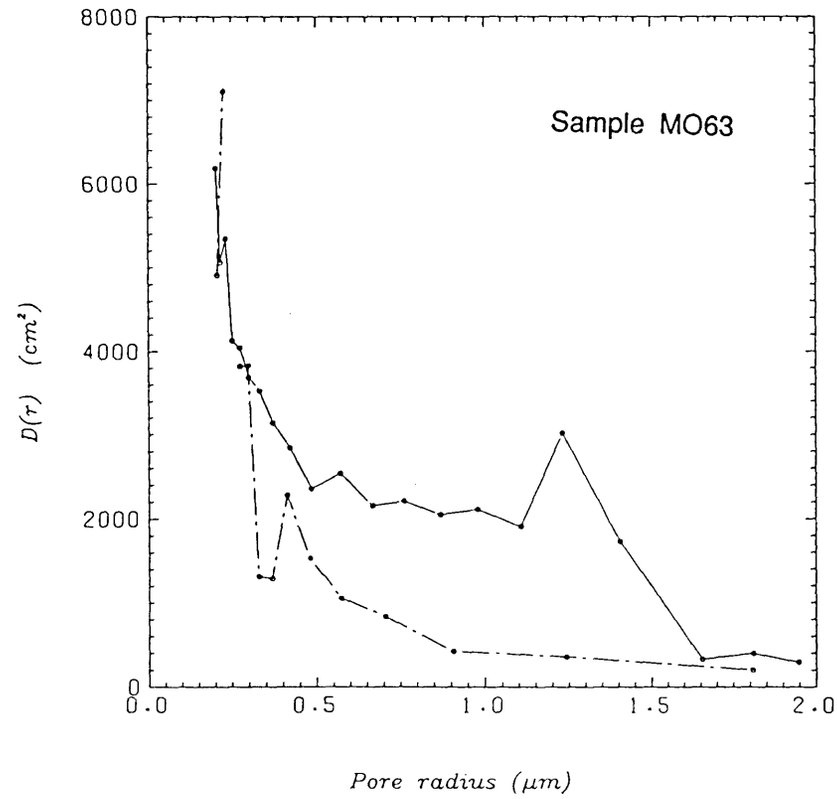


Fig. 6. 32 Pore throat size distribution curves.

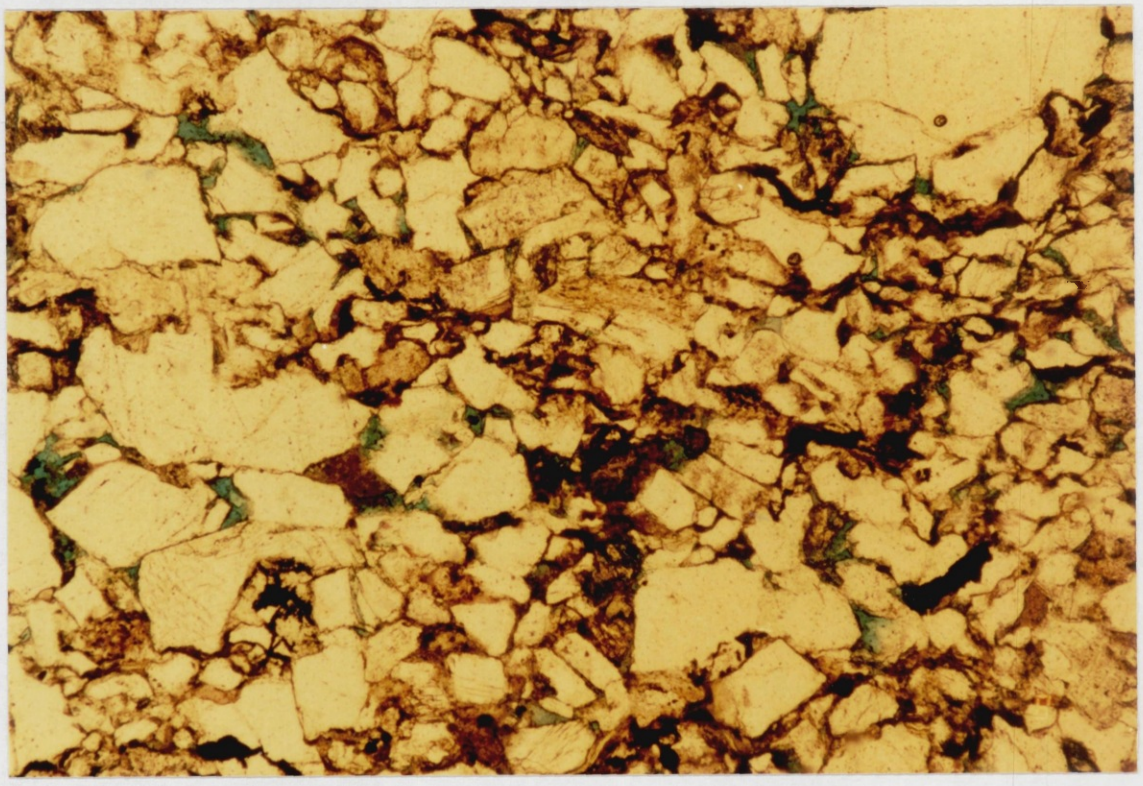


Fig. 6.33 Photomicrograph of sample M11003. Magnification x10.

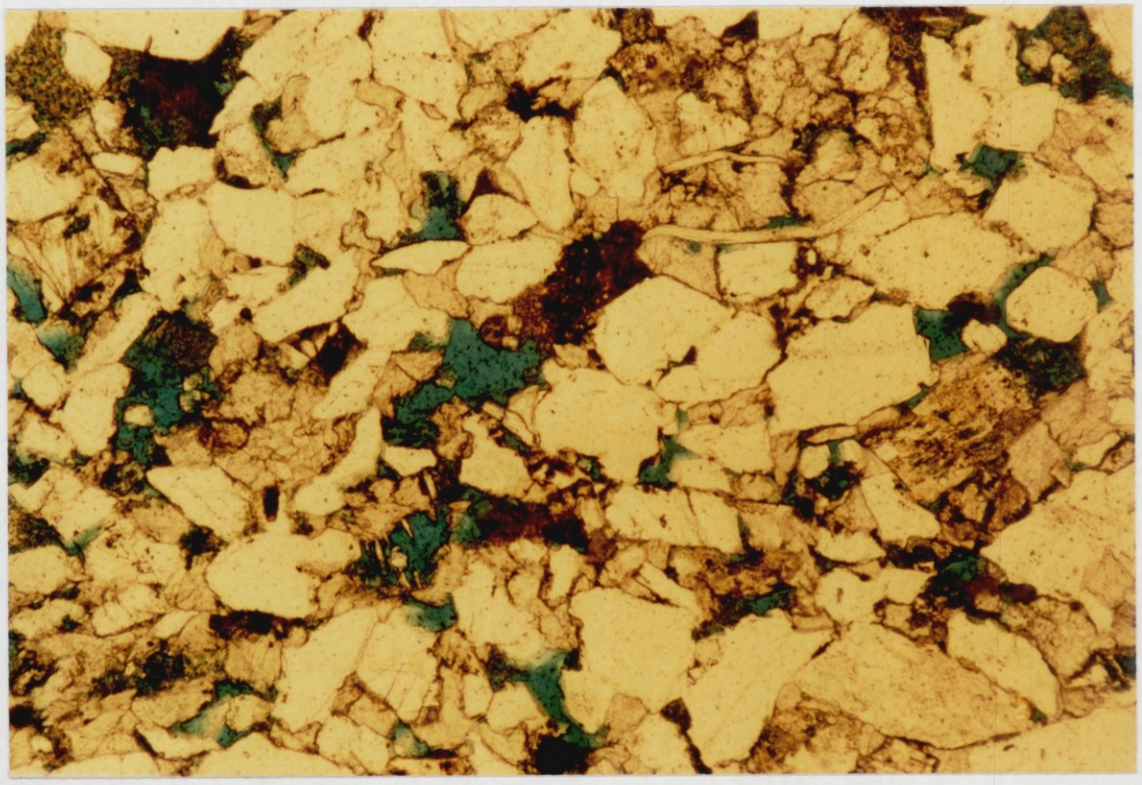
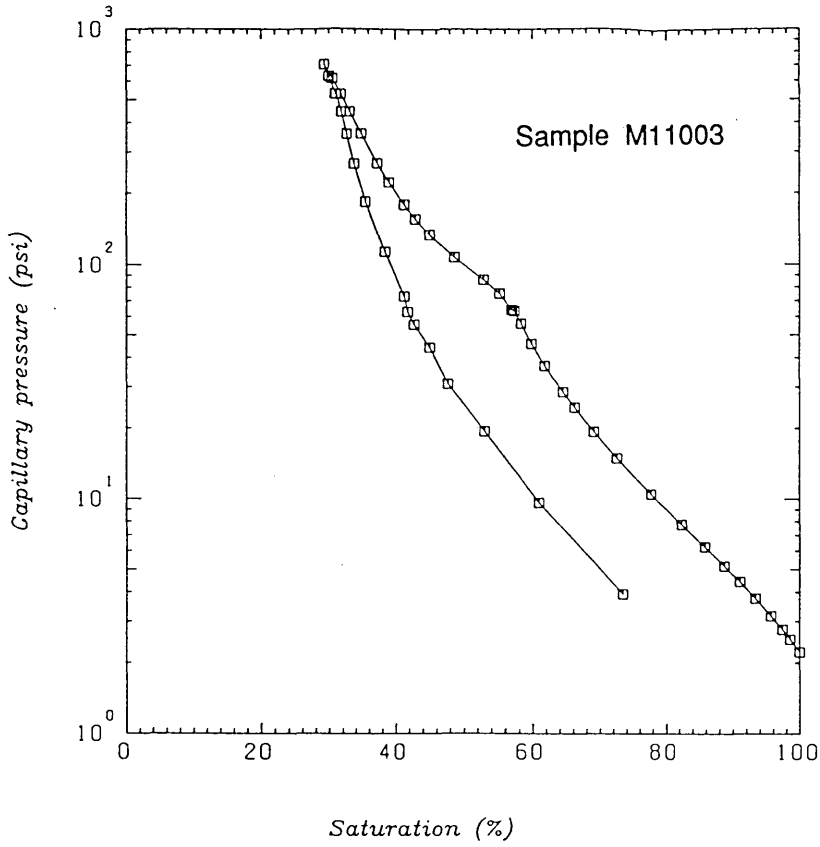


Fig. 6.34 Photomicrograph of sample M73004. Magnification x10.



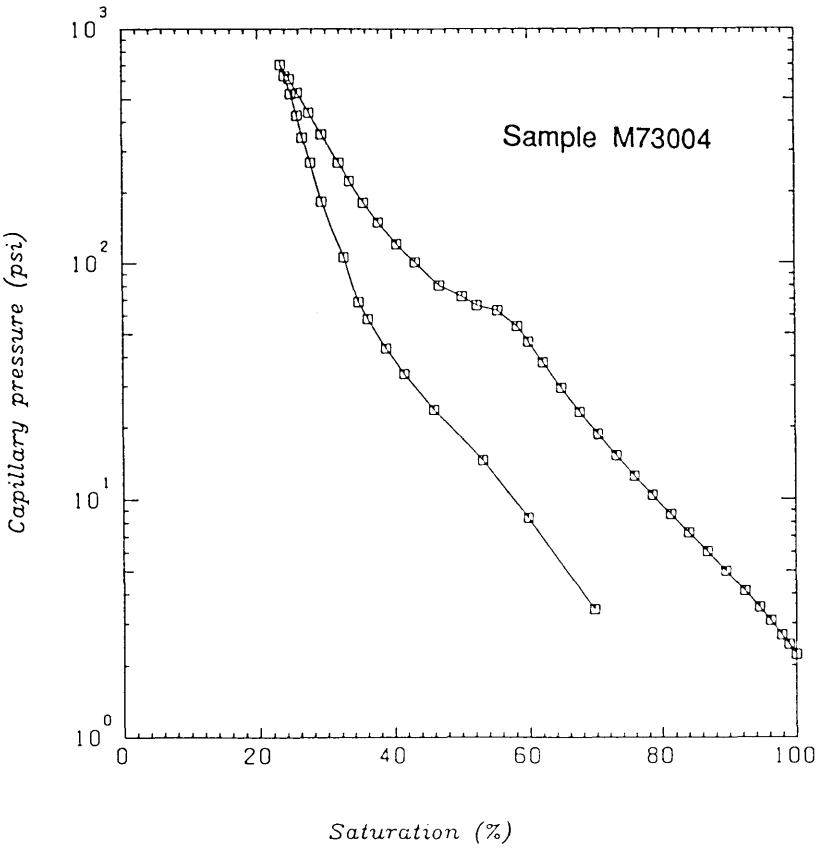
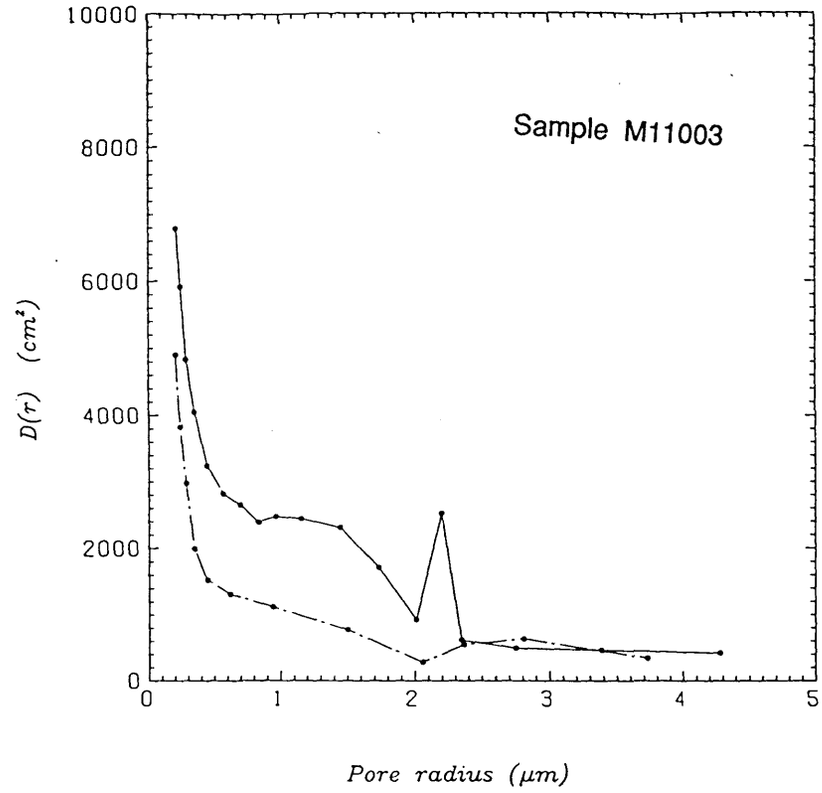


Fig. 6.35 Capillary pressure curves.



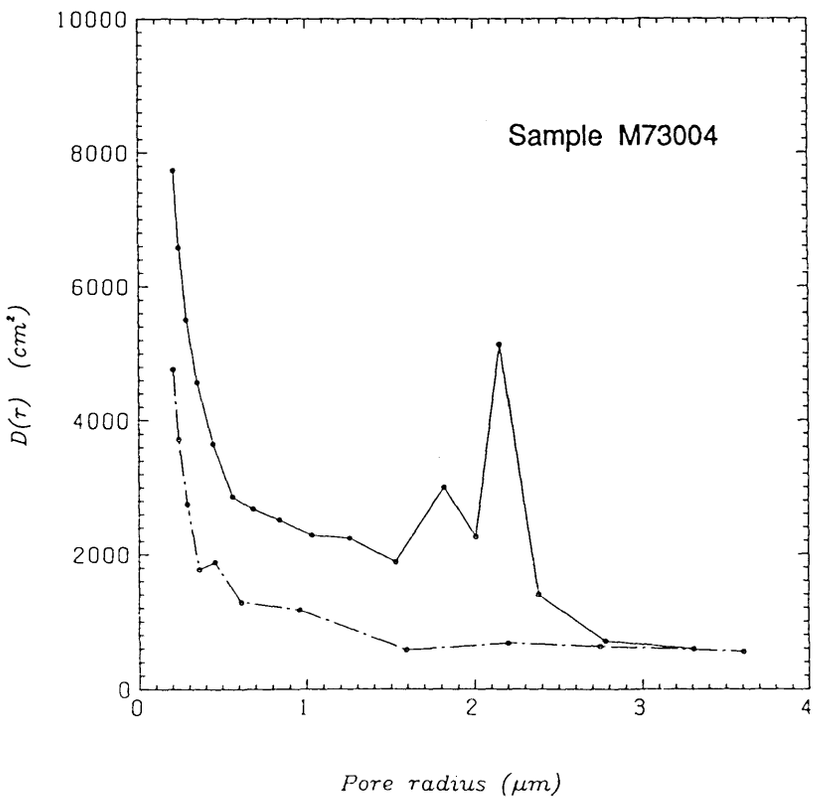


Fig. 6. 36 Pore throat size distribution curves.

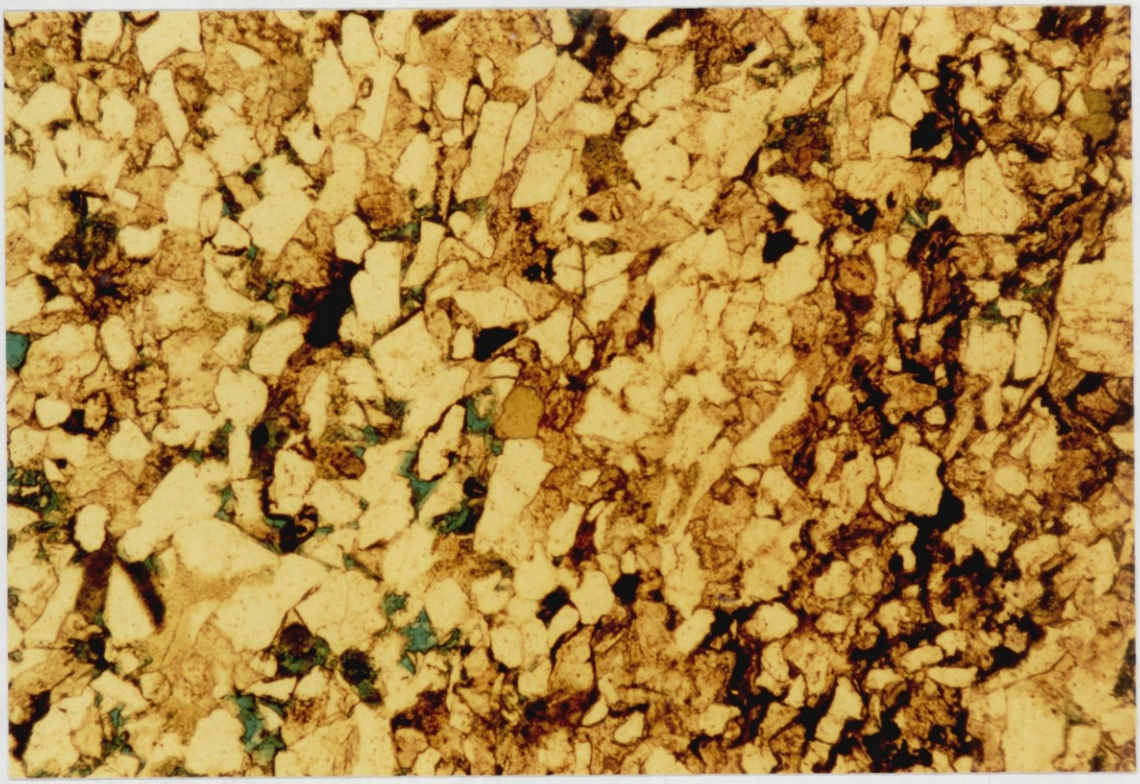


Fig. 6.37 Photomicrograph of sample M11011. Magnification x10.

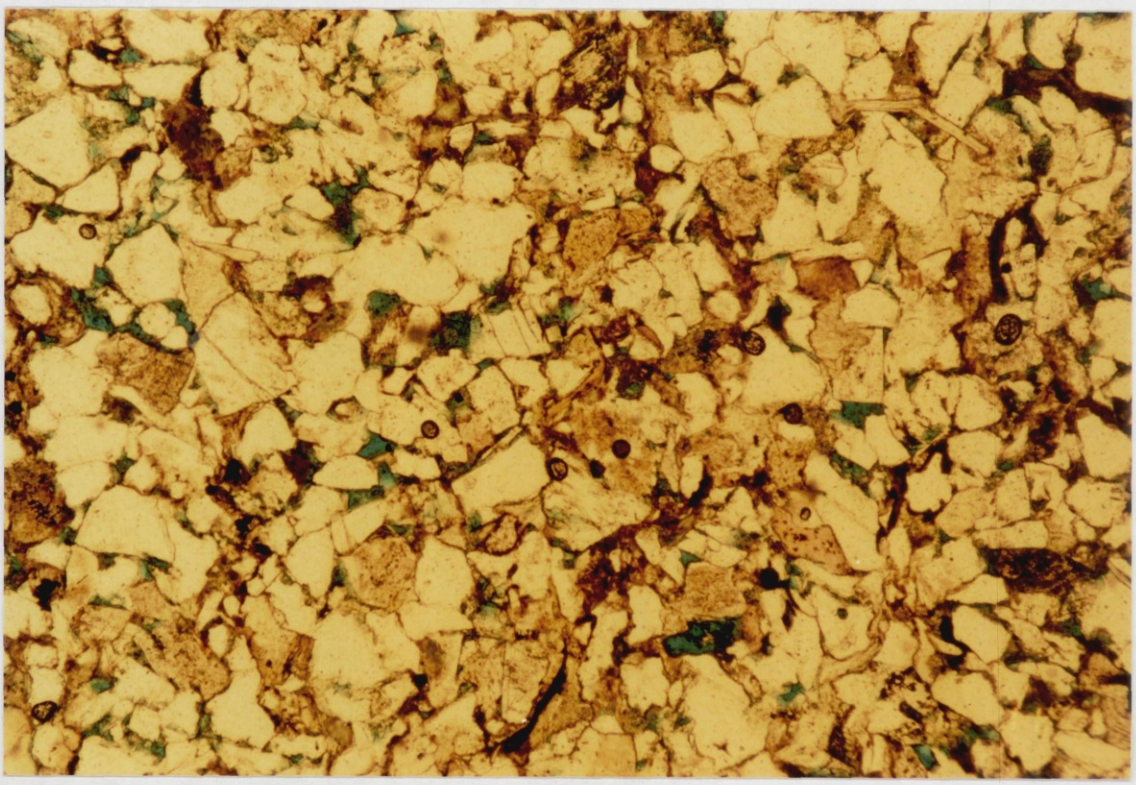
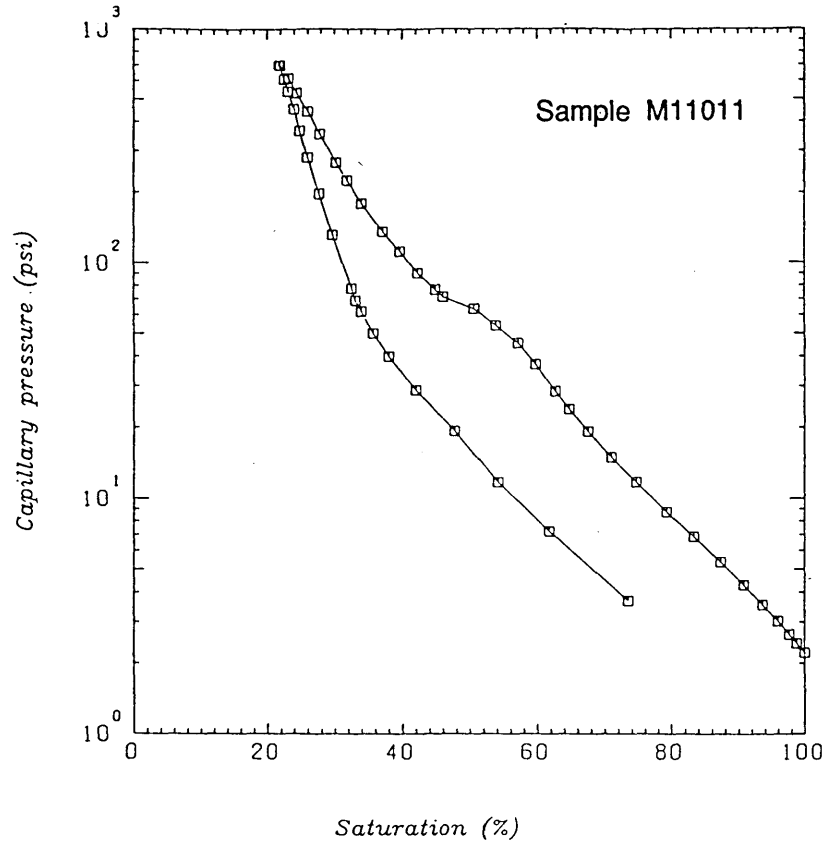


Fig. 6.38 Photomicrograph of sample M11008. Magnification x10.



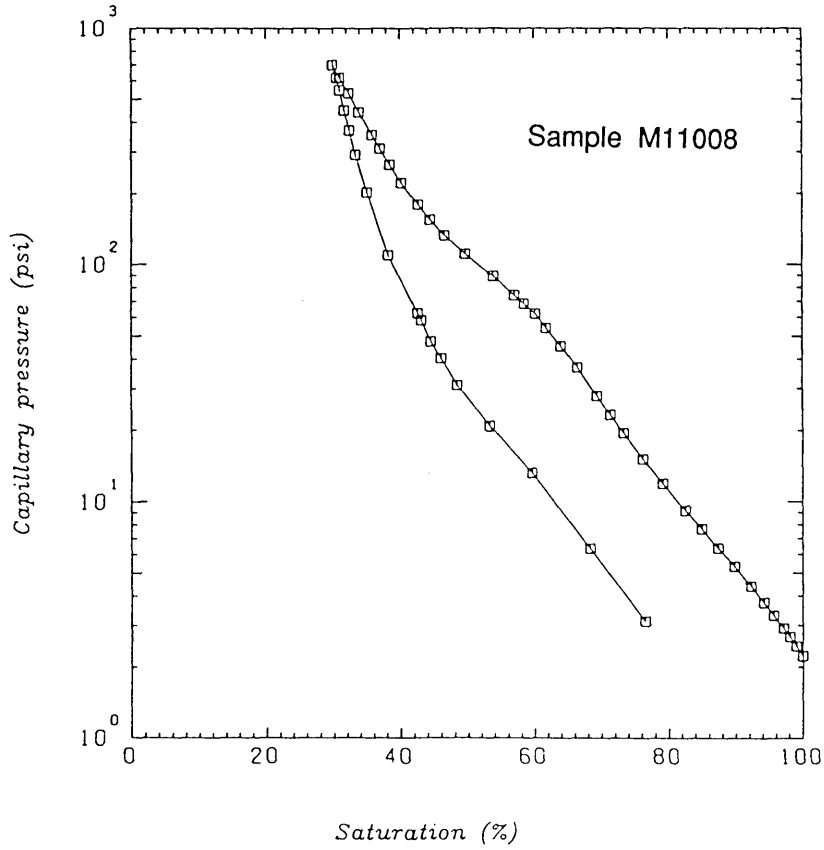
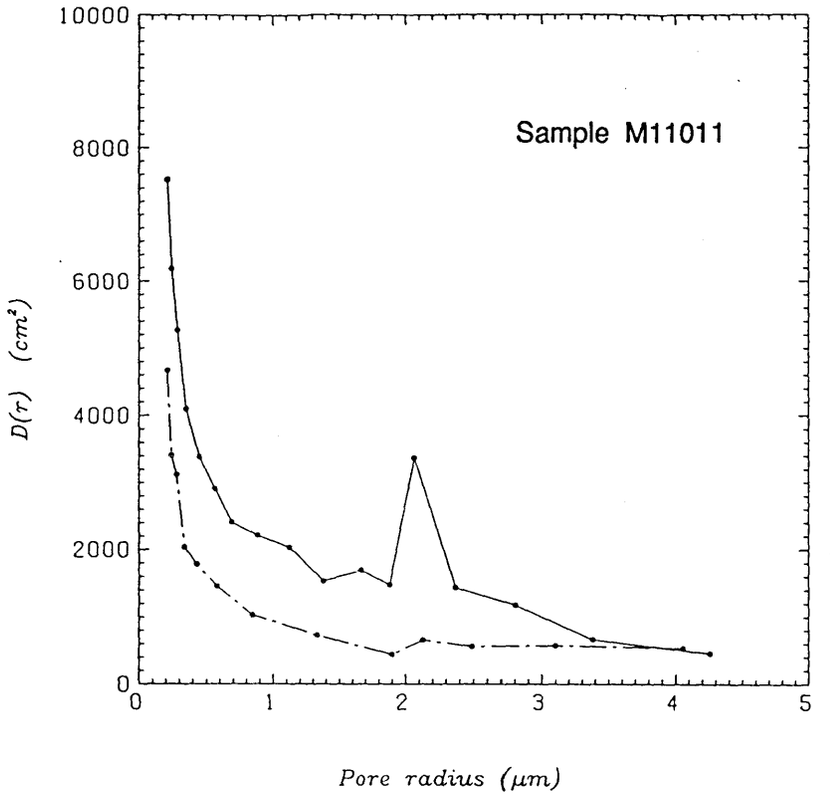


Fig. 6.39 Capillary pressure curves.



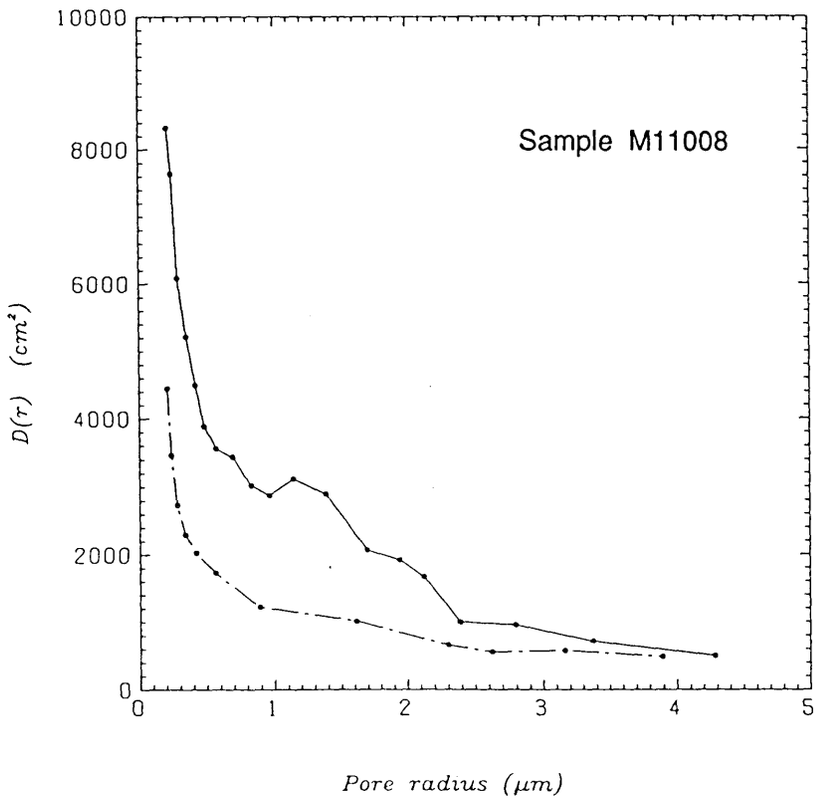


Fig. 6.40 Pore throat size distribution curves.

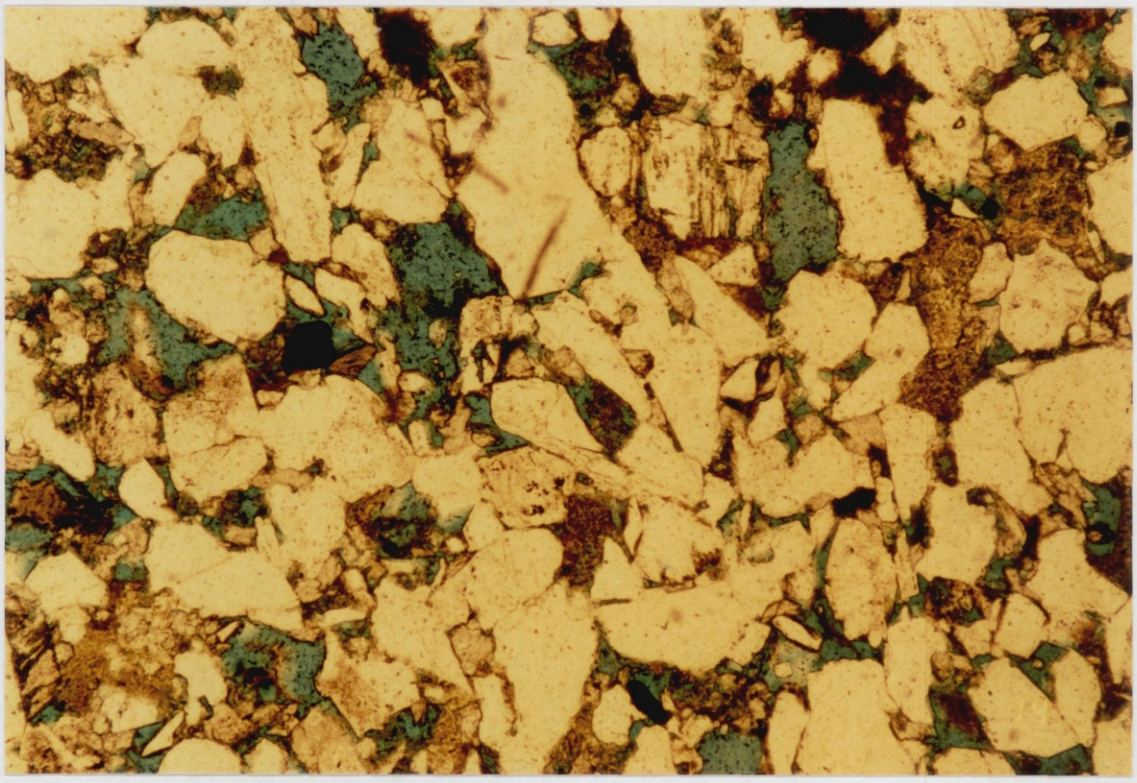


Fig. 6.41 Photomicrograph of sample M73006. Magnification x10.

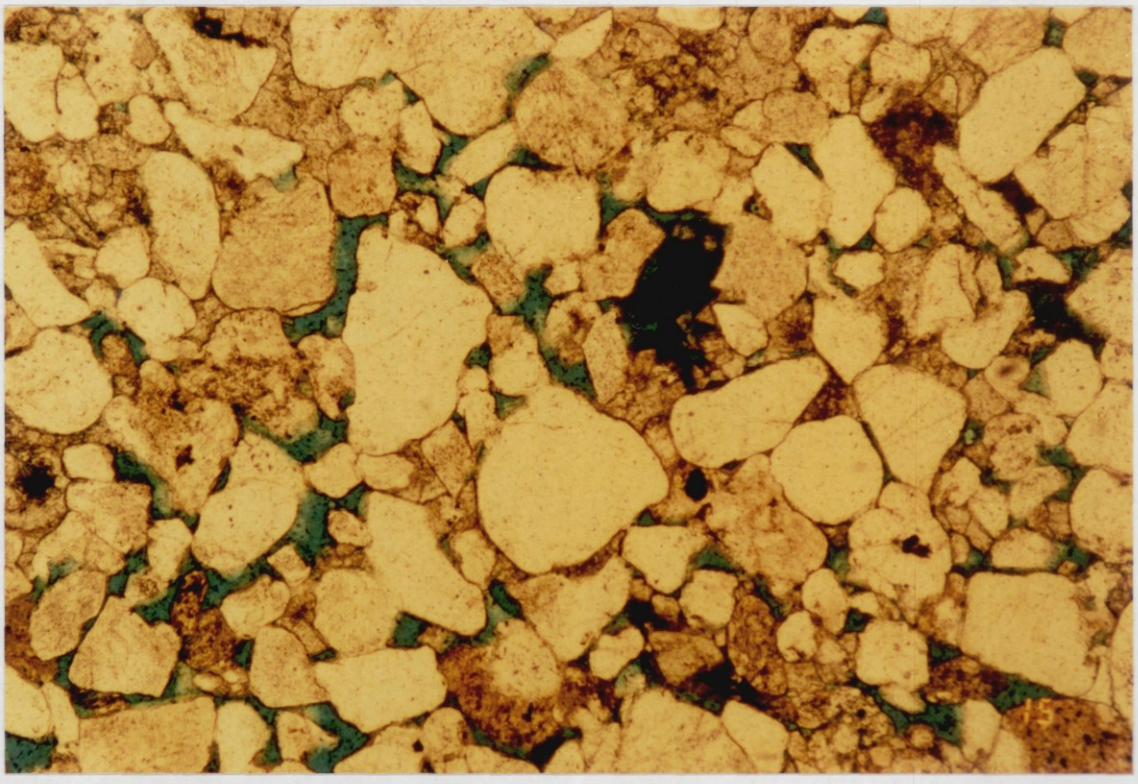
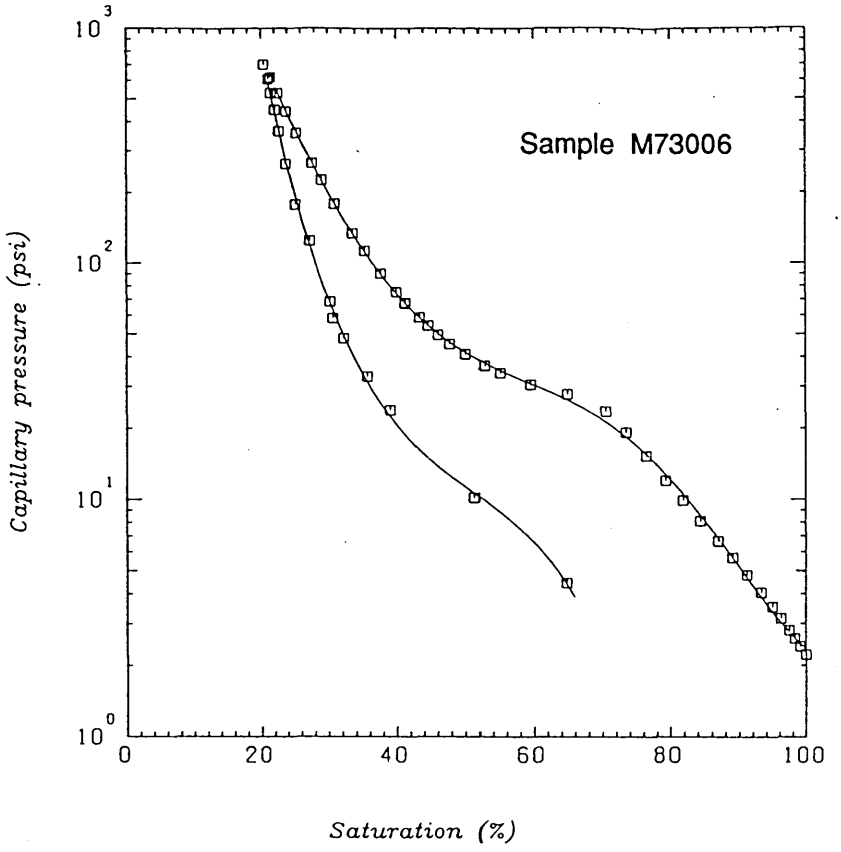


Fig. 6.42 Photomicrograph of sample RH97. Magnification x10.



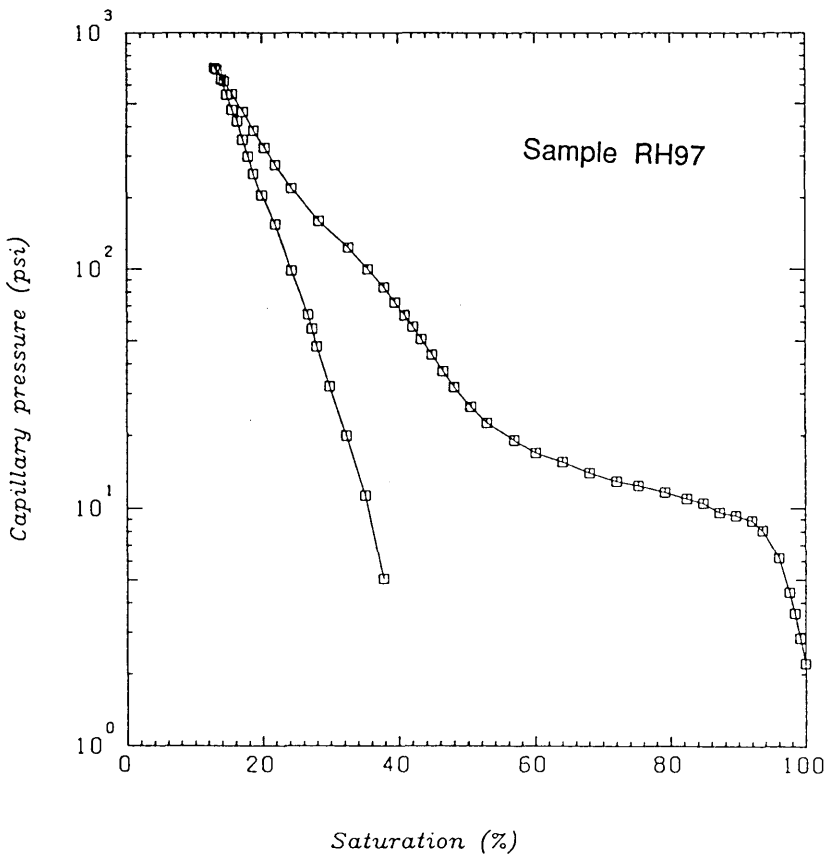
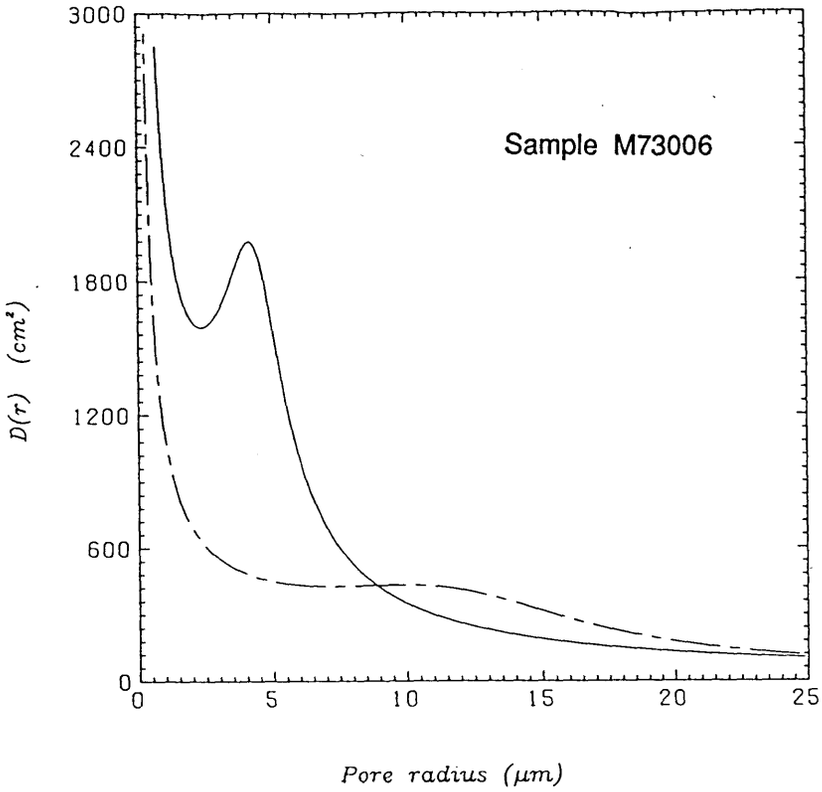


Fig. 6.43 Capillary pressure curves.



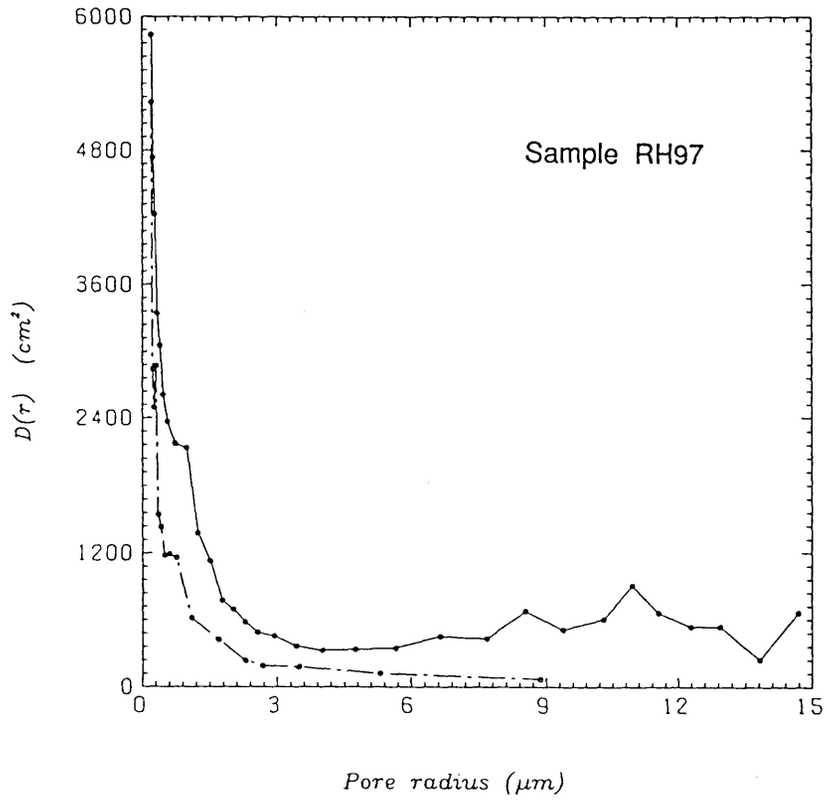


Fig. 6. 44 Pore throat size distribution curves.

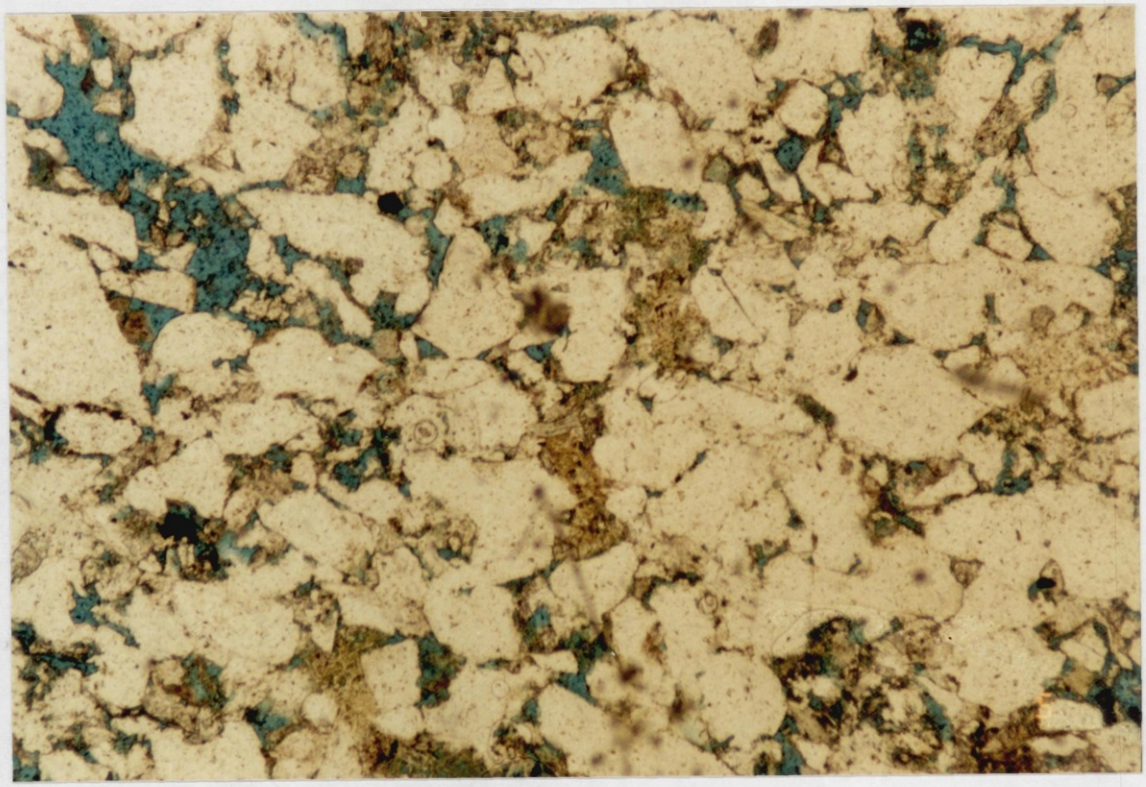


Fig. 6.45 Photomicrograph of sample M73005. Magnification x10.

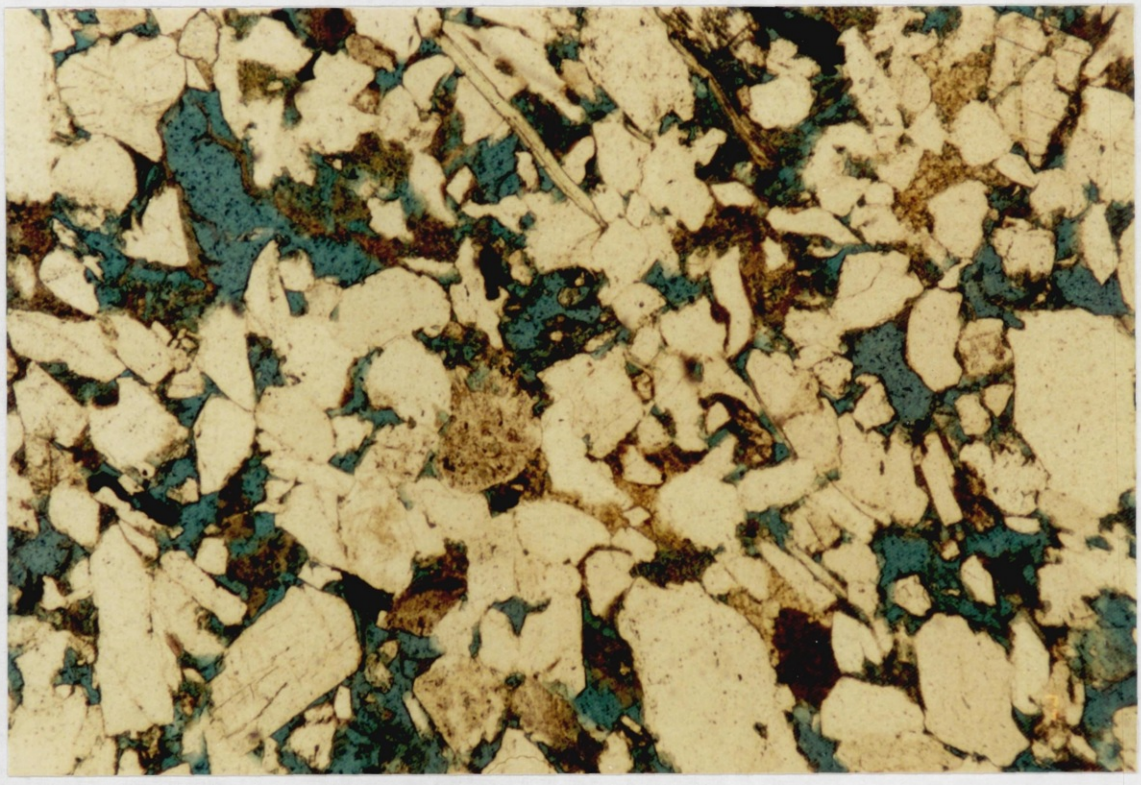
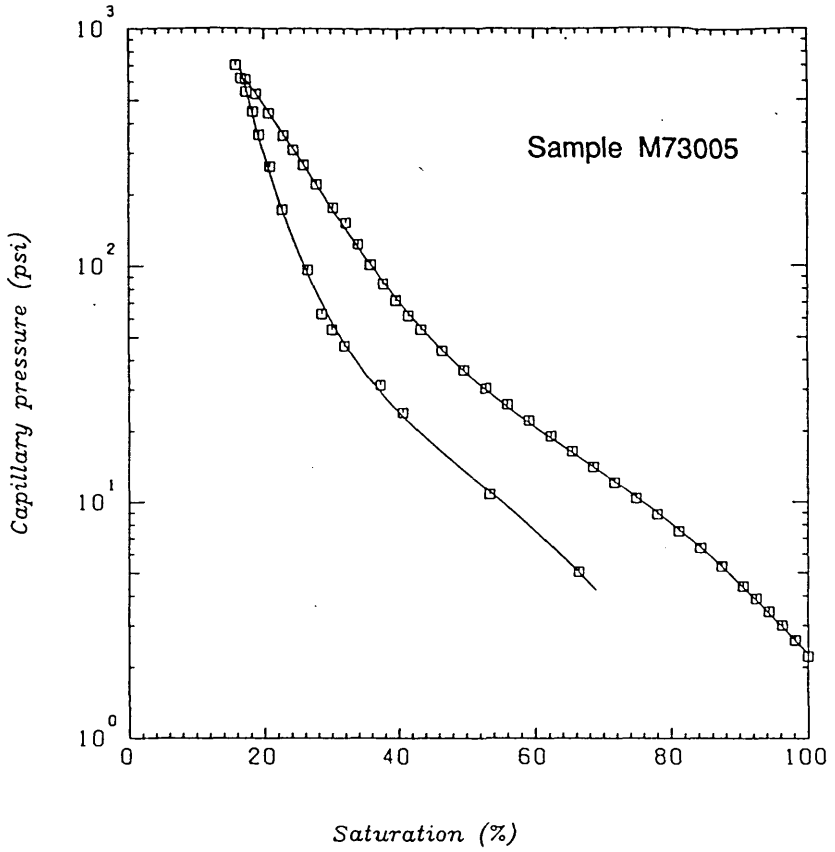


Fig. 6.46 Photomicrograph of sample M73009. Magnification x10.



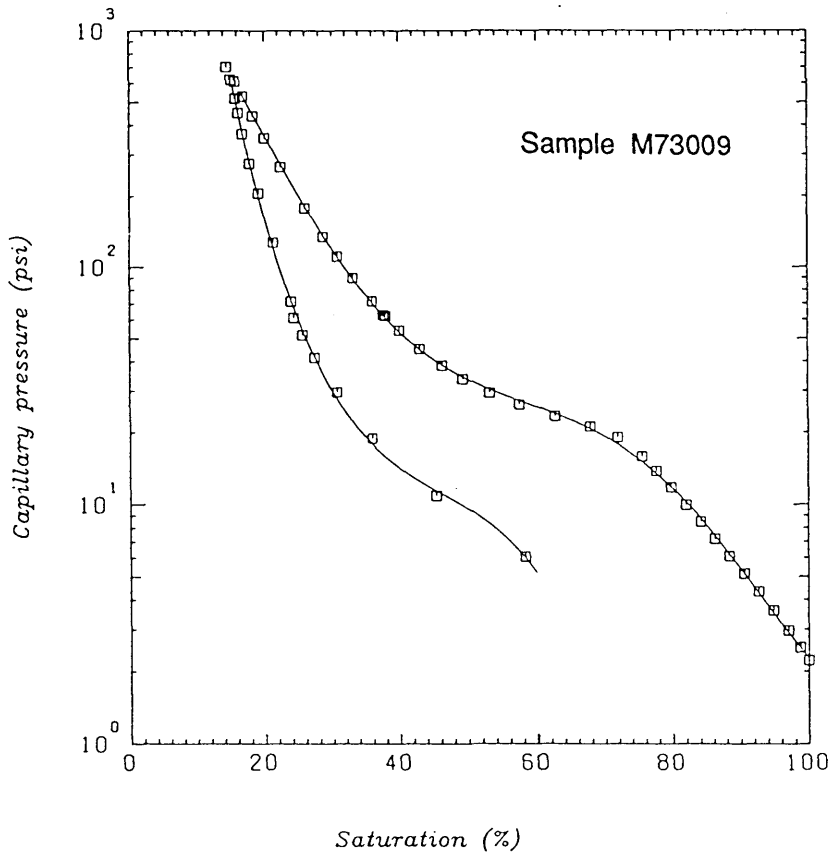
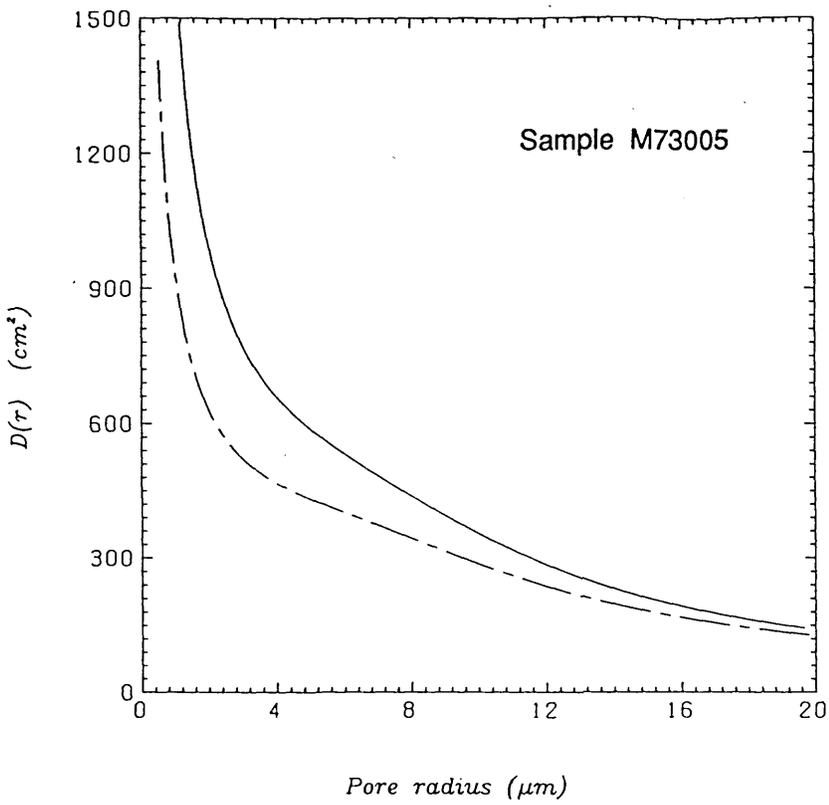


Fig. 6.47 Capillary pressure curves.



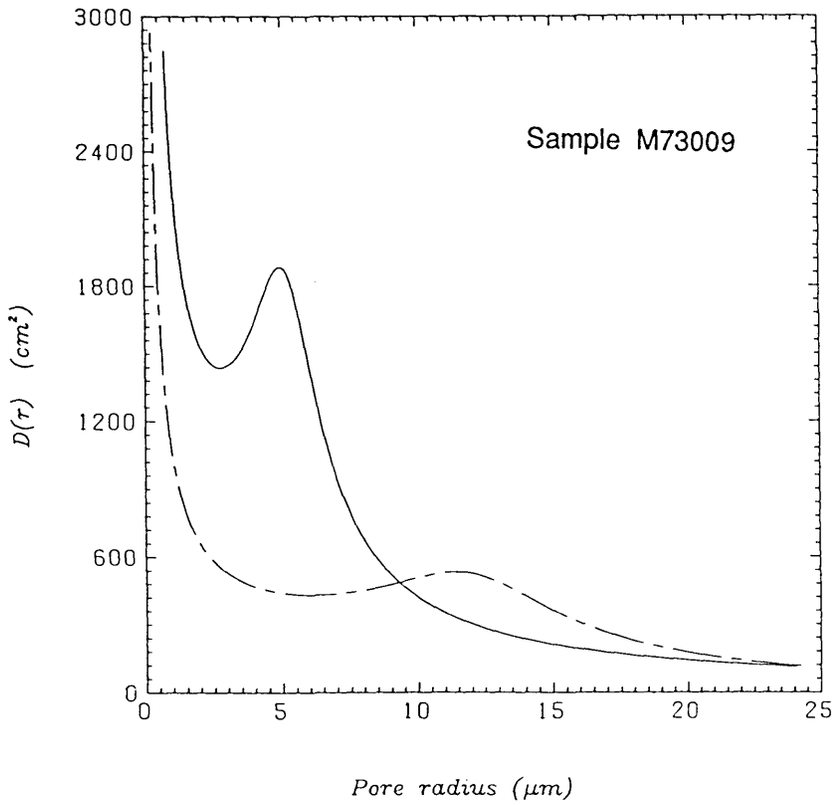


Fig. 6. 48 Pore throat size distribution curves.

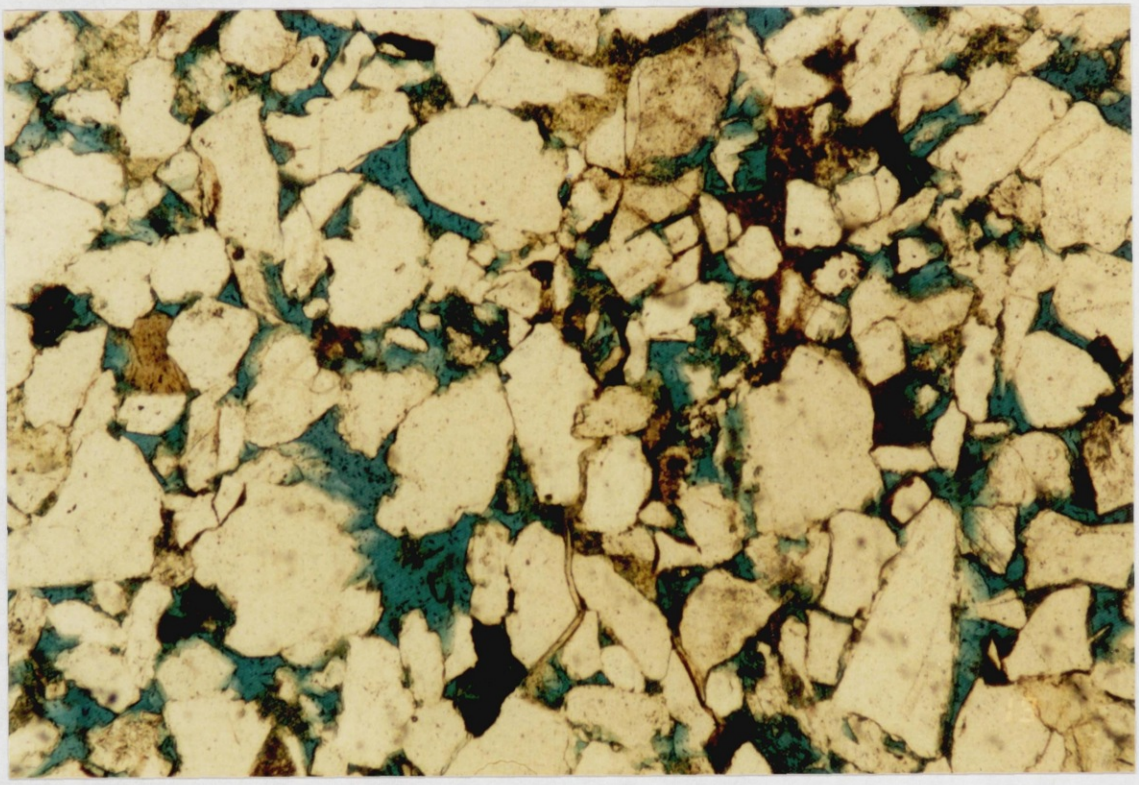
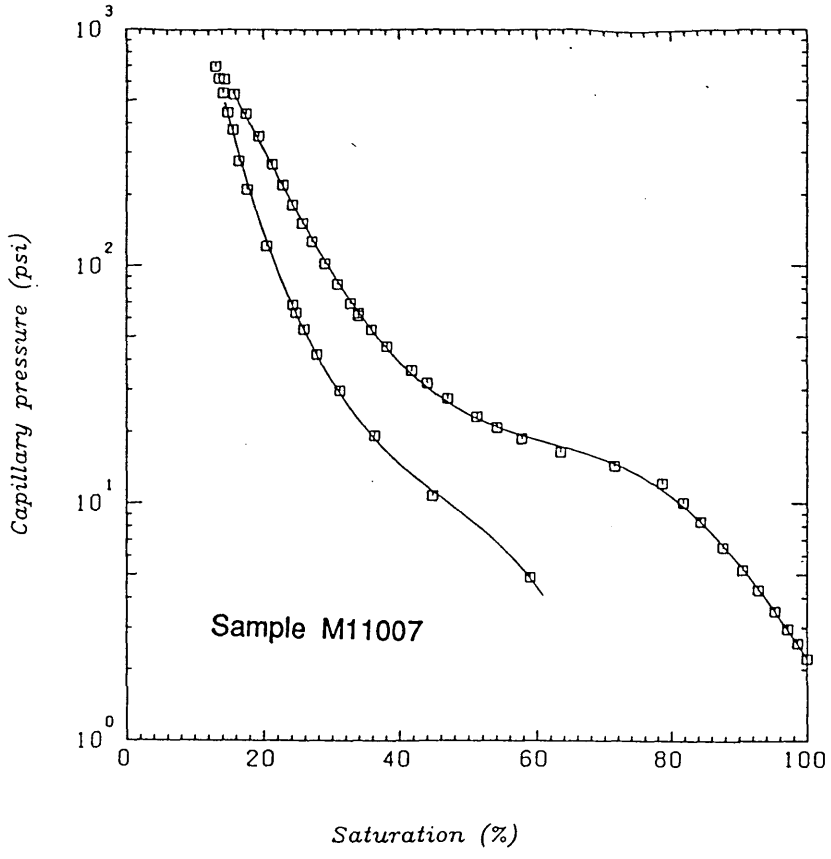


Fig. 6.49 Photomicrograph of sample M11007. Magnification x10.



Fig. 6.50 Photomicrograph of sample LE249. Magnification x10.



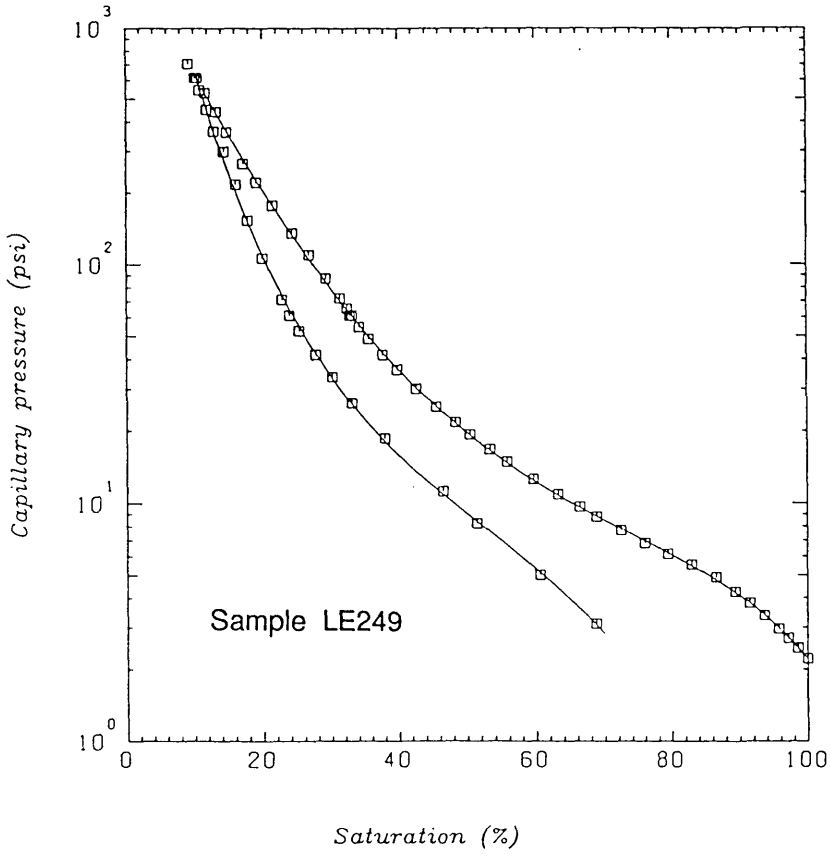
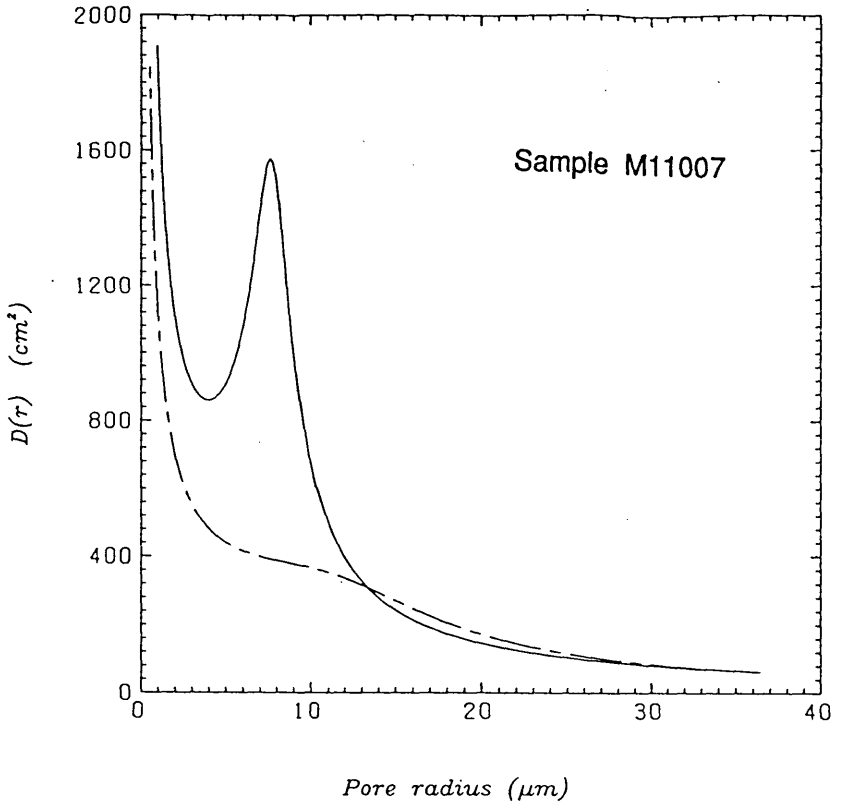


Fig. 6.51 Capillary pressure curves.



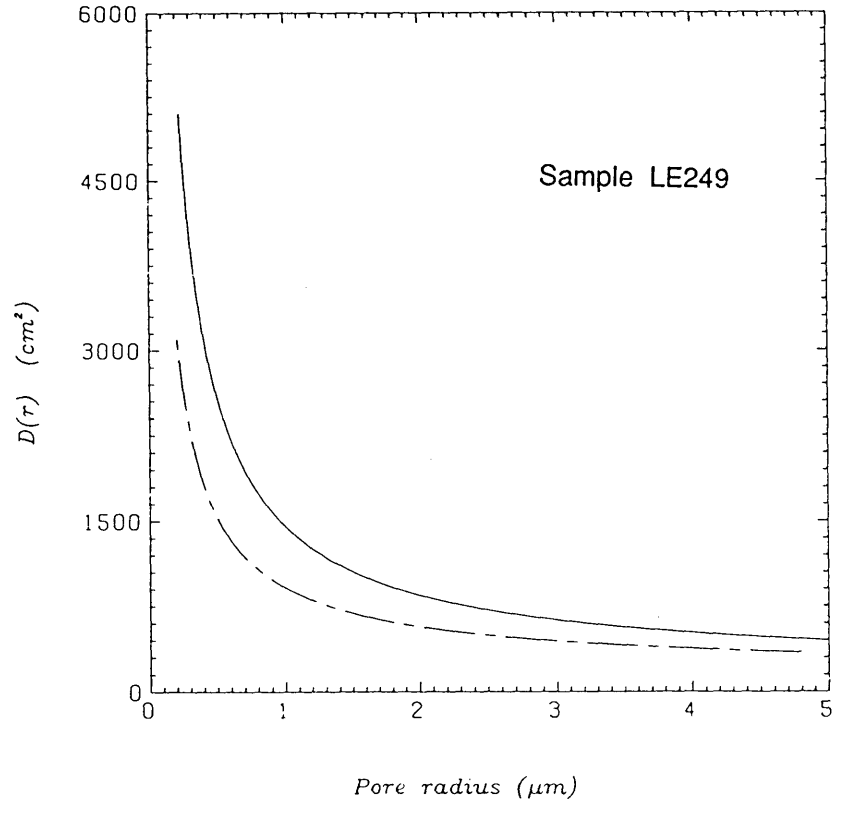


Fig. 6.52 Pore throat size distribution curves.

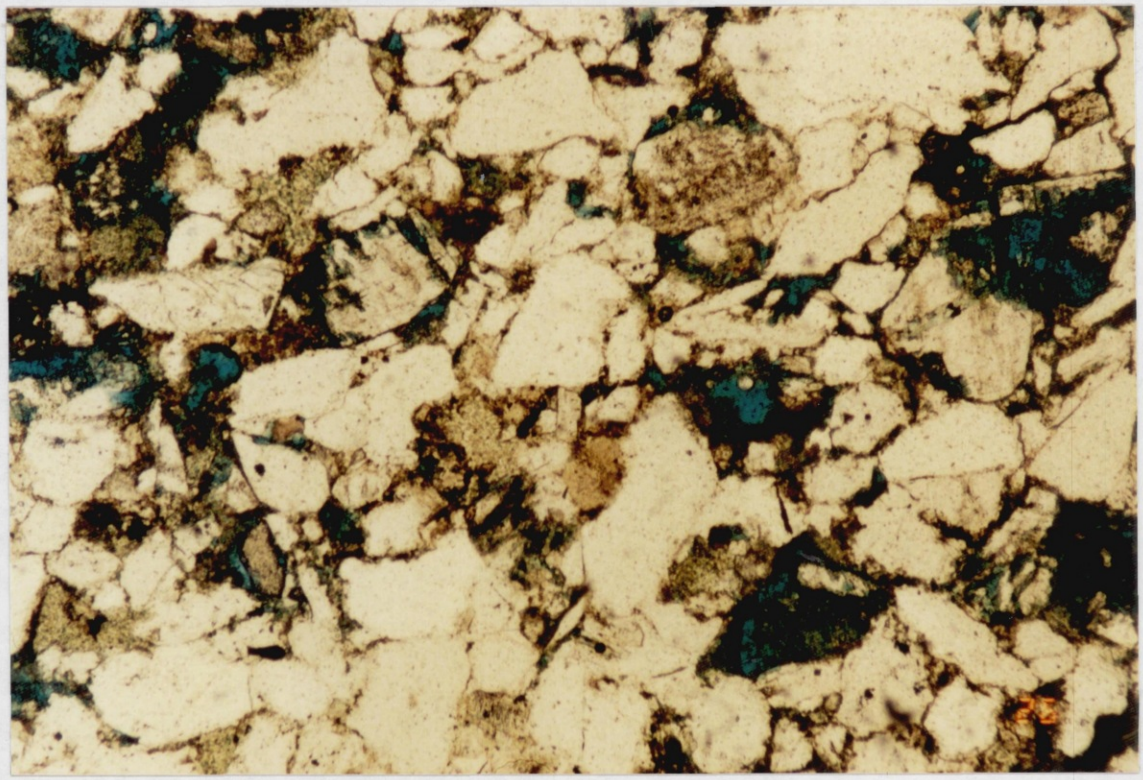


Fig. 6.53 Photomicrograph of sample M73001. Magnification x10.

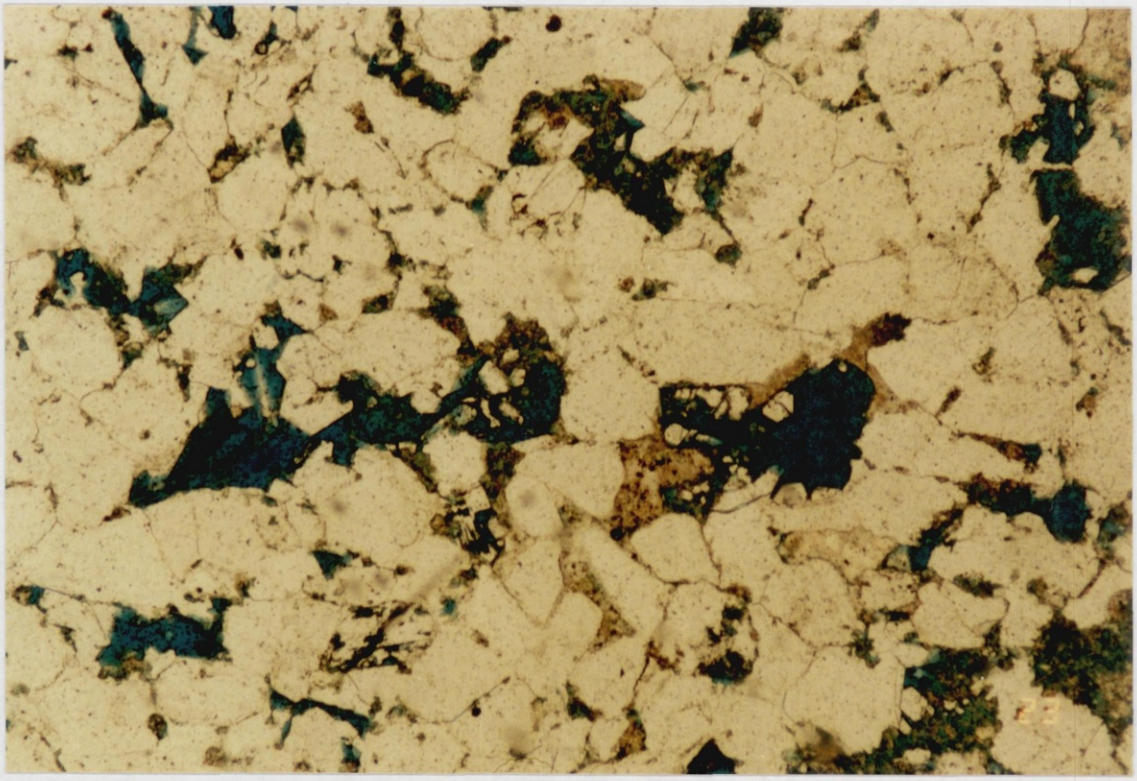
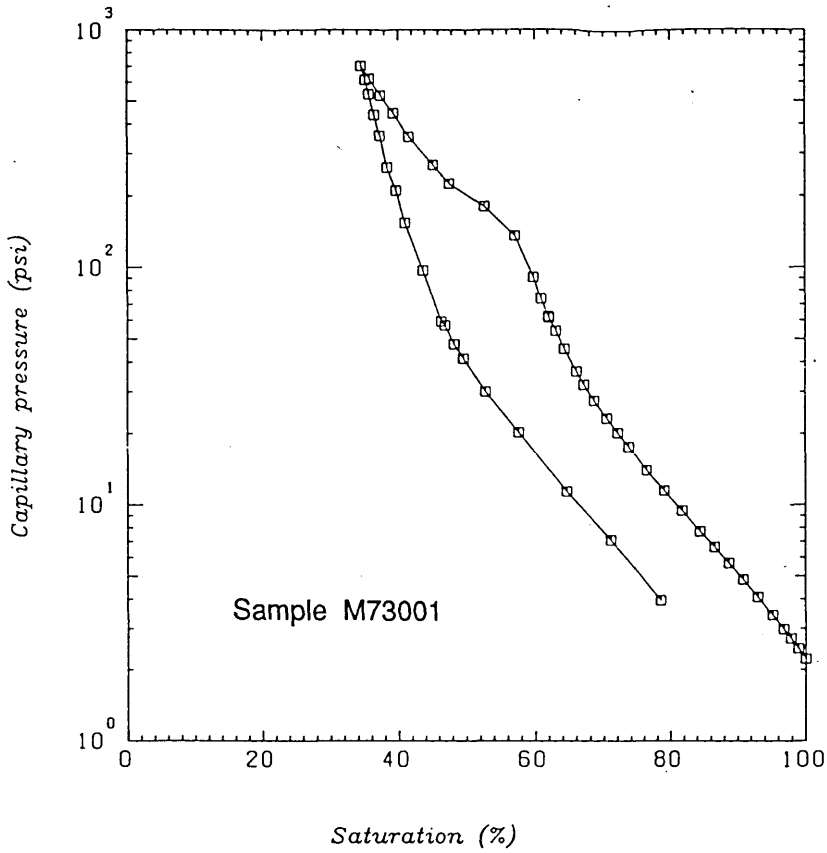


Fig. 6.54 Photomicrograph of sample AL118. Magnification x10.



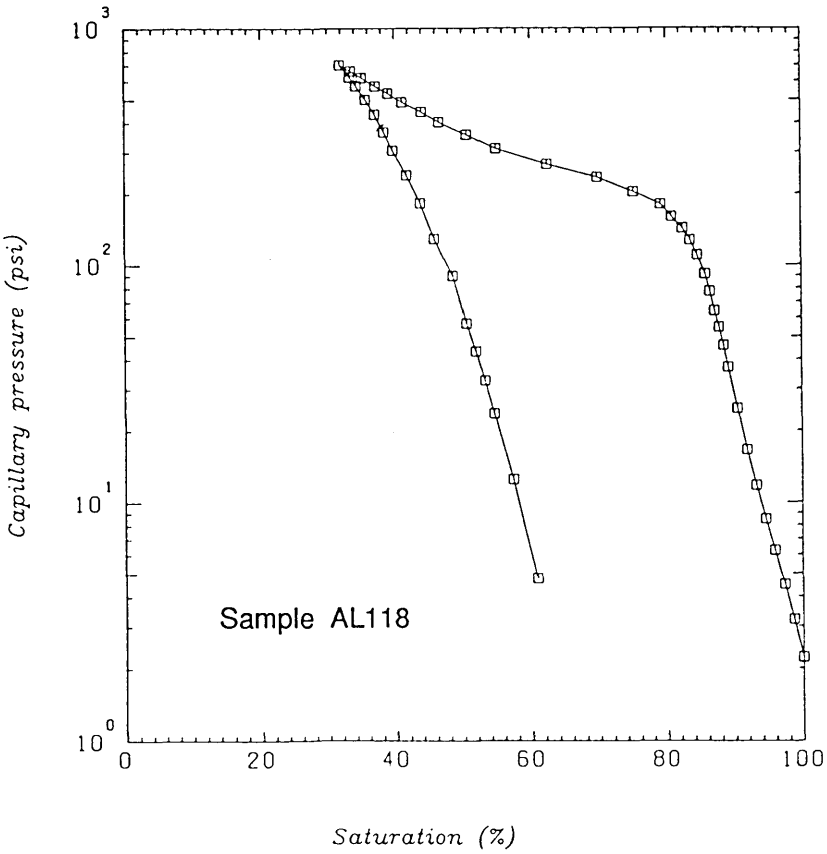
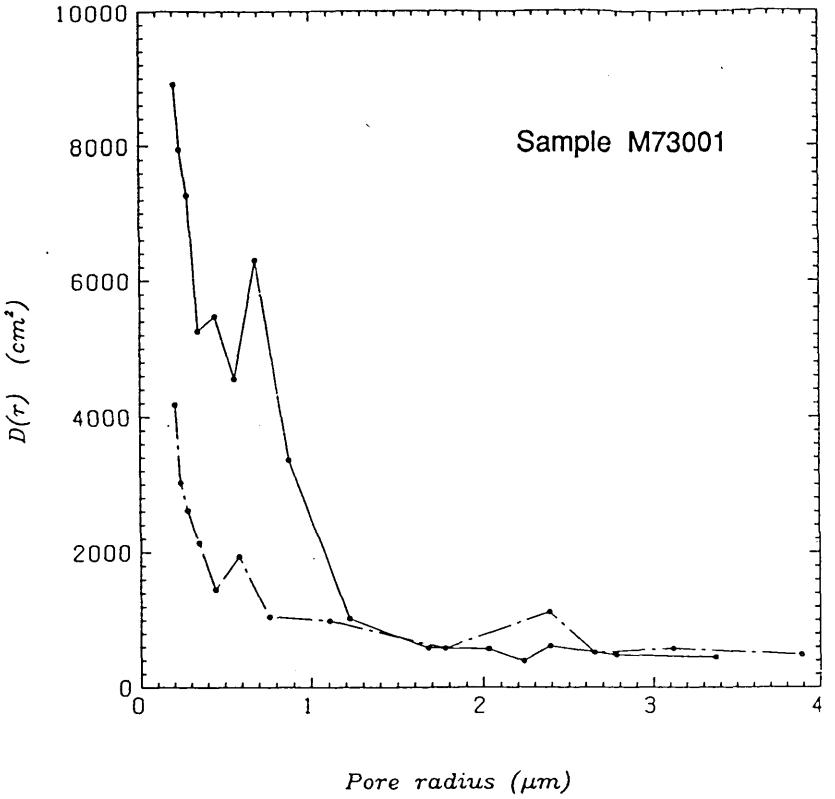


Fig. 6.55 Capillary pressure curves.



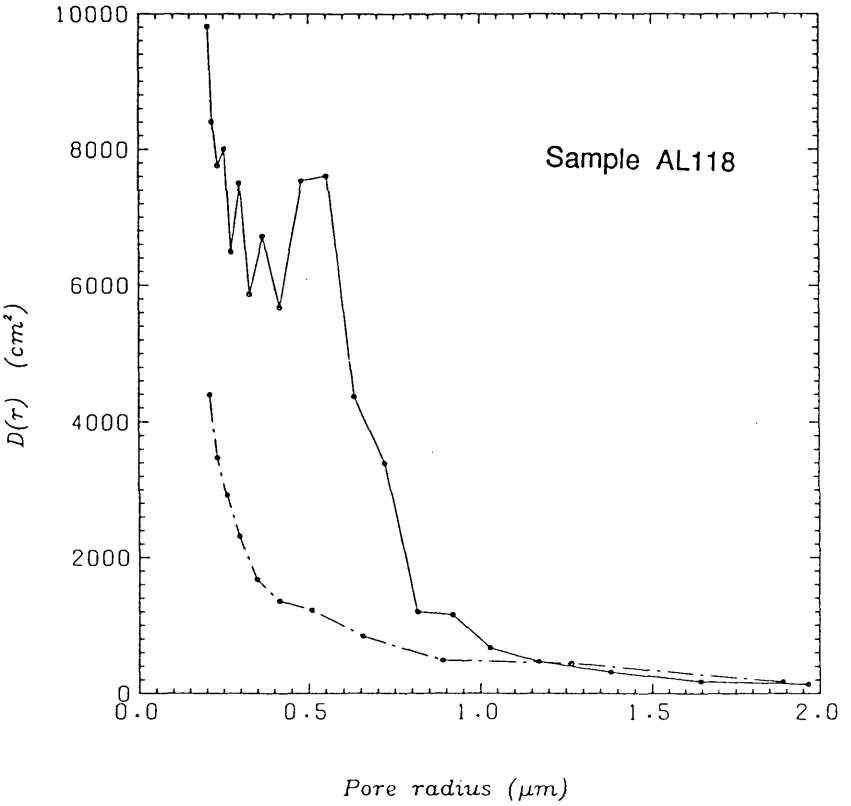


Fig. 6.56 Pore throat size distribution curves.

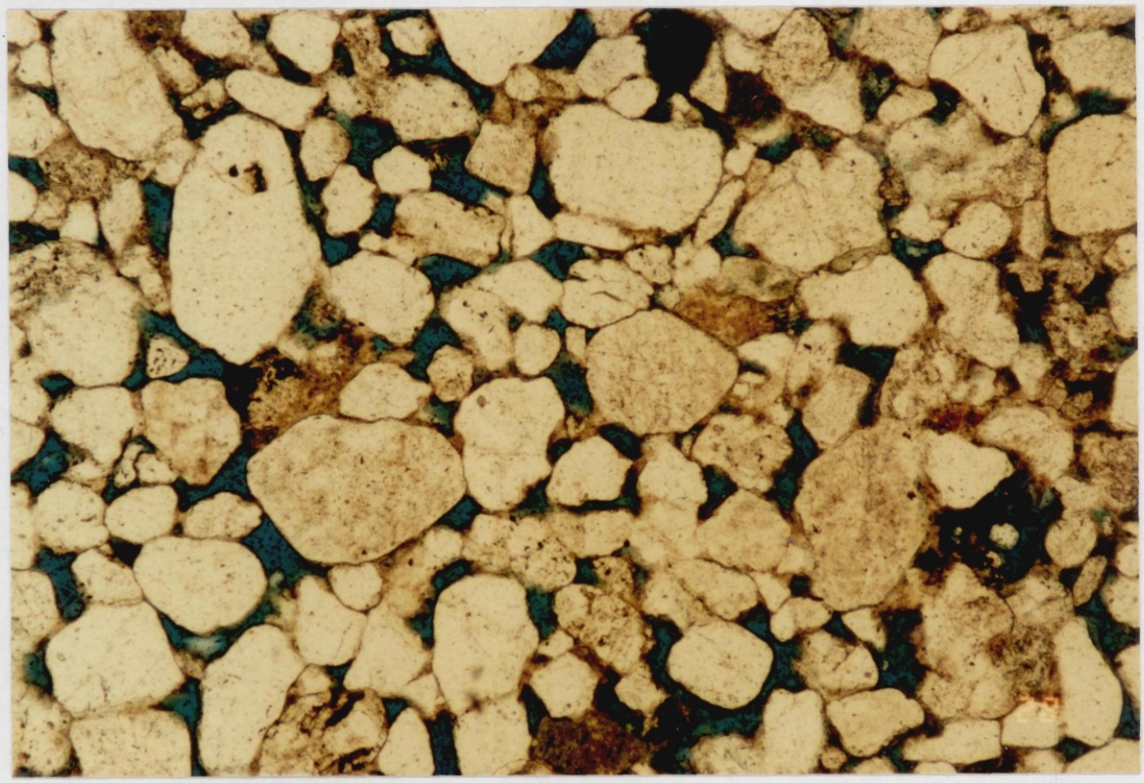


Fig. 6.57 Photomicrograph of sample RH94. Magnification x10.

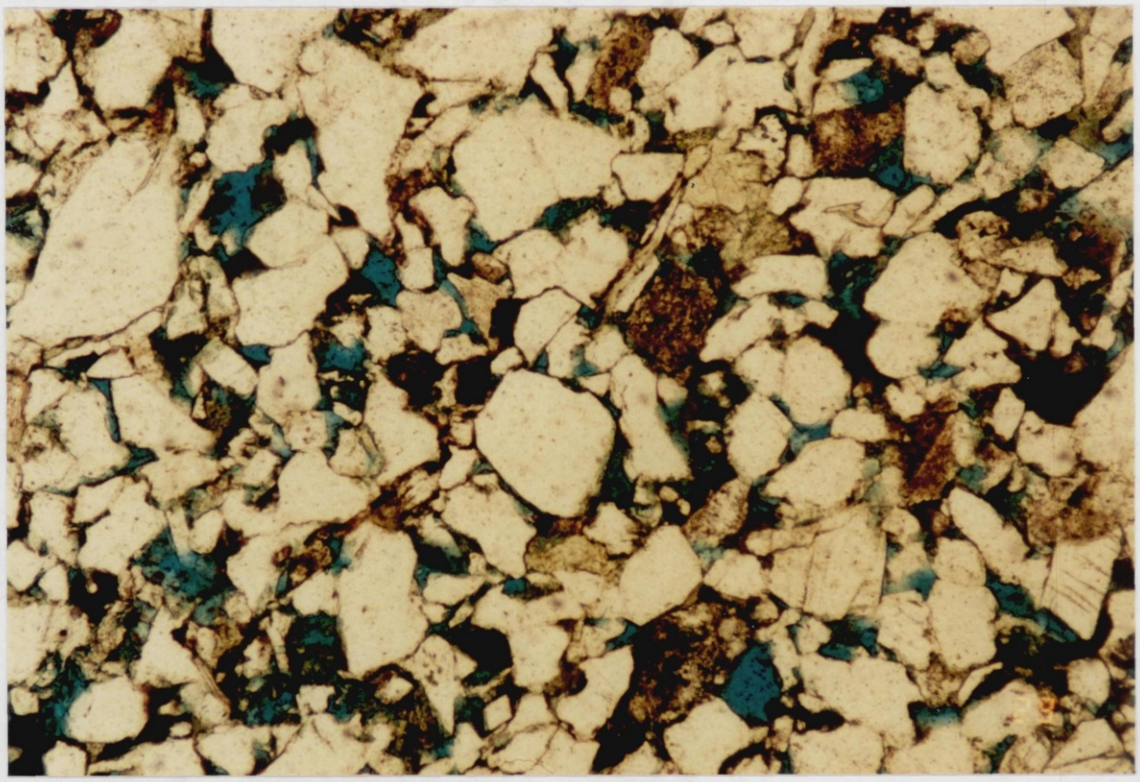
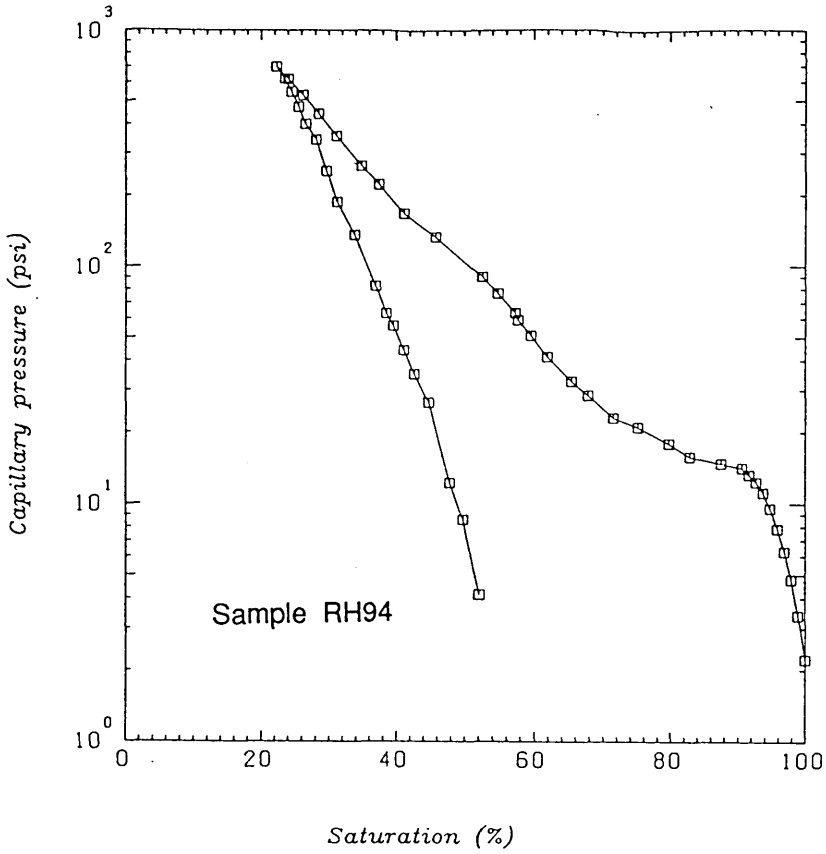


Fig. 6.58 Photomicrograph of sample M11002. Magnification x10.



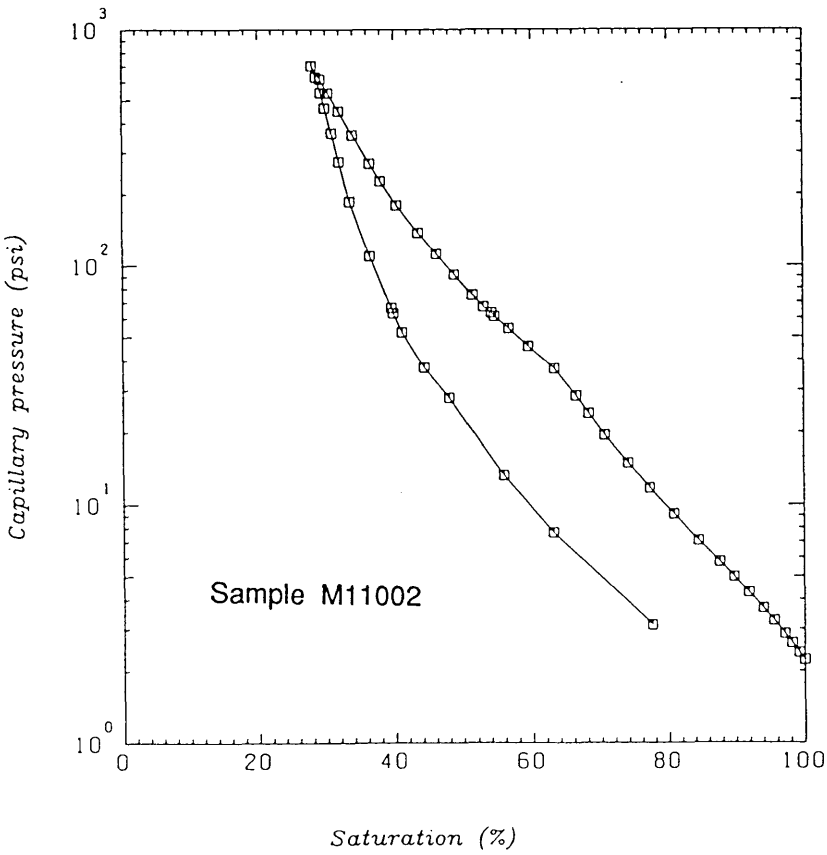
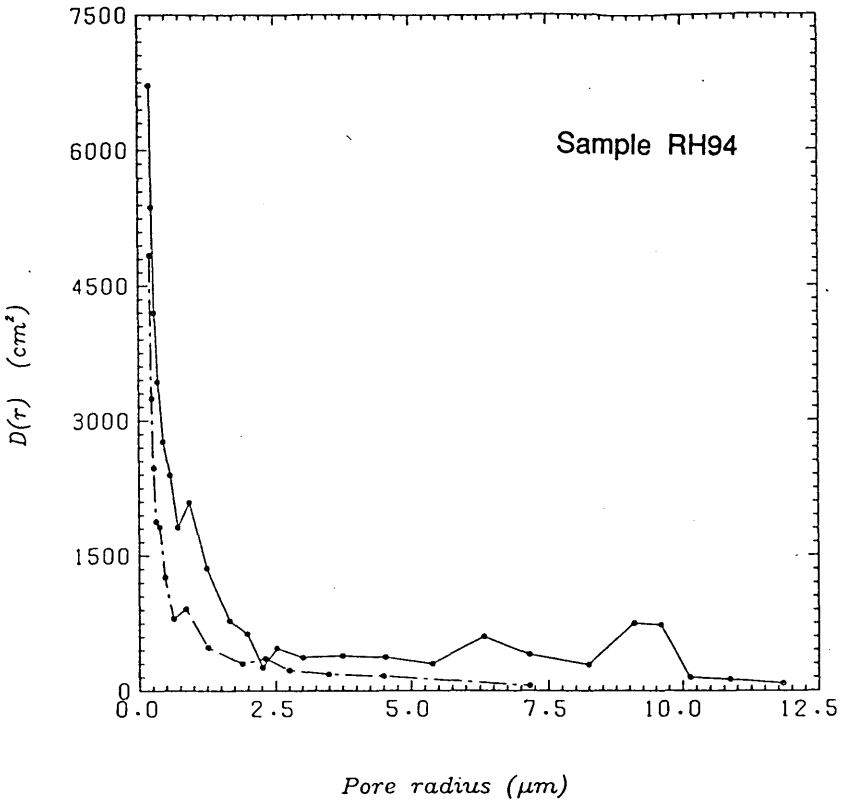


Fig. 6.59 Capillary pressure curves.



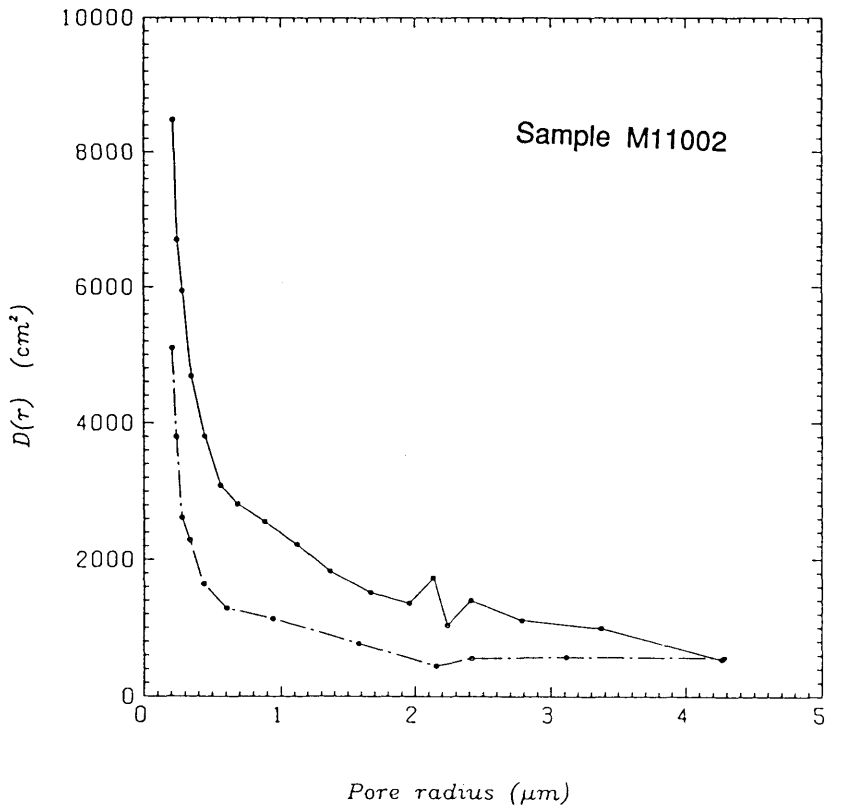


Fig. 6.60 Pore throat size distribution curves.

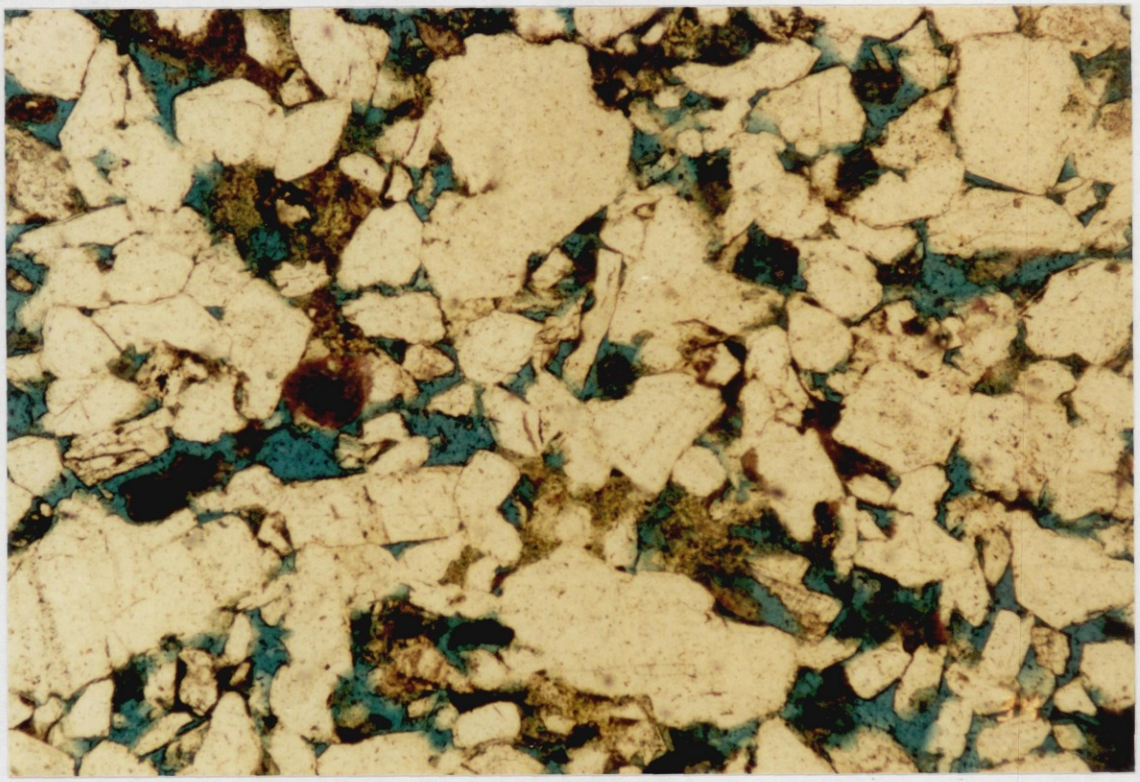


Fig. 6.61 Photomicrograph of sample M11001. Magnification x10.

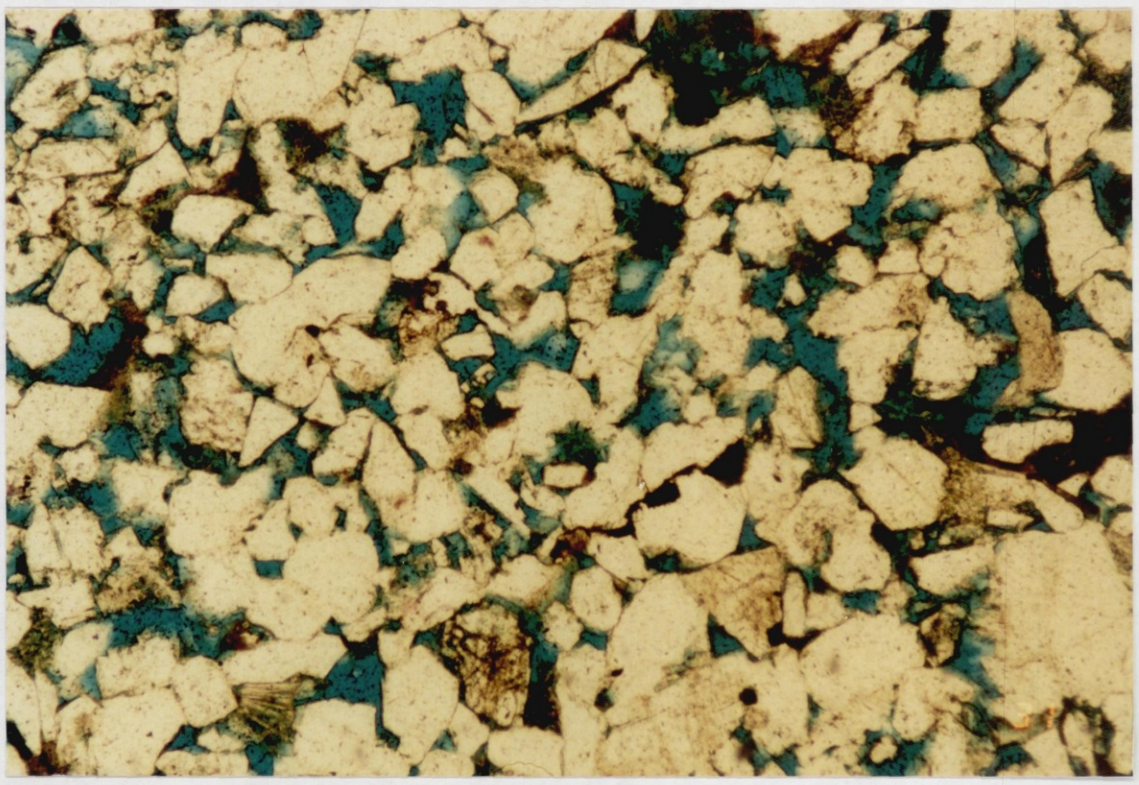
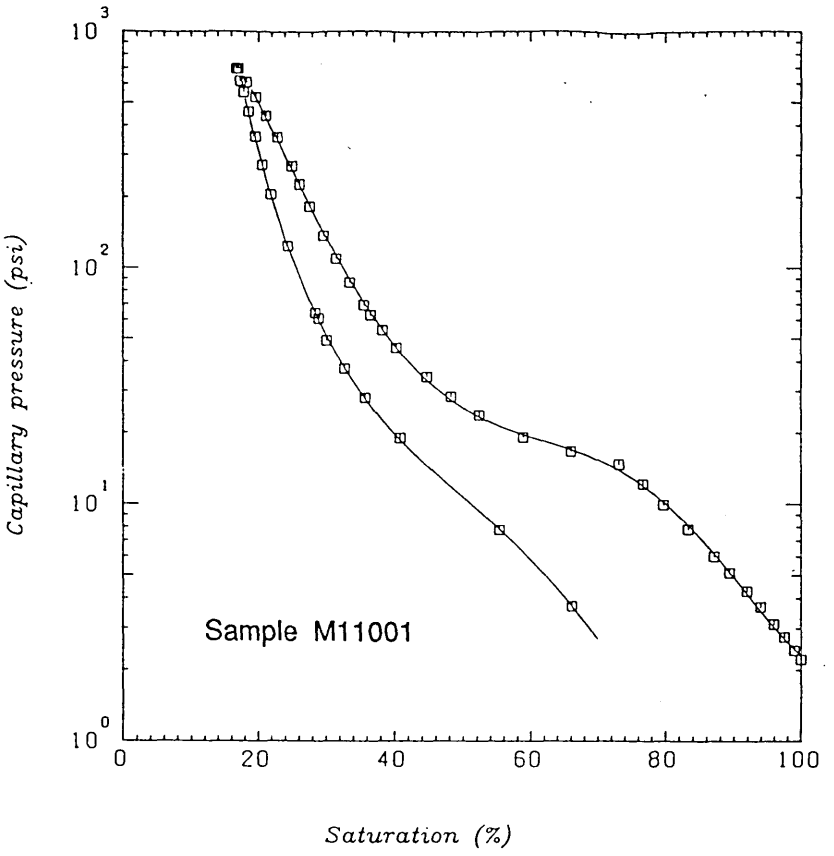


Fig. 6.62 Photomicrograph of sample M11009. Magnification x10.



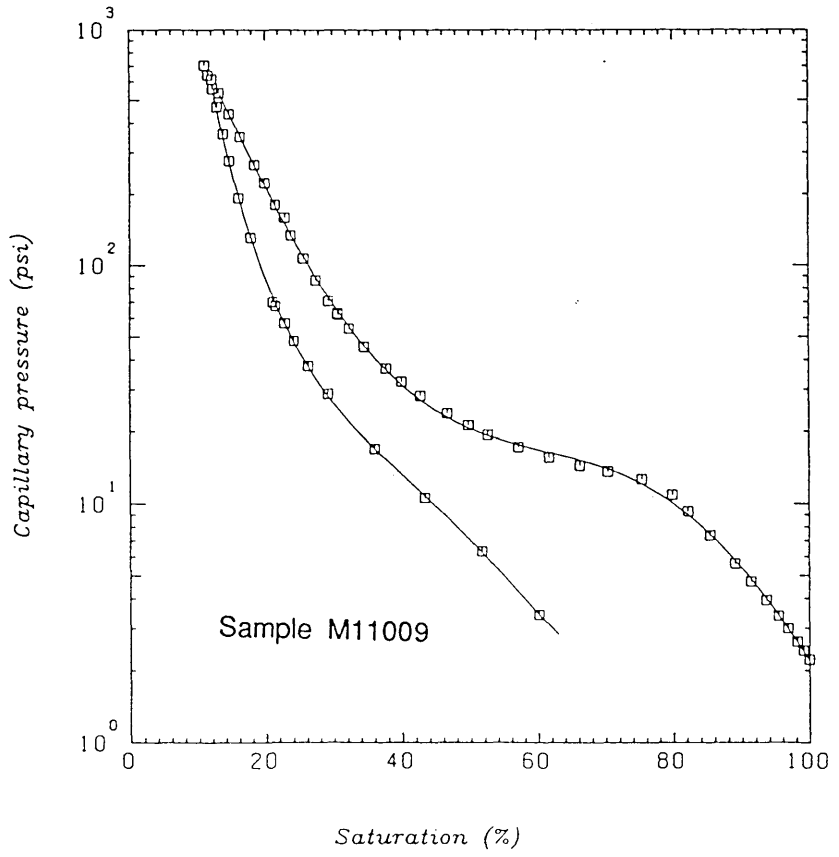
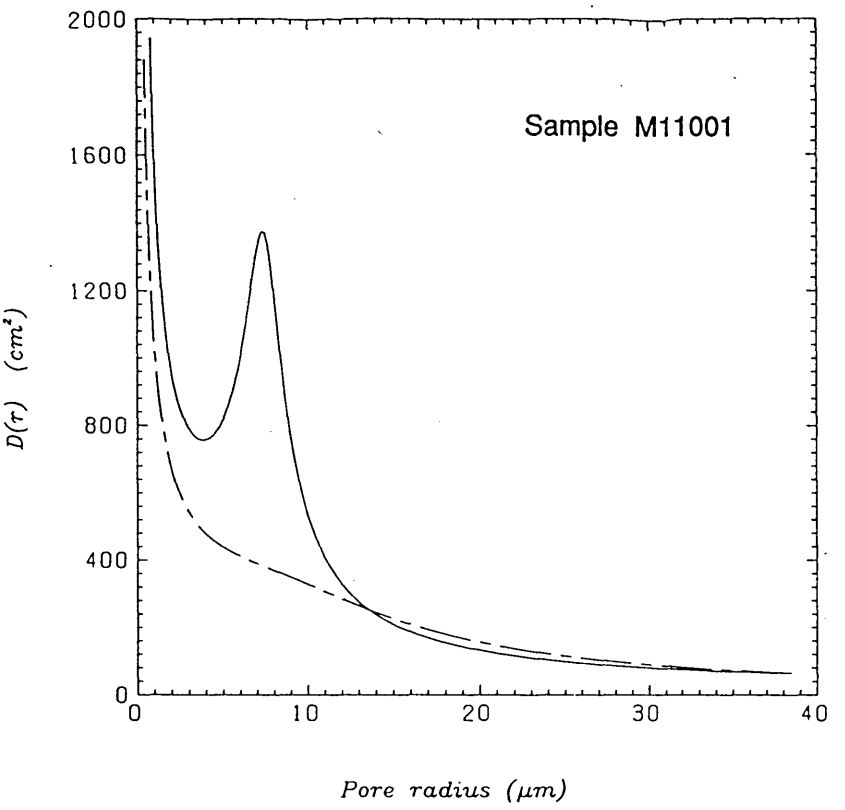


Fig. 6. 63 Capillary pressure curves.



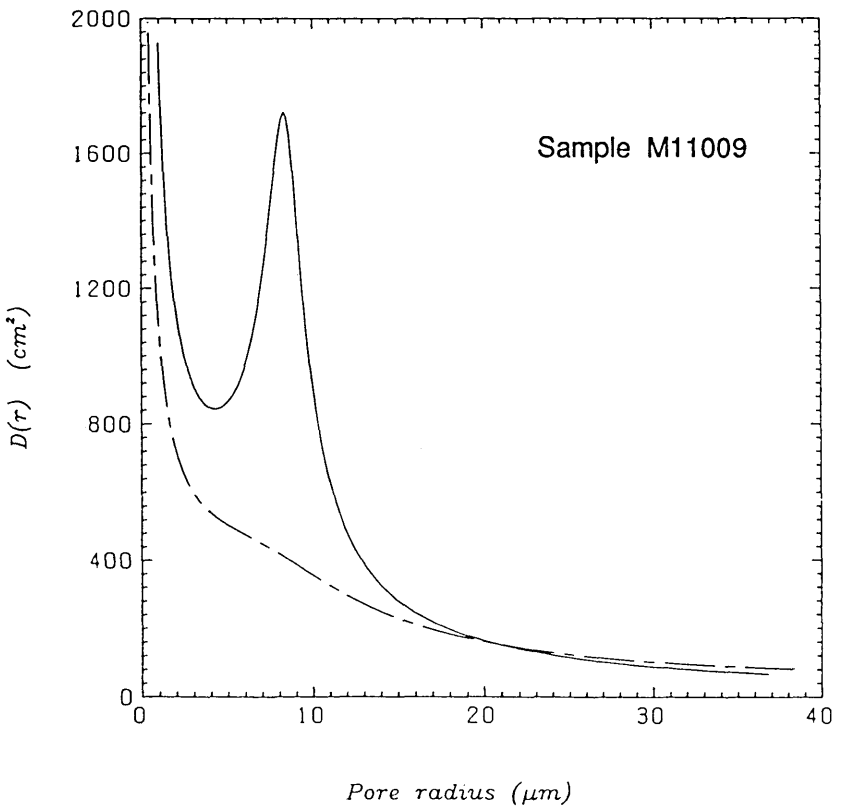


Fig. 6.64 Pore throat size distribution curves.

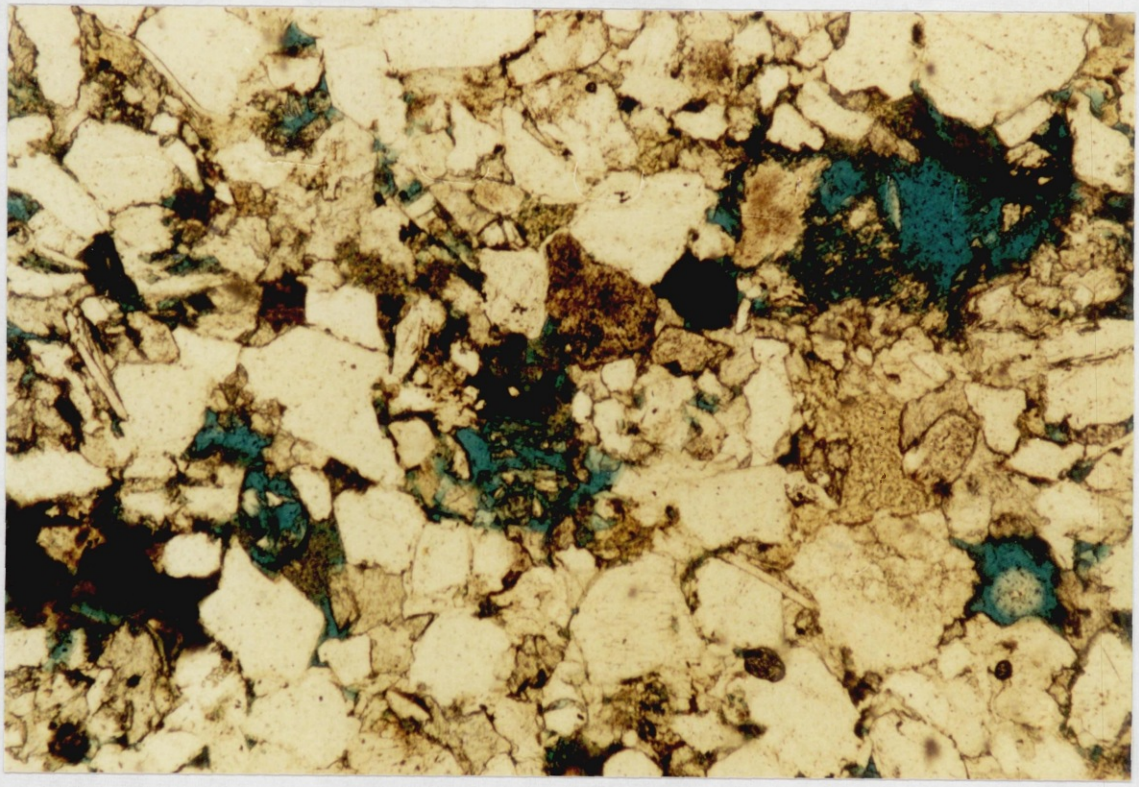


Fig. 6.65 Photomicrograph of sample M73003. Magnification x10.

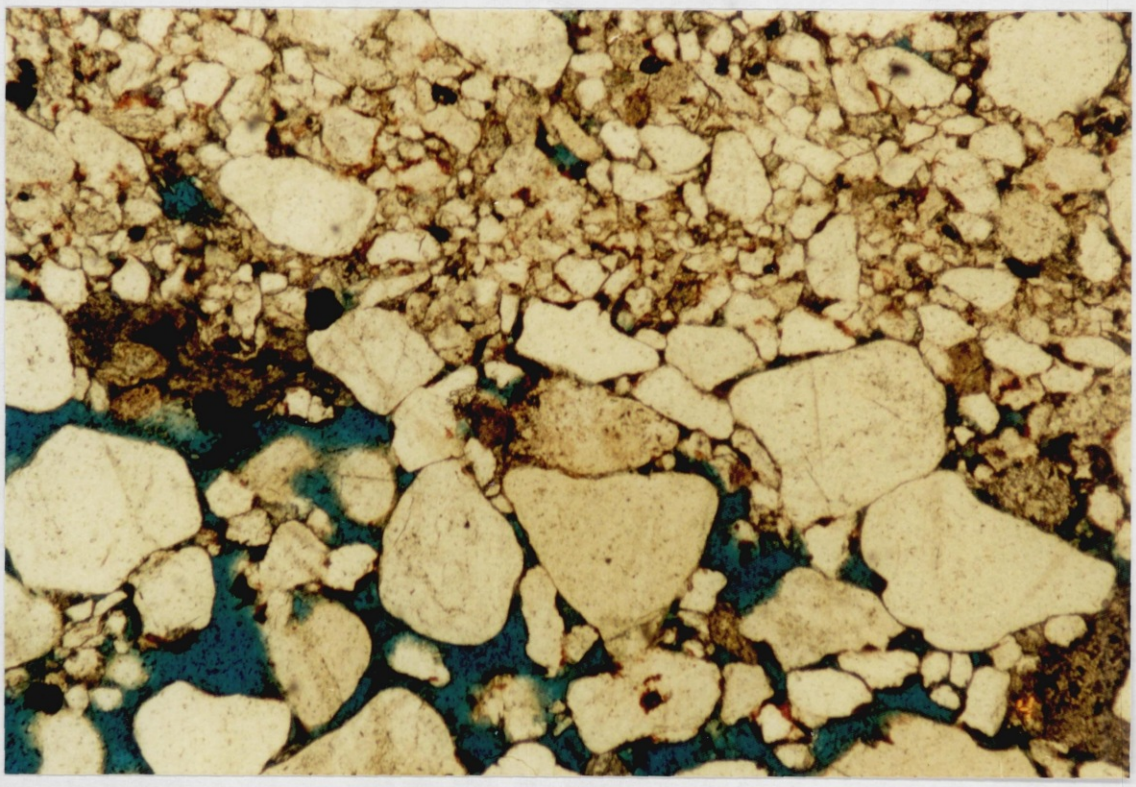
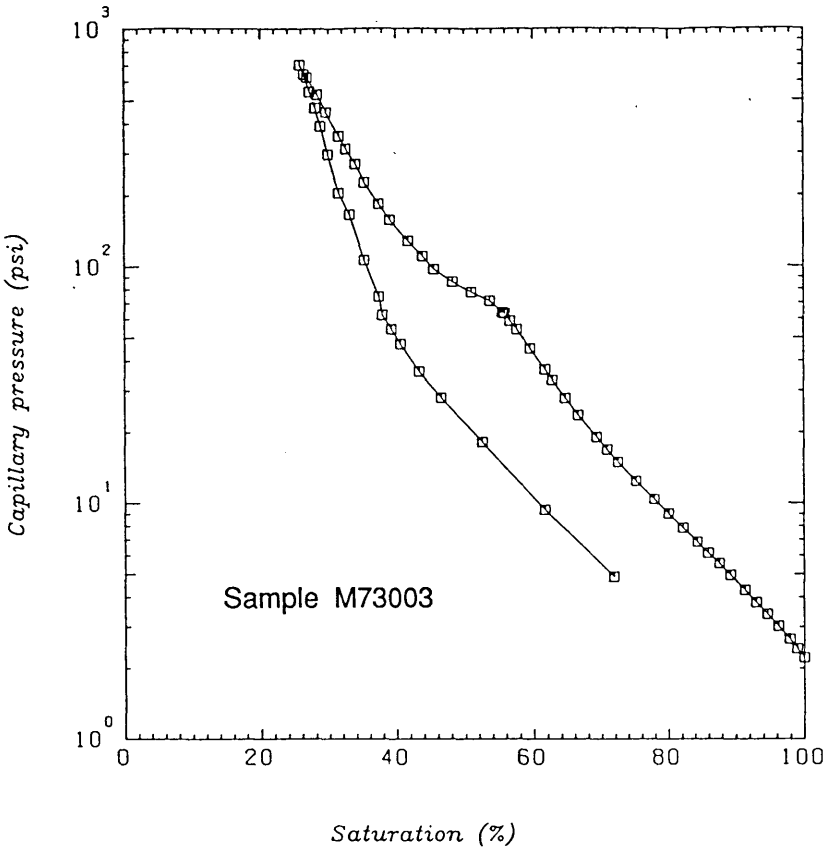


Fig. 6.66 Photomicrograph of sample LE253. Magnification x10.



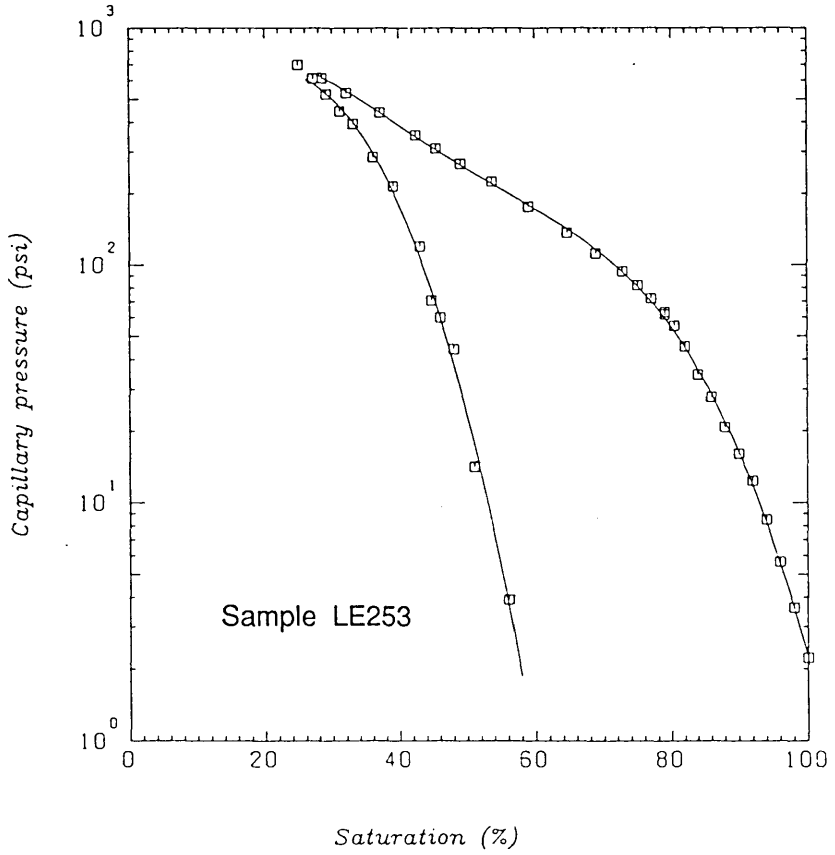
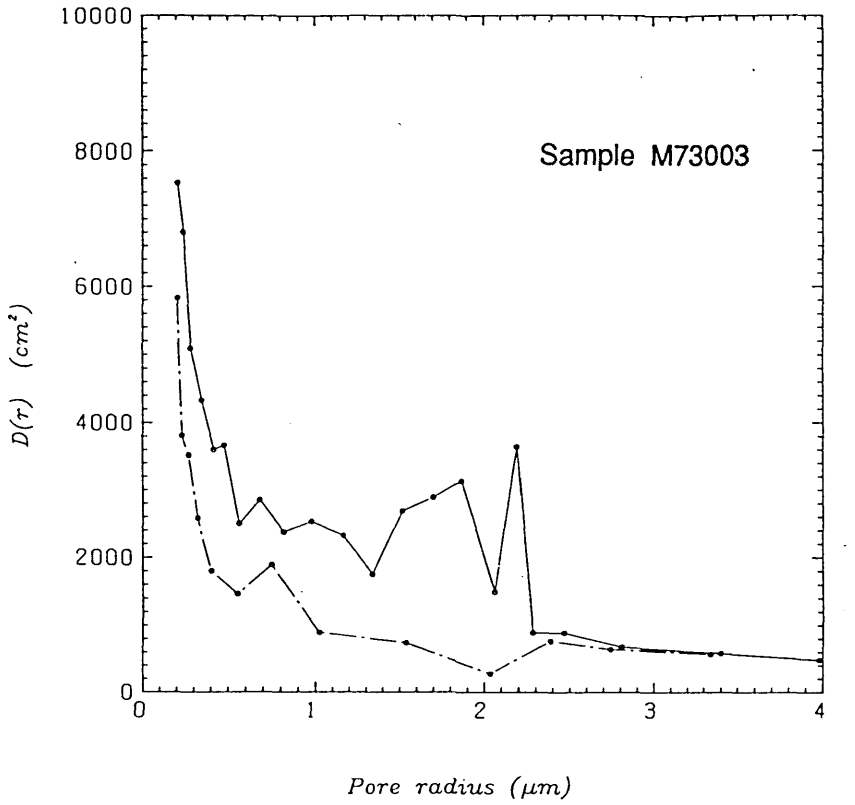


Fig. 6. 67 Capillary pressure curves.



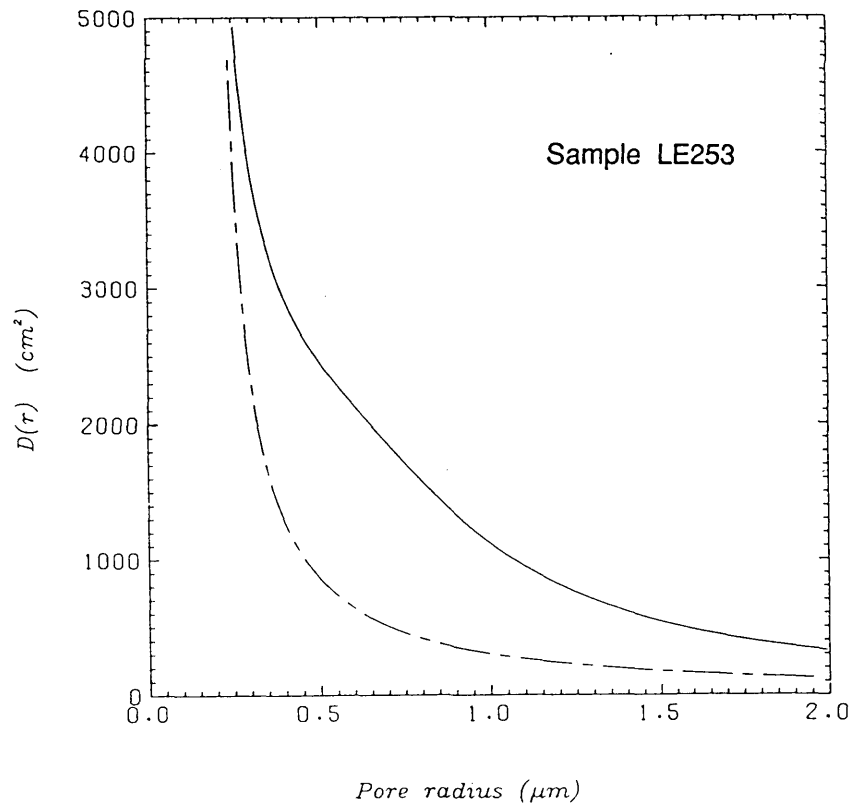


Fig. 6.68 Pore throat size distribution curves.

Chapter 7

EFFECT OF LIQUID SATURATION ON HIGH VELOCITY GAS FLOW

7.1 INTRODUCTION

Deviation from Darcy's law due to the effect of inertial forces has already been discussed in the previous chapters. In practice, this phenomena is usually encountered in gas wells where the velocity near the wellbore can become very high. The pressure gradient is also at its highest in this region. In gas condensate wells for example, liquid saturation could build up due to retrograde condensation which is caused by a large pressure drop. In the presence of a liquid phase the non-Darcy effect in the gas phase can increase considerably thereby causing a loss of productivity. High liquid saturation in the vicinity of a wellbore may also be caused by acidizing or mud filtrate invasion.

The increase in the inertial effect in liquid saturated porous media has been clearly demonstrated by Gewers and Nichol [1] who carried out experimental measurements on micro-vugular carbonates with a static liquid phase. Their work was later extended by Wong [2] for a mobile phase using the same cores. The work on carbonates [1] suggested that the inertial coefficient (often wrongly termed as 'turbulence factor') actually decreases on increasing the liquid saturation from 0 to 10% and then rapidly increases with any further increase in saturation. It was also reported [2] that the inertial coefficient increases by as much as eight fold on increasing the liquid saturation from 40 to 70%. It has been assumed [3] that the same behaviour would also be observed in sandstones.

Due to lack of information on consolidated sandstones in the literature the present work was carried out to check if this assumption is true. This study using sandstones therefore extends the earlier work carried out by Gewers and Nichol on carbonates and some of it has been reported by the author elsewhere [4]. Subsequently, similar work carried out independently by Evans et al [5] has been reported. Investigations have also been carried out on unconsolidated Trinidad sands by Jagai [6]. The experimental procedure of these two group of workers are essentially similar to that described here and the conclusions arrived at from the present study are generally in agreement with those found by the others.

To have a proper understanding of the effect of liquid saturation on the inertial coefficient it is necessary to have a knowledge of the distribution of the liquid phase within the pores. For this purpose, a method using coloured epoxy resins has been developed [7] to enable a direct observation of the liquid and gas phase to be made at the pore scale.

7.2 EXPERIMENTAL WORK

7.2.1 Flow measurement

The experiments were carried out on four sandstone core plugs obtained from an Upper Jurassic submarine-fan sandstone of the northern North Sea. The four samples were chosen from the sample set (see Table 4.3) because of the wide range of permeabilities covered by them. The plugs were cleaned using toluene and then by methanol in a Soxhlet extractor. Grain volumes were measured using a helium gas expansion porosimeter. The bulk volumes were measured using a caliper since the plugs had very sharp edges, and from these measurements the porosity was calculated.

Flow measurements on dry cores were carried out by placing the cores in a Hassler cell and flowing gas at increasingly high rate. A schematic diagram of the apparatus is shown in Figure 7.1. For saturated cores, the samples were first weighed and then completely saturated under vacuum. The samples were then placed in a porous plate capillary pressure cell and brought to an equilibrium saturation by imposing a pressure of 150 psig. The irreducible liquid saturations for the cores were obtained from the asymptotic values of drainage capillary pressure curves measured using a hydrocarbon-air system. The values are shown in Table 7.1. The liquid used for saturating the cores was a refined oil - Isopar™, which is a mixture of various iso-paraffins. The physical properties and the chemical composition of this liquid are given in Section 4.2.2. Water and glycerol were used in some of the reported works [1,2,6] but these are unsuitable for sandstones as they may cause swelling of the interstitial claysand cementing.

Typically, a plug was weighed and then placed in the Hassler cell for flow tests. The saturation was calculated gravimetrically, ie from the weight of the dry and saturated core. The gas flowing into the core was saturated to minimize any loss from the plug due to evaporation. This was done by bubbling the gas through a long column which was half filled with the liquid and partly filled with glass beads to break up the bubbles. Each core was reweighed after the test and if the saturation was found to have changed by more than ±3% then the results were discarded and the above procedure repeated.

For measurements below the 'irriducible' minimum, the liquid saturation was decreased by evaporation [1]. The cores were gently heated in an oven at 50° C until the required saturation was achieved and were then left in an air tight container for 10 to 12 hours before the start of the flow tests.

7.2.2 Flow visualization

The core plugs were saturated by a low viscosity thermal setting epoxy resin under vacuum. The resin, (Araldite™ AY18) was mixed with the hardener (HZ18) in a ratio of 1.0 of the former to 0.75 of the latter (by weight). Viscosity of the epoxy after mixing with the hardener was about 15cp at 25°C. The mixture was dyed blue prior to saturation using 0.5% (w/w) Sudan blue dye.

After saturation, the sample was placed in a Hassler-type core holder which was installed inside an oven. The resin was displaced from the core very slowly by injecting air at a very low rate to minimize any bypassing due to the viscosity contrast. The air flow rate was then gradually increased until the flow was sufficiently high for inertial effect to be significant. The temperature of the oven was then increased to 120°C and gas was flowed continuously for some 48 hours to give the epoxy sufficient time to set and harden in-situ.

After the sample was taken out of the core holder and cooled to ambient temperature, it was then vacuum saturated with similar epoxy which had been coloured with Sudan red dye (1% w/w). The sample was then placed in an oven at 80°C for 24 hours for the resin to set. The red resin would now be occupying the pore spaces through which gas was flowing, and the blue resin would be distributed as the wetting phase. Thin sections of the rock samples were prepared for visual examination under an optical microscope. The sections prepared were cut at the two end faces as well as along the long axis of the core. The latter shows significant channeling caused by the viscosity contrast and also liquid accumulation near the downstream end face due to the discontinuity.

7.3 RESULTS

7.3.1 Dry cores

Measurements of flow rate and pressure drop were carried out to determine the permeability and inertial coefficient. Permeability was determined by plotting the data according to the equation proposed by Klinkenberg [8] which takes account of gas slippage effects.

The apparent permeabilities k_a, were calculated using Darcy's law. From a plot of the apparent permeability against the inverse of mean pressure $1/P_m$, the true permeability can be obtained as the extrapolated straight line to infinite pressure. An example of this type of plot is shown in Fig 7.2. For liquid saturated cores the 'true' permeability is equivalent to the 'effective' permeability for that saturation.

It should be noted that in both the Klinkenberg and Forchheimer type of plots the data points show a downward warp, which was previously recognised by Dranchuk et al [9]. In the Klinkenberg plots this is due to inertial effects becoming significant while in the Forchheimer plots it is due to slippage becoming important at lower rates. In the case of Klinkenberg plots (Fig. 7.3), it was often necessary to impose some back pressure to be able to obtain a straight line while being able to vary the mean pressure. If this was not done inertial effects would start to become significant and a straight line drawn through any set of data points will give erroneous results [9]. Similarly for the inertial coefficient plots, it is necessary to have a sufficiently high flow rate (and mean pressure) to minimise any effect of gas slippage. The evaluated data are shown in Table 7.1.

To check for the movement of any fine particles, gas was flowed through both ends of the core. This was done by taking the core plug out of the holder and then altering its orientation so that the downstream end became the upstream end. The permeability and inertial coefficient were calculated for flow in both directions and were found to be in very close agreement. The possibility of any fines movement was therefore discounted.

TABLE 7.1
Core Data

SAMPLE	ϕ (%)	k (md)	β (cm^{-1})	S_{wirr} (%)
M01	20.8	64.5	4.49×10^6	20.0
M03	10.0	0.60	6.17×10^9	35.0
M10	20.9	205	0.91×10^6	9.5
M11	11.6	1.10	3.04×10^8	22.5

7.3.2 Saturated Cores

The procedures followed for the saturated plugs were essentially similar to those for the dry cores. The effective ('true') permeabilities were calculated at various saturations using Klinkenberg plots and the inertial coefficients from Forchheimer plots. The decrease in effective permeability with increasing liquid saturation are shown in Figures 7.4 to 7.7, and the corresponding increase in inertial coefficient are shown in Figures 7.8 to 7.11.

The experimental work was carried out in two stages. The second set of data (represented in the Figures by the squares) were obtained after an interval of some four weeks from the first set (represented by the circles). The results from both these sets are in good agreement.

7.4 PROPOSED CORRELATION

In Fig 7.8 the values predicted by correlations proposed by Katz and coworkers [10,11] and Geertsma [3] are also shown. The correlation mentioned by Tek et al [11] can be written as :

$$\beta = \frac{5.5 \times 10^{9}}{k^{1.25}\ \phi^{0.75}} \qquad (7.4\text{–}1)$$

The correlation proposed by Geertsma [3] is :

$$\beta = \frac{0.005}{\sqrt{k}\ \phi^{5.5}} \qquad (7.4\text{–}2)$$

These correlations were derived for dry cores but are widely used by replacing absolute permeability with effective permeability and using reduced porosity ie $\phi.S_g$, instead of the true porosity. Even with such adaptations these correlations do not appear to be particularly useful. Geertsma's relation is found to be completely inadequate since it puts too much emphasis on the porosity term (see Fig 7.8) in the ranges of interest.

The relation mentioned by Katz et al was often found to predict the value of β by as much as one order of magnitude away from the observed value. It however follows the general trend fairly closely. We have found that the inertial coefficients at higher saturations could be predicted with reasonable accuracy if an equation of the following type is used :

$$\beta = \text{const} / k_e^{1.25} \qquad (7.4\text{-}3)$$

where the constant in the equation could be evaluated if the value of β and k are known for the dry plug. At subsequent higher saturations only the effective permeability needs to be known to obtain a good approximation of β. The predicted values obtained in this manner are shown with broken lines in Figures 7.8 to 7.11.

An attempt was made to include the porosity term in Eq.(7.4-3) but this was found to have no improvement on the correlation and in some cases in fact deterioration was noticable. This is likely

due to the distribution of the liquid phase. The saturating liquid does not simply reduce porosity by being present as a thin film spread evenly throughout, as would be implied by the inclusion of the term $\phi.S_g$.

7.5 DISCUSSION

For measurements in saturated cores it is important that any change in the liquid saturation during the flow test should be minimal. This was achieved by saturating the gas before it entered the Hassler cell. At higher liquid saturations the loss usually did not exceed 2% and at lower saturations, the cores often gained by about 1% due to liquid deposition as the gas expanded through the core.

The most important requirement for measurements in saturated cores is that the saturating liquid should not move significantly during the flow test and that it should remain distributed uniformly throughout. This criterion is, however, difficult to evaluate since the saturations were measured gravimetrically and therefore is an average value for the sample. More advanced techniques, eg. nuclear magnetic resonance (NMR) or X-ray computer assisted tomography (CAT) would be required to measure the saturation in-situ and to be able to look at the saturation profile.

To find out if there was any significant movement of the liquid in the cores, the pressures were monitored at increasing gas flow rate up to a maximum upstream pressure of 689.5 kPa (100 psi) and then at decreasing flow rates. Any difference of the pressure-flow rate relation in the increasing and decreasing cycle could be interpreted as due to a hysteresis effect of the liquid movement. The hysteresis effect was indeed observed for high liquid saturations. This effect in the Forchheimer plot is shown in Fig.7.12 for sample M11 at 38% saturation, which is far in excess of its irreducible minimum. For saturations near the irreducible minimum and lower, no significant hysteresis effect was noticeable in any of the runs. This is to be expected since at such low saturations capillary adhesion forces required to move the liquid are far higher than the pressure difference imposed to move the gas through the core sample.

In Fig. 7.12 the lower portion represents the increasing flow rate cycle and the upper portion the decreasing cycle. The effective permeability evaluated from the upper portion is lower than for the increasing flow rate. The gradient of the upper portion is also slightly higher, which would therefore give a higher value of β. This phenomenon suggests that during the increasing pressure gradient cycle, the mobile wetting liquid moves and rearranges itself in such a manner that upon lowering the pressure gradient, the wetting liquid is unable to redistribute back to its original state, thereby causing the effective permeabilities to be different.

Gewers and Nichol [1] found that the values of β was at a minimum for 10% saturation. They attributed this principally to the streamlining of pores, ie. liquid tending to "smooth" out the sharp edges. From the present work, it can be seen (Figures 8 to 11) that the increase in inertial coefficient is not as rapid as had been reported for carbonates [2]. Furthermore, no minimum could be found at 10% saturation or at any other value as was observed for carbonates. The inertial coefficients in the present study were found to increase continuously with increasing saturations. The reason for not finding any minimum is likely to be due to the fact that the wetting phase mostly fills dead end pores as well as very narrow pore throats which would not be expected to contribute significantly to the overall flow process. This might also explain why the inertial coefficient values seem to increase very little until the saturation is close to the irriducible minimum. The differences are also likely due to the difference in pore structures between sandstones and micro-vugular carbonates. In the carbonates, micro-vugs alternate with pores whereas in sandstones the pores are much more homogeneous. The explanation of Gewers and Nichol for the lowering of β at 10% saturation no longer seems plausible. Photomicrographs (see Fig 7.13(a)) clearly show that the liquid phase is not distributed evenly as a thin layer which could cause the pore spaces to become more "smooth" and it is not expected that such behaviour could be found in sandstones. Investigations by others [5,6] also confirm this.

A number of interesting observations can also be made from the photographs of the impregnated thin sections. The wetting phase (shown in blue) is normally found to occupy relatively smaller intergranular pores than the non-wetting phase (shown in red) . This is likely due to the very high capillary forces required to displace the wetting phase from smaller pores.The wetting phase is also generally found to occur in regions of high surface curvature, eg inside pore filling aggregates, in points of contact between the grains, and inside intragranular porosity formed by the partial dissolution of unstable grains (Fig.7.13 (b),(c)). The non-wetting phase tends to occupy regions of low surface curvature. The passages through which gas flow takes place are often found to be almost cylindrical in shape (Fig.7.13 (d)).

The nonwetting phase can often be seen to be in direct contact with the sand grains. The reason for this is due to the tortuous nature of the flow channels. Although on average gas flow takes place perpendicular to the cross-section, however due to the tortuous path of individual channels gas could be impinging against the grain solid matrix perpendicularly. In this case any wetting phase present would be displaced away from there. It is possible that a layer of the wetting phase, a few molecules thick, would still be present due to adsorption. This however cannot be seen under an optical microscope and in any case the presence of such a thin layer would do little to reduce the frictional forces experienced by the gas phase.

Although quantitative measurements have still to be made, it can be seen from the photographs that very little of the wetting phase (blue) is present at the upstream end of the sample.

Comparitively there is a much higher quantity of it present at the downstream end. The commonly accepted explanation for this is the presence of capillary "end effect", arising from the outlet face discontinuity.

The capillary "end effects" of the mobile liquid phase can also have very significant influences on the inertial effect since an increase in the liquid saturation would decrease the effective permeability and hence increase the inertial coefficient. Such effects however were not taken into account by Wong [2]. It is probably the main reason why he found inertial coefficients increasing eight fold on increasing the saturation from 40 to 70%. Although it is easier to eliminate the end effects, it is however much more difficult to maintain an even saturation throughout the core with a mobile liquid phase. This is due to the very high pressure gradient required for the measurement of the inertial coefficient of the gas phase.

The above method provides an excellent means of visualizing the wetting phase. For any detailed quantitative work however, the method is inadequate. There are a number of significant differences between the experiments carried out to determine the inertial coefficients and those conducted with the epoxy resin. In the former, the cores were saturated with a hydrocarbon and then brought to their irreducible liquid saturation by placing them in a capillary pressure cell and imposing a high pressure. In the experiments with resin, air was used to displace the epoxy out of the cores. It was therefore not possible to reach an irreducible saturation throughout the core due to the presence of the end effect. Furthermore due to the large difference in the viscosity of the gas and the epoxy, the gas was found to channel through the core leaving behind unswept zones. This could be seen in the photomicrographs clearly as patches of red and blue distributed unevenly. Differences in the wettability between hydrocarbons and epoxy resins could also cause the distribution of the liquid phase to be different in the two cases.

Further work could be carried out to make the experiment more realistic. This could be achieved by injecting a fluid mixture which would be found in the real gas condensate reservoirs. By flowing such a fluid the quantity of the liquid dropout could be monitored for different flow conditions to simulate reservoir behaviour in a more realistic fashion. The liquid distribution could possibly be observed in-situ by such techniques as NMR. Reports of such experiments do not seem to be available in the open literature.

The degree of fit of the proposed correlation Eq. (7.4-3) can be expected to be dependent on the pore structure for a given medium. The four samples tested have varying "goodness of fit" (Fig.7.8-11). The capillary pressure and pore size distribution curves for these samples (Fig. 7.14-15) show that the pore structures are indeed quite different. A generalization of this idea will not be pursued here. It should however be noted that the Eq. (7.4-3) enables the value of β to be predicted more accurately than any of the existing correlations (Fig. 7.8).

7.6 CONCLUSIONS

Increasing the liquid saturation in sandstones decreases the effective permeability to gas and hence increases the inertial coefficient. The increase in inertial coefficient is however does not seem as rapid as has been reported for carbonates. Furthermore no minimum value have been found in the trend.

The inertial coefficient of gas flow in sandstone cores in the presence of a liquid saturation can be approximated with a β - k correlation provided that the value of β is known for a dry core and the effective permeabilities are known.

A method has been developed for visualization of the wetting and non-wetting phase distribution using coloured epoxy resins. The method has provided a means for making direct observations of the distribution of the liquid phase during high velocity gas flow in porous media.

REFERENCES

1. Gewers, C.W.W. and Nichol, L.R. : Gas turbulence factor in a microvugular carbonate, *J.Can.Pet.Tech.* (April 1969), 5
2. Wong, S.W. : Effect of liquid saturation on turbulence factors for gas-liquid systems, *J.Can.Pet.Tech.* (Oct. 1970), 274
3. Geertsma, J. : Estimating the coefficient of inertial resistance in fluid flow through porous media, *Soc.Pet.Eng.J.* (Oct. 1974), 455.
4. Noman, R. : High velocity gas flow in liquid saturated porous media, Student paper contest, Offshore Europe '85 Conference, Aberdeen, 10-12 Sept, 1985.
5. Evans, R.D., Hudson, C.S. and Greenlee, J.E. : The effect of an immobile liquid saturation on the non-Darcy flow coefficient in porous media, Paper SPE 14206 presented at the 60th Annual Fall Conf. of the SPE, Las Vegas, NV, Sept. 22-25, 1985; see also *SPE Prod. Engr. J.*, (Nov. 1987) p.331.
6. Jagai, T. : A laboratory investigation of the inertial coefficient of unconsolidated Trinidad sandstones, M.Phil. thesis (unpublished), Dept. of Chemical Engineering, University of W. Indies, Trinidad, Nov. 1982.
7. Noman, R. and Archer, J.S. : Resistance to high velocity gas flow in liquid saturated porous media and its visualization, *J. Can. Pet. Tech.* (to appear), 1988.
8. Klinkenberg, L.J. : The permeability of porous media to liquids and gases, *Drill. & Prod. Prac.*, A.P.I., (1941), p.200.

9. Dranchuk, P.M. and Kolada, L.J. : Interpretation of steady linear visco - inertial gas flow data, *J.Can.Pet.Tech.* (Jan. 1968), 36-40.

10. Katz, D.L. et al : *Handbook of Natural Gas Engineering*, McGraw Hill Book Co., New York (1959).

11. Tek, M.R., Coats, K.H. and Katz, D.L. : The effect of turbulence on flow of natural gas through porous reservoirs, *J.Pet.Tech.*, (July 1962), 799.

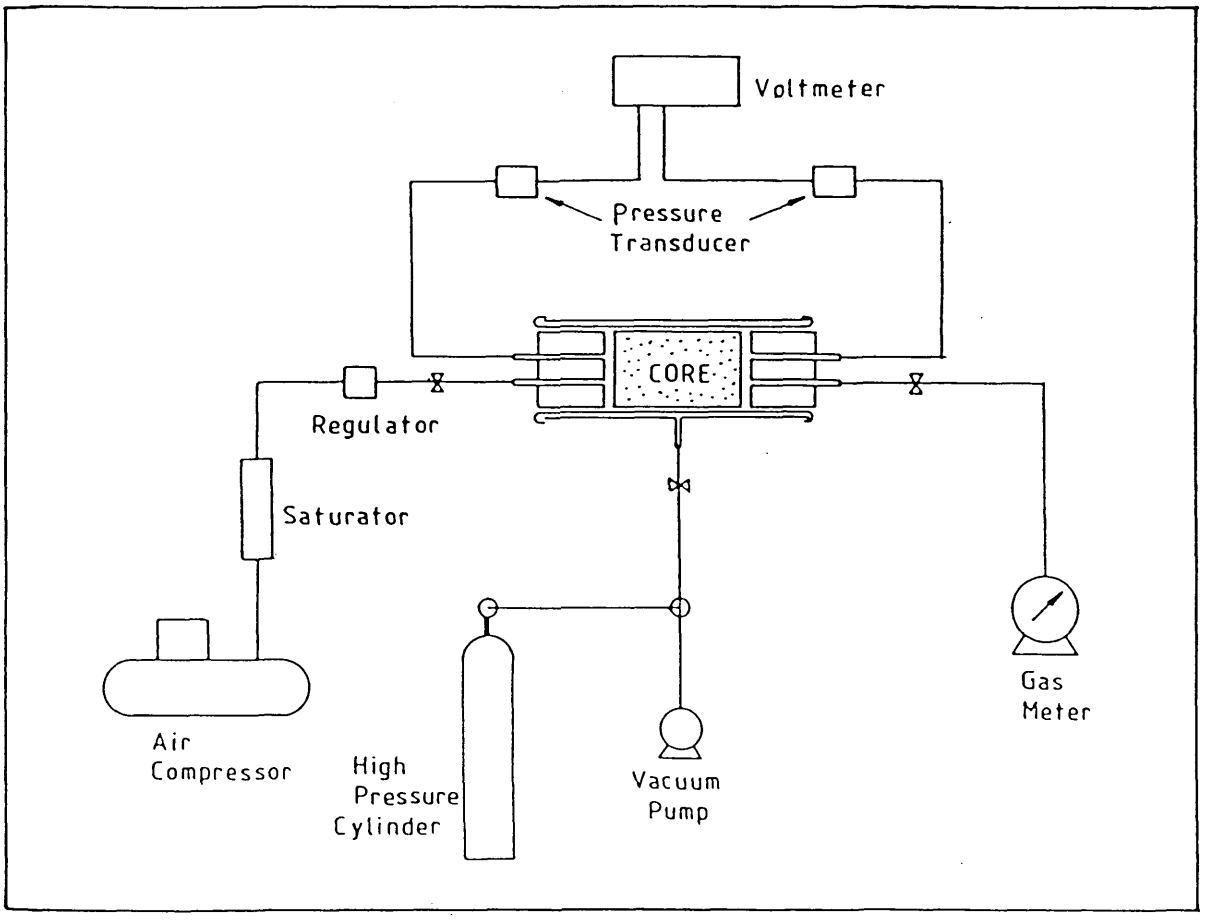


Fig. 7.1 Schematic arrangement of the apparatus for flow measurement.

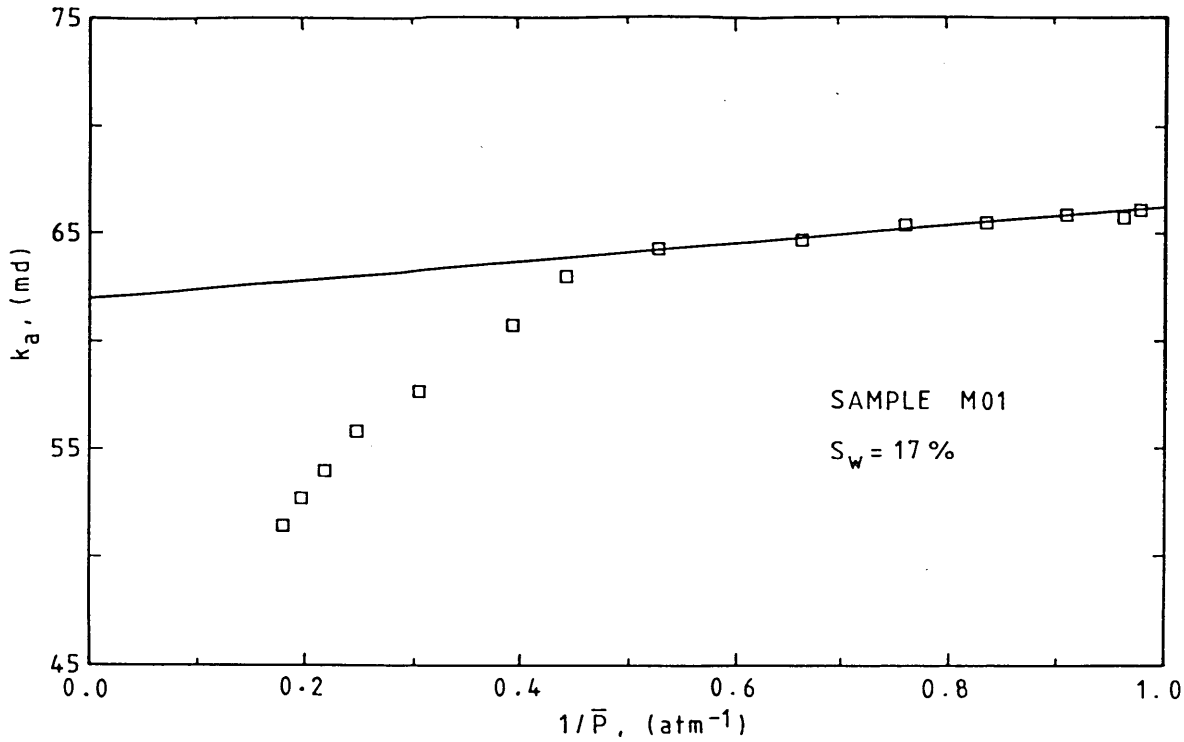


Fig. 7.2 An example of Klinkenberg plot.

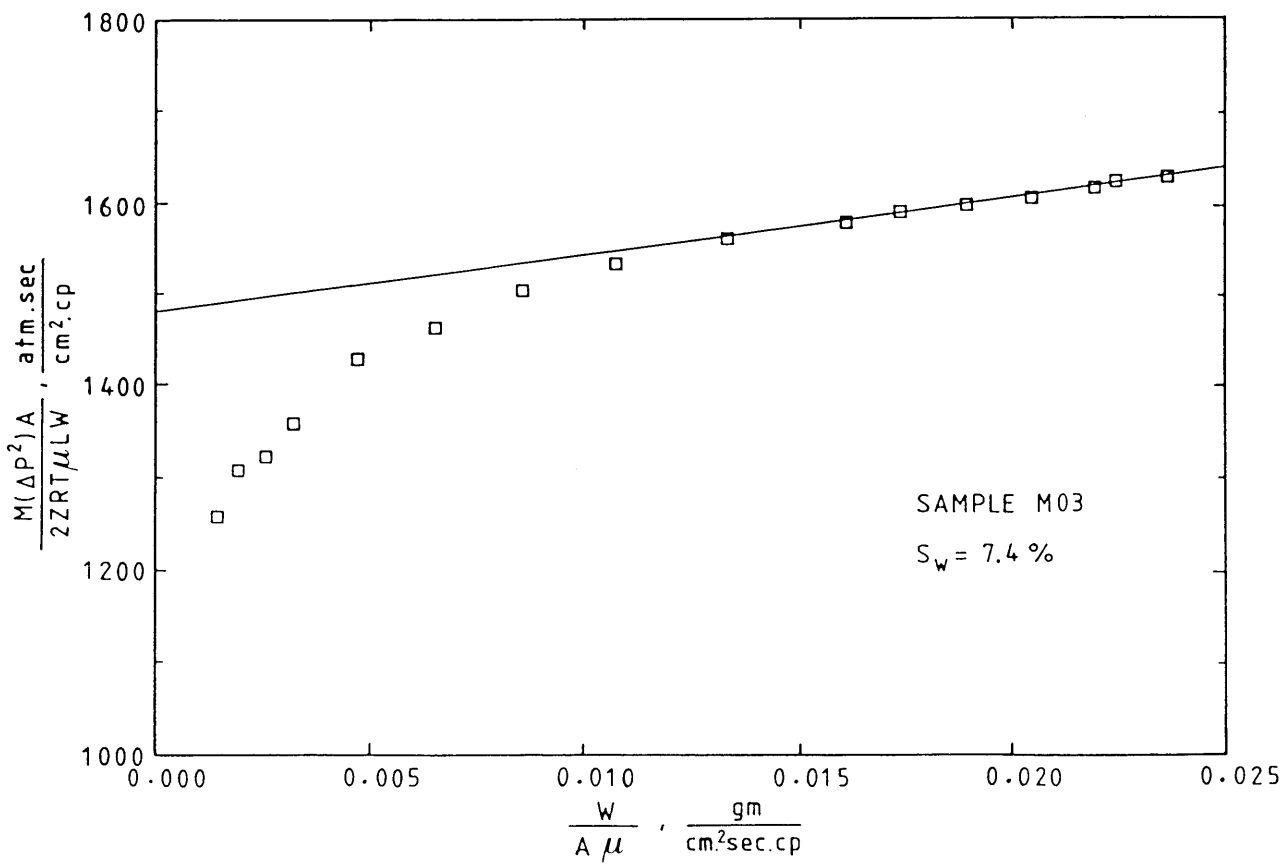


Fig. 7.3 An example of Forchheimer plot.

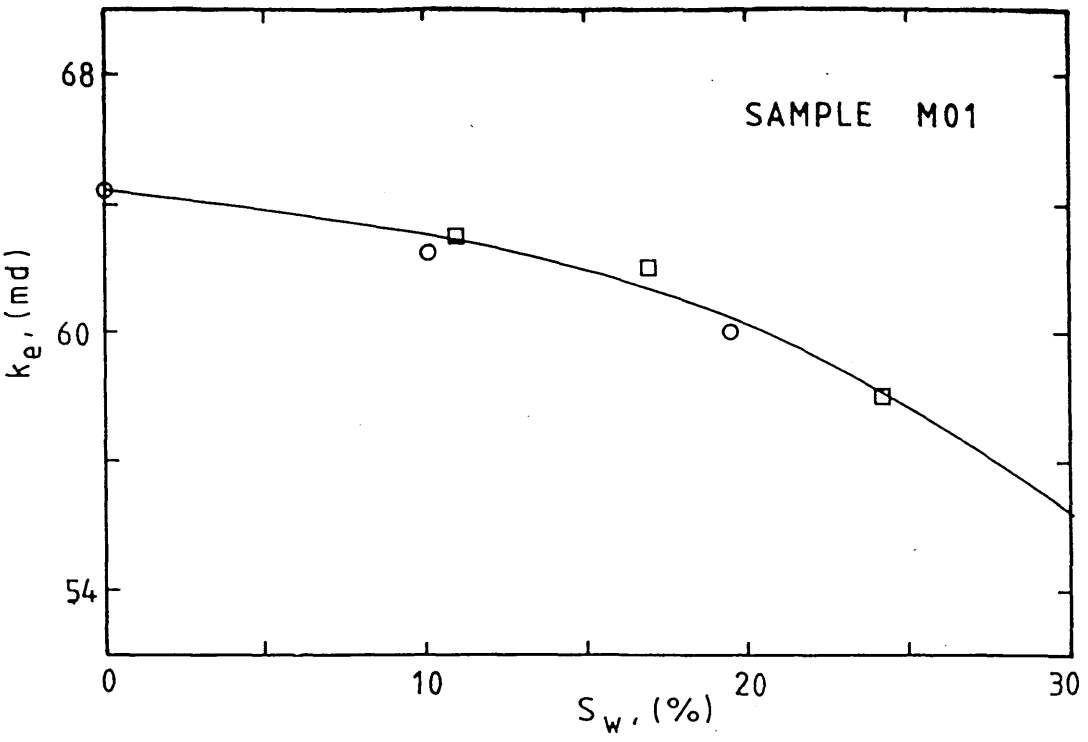


Fig. 7.4 Effect of wetting phase saturation on gas permeability. Sample M01.

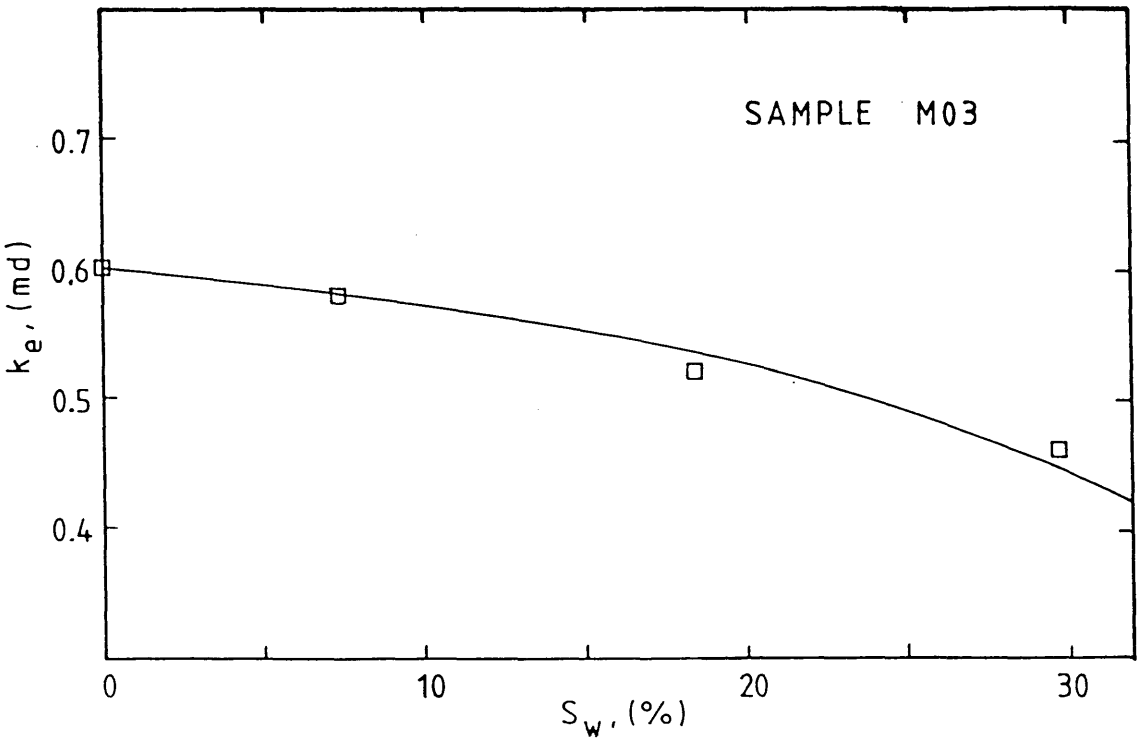


Fig. 7.5 Effect of wetting phase saturation on gas permeability. Sample M03.

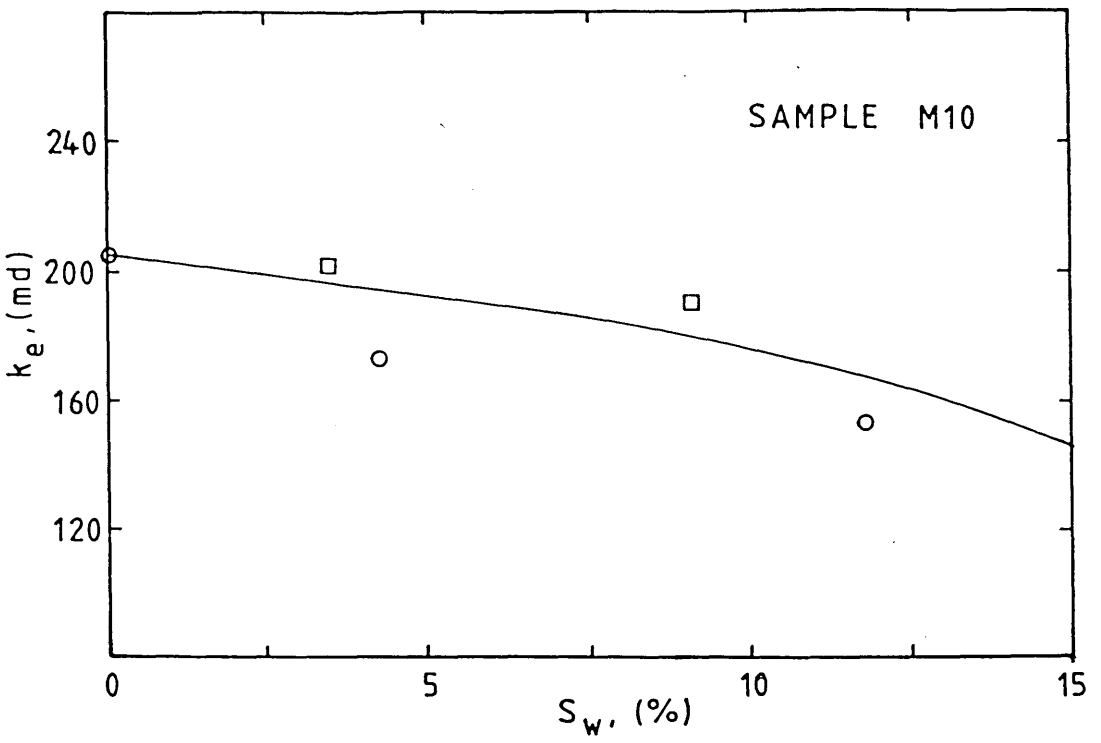


Fig. 7.6 Effect of wetting phase saturation on gas permeability. Sample M10.

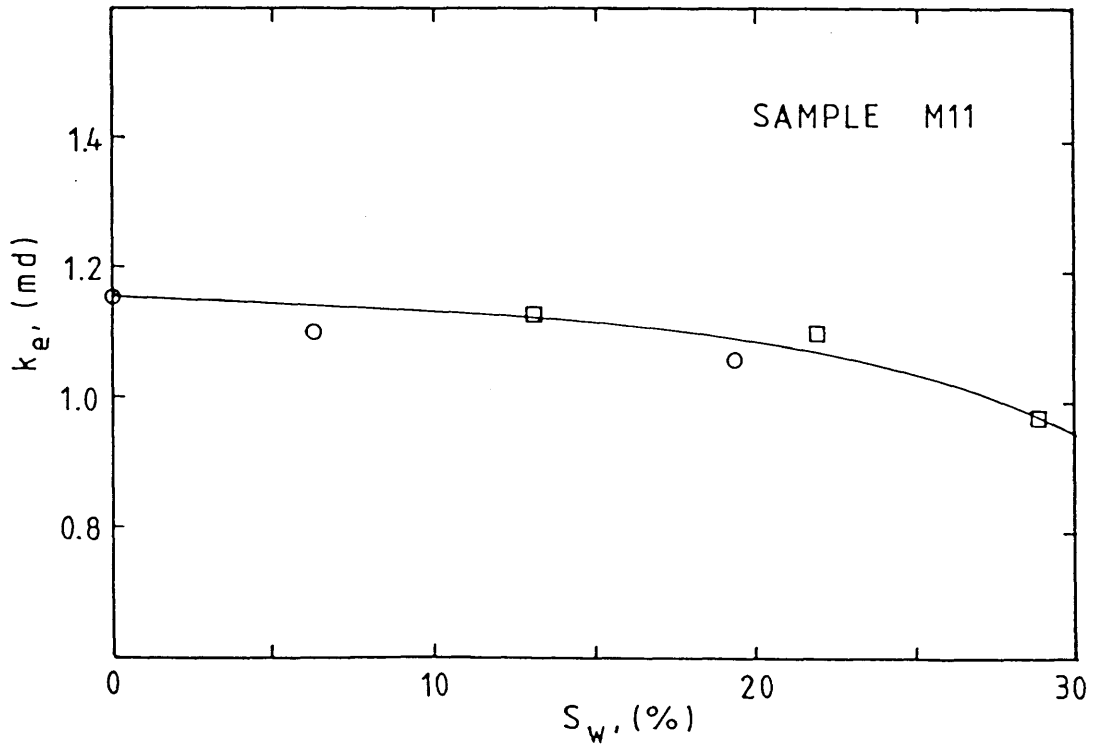


Fig. 7.7 Effect of wetting phase saturation on gas permeability. Sample M11.

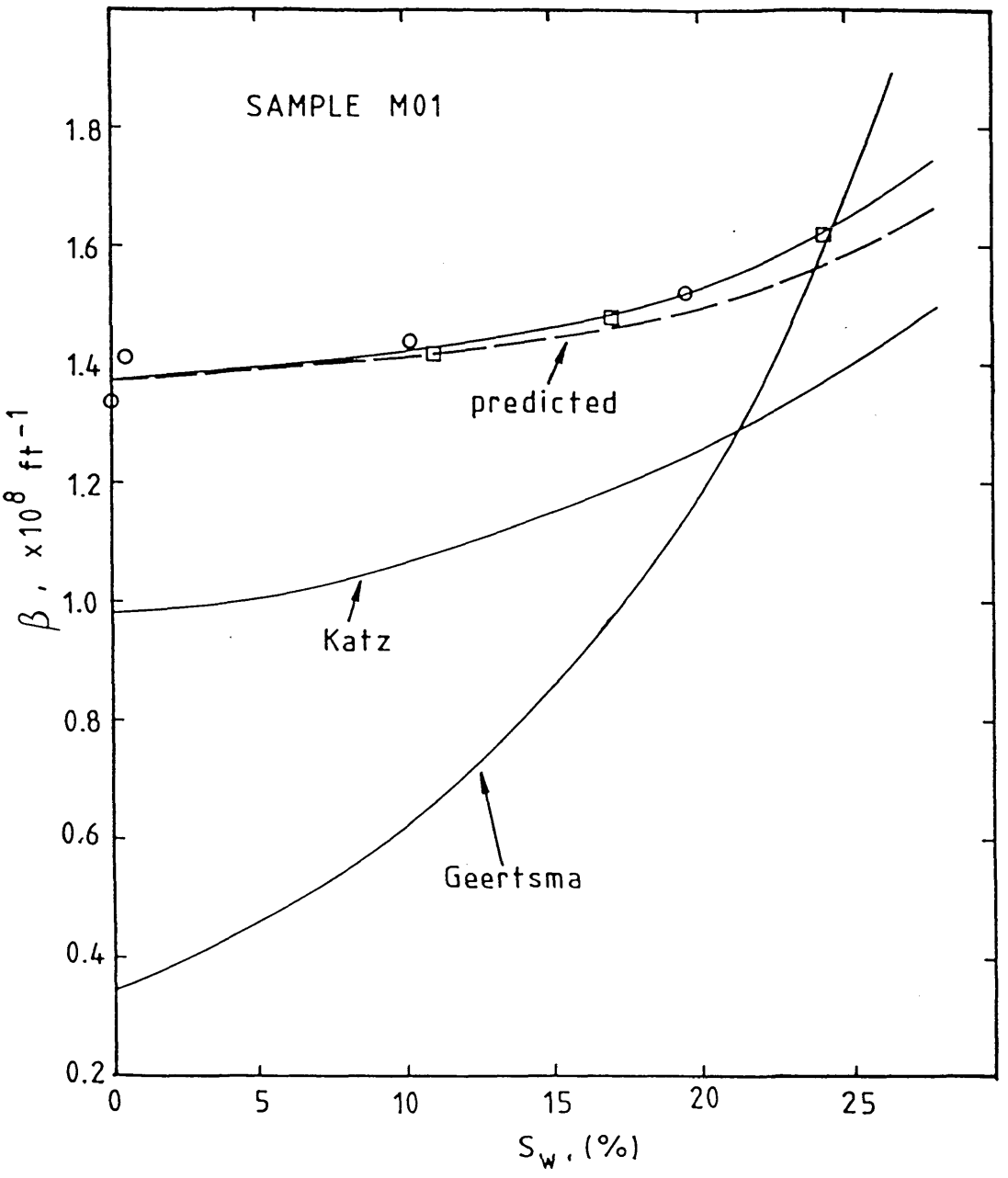


Fig. 7.8 Effect of wetting phase saturation on inertial coefficient. Sample M01.

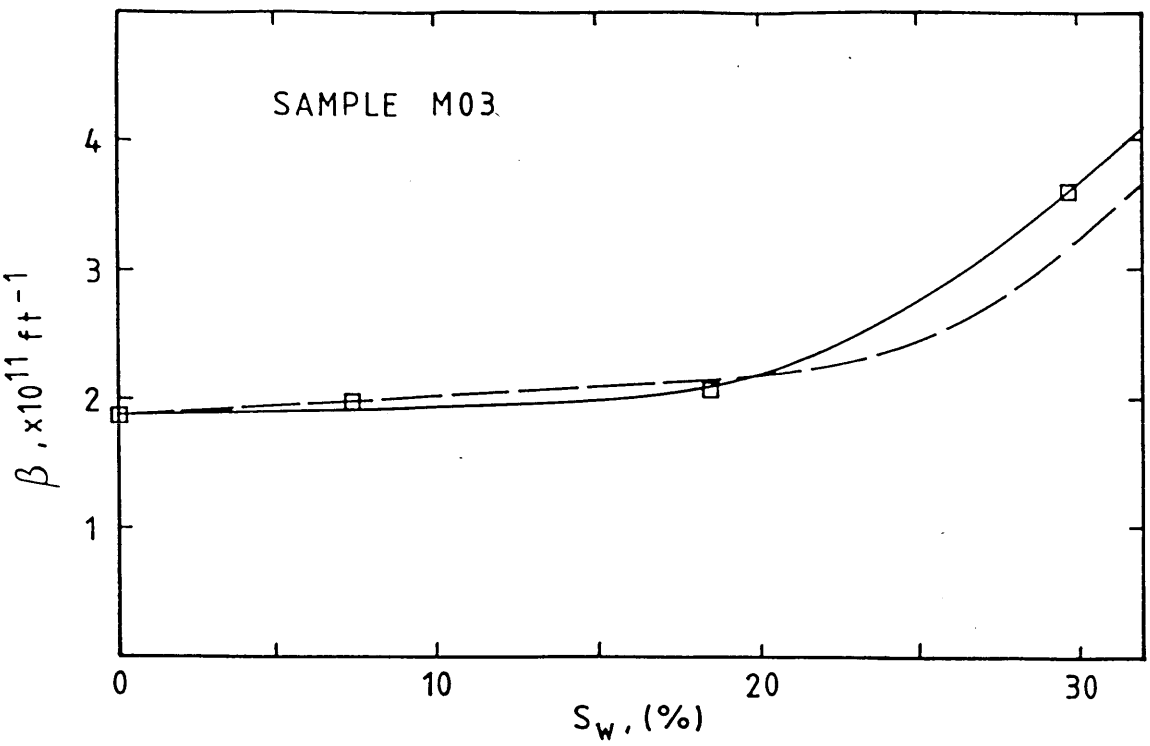


Fig. 7.9 Effect of wetting phase saturation on inertial coefficient. Sample M03.

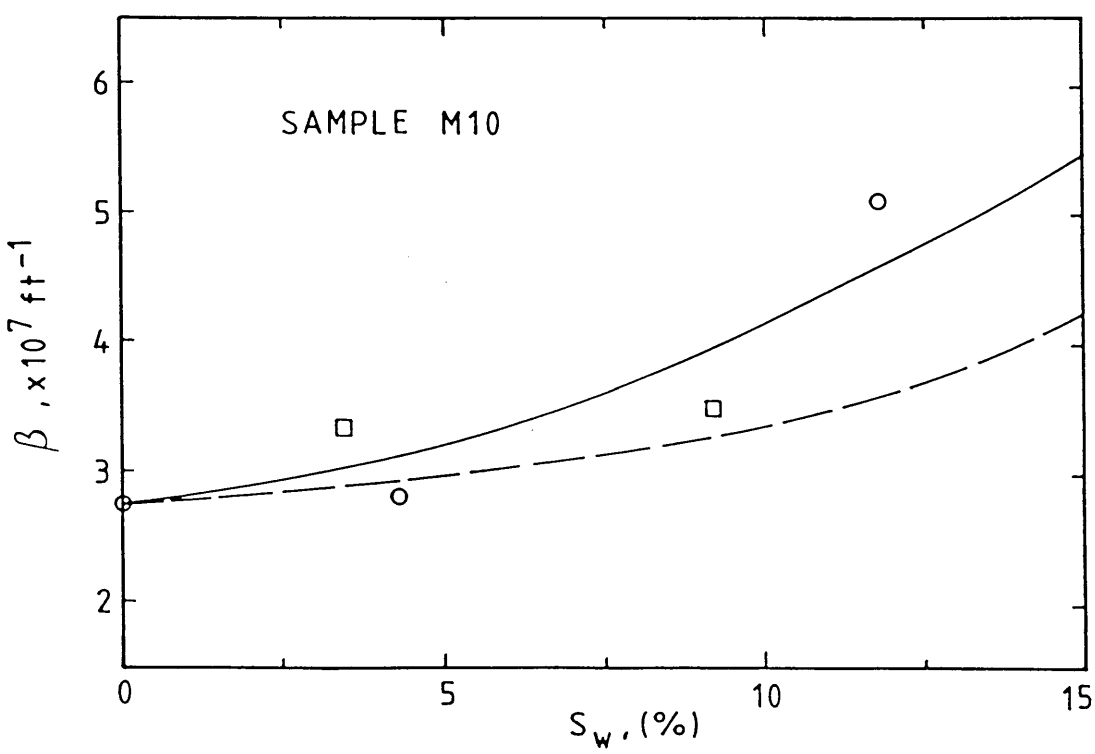


Fig. 7.10 Effect of wetting phase saturation on inertial coefficient. Sample M10.

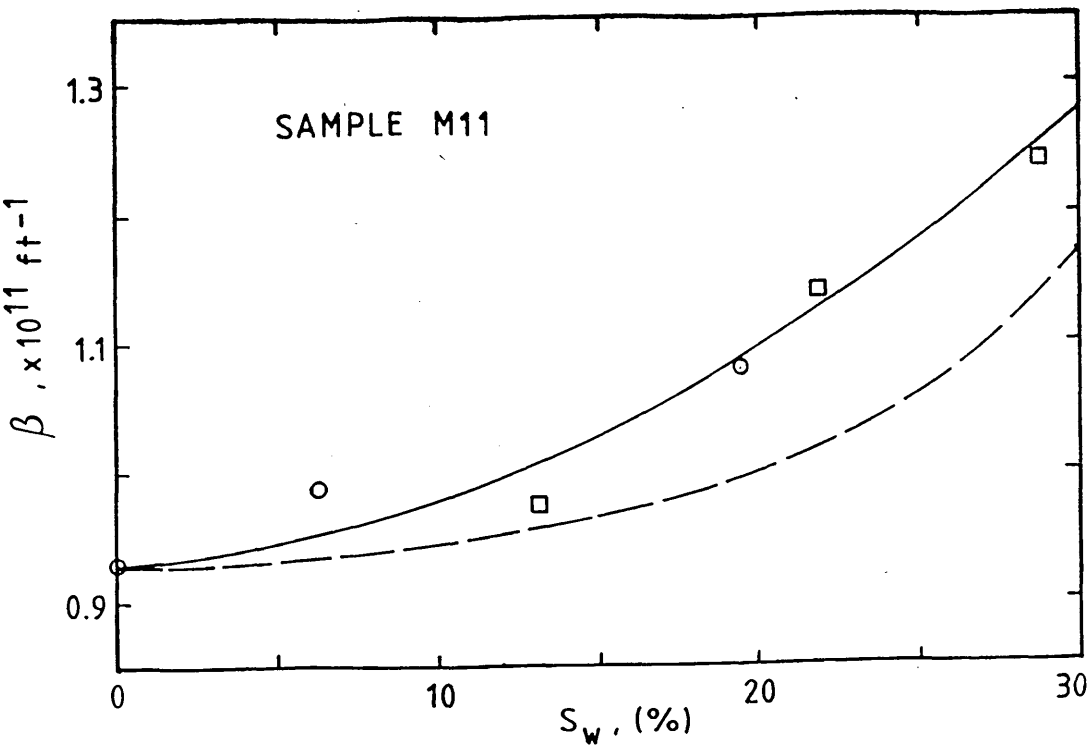


Fig. 7.11 Effect of wetting phase saturation on inertial coefficient. Sample M11.

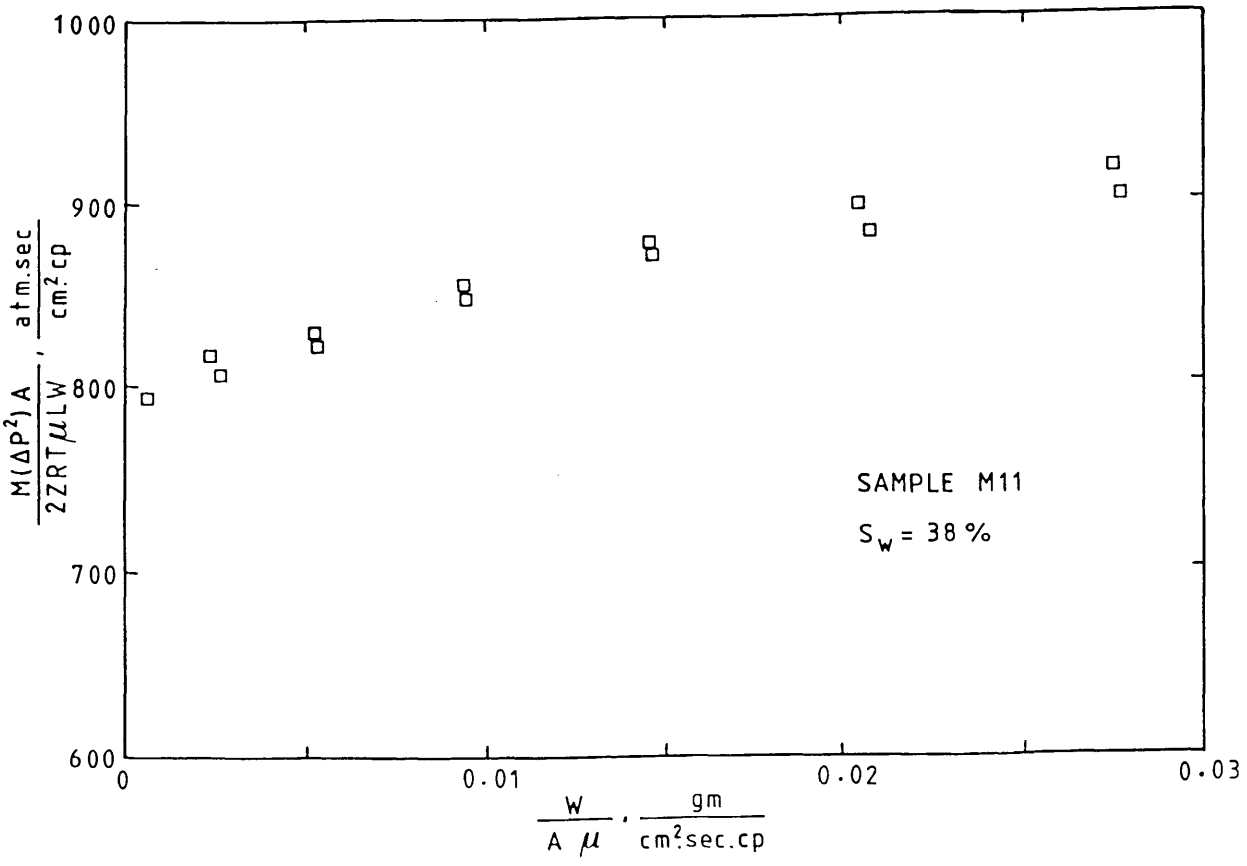
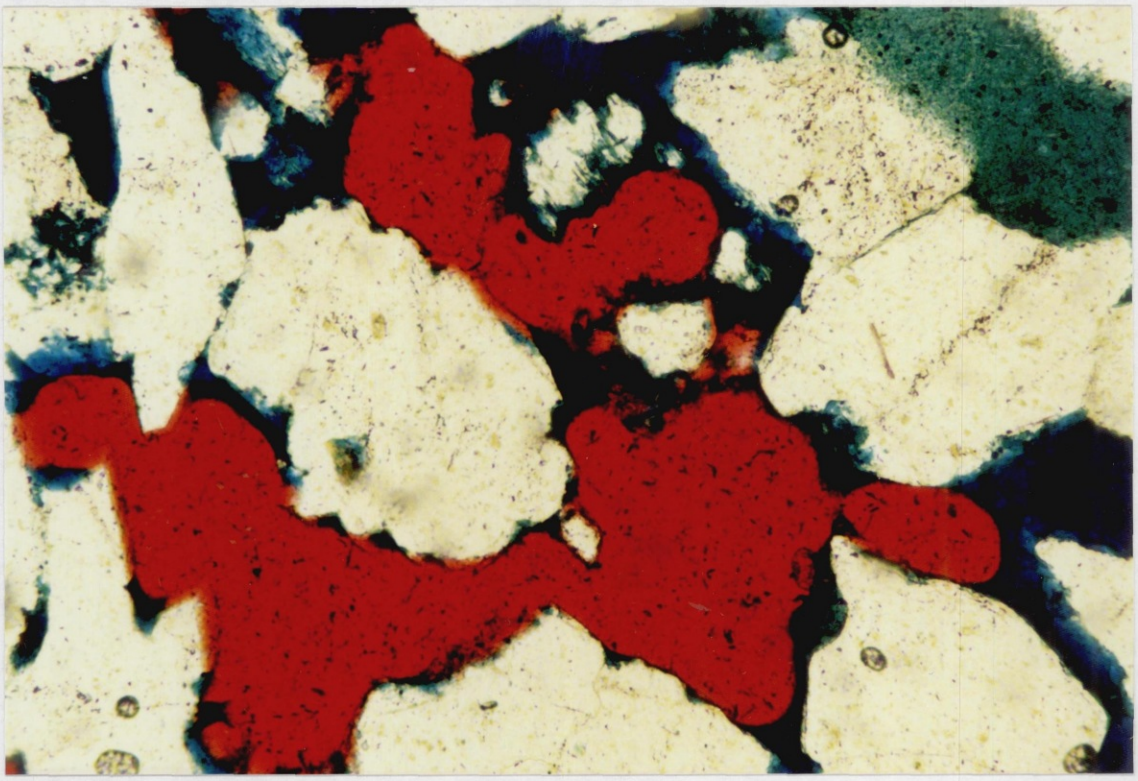


Fig. 7.12 Hysteresis in the inertial coefficient plot at liquid saturations above the irriducible minimum. Sample M11. Lower portion represents increasing flow rate and the upper portion decreasing flow rate.



(a)

(b)

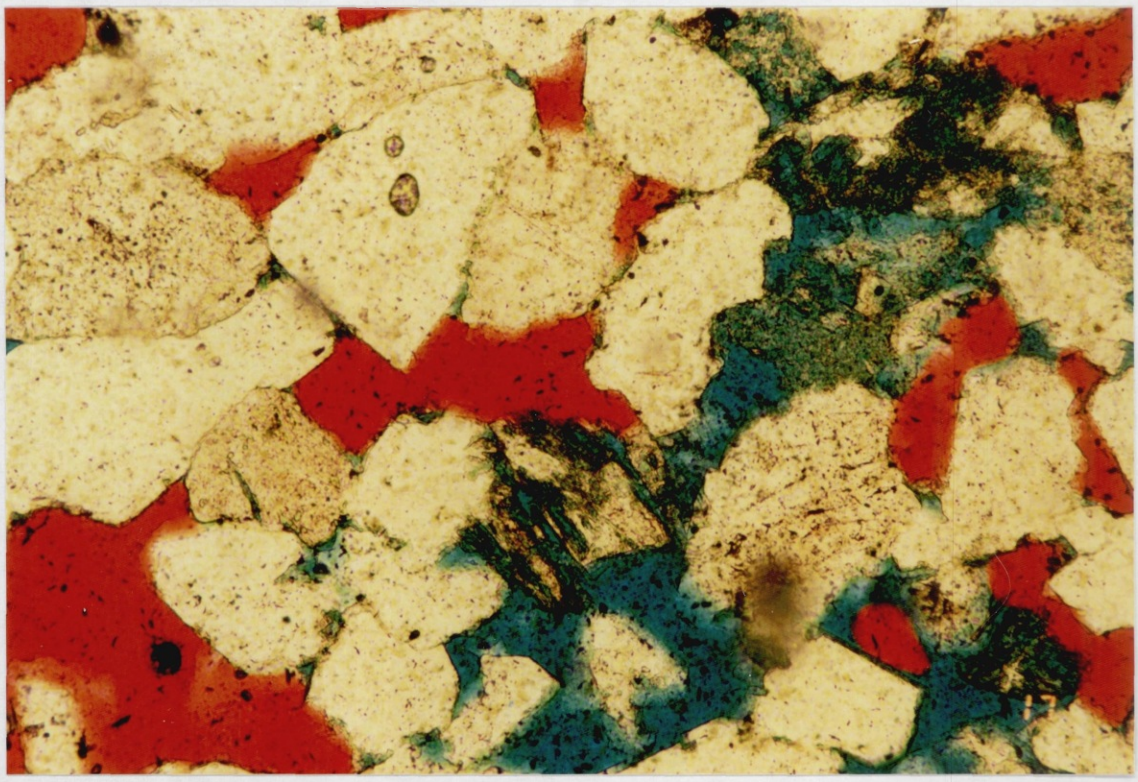
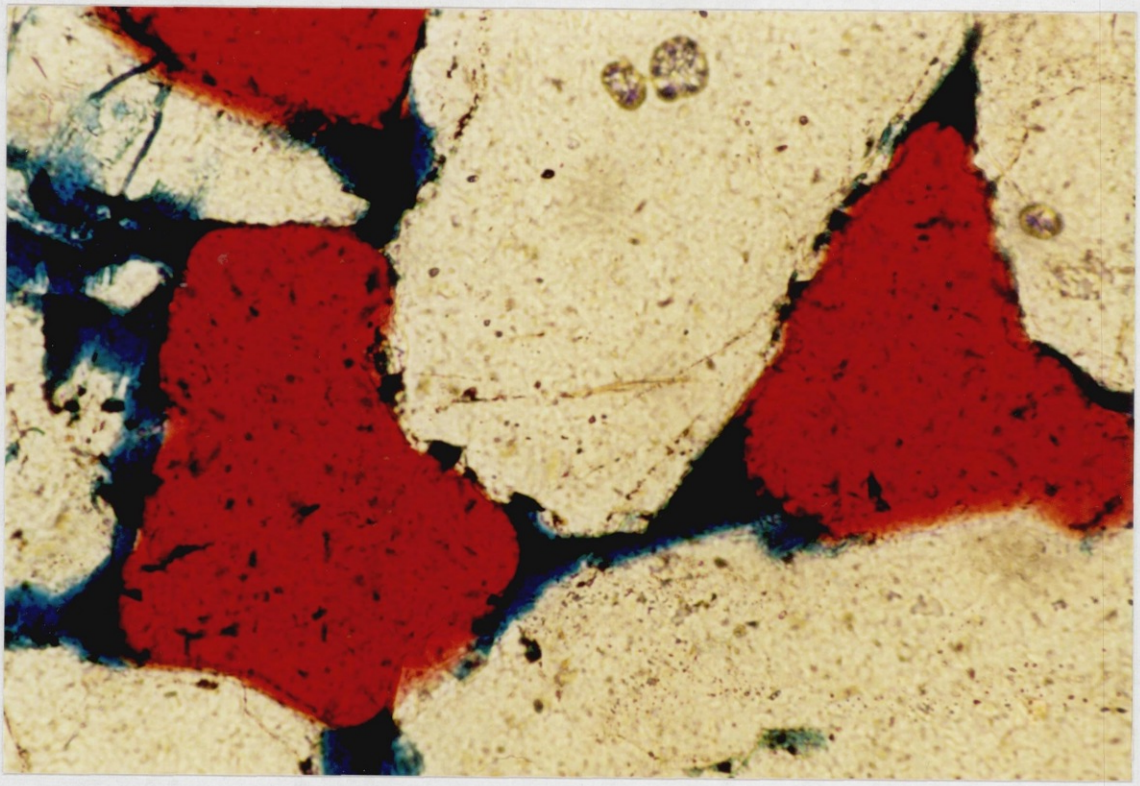
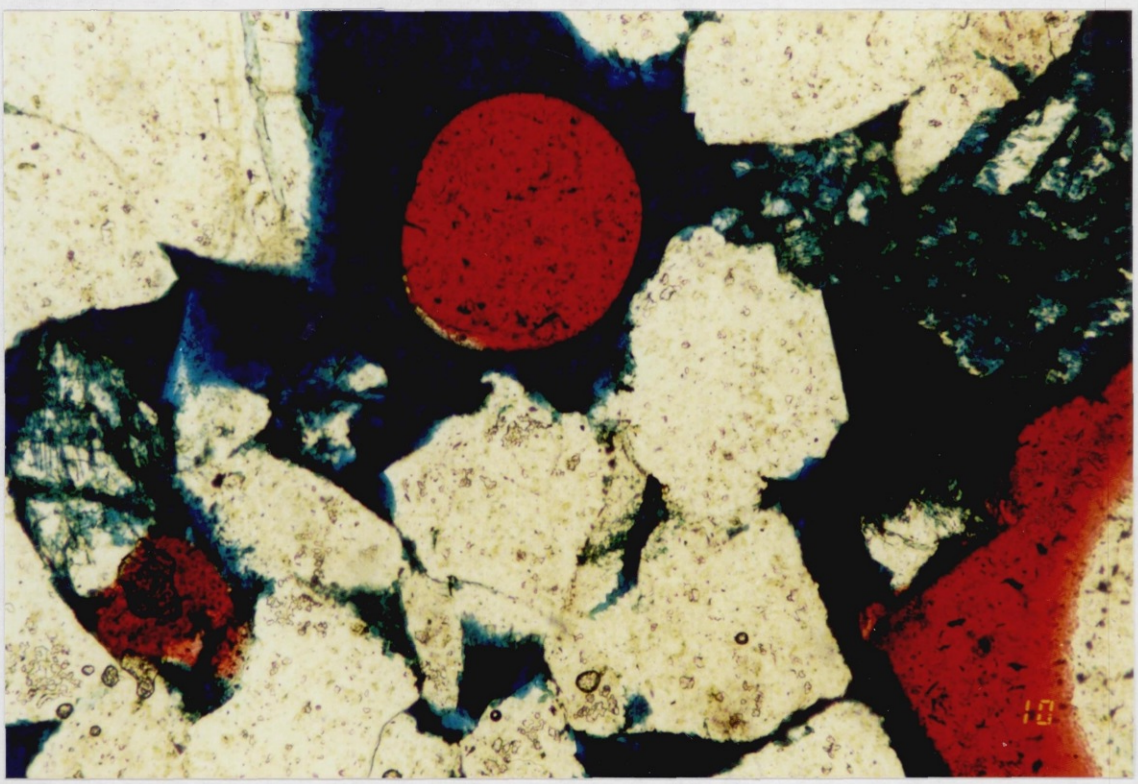


Fig. 7.13 Photomicrographs showing the distribution of the wetting (blue) and the nonwetting (red) phases in a sandstone rock sample. See text for discussion.



(c)



(d)

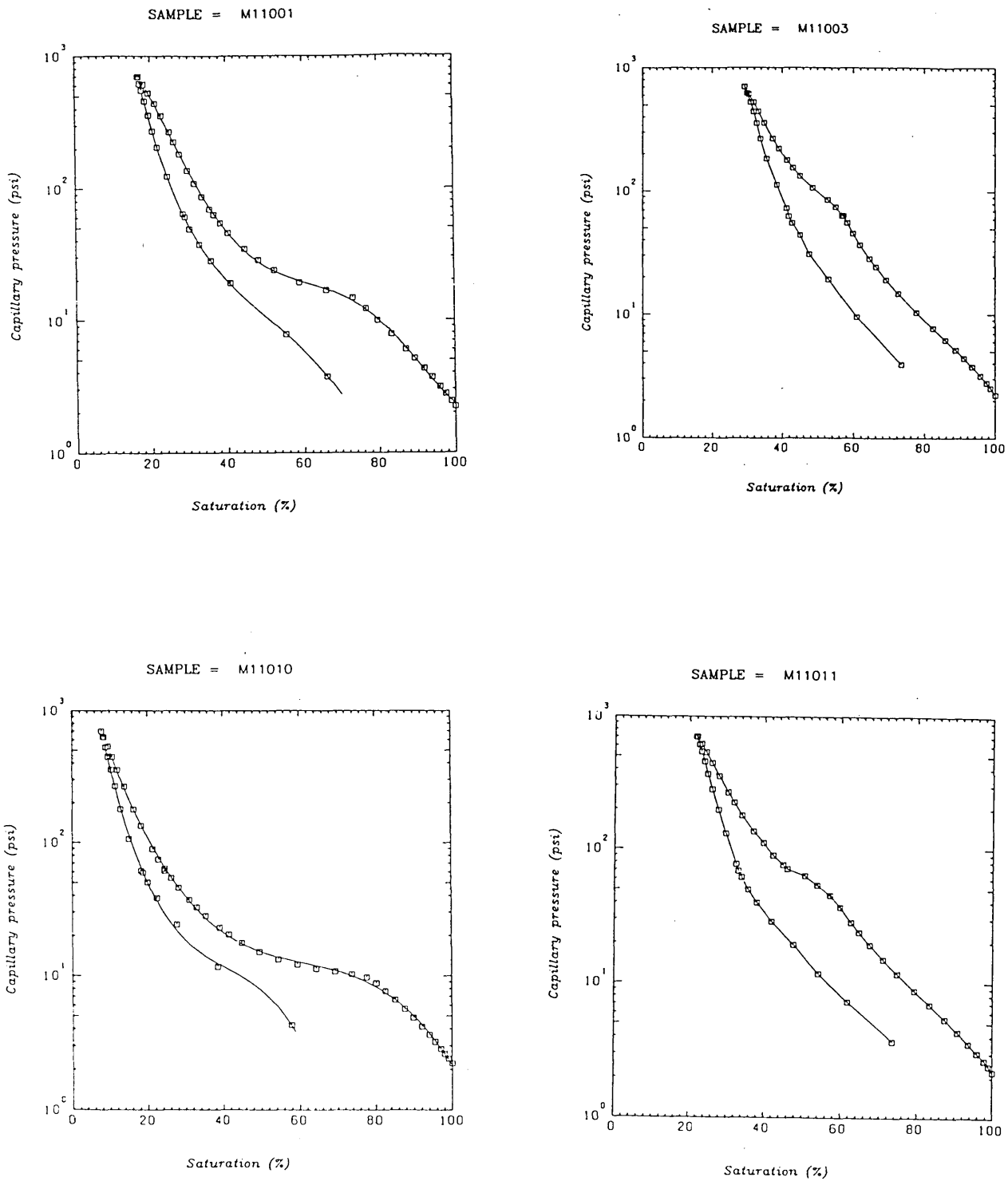


Fig. 7.14 Capillary pressure curves of sample (a) M11001, (b) M11003, (c) M11010 and (d) M11011.

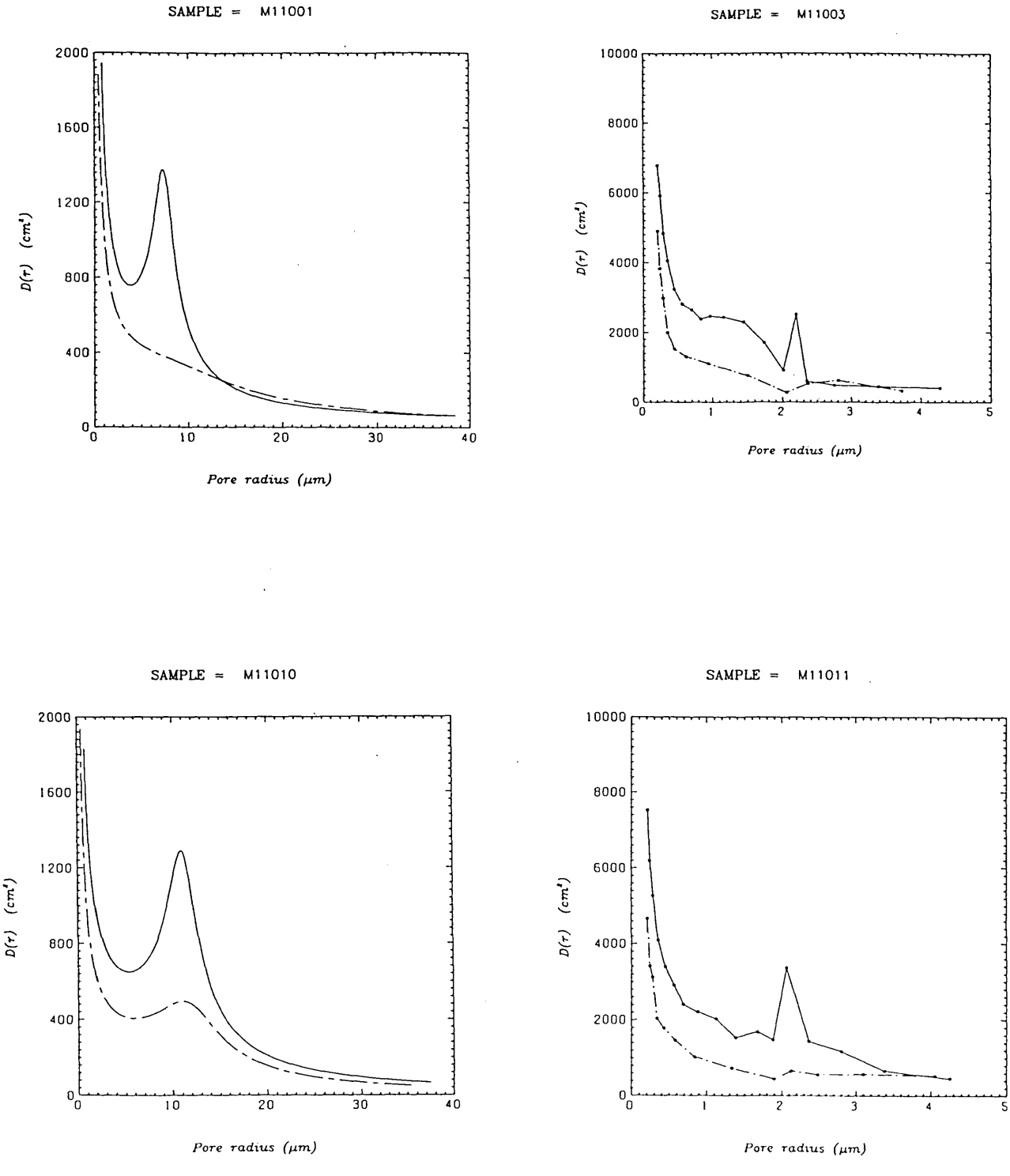


Fig. 7.15 Pore size distribution curves of sample (a) M11001, (b) M11003, (c) M11010 and (d) M11011.

Chapter 8

ESTIMATION OF INERTIAL COEFFICIENTS IN HIGH RATE GAS WELLS

8.1 INTRODUCTION

The inertial coefficient, β, for a rock can be estimated from either laboratory measurements on core plugs or from multi-rate pressure tests conducted in a well. Correlations published in the literature have all made use of the former method, and are often found to predict values of β by as much as two orders of magnitude away from those obtained from producing gas wells where conditions may be quite different. Extrapolation of the existing correlations to very tight (< 1md) reservoir rocks have also shown that the predicted values may by lower by an order of magnitude or more.

In this work β has been calculated from analysis of multi rate pressure transient tests conducted in over one hundred gas wells. The β -factors so obtained have then been correlated with available reservoir parameters, and experimental measurements on core plugs were also carried out for comparision. The empirical correlations obtained by this method could be used in predicting the non-Darcy pressure drop for other wells where, due to reservoir or operational constraints it may be difficult to conduct any extended multi-rate flow test. This chapter is based on results of this approach which has already been reported elsewhere [1].

8.2 RELATION BETWEEN α AND β

The quadratic equation which was first proposed by Forchheimer [2] to account for deviation from Darcy's law may be expressed as :

$$-\frac{dP}{dL} = \alpha \mu v + \beta \rho v^2 \qquad (8.2\text{-}1)$$

where α is the coefficient of viscous flow resistance, equivalent to 1/k at low flow rate. The other coefficient β is known as the coefficient of inertial flow resistance although other names have been suggested [3-5] in the literature.

Since β is generally much more difficult to measure than α (or permeability), numerous attempts have been made in the past to relate β to other petrophysical properties of rocks. These have shown that β can be related in various ways to porosity, permeability, tortuosity, specific surface area, size distribution of grains and pores, surface roughness, etc. However no universally applicable quantitative relationship has emerged (see Chapter 2). It would seem that each of these attempts are valid for only the specific conditions for which they were derived. In this section we shall attempt to show the relationship between β and other rock properties, firstly using dimensional analysis and then using the Kozeny - Carman equation. Although they are not exact, they do however provide a basis for deriving the regression based equations in later sections.

8.2.1 Dimensional Analysis

A simple dimensional consideration of Eq.(8.2-1) will show that α, the viscous coefficient, has dimensions of $[L]^{-2}$ and β, the inertial coefficient, has dimensions of $[L]^{-1}$. These two coefficients are independent of the fluid properties. Since they are both related to the characteristic length scale describing the structure of the porous medium, they may be expected [6] to be related to one another.

A more detailed dimensional analysis shows [7] that the pressure gradient during viscous fluid flow through a porous medium can be expressed as :

$$-\frac{dP}{dL} = c_1 \frac{\mu^2}{\rho \delta^3} F\left(\frac{\rho v \delta}{\mu}\right) \qquad (8.2\text{-}2)$$

where c_1= dimensionless constant

δ = a length parameter characterizing pore opening

F = an unknown function

At low values of Reynold's number the value of the function F has been found to be equal to its argument, ie.

$$-\frac{dP}{dL} = c_1 \frac{\mu v}{\delta^2} \qquad (8.2\text{–}3)$$

For flow at high velocity, ie. at high Reynolds number, the function F is found to be proportional to the square of its argument; Eq. (8.2-2) then becomes

$$-\frac{dP}{dL} = c_2 \frac{\rho v^2}{\delta} \qquad (8.2\text{–}4)$$

Equations 8.2-3 and 4 are equivalent to the viscous and inertial terms in the Forchheimer formula, where

$$\alpha = c_1 / \delta^2$$

$$\beta = c_2 / \delta \qquad (8.2\text{–}5)$$

The coefficients α and β are both related to a characteristic length scale of the medium and have dimensions of $[L]^{-2}$ and $[L]^{-1}$ respectively. The two coefficients can therefore be related to one another by

$$\beta = c_3 \alpha^{-0.5}$$

$$\beta = c_3 / \sqrt{k} \qquad (8.2\text{-}6)$$

8.2.2 Kozeny - Carman Relation

An alternative method is to use the Kozeny - Carman equation to establish a relation between the two coefficients. For a randomly packed bed of spherical particles, the particle sizes can be eliminated in favour of specific surface and porosity. The permeability of such a bed can be expressed [8,9] by the relation

$$\alpha = k_1 S_0^2 \frac{(1 - \phi)^2}{\phi^3} \qquad (8.2\text{-}7)$$

Using some simplifying assumptions, it can be shown [9] that for high velocity flow situations, the coefficient β in the Forchheimer equation may be expressed as

$$\beta = k_2 S_0 \frac{1 - \phi}{\phi^3} \qquad (8.2\text{-}8)$$

where k_1 and k_2 are dimensionless constants, and S_0 is the specific surface. The two coefficients α and β can therefore be related to one another via porosity and surface area by

$$\beta = (k_2 / k_1)\ \phi^{-1.5}\ \alpha^{0.5} \qquad (8.2\text{–}9)$$

which may be rewritten as

$$\beta = \frac{\text{const}}{\phi^{1.5} \sqrt{k}} \qquad (8.2\text{–}10)$$

The value of k_1, known as the 'Kozeny constant', has been found to be about 5 and that of k_2 around 0.4. These values and Eq. (8.2-10) has to be used with great caution when applying to consolidated reservoir rocks. For such rocks, diagenetic changes make it virtually impossible to predict the values of these constants from theoretical reasons alone.

8.2.3 Empirical Relations

A number of correlations are available in the literature, relating β to other petrophysical properties of rock samples. They have all been derived from experimental data often from small sets of data. Most of these are in fact variations of Eq. (8.2-10) with the coefficients found

empirically. Among the well known ones are those proposed by Katz and coworkers [10,11] and Geertsma [4] which have already been mentioned in the previous chapter. In the presence of an immobile liquid saturation, Katz' equation has been modified [12] to read as

$$\beta = \frac{5.5 \times 10^9}{k^{1.25} (\phi S_g)^{0.75}} \qquad (8.2\text{–}11)$$

This equation is however dimensionally incorrect, as are many of the other correlations proposed in the literature. By plotting ϕ against $\beta.k^{0.5}$ Geertsma [4] was able to obtain a straight line from which he proposed a dimensionally consistent relationship. The arguments used to propose this form of relationship are valid only for unconsolidated media having fairly uniform grain size distribution. For consolidated rocks such a relationship is not necessarily valid and the application of Geertsma's relation has been found to give erroneous results in many instances. It is necessary to note that his relation was formed from data which included porous metals, vuggy carbonates as well as various other media having pore structures quite dissimilar to consolidated sandstones.

In the present study we have also sought to relate β from well tests to porosity, permeability and saturation. Of necessity, some of these relations are dimensionally inhomogeneous. Fractional dimensions however may be reasonable in the description of porous media [13].

8.3 MEASUREMENT OF β FROM WELL TESTS

Using the real gas pseudo pressure, the inflow equation for a gas well may be written [14] as

$$m(p) - m(p_{wf}) = AQ + BQ^2 \qquad (8.3\text{-}1)$$

where A is the Darcy coefficient and for a semi steady-state flow may be represented in oilfield units by

$$A = \frac{1422\,T}{k\,h}\left(\ln\frac{r_e}{r_w} - \frac{3}{4} + S \right) \qquad (8.3\text{-}2)$$

In Eq. (8.3-1), B is the non-Darcy rate-dependent term, and can be found [15] from the expression

$$B = \frac{3.161 \times 10^{-12}\,\beta\,\gamma\,T}{\mu\,h^2}\left(\frac{1}{r_w} - \frac{1}{r_e} \right) \qquad (8.3\text{-}3)$$

Since in general $1/r_e$ is negligibly small compared to $1/r_w$, Eq. (8.3-3) may be simplified to

$$B = \frac{3.161 \times 10^{-12} \beta \gamma T}{\mu h^2 r_w} \qquad (8.3\text{-}4)$$

From a multi rate pressure test, the apparant skin S' can be calculated [15] for each rate of production. The apparent skin S' is related to the flow rate by

$$S' = S + DQ \qquad (8.3\text{-}5)$$

where

$$D = \frac{B k h}{1422 T} \qquad (8.3\text{-}6)$$

A plot of S' against Q from multi-rate drawdown can be used to obtain the value of S as the intercept and D as the gradient, according to Eqn.8.3-5. The value of B can therefore be found from Eq.(8.3-6) since D is already known, and hence the value of β can be evaluated from Eq.(8.3-4) for the particular well.

Excepting for a few cases, all the pressure test data reported here were analysed using the real gas pseudo pressure and the method of superposition [14,15].

8.4 DATA USED

Data from wireline logs and isochronal or flow-on-flow tests followed by an extended build-up were available for 105 gas wells. These wells are spread across 5 major sandstone gas reservoirs of the southern North Sea. The fields are referred to as A,B,C,D and E in Table 8.1.

The values of (kh) were calculated from buildup test and the apparent skin S', and hence β were calculated from drawdown. The net formation thickness, h, at a well was estimated from wireline logs. The net reservoir thichkness in these reservoirs was not considered to change significantly from that indicated at a well. The values for porosity and gas saturation are the thickness weighted averages for the cross section of the formation found from the logs for the individual well. Many of the southern North Sea gas reservoirs are characterized by a high liquid saturation which is immobile. The values for perforated intervals are subject to some uncertainity since production logs were available for less than one third of all the wells. For the rest, original well completion records were used. In some cases the perforated thickness, h_p, was found to be greater than h where the wells were highly deviated. The relevant data for the five fields are given in Table 8.1. Plots of permeability against porosity for all the wells are shown in Fig.8.1 and the distribution of data are shown in Figs. 8.2 to 8.4.

8.5 PROPOSED CORRELATION

Several different statistical models were tested to fit the observed field data. Both single and multiple regression methods were used to correlate β to other variables as described below.

(a) Linear Regression

The best correlations were obtained when power curve regression models were used. These are of the form

$$y = c\,x^{m} \tag{8.5-1}$$

They were linearised by taking logarithms

$$\log y = m \log x + c' \tag{8.5-2}$$

Standard techniques [16] of regressing y on x or alternatively x on y are not suitable in this sort of situations since errors are inherent in the calculation of all the variables. Use of such standard methods can lead to erroroneous results and can sometimes even fail completely. An alternative method [17] of minimizing the distance perpendicular from the data point to the regression line was adopted in the present work.

Some of the results found by using the above method are shown in Table 8.2 along with their correlation coefficient and standard errors of estimate.

(b) Multiple Regression

Using a linear regression it is possible to treat only one independent variable at a time. A standardized multiple regression technique was used to include more significant variables. Power curve models were again chosen and linearized for the purpose of regression by taking logarithms. A number of different relationships were tested and are given in Table 8.2. The best fitting correlation was found to be Eq. (8.5-3).

8.6 LABORATORY MEASUREMENTS

In the present study measurements were carried out in the laboratory on a number of core plugs from the study fields and also from other adjoining fields. Measurements were carried out by flowing gases at increasingly high rate. Porosity, permeability and inertial coefficient were calculated in the usual manner as described in Chap.4. Results are given in Table 8.3.

8.7 DISCUSSION

Some of the results obtained from regression are presented in Figures 8.5 to 8.11. The results indicate that an acceptable and useful correlation can be obtained by relating β directly to permeability as shown in Fig 8.5. The plot also shows lines obtained from Katz's equation [10] for 10% and 20% porosity values as well as the line obtained from Geertsma's relation [4] assuming the porosity is 15%. In both cases it is clear that the existing correlations are unable to predict the observed values with acceptable accuracy. The best fitting straight line is given by Eq. (8.5-3). A plot according to Eq. (8.5-6) is shown in Fig 8.6.

The best relationship was obtained when β was related to $\sqrt{(k / \phi.S_g)}$ as shown in Fig.7. This may suggest that β is directly related to pore geometry through ϕ. The term $\sqrt{(k / \phi)}$ has been used widely in the literature as a length parameter characterizing a porous media, eg in Leverett's "J-function" [18]. According to Eq. (8.5-3), the relationship is also dimensionally homogeneous. The gas saturation term is included since the presence of a liquid saturation will reduce the effective porosity. In the present study it has been assumed that the liquid phase present is immobile for all the wells. The liquid production in all cases hardly ever exceeded 3-4 bbl/MMscf and this is most likely due to the pressure and temperature changes from wellbore to the surface separators.

The experimental results have been plotted in Fig 8.8 using β and k as the axes. The line according to Eq.(8.5-4) is shown as well as the line of best fit given by the dashed line. It can be seen that Eq. (8.5-4) can predict the values of β far better than existing relations. The experimental results obtained in the laboratory therefore supports the correlation derived from field data. Further, the experimental results show that for low permeability rocks (ie . $0.1 < k < 1.0$ md.) the values of β may be at least an order of magnitude higher than those predicted by existing correlations.

Plots according to Geertsma's procedure are shown in Fig 8.9 and 8.10. A plot of ϕ against β can be used to obtain a very good straight line (Fig 8.11). However correlations formed from such plots may be unreliable since the range of porosity is far too narrow to form any valid relationship.

It has been suggested [15] that the perforated interval, h_p, should be used in Eq.(8.3-4) instead of h, the net formation thickness. This suggestion is based on the assumption that non-Darcy flow is significant only very near to the wellbore. Also implicit is the assumption that the flow is completely radial. In this study it was found that the correlation coefficients for Eqns.(8.5-3) to (8.5-11) improved considerably when h was used instead of h_p in calculating β from Eq.(8.3-4). The correlations were also tested for all the data where h_p was less than h. It

was found that the correlations again improved by a similar magnitude. This suggests that inertial effects may be significant at larger distances away from the wellbore so that it would be more appropiate to use h instead of h_p. The situation is depicted in Fig. 8.12. The flow is such situations are neither completely radial nor spherical. If the inertial effect is significant some distance away from the wellbore, then the formation thickness would be a better quantity to use. Some uncertainity is also attached to the values of h_p. In this study production logs were not available for most of the wells and even when available their interpretation was ambiguous. In contrast, the net formation thickness can be evaluated with much more reliability from wireline logs. The net formation thickness h therefore provides a more reliable parameter to use than h_p. For this and the above mentioned reason only h was used in Eqn.8.3-4 for calculating β as shown in Table 8.1. The reported ratios between h_p and h are also shown in Table 8.1.

Permeability near the wellbore is almost always different from that of the bulk formation due to mud filtrate invasion, acidizing etc. This is precisely the region where the non-Darcy effects are more significant. It was therefore thought that the correlations could be improved further if β was related to the altered permeability. An equation for calculating k_a, the permeability of the altered zone has been given by Hawkins [19] which is

$$S = \left(\frac{k}{k_a} - 1\right) \ln \frac{r_a}{r_w} \qquad (8.7\text{-}1)$$

This equation is however not particularly useful since r_a, the radius of zone of the altered permeability is also unknown. By analogy with the concept of effective wellbore radius [15] we can relate the two permeabilities.

$$k_a = k \exp(-nS) \qquad (8.7\text{-}2)$$

where n is a constant to be found by trial and error. A negative skin would therefore increase the value of k_a and a positive skin would have the opposite effect.

Using this method Eqns. 8.5-5 and 11 were modified (see Table 8.2). The improvement using the first equation was small, although in the second case it was significant. The bulk formation permeability therefore seems to be adequate in formulating the correlations especially since inertial effects may be present at some distance away from the wellbore.

The major limitation of the various correlations proposed in this work and by others in the literature is that only porosity and permeability have been taken as the independent variables controlling inertial effects. However, as we have shown in the previous chapters, porosity and permeability alone cannot characterize the geometry of the porous medium sufficiently well.

8.8 CONCLUSIONS

1. Data from over one hundred gas wells were analysed to obtain the coefficient of inertial resistance. The coefficients were correlated with reservoir parameters. These correlations, which are supported by experimental measurements using core plugs, are shown to be better than existing relations in predicting β.

2. The best correlation can be formed when β is related to $(k / \phi.Sg)^{-0.5}$. This is because the parameter $(k / \phi)^{0.5}$ is found to be a good estimate of the mean characteristic length of a porous media.

3. Correlations according to Geertsma's method give unreliable results since the porosity range in producing sandstone reservoir rocks is generally narrow.

4. Laboratory measurements of β show that for low permeability (ie. $k < 1$md) sandstones, the value of β can be at least an order of magnitude higher than those predicted by existing correlations.

5. Correlations were found to be much improved if β was calculated using the formation thickness. This is thought to be due to non-Darcy effects existing at some distance away from the wellbore. It was therefore found preferable to use the net formation thickness rather than the perforated interval thickness in Eq. (8.3-4).

6. Although it may be preferable to relate β to the permeability of the altered zone near the wellbore, the bulk formation permeability appears to be adequate for use in predicting the value of β.

7. No unique correlation could be found for predicting β from k and ϕ alone which would fit the data perfectly. This is because β is also a function of other pore structural parameters for which k and ϕ alone cannot provide adequate description.

REFERENCES

1. Noman, R., Shrimanker, N. and Archer, J.S. : Estimation of the coefficient of inertial resistance in high rate gas wells, Paper SPE 14207 presented at the 60th Annual Fall Conference of the SPE, Nevada, Sept. 22-25, 1985.
2. Forchheimer, P. : *Hydraulik*, Leipzig and Berlin (1914) Chap 15, Sec 116-118.
3. Firoozabadi, A. and Katz, D.L. : An analysis of high velocity gas flow through porous media, *J. Pet. Tech.* (Feb. 1979) p.211.
4. Geertsma, J. : Estimating the coefficient of inertial resistance in fluid flow through porous media, *Soc. Pet. Eng. J.* (Oct. 1974) **5**,445.
5. Cornell, D. and Katz, D.L. : Flow of gases through consolidated porous media, *Ind. Eng. Chem.* (Oct. 1953) **45**, 2145.
6. Green, L. and Duwez, P.J. : Fluid flow through porous metals, *J. Appl. Mech.* (1951) **18**, 39.
7. Muskat, M. : *Flow of Homogeneous Fluids Through Porous Media*, Edward Arnolds, New York (1934)
8. Ergun, S. and Orning, A.A. : Fluid flow through randomly packed columns and fluidized beds, *Ind. Eng. Chem.* (1941) **41**, 1179-1184.
9. Carman, P.C. : *Flow of Gases Through Porous Media*, Butterworth, London (1956).
10. Katz, D L et al : *Handbook of Natural Gas Engineering*, McGraw Hill Book Co, New York (1959).
11. Tek, M. R., Coats, K.H. and Katz, D.L. : The effect of turbulence on flow of natural gas through porous reservoirs, *J. Pet. Tech.* (July 1962) 799.
12. Ramey, H. J. : Non-Darcy flow and wellbore storage effects in pressure buildup and drawdown of gas wells, *J. Pet. Tech.* (Feb. 1965) 223.
13. Mandelbrot, B.B. : *Fractal Geometry of Nature*, W H Freeman & Co, San Francisco (1982).
14. Alberta Energy Resource Conservation Board : *Theory and Practice of the Testing of Gas Wells*, Alberta, Canada (1975).
15. Dake, L. P.: *Fundamentals of Reservoir Engineering*, Elsevier Scientific, Amsterdam (1978)
16. Davis, J.C. : *Statistics and Data Analysis in Geology*, J Wiley & Sons, New York (1973)
17. Dorn, W.S. and McCrakin, D.D. : *Numerical Methods and Fortran IV Case Studies*, J.Wiley & Sons, New York (1972) p. 357.
18. Leverett, M. C. : Capillary behaviour in porous solids, *Trans AIME* (1941) **142**, 153.
19. Hawkins, M. F. : A note on the skin effect, *J.Pet. Tech* (Dec. 1956) p. 65.

Table 8.1

Field Data

Well No.	β (ft^{-1})	k (md)	ϕ (%)	S_g (%)	h_p/h	S
	$x10^9$					
			FIELD A			
1	0.89	63.0	11.0	45.0	1.0	-4.2
2	2.15	118.0	11.7	63.0	1.0	-5.0
3	4.38	48.0	10.9	52.0	1.0	-0.6
4	3.05	7.0	12.1	50.0	1.0	-3.5
5	0.58	80.0	12.9	52.0	1.0	-4.0
6	22.86	2.5	11.4	53.0	1.0	-5.0
			FIELD B			
7	10.45	13.10	14.1	74.0	.42	0.2
8	1.11	64.20	12.5	69.0	.67	-3.7
9	171.15	.88	12.2	65.0	.55	-1.4
10	16.20	16.20	13.1	70.0	.45	-3.6
11	107.83	.96	14.8	71.0	.60	-4.0
12	4.09	12.10	12.3	70.0	.65	- .7
13	3.07	22.60	14.1	73.0	.94	11.9
14	4.63	25.20	13.9	72.0	.89	-5.0
15	9.47	12.90	14.0	71.0	.43	-2.0
16	2.12	27.10	14.4	72.0	.75	-3.8
17	2.87	48.00	19.5	68.0	.98	6.6
18	4.67	8.77	16.4	73.0	.75	-2.3
19	8.11	6.40	15.7	68.0	.86	-4.7
20	2.20	21.80	13.2	71.0	.55	6.2
21	5.42	42.30	16.0	65.0	.78	1.8
22	1.94	202.00	17.9	72.0	.77	-4.8
23	12.38	6.50	15.8	63.0	.52	-4.4
24	2.56	121.00	19.1	66.0	.79	- .8
25	6.67	3.31	17.0	55.0	.47	-2.4
26	2.20	23.60	15.6	75.0	.80	-1.4
27	2.07	28.10	16.0	74.0	1.19	4.7
28	1.44	28.40	15.7	72.0	1.18	-2.5
29	2.17	22.60	15.3	70.0	.86	-3.2
30	47.72	.74	14.6	60.0	1.15	-4.3
31	3.09	10.50	13.4	74.0	.68	.9
32	7.86	2.68	11.8	50.0	.98	-2.8
33	1.90	14.40	14.9	73.0	.68	-3.3
34	3.33	65.50	17.6	77.0	.96	-5.0
35	5.79	51.70	16.9	79.0	.76	-1.4
36	.74	89.20	14.9	76.0	.77	.9
37	2.49	24.20	10.1	63.0	.65	- .4
38	1.42	174.00	18.2	77.0	.88	8.1
39	.23	418.00	19.5	75.0	.43	2.7
40	1.13	104.00	17.0	73.0	.37	-5.0
41	1.67	68.60	17.3	73.0	.51	-5.0
42	8.60	42.60	14.8	64.0	.50	22.0
43	.25	112.00	16.0	74.0	.50	4.9
44	.91	134.00	15.7	75.0	.50	3.4
45	.27	59.10	14.7	70.0	.50	9.2
			FIELD C			
46	80.82	8.47	12.7	60.0	1.04	-1.8
47	5.77	64.30	12.6	67.0	1.04	5.2
48	14.50	40.00	13.1	60.0	1.05	11.9
49	2.23	42.50	10.9	53.0	1.05	- .9
50	27.83	19.70	14.6	59.0	.80	1.8
51	.12	606.00	17.3	55.0	1.11	4.2
52	2.92	68.00	16.9	71.0	.81	2.0
53	.88	82.00	15.5	56.0	.47	.9

Well No.	β (ft^{-1})	k (md)	ϕ (%)	S_g (%)	h_p/h	S
	$\times 10^9$					
			FIELD D			
54	16.29	71.00	12.3	54.0	.66	.01
55	514.85	.10	13.6	61.0	.59	-1.80
56	55.89	4.30	13.0	61.0	.47	-4.00
57	294.00	.35	11.4	64.0	.61	-1.00
58	204.24	1.20	13.7	58.0	.50	.80
59	96.28	.23	12.0	56.0	.61	- .80
60	131.86	6.80	14.6	62.0	.45	.01
61	295.68	.26	13.2	41.0	.37	- .20
62	1183.45	.04	13.3	60.0	.28	-1.20
63	89.43	6.90	12.1	61.0	.44	.01
64	305.61	1.23	15.5	62.0	.63	-2.30
65	78.72	6.90	13.9	63.0	.37	-2.10
66	381.02	.50	14.2	48.0	.36	- .60
67	275.94	1.10	13.8	48.0	.39	.01
68	259.51	.60	15.6	43.0	.40	-4.10
69	192.39	1.49	13.9	43.0	.33	.01
70	399.59	.48	13.3	48.0	.26	-2.60
71	341.77	.38	11.3	49.0	.32	4.00
			FIELD E			
72	71.41	.91	14.8	57.5	1.0	- .16
73	201.84	.88	14.6	68.0	1.0	-3.80
74	408.32	.28	12.9	59.9	1.0	-3.50
75	182.80	.52	14.7	56.7	1.0	-2.71
76	229.90	.52	11.4	60.0	1.0	-3.27
77	12.41	25.80	15.4	63.4	1.0	- .30
78	24.27	.54	12.1	54.4	1.0	-1.70
79	397.42	.73	14.1	58.4	1.0	-2.60
80	39.09	3.02	16.6	53.8	1.0	-2.96
81	4.05	5.13	17.9	62.1	1.0	.44
82	82.81	2.36	14.4	57.5	1.0	-1.37
83	52.23	2.16	12.4	58.6	1.0	-4.40
84	773.62	.50	12.1	56.6	1.0	.15
85	1739.69	.23	10.6	54.9	1.0	.15
86	12.18	4.20	16.6	59.9	1.0	-1.60
87	56.76	1.70	16.9	61.0	1.0	-4.60
88	158.74	.88	17.3	58.5	1.0	-3.60
89	12.12	2.55	20.2	65.9	1.0	-4.30
90	34.18	3.32	17.9	65.0	1.0	.90
91	7.37	2.57	13.7	45.6	1.0	-1.70
92	87.71	1.51	14.8	60.8	1.0	.39
93	13.22	6.70	16.6	66.3	1.0	-2.10
94	18.51	4.10	15.9	31.5	1.0	-3.40
95	25.22	2.80	15.8	57.3	1.0	-2.40
96	19.94	4.56	13.6	45.6	1.0	-3.10
97	20.64	1.23	14.0	53.2	1.0	-3.50
98	42.09	.95	15.6	58.9	1.0	-2.50
99	7.34	1.70	16.5	60.6	1.0	-2.30
100	102.04	.54	11.8	48.2	1.0	-3.90
101	149.51	.65	13.4	55.8	1.0	-3.50
102	32.17	1.31	10.2	35.1	1.0	-1.00
103	1.25	12.61	16.0	57.7	1.0	- .70
104	3.16	17.60	15.0	49.2	1.0	-2.70
105	6.97	6.98	15.8	57.6	1.0	-3.20

Table 8.2

Regression Equations

Eqn.	Regression Equation	Correlation Coeff (R) Standard Error (S)
8.5-3	$\log \beta = m \log (k/\varphi . S_g)^{-0.5} + c$ $m = 2.4388,\ c = -2.4071$	$R = 0.9821$
8.5-4	$\log \beta = m \log k + c$ $m = -1.0609,\ c = 11.0485$	$R = 0.8883$
8.5-5	$\log \beta = m \log k_a + c$ $m = -1.0805,\ c = 11.0756$ $k_a = k. \exp(-0.03S)$	$R = 0.8903$
8.5-6	$\log \beta = m \log (k.\varphi) + c$ $m = -1.0356,\ c = 10.1544$	$R = 0.8895$
8.5-7	$\log \varphi = m \log \beta + c$ $m = -0.0233,\ c = -0.6068$	$S = 0.0628$
8.5-8	$\log \beta\sqrt{k} = m \log \varphi + c$ $m = -30.0799,\ c = -21.7707$	$S = 1.1918$
8.5-9	$\log \beta\sqrt{k} = m \log (\varphi . S_g) + c$ $m = -13.4639,\ c = -10.7036$	$S = 1.4922$
8.5-10	$\beta = \dfrac{b0}{k^{b1}.(\varphi . S_g)^{b2}}$ $b0 = 4.7543 \times 10^{10}$ $b1 = 0.9212$ $b2 = 0.2429$	$R = 0.6787$
8.5-11	$\beta = \dfrac{b0}{k^{b1}.(\varphi . S_g)^{b2}}$ $b0 = 1.3633 \times 10^{10}$ $b1 = 0.8804$ $b2 = 0.7770$ $k_a = k. \exp(-0.19S)$	$R = 0.7262$

Table 8.3
Laboratory Data

Sample No.	β (ft^{-1}, $x10^9$)	k (md)	φ (%)
1	0.36	59.0	20.76
2	14.90	2.18	13.82
3	119.0	0.98	10.19
4	179.0	1.23	12.74
5	17.30	2.21	12.17
6	2.02	17.0	16.92
7	7.380	5.90	14.90
8	7930	0.14	5.87
9	1130	0.23	9.96
10	0.76	99.5	15.17
11	803.0	0.41	7.43
12	31310	.041	6.83
13	1140	.260	11.39
14	42470	.064	12.31
15	17400	.102	11.50
16	865.0	.460	10.01
17	726.0	.515	11.00
18	0.51	33.0	21.00
19	1.17	15.2	20.50
20	2.01	10.5	20.90
21	1.08	13.0	23.90
22	0.26	32.5	25.60
23	0.63	28.4	19.60
24	0.81	20.8	19.01

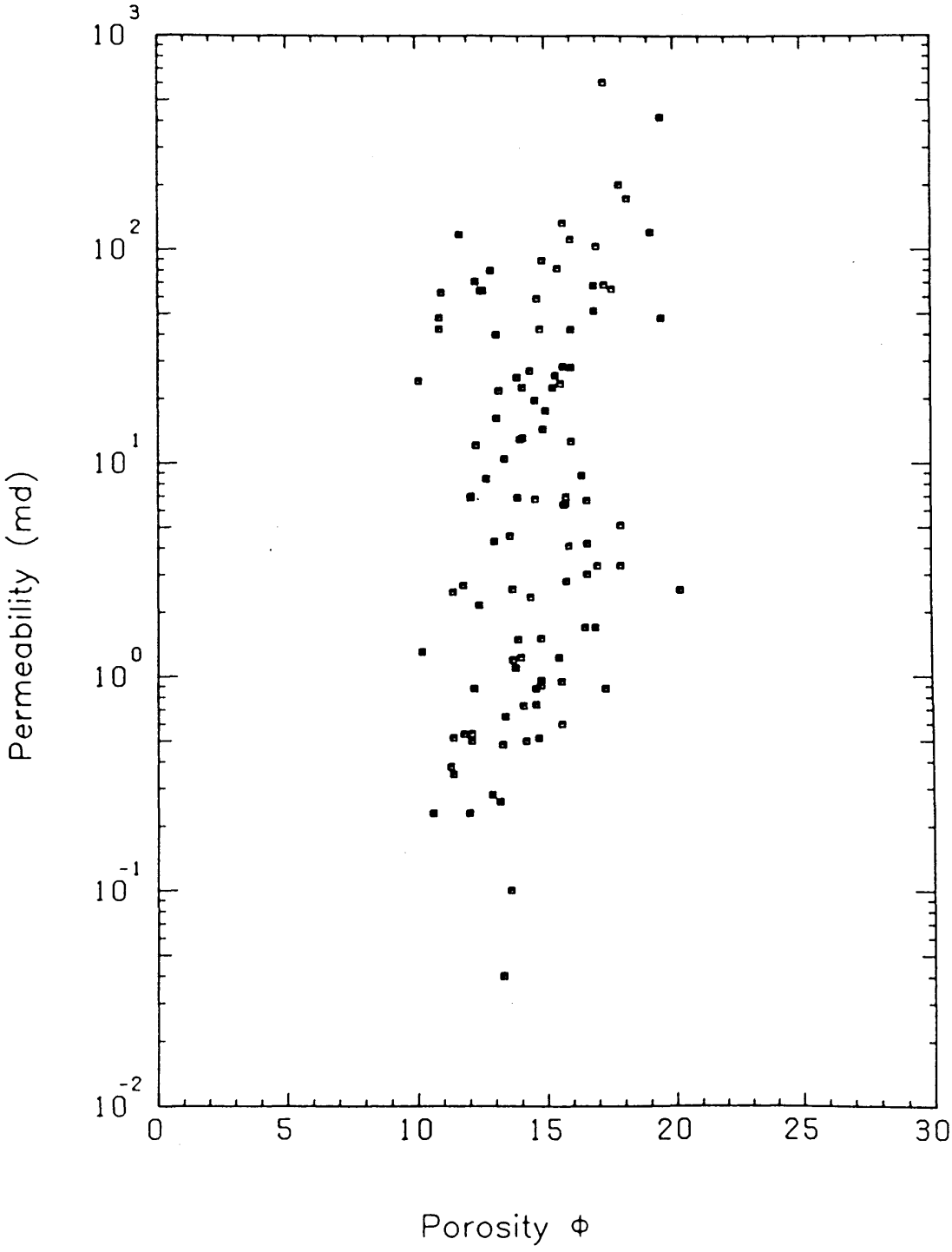


Fig. 8.1 Relationship between porosity and permeability.

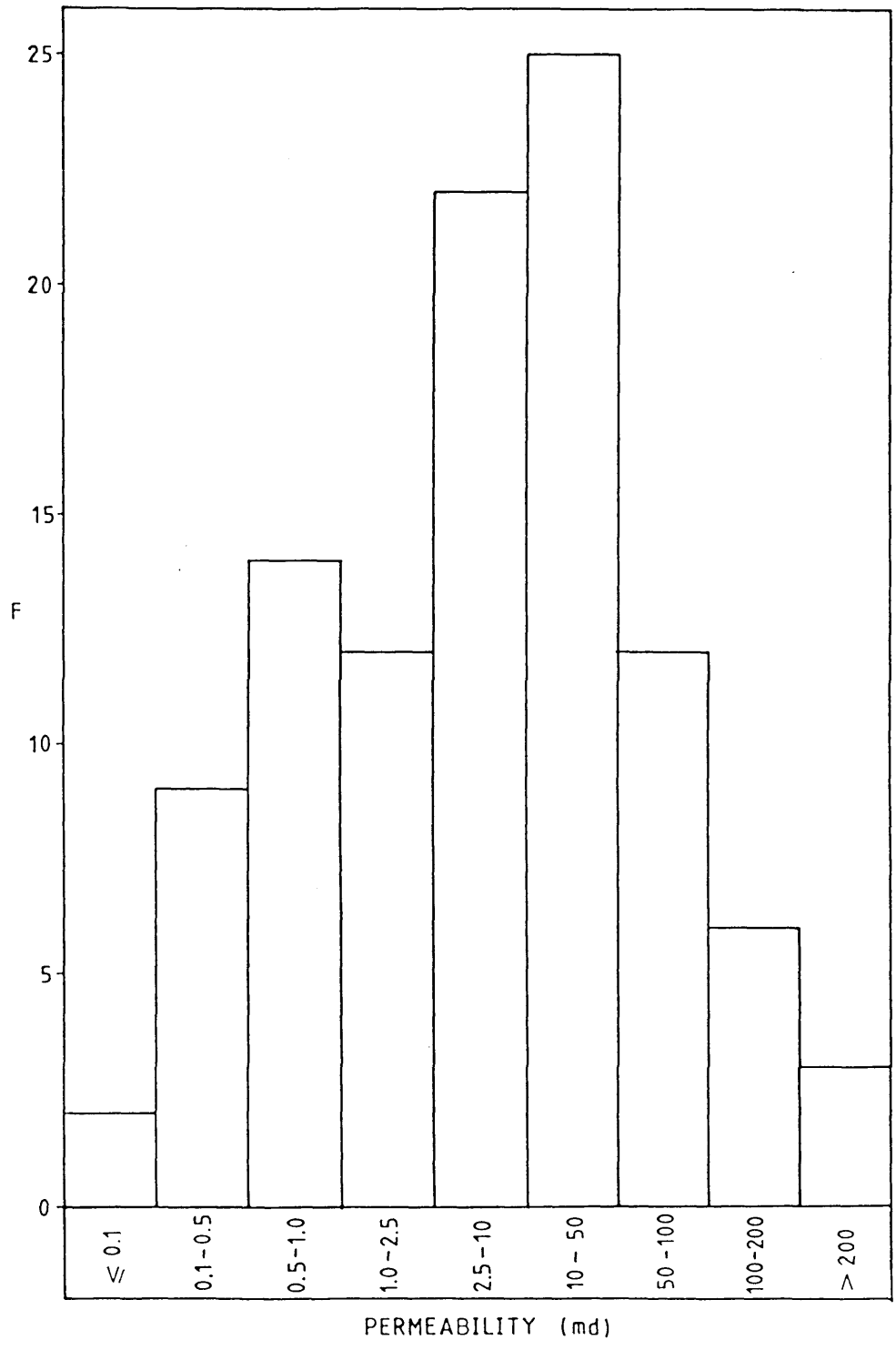


Fig. 8.2 Permeability distribution of the sample set.

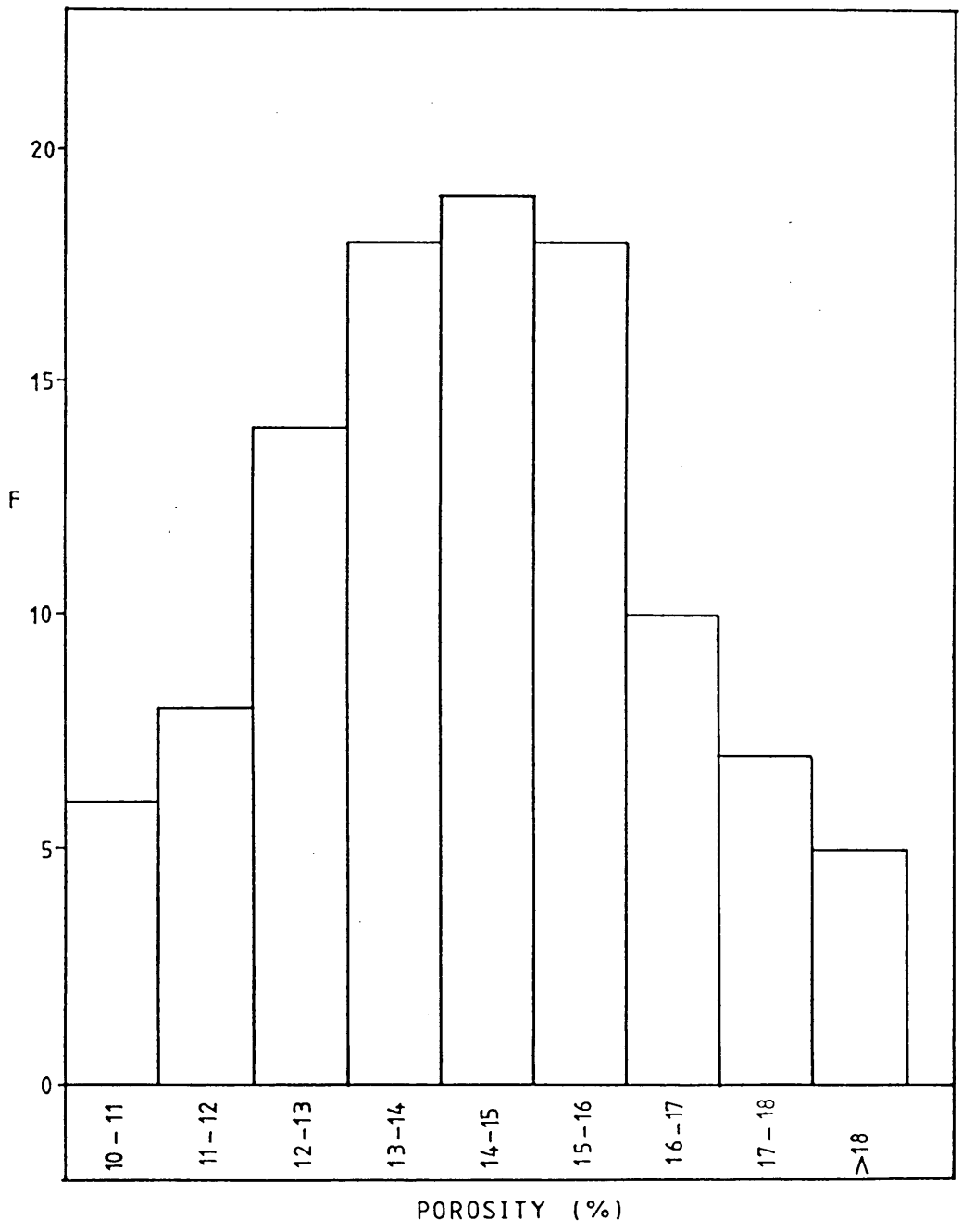


Fig. 8.3 Porosity distribution of the sample set.

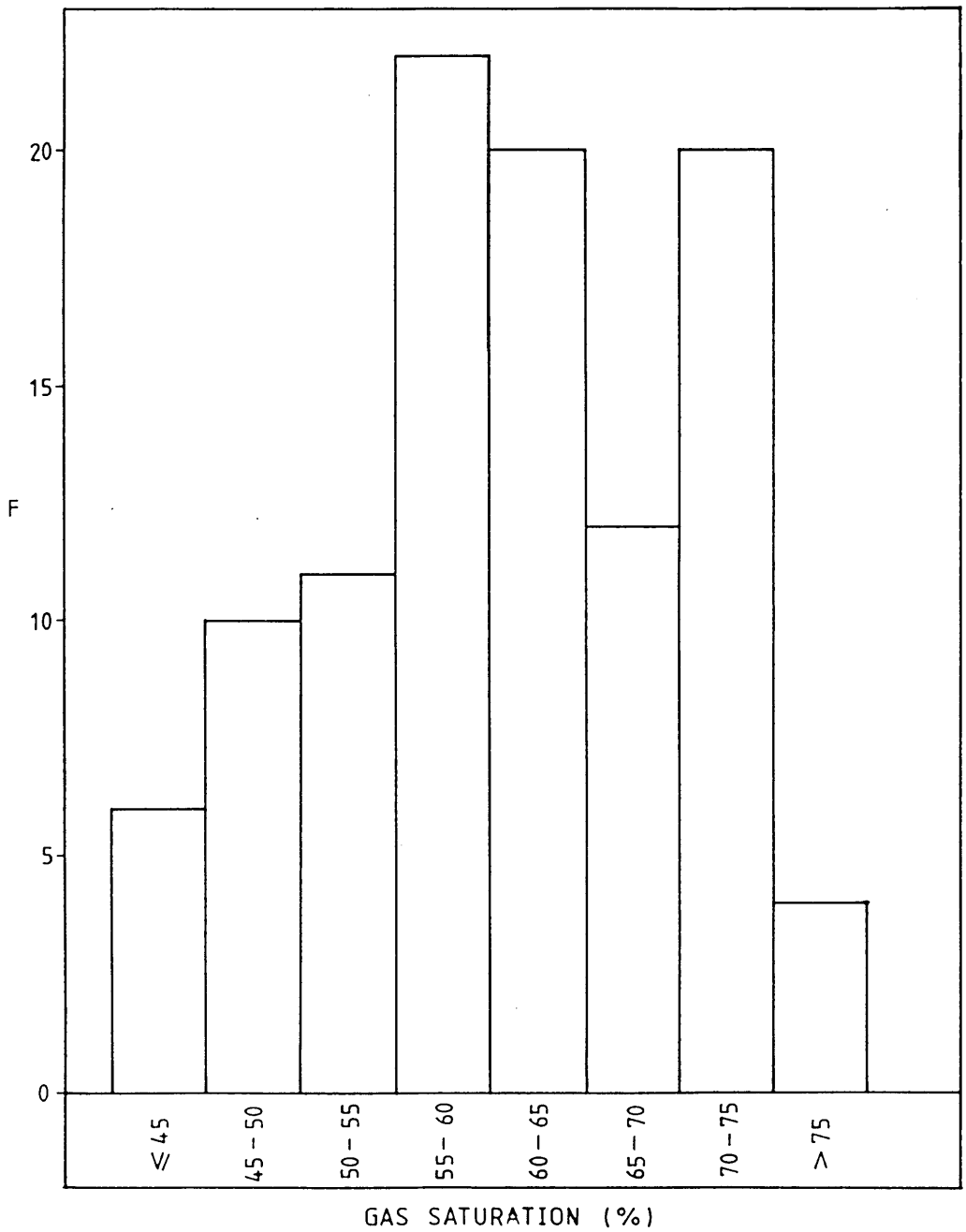


Fig. 8.4 Gas saturation distribution of the sample set.

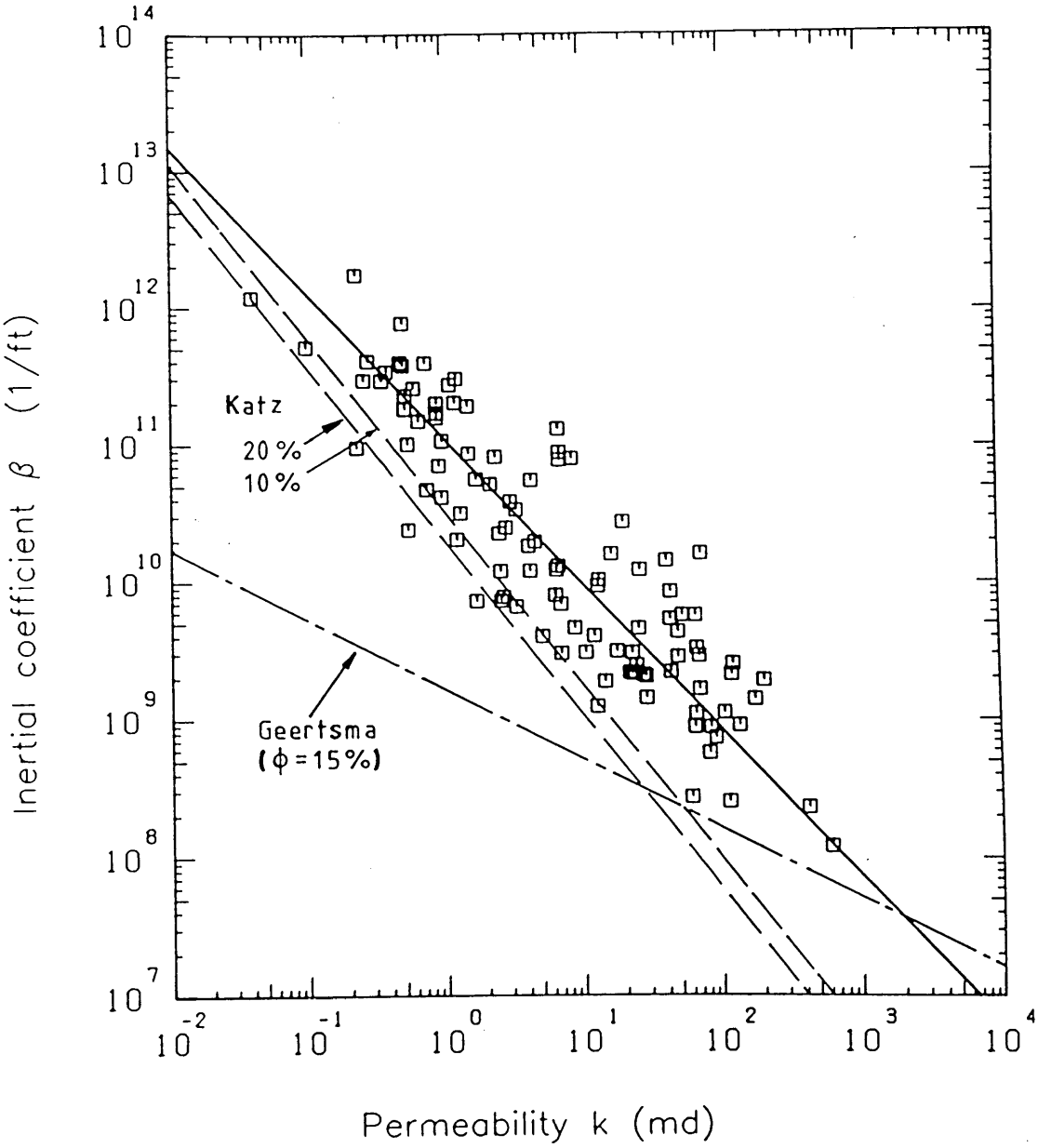


Fig. 8.5 Correlation of β with permeability.

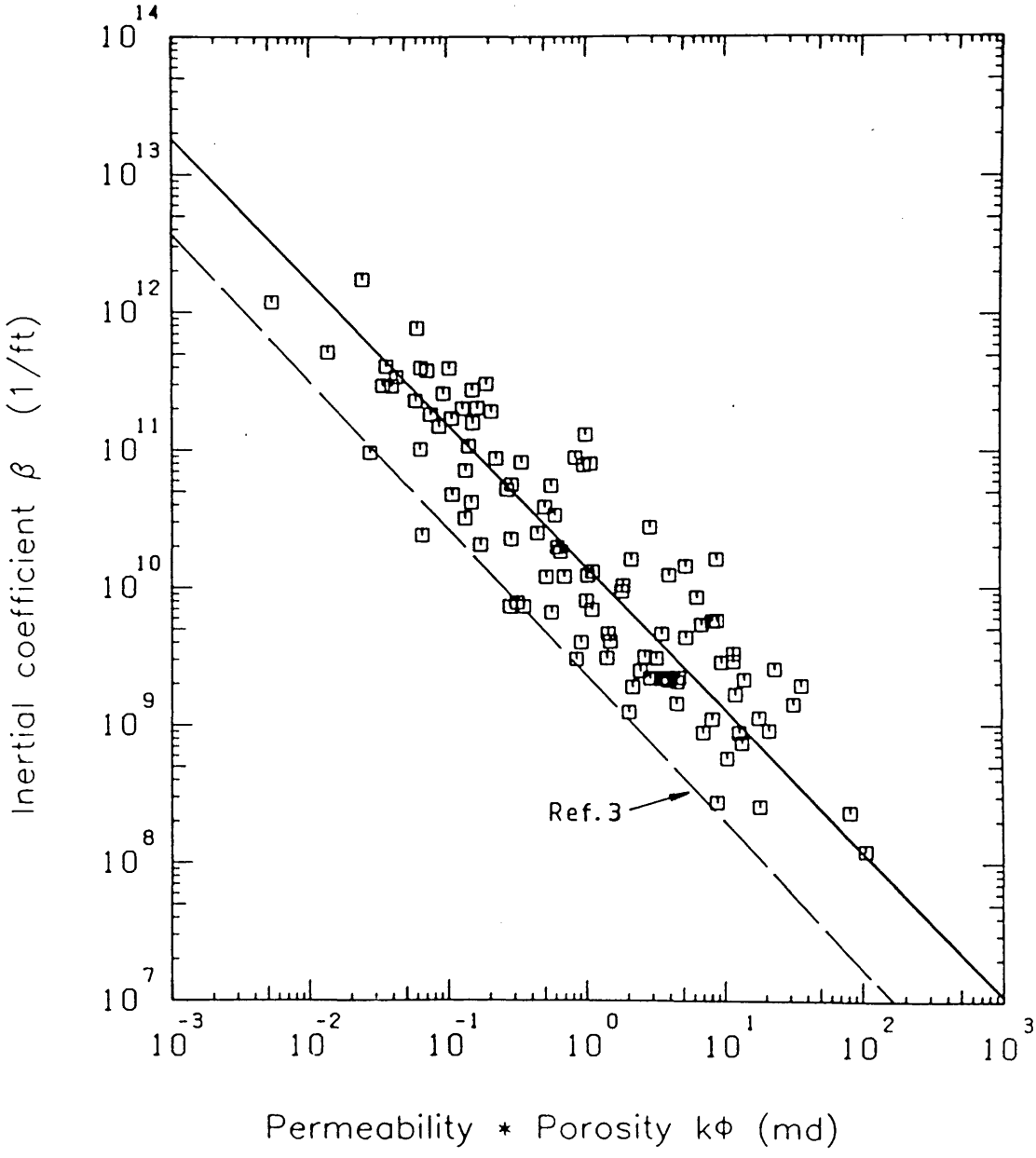


Fig. 8.6 Plot according to Eqn. (8.5-6)

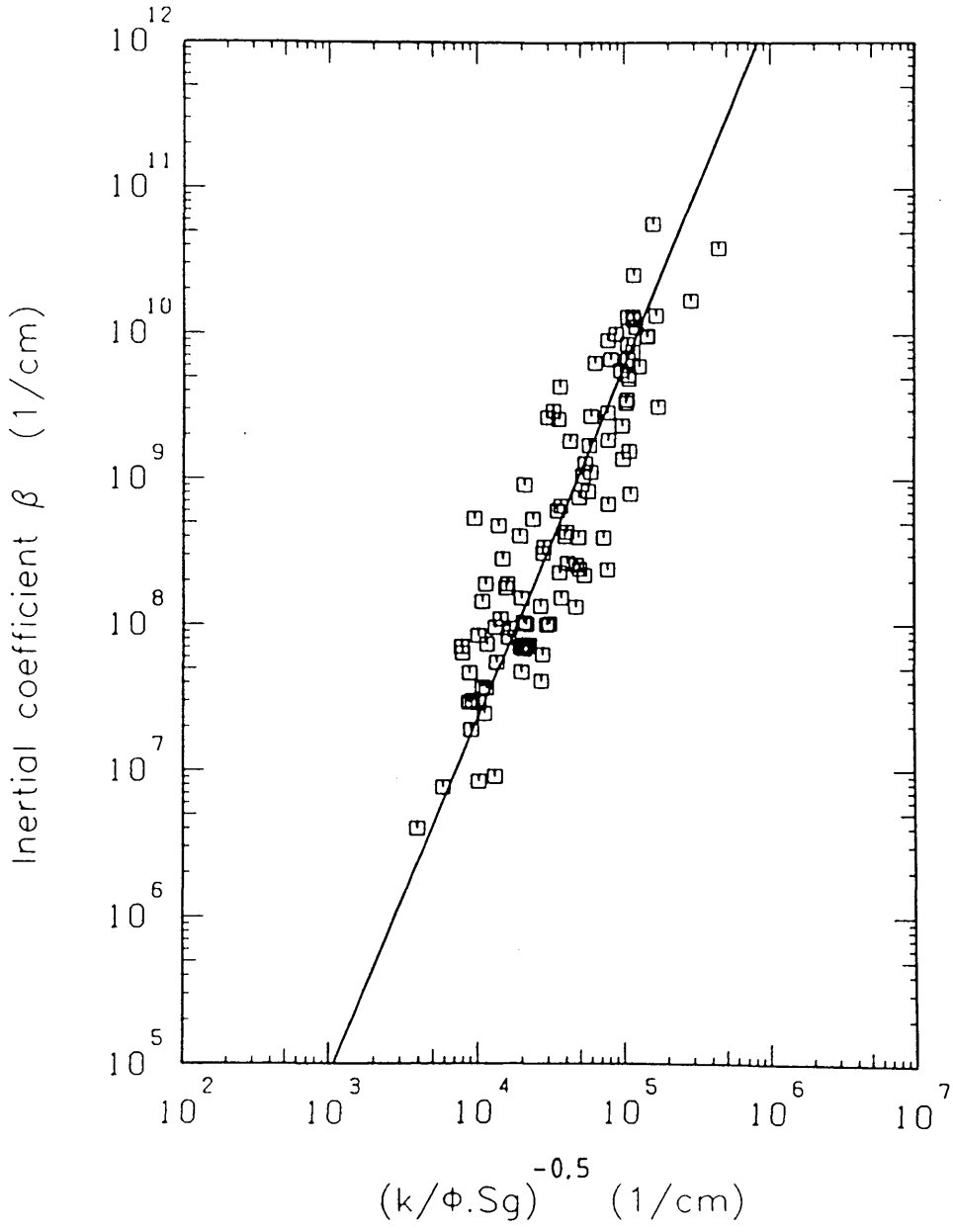


Fig. 8.7 Plot according to Eqn. (8.5-3)

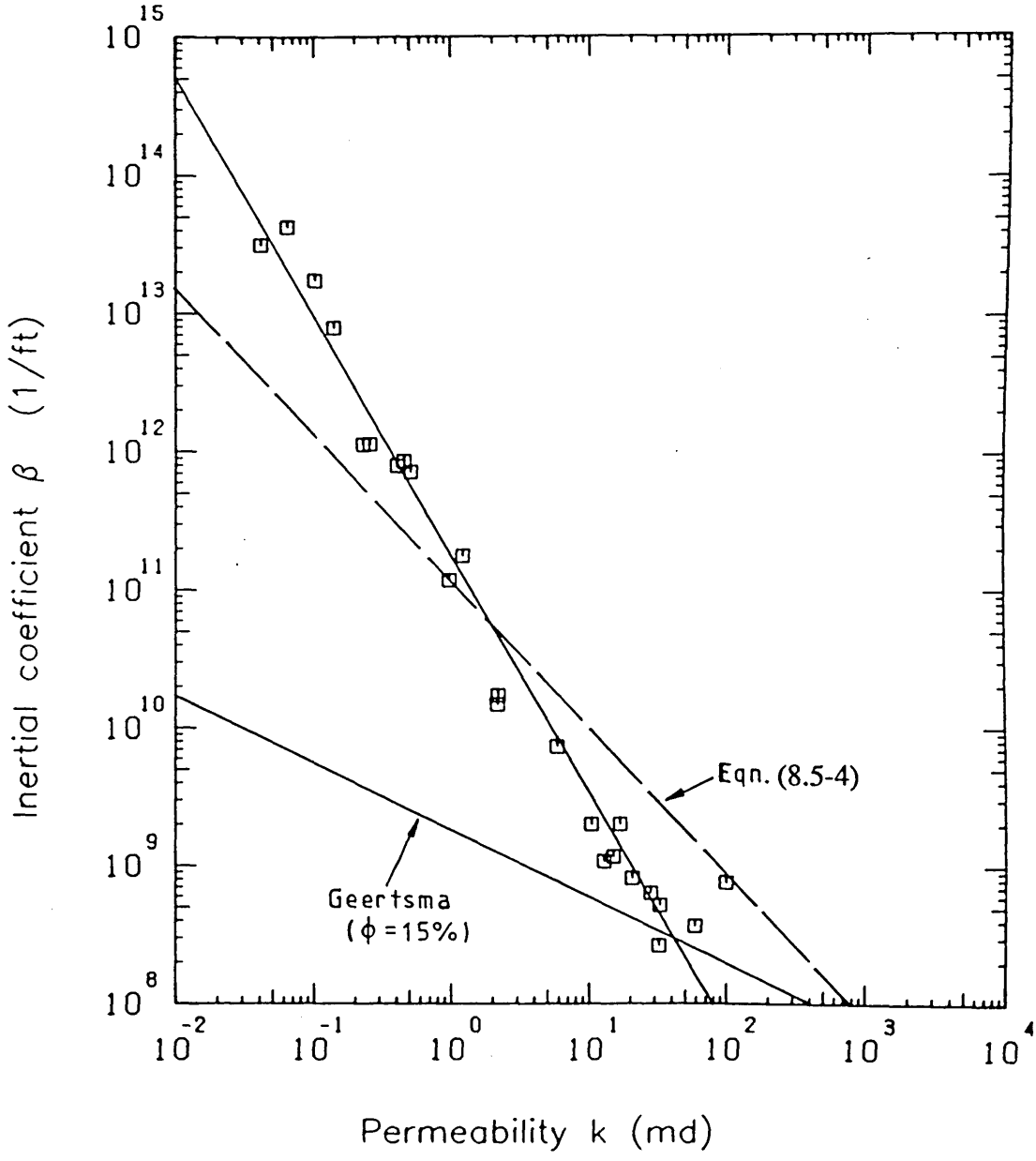


Fig. 8.8 Correlation of β for experimental data.

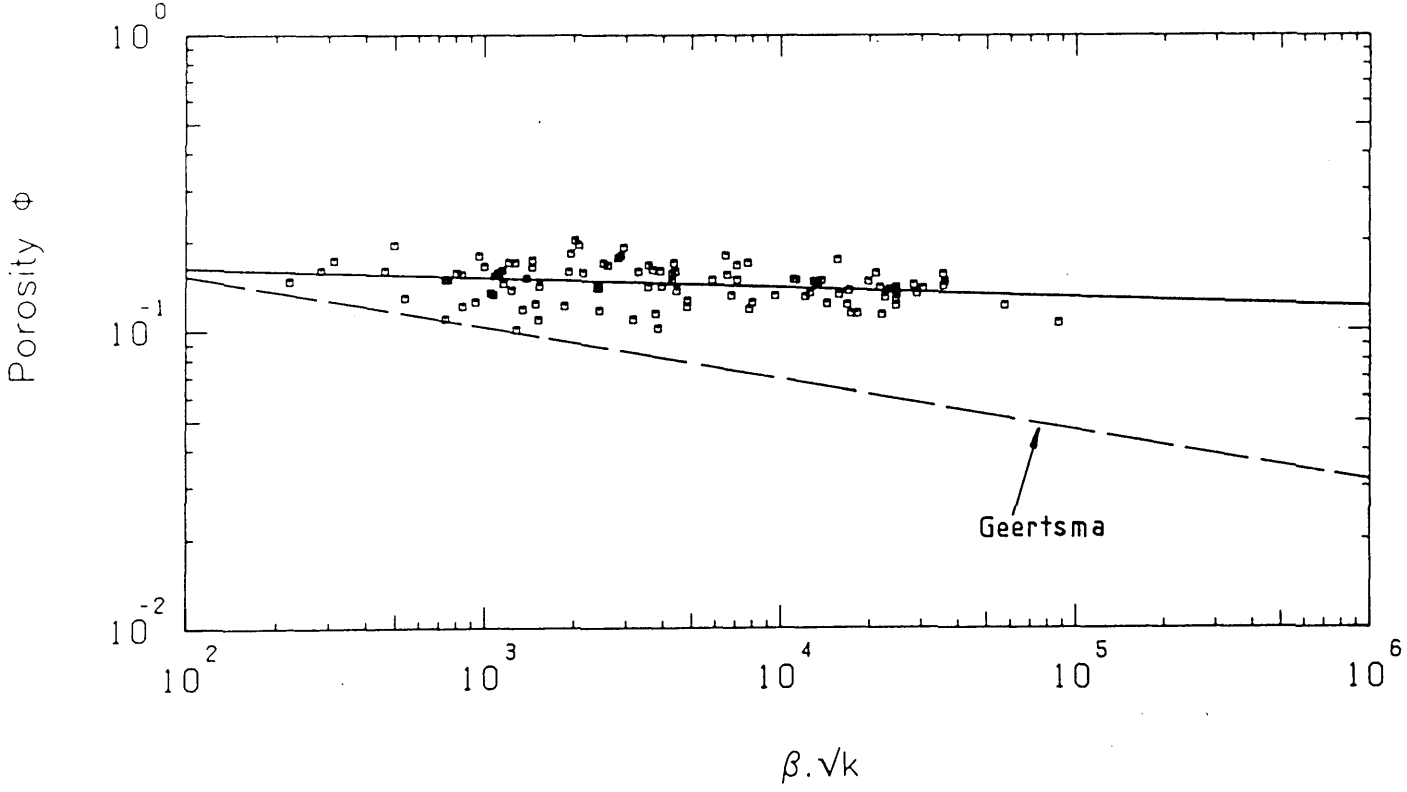


Fig. 8.9 Correlation between ϕ, β and k.

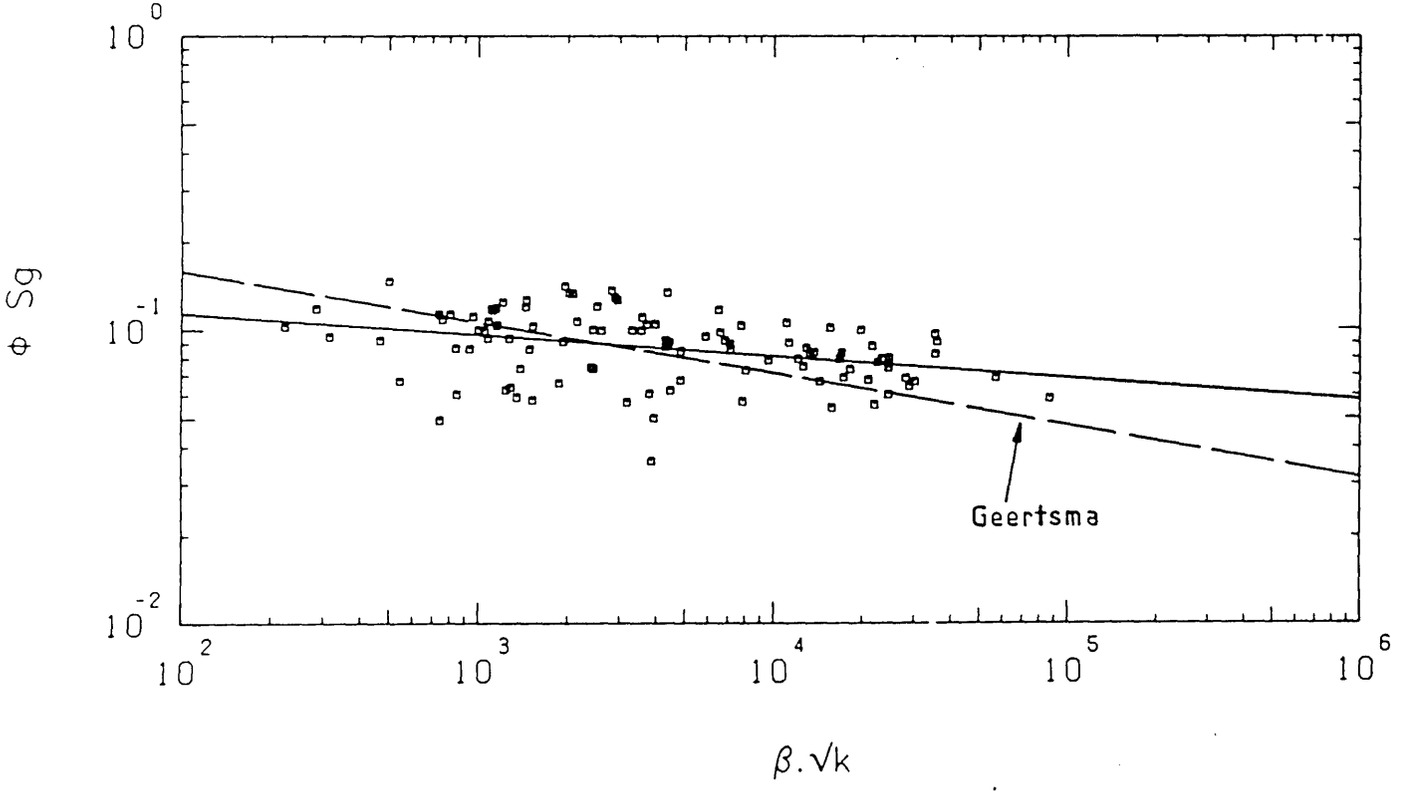


Fig. 8.10 Correlation between reduced porosity, β and k.

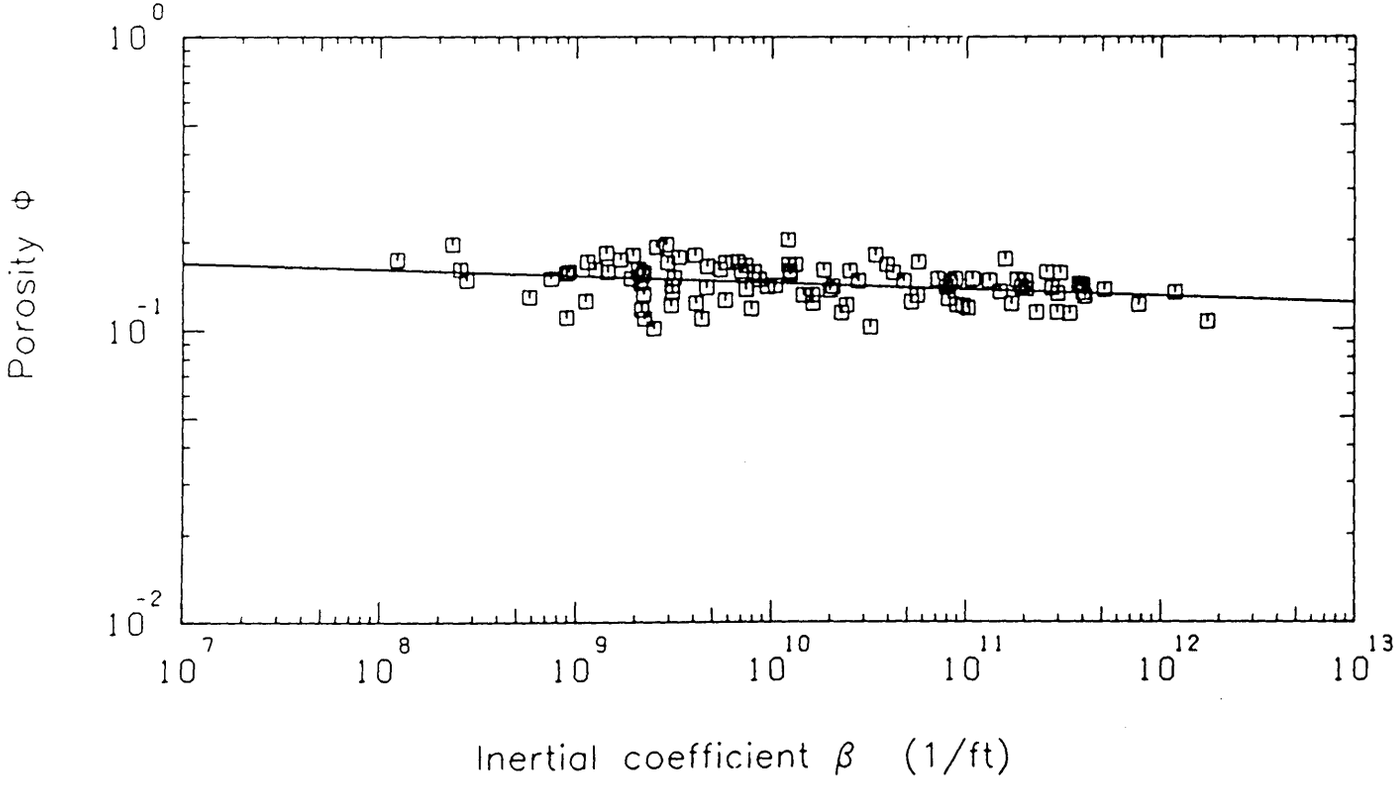
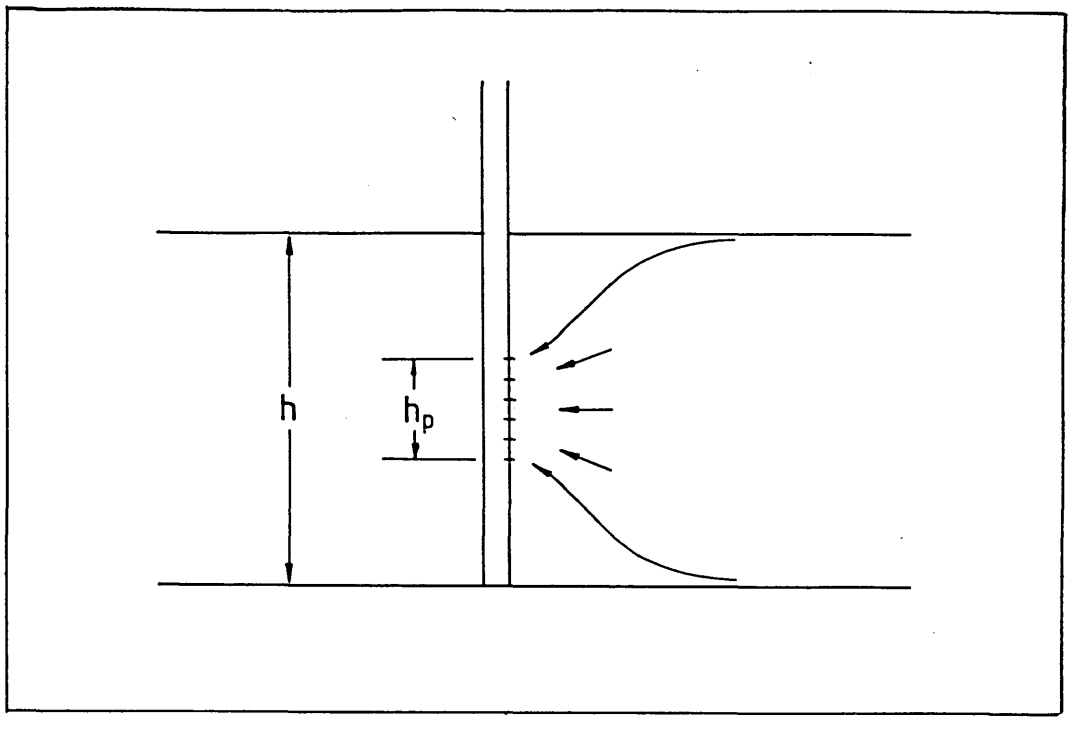
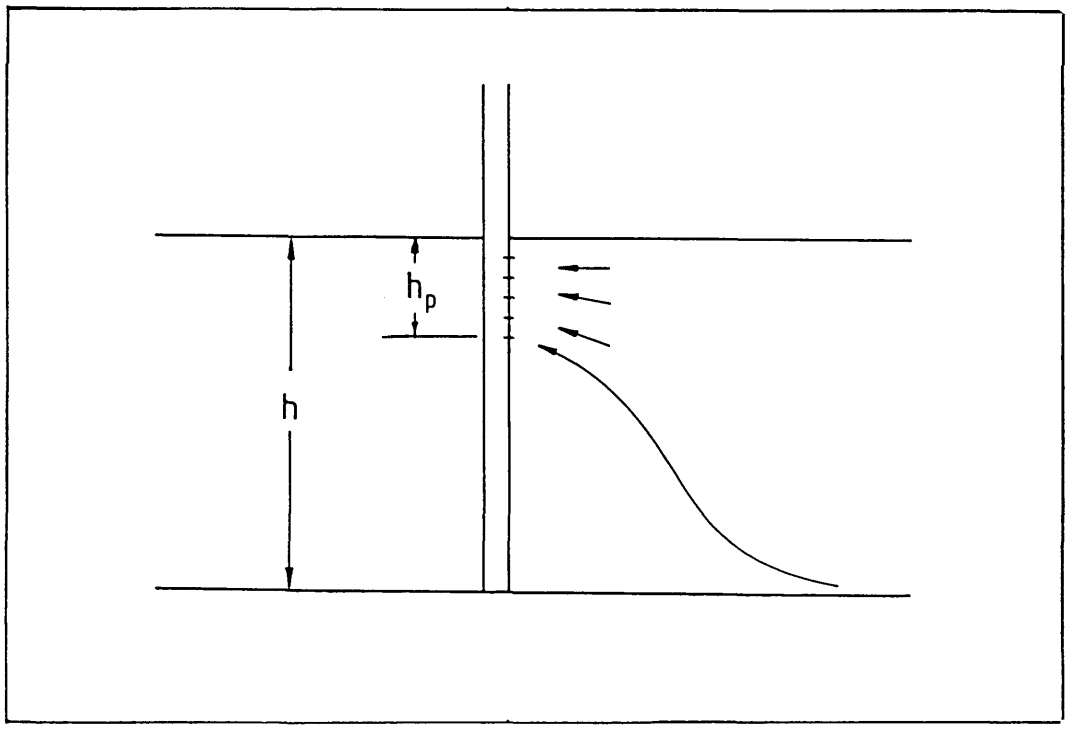


Fig. 8.11 Correlation between porosity and inertial coefficient.





8.12 Sketches of flow streamlines in a reservoir being produced by partially completed wells.

Chapter 9

SUMMARY AND CONCLUSIONS

This chapter summarises the major achievements of the present study and provides conclusions and suggestions for further study.

The physics of flow through porous media has been studied at both the microscopic and the macroscopic scales. Physical and mathematical descriptions of the causes of deviation from Darcy's law have been provided. Measurements of the flow rate and pressure gradient were carried out on over 40 sedimentary sandstone core samples. Porosity for all the samples were measured using the helium gas expansion method. Permeability was calculated from plots according to the Klinkenberg equation and the inertial coefficients calculated from plots according to the Forchheimer equation - modified for compressible fluid. Capillary pressures were measured using both the mercury intrusion and the porous membrane techniques. The pore throat size distributions were calculated directly from the gradients of the capillary curves. Visual observations were also made using both the optical and scanning electron microscopes.

9.1 THE ROLE OF INERTIA

The present study has shown that the physics of flow in porous media is inherently different from that of flow in capillaries or tubes. In the past, all too often, an analogy has been drawn between these two. During steady flow in a straight capillary, the fluid particles move in a rectilinear path with constant velocity and therefore have no acceleration, unless the flow is sufficiently large for turbulence to set in. In contrast, during flow in porous media, the fluid particles will move along a continuously curvilinear path and hence at a continuously varying acceleration. As the flow rate increases, this produces distortions in the streamlines which result in the streamlines getting crowded where the curvature is sharp. The distortions will increase the terms dependent on viscous forces. The forces due to inertia increase as the square of the velocity, and are non-linear with respect to v. The resistance to flow therefore increases at a progressively greater rate as the velocity is increased. Darcy's law remain valid only if the fluid velocity is small enough so that the forces of inertia are negligible compared to the viscous forces.

Besides the curvilinear nature of the flow path, it is also essential to consider the expansions and contractions of the pore spaces. The changing cross sectional area causes convective acceleration and deceleration of the fluid particles, thereby causing further losses. These losses are known to be dependent on the square of the velocity, ie they are non-linear with respect to v. This is the other cause of deviations from Darcy's law at increasing velocity.

It is important to realise that deviation from Darcy's law need not be caused by turbulence. The above discussion show that nonlinear flow arises due to the inertial forces becoming more

significant than the viscous forces. Indeed, all experimental evidence suggest that this is the cause of deviation from Darcy's law at increasing flow rate, and turbulence plays an insignificant part.

The discussion in Chapter 3 has shown that the inertial forces arising in flow through porous media can be understood fully only when the flow phenomena is considered at the microscopic scale. By employing averaging processes it has been possible to take into consideration the flow behaviour at both the micro- and the macroscopic levels. This has shown that streamline curvature at the microscopic level plays a vital role in the inertial effect which is felt at the macroscopic scale.

9.2 TRANSITION FROM LINEAR TO NONLINEAR FLOW

The flow rate at which deviation from Darcy's law occurs could be found by plotting the pressure gradient against the flow rate. According to Darcy's equation this should yield a straight line passing through the origin. The point of departure from the straight line indicates the onset of nonlinear flow.

For gas flow, it is necessary to plot the pressure gradient squared versus the flow rate due to its compressibility. However such plots were found to give a very low value of the flow rate at the point of departure from the straight line. This is thought to be due to both molecular slippage and inertial effects occuring simultaneously. Correction for the slippage can be made by introducing the Klinkenberg equation into the Forchheimer equation. This yields plots where the point of departure from linear flow occur much later.

The modified plots were made for a number of the samples. It was found that there is a correlation between the rate at the onset of nonlinear flow and the permeability of the sample, although there is a wide scatter of the data. Obviously, permeability on its own is inadequate for describing the medium. It was thought that the parameter (β k) could be used as a length scale for describing the medium. However this length scale is found to decrease with increasing permeability and its use for characterizing porous medium seems to be suspect. This parameter has been used extensively by others for calculating both the friction factor and the Reynolds number. Various other definition of the friction factor and the Reynolds number are available in the literature for estimating the flow rate at which nonlinear flow will occur, but none of them are satisfactory due to the difficulty of finding a single length parameter which will describe the shape of pore spaces. It seems that the best method for finding the rate at the onset of nonlinear flow is to plot the pressure gradient against the flow rate with appropiate modifications as already mentioned above. The study has shown that the 'critical' flow rate is a unique value for a given porous medium and is dependent on its pore structure.

9.3 EFFECTS OF PORE STRUCTURE

Numerous correlations are available in the literature for predicting the inertial coefficient from porosity and permeability of the rock samples. The estimated values from these correlations can however be very inaccurate, often by as much as one order of magnitude. This is because only the bulk properties of the rock samples were considered. Experimental measurements have shown that two core samples may have very similar porosity and permeability but widely different values of β. The differences could only be explained in terms of different pore structures in the two samples.

The present study has shown that the inertial coefficient β is related inversely to the permeability of a rock and is also a function of other pore structural parameters. Some of the important factors, besides porosity and permeability which were found to influence the inertial coefficient are as follows:

(a) The inertial effect is strongly influenced by the pore-to-throat size (aspect) ratio. Higher aspect ratio leads to an increase in the inertial coefficient.

(b) High coordination number leads to a more complicated network of pores. Fluid flowing in such a rock encounters a more tortuous path with more expansion and contraction losses. The β values are generally found to be higher in these cases.

(c) The presence and orientation of small-scale heterogeneities - random micro-scale or laminations, usually help to lower the value of β. The presence of any laminae with high permeability is likely to be a primary cause in the lowering of inertial coefficient values.

(d) The geometry of the pore spaces is found to be vital; the presence of clays, authigenic or detrital, pore lining or pore bridging, increases the 'roughness' and thereby significantly increases the inertial coefficient for a rock sample.

9.4 EFFECTS OF LIQUID SATURATION

In the present study the effect of a static liquid saturation on non-Darcy gas flow was investigated. This phenomena is of particular importance in gas condensate reservoirs where the pressure drop near the wellbore can be sufficiently high for liquid drop-out to occur. Previous reported studies have been restricted to micro-vugular carbonates. Those studies also showed an anomalous behaviour; the inertial coefficient was found to decrease to a minimum at 10% saturation.

The present study has been conducted on consolidated sandstone reservoir rock samples. Experiments were carried out to measure the inertial coefficient for these samples at various liquid saturations, up to the irreducible minimum. The experiments did not show any minimum value of the inertial coefficient with increasing saturation; there was only a steady increase of the coefficient. The increase was also found to be much smaller than that for carbonates.

A method was developed for visualization of the liquid phase distribution. This was done by firstly saturating the sample with a thermo-setting epoxy resin which was dyed blue. The resin was displaced by injecting air and was subsequently solidified while gas was flowing at high velocity. The remaining pore space was filled with a similar resin dyed red. Finally, thin sections were prepared for visual observations under optical microscopes.

The wetting phase was normally found to occupy relatively smaller intergranular pores. It was also generally found in regions of high surface curvature, eg. intragranular pores, inside pore filling aggregates etc. It was found that the inertial coefficient could be predicted if the value of β is known for the dry sample. The value of the constant in Eqn.(7.4-3) could then be calculated, and hence the value of β at any particular saturation estimated from the effective permeability.

9.5 ESTIMATION OF β IN HIGH RATE GAS WELLS

All the known correlations available for estimating the value of coefficient of inertial resistance have been derived from measurements done on small core samples at laboratory scale and are found to predict values with an unacceptable level of accuracy. An attempt was therefore made to form correlations for estimating the inertial coefficient from producing gas wells.

The value of inertial coefficient has been measured for over one hundred gas wells from analysis of multi-rate pressure transient test data. The wells are spread across five producing gas reservoirs of the southern North Sea. The inertial coefficients so obtained were correlated with available reservoir parameters. Comparisions were also made with existing correlations and with data from experimental measurements.The important conclusions from this study were as follows:

(a) The best correlations were formed when β is related to the parameter $(k / \phi)^{0.5}$, since this provides a good estimate of the mean characteristic length of a porous medium.

(b) Correlations formed according to Geertsma's method give unreliable results since the porosity range in producing sandstone reservoir rocks is generally narrow.

(c) Correlations were found to be much improved if β was calculated using the formation thickness. This is thought to be due to non-Darcy effects existing at some distance away from the wellbore.

(d) Although it may be preferable to relate β to the permeability of the altered zone near the wellbore, the bulk formation permeability appears to be adequate for use in predicting the value of β

9.6 SUGGESTIONS FOR FURTHER WORK

(a) The quality and quantity of mechanical breakdown of clays during high velocity flow in porous media and its transport at various velocities need to be understood better. This would be important in interpreting experimental work more accurately and also in understanding the physical conditions of the porous media near a wellbore.

(b) Virtually all the numerical work carried out so far to simulate the high velocity phenomena makes use of symmetrical pore and throat arrangements. The introduction of asymmetric arrangement of pores and throats will introduce 'tortuosity' and will therefore better represent the pressure drop in numerical calculations since it will take account of the streamline curvature as well as the expansion / contraction effects.

(c) Further work is required to better understand the energy balance during flow of compressible fluids through porous media. No reported experimental or theoretical work could be found in the literature. If the temperature of the fluid changes even by a few degrees, it may have important implications, for example, in the production of gas condensate reservoirs.

(d) The influence of aspect ratio and coordination number on the inertial coefficient needs to be quantified. This could be investigated using numerical models of large pore networks. Further quantification is also possible by carrying out measurements directly on the photo-micrographs of resin pore casts of the samples.

(e) The experimental work involving high velocity gas flow in the presence of a liquid saturation, as described in Chapter 6, could be extended to make it more realistic. This could be done by injecting at reservoir conditions a gas similar in composition to those found in condensate reservoirs. By flowing such a gas, the quantity of the liquid dropout could be monitored for different flow conditions to simulate reservoir behaviour.

(f) Further theoretical and experimental work needs to be carried out to understand the physics of multiphase flow in porous media at high velocities. Although a number of studies have been reported on flow through packed columns and towers, however, very little has been done on consolidated rocks. Forchheimer's equation has not been extended to multiphase flow with any rigour as yet.

(g) Quantification of the pore structural parameters could also be possible through the use of electrical resistivity measurement of the core samples. It is of course well known that resistivity measurements can yield useful information on the pore structure, types and quantity of clays and their distribution and cementation.

Appendix

EQUATIONS OF NONLINEAR FLOW

Numerous equations have been proposed in the literature for describing nonlinear flow in porous media [1]. Here a summary of some of the important equations is provided. These equations can be classified broadly under three groups as follows:

GROUP 1

In this group the various empirical equations which have been proposed on the basis of experimental results alone are placed. These equations contain coefficients which are not related to any specific properties of either the fluid or the solid matrix. The coefficients have to be evaluated directly from experiments. Among the well known ones are the those due to -

Forchheimer [2] $J = aq + bq^2$ (A1-1)

Forchheimer [2] $J = aq + bq^2 + cq^3$ (A1-2)

Forchheimer [3] $J = aq + bq^m$ (A1-3)

White [1] $J = aq^{1.8}$ (A1-4)

Polubarinova-Kochina [4]

$$J = aq + bq^2 + c\,\partial q/\partial t \qquad \text{(A1-5)}$$

where J is the hydraulic gradient, q the Darcy velocity and a,b,c,m are the empirical coefficients.

White's equation (A1-4) was found from air flow through packed towers. The constant in Forchheimer's equation (A1-3) has a value of $1.6 < m < 2$ depending on the media. The equations of Polubarinova -Kochina contains a time dependent term but this has been found to be negligibly small. These relations are basically curves or equations devised to fit experimental data. Due to the very empirical nature of these relations they often contradict one another and are generally found to be useful only for a limited range. Generalizations are therefore not possible. Use of such relations can give inaccurate results if they are applied to porous media which are dissimilar to the ones on which they were based. They are nevertheless sometimes useful in specific engineering calculations.

The equations of Forchheimer were proposed by analogy with turbulence phenomena occuring in tubes. The third order term in (A1-2) was included to fit the experimental data better. Recently Ezeudembah et al [5] have attempted to provide a physical basis for the use of a cubic

term. The third coefficient, c, was found to be related to a characteristic dimensionless shape factor which is significant at very high rates of flow. The authors used the boundary layer theory to provide a physical explanation of the flow behaviour.

In Eq. (A1-4) the exponent of 1.8 has been found to be unreliable, and others have even proposed

$$J = aq^m \qquad \text{(A1-6)}$$

where m has been claimed to be anywhere from 1 to 2.5 depending on the pore structure of the media [3].

Many papers have also proposed correlations between friction factors and Reynolds number based on experimental data. Some of these are reviewed in Chapter 5.

GROUP 2

Under this group we can place the number of equations which contain parameters relating the fluid and the porous medium properties to the overall flow behaviour. The expressions nevertheless contain unspecified coefficients reflecting the various geometries of the pore structure and which can be evaluated only from experiments. Some of the important ones in this category are:

Burke & Plummer [1]

$$J = [K_o (1-\phi)/g\phi^3 d^2] q^2 \qquad \text{(A2-1)}$$

where K_0 is a constant and J the hydraulic gradient. The equation is thought to be valid only for flow at very high Re.

Ergun & Orning [6]

$$J = \frac{180 \alpha \nu (1-\phi)^2}{g\phi^3 d^2} q + \frac{3\beta(1-\phi)}{4 g\phi^3 d} q^2 \qquad \text{(A2-2)}$$

Here, the coefficients α and β are the shape factors, being constant for a given medium; d is the average particle diameter.

Irmay [7]

$$J = \frac{\alpha \nu (1-\phi)^2}{g \phi_e^3 d^2} q + \frac{\beta (1-\phi)}{g \phi_e^3 d} q^2 + \frac{1}{g \phi_e} \frac{\partial q}{\partial t} \qquad \text{(A2-3)}$$

where α and β are the constants describing the geometry of the porous medium and ϕ_e is the effective porosity. This is very similar to the Ergun equation (A2-2) since both of them are based on the Kozeny model (see chapter 2) of porous media.

Scheidegger [8]

$$J = C_1 \frac{\nu T^2}{g \phi} q + C_2 \frac{T^3}{g \phi^2} q^2 \qquad \text{(A2-4)}$$

where C_1 and C_2 are constants dependent on the grain size distribution and T is a "tortuosity constant" for the medium.Scheidegger obtained this equation by assuming the porous medium to be composed of a bundle of parallel capillaries.

Bachmat [9]

$$\mathbf{k} \cdot \mathbf{J} = \frac{\nu}{g} \mathbf{q} + \left(\frac{\beta q}{g \phi} \right) \mathbf{q} \qquad \text{(A2-5)}$$

where **k** is the permeability tensor and β a geometrical coefficient. This seems to be the only equation of nonlinear flow where anisotropy of the media has been taken into account.

Blick [10]

$$J = \frac{32 \nu}{g \phi D^2} q + \frac{C_D}{2 g \phi^2 D} q^2 \qquad \text{(A2-6)}$$

where $D = 3 [(1 - \phi) / \phi]$ is the diameter of the capillary, $C_D = [(1-d^2/D^2)(D^4/d^4 - 1) / C_o^2]$, d being the diameter of the narrow opening and C_o the discharge coefficient of the opening.

Rumer & Drinker [11]

$$J = \frac{\alpha C_D}{\phi^2} \left[\frac{(1-\phi)}{\lambda \beta k} \right]^{1/2} q^2 / 2g \qquad \text{(A2-7)}$$

where α and β are volume and surface -shape factors respectively, λ is an empirical

coefficient taking account of the effect of neighboring spheres, C_D is a drag coefficient which depends on the Re and k is the permeability of the medium.

Ahmed [12]

$$J = (\mu/\gamma k)\, q + (1/g\sqrt{C k})\, q^2 \qquad \text{(A2-8)}$$

where C is the constant in the equation $k = C\, d^2$

GROUP 3

In this group equations contain coefficients which relate to the fluid and porous medium properties in an exact manner. There are therefore no unknown parameters in these equations.

Ergun [13]

$$J = 150\frac{(1-\phi)^2 \nu}{\phi^3 g d^2}\, q + 1.75\frac{(1-\phi)}{\phi^3 g d}\, q^2 \qquad \text{(A3-1)}$$

where d is the average particle diameter.

Schneebeli [14]

$$J = 1100\frac{\nu}{g d^2}\, q + \frac{12}{g d}\, q^2 \qquad \text{(A3-2)}$$

This equation is said to be applicable for $Re > 2$, where Re is calculated using d, the diameter of the spherical particles.

Carman [15]

$$J = 180\frac{(1-\phi)^2 \nu}{\phi^3 g d^2}\, q + 2.87\frac{(1-\phi)^{1.1} \nu^{0.1}}{\phi^3 g d^{1.1}}\, q^{1.9} \qquad \text{(A3-3)}$$

The equation was obtained from experimental data.

Ward [16]

$$J = \frac{\nu}{g k}\, q + \frac{0.55}{g\sqrt{k}}\, q^2 \qquad \text{(A3-4)}$$

where k is the permeability of the medium.

Irmay [7]

$$J = 180 \frac{(1-\phi)^2 \nu}{\phi^3 g d^2} q + 0.6 \frac{(1-\phi)}{\phi^3 g d} q^2 \qquad \text{(A3-5)}$$

This equation is thought to be applicable for Re > 0.1, where d is calculated to be the average particle diameter. This is very similar to the Ergun equation (A3-1).

REFERENCES

1. Bear, J. : *Dynamics of Fluids in Porous Media,* American Elsevier, New York (1972)
2. Forchheimer, P. : Wasserbewegung durch Boden, *Z. Ver. deuts. Ing.* (1901) **45**, 1782.
3. Forchheimer, P.: *Hydraulik*, 2nd Ed., Teubner, Leipzig and Berlin (1914).
4. Polubarinova-Kochina, P. Ya. : *Theory of Groundwater Movement,* (English trans. by R.J.M. DeWeist) Princeton Univ. Press., Princeton, N.J., (1962).
5. Ezeudembah, A.S. and Dranchuk, P.M. : Flow mechanism of Forchheimer's cubic equation in high-velocity radial gas flow through porous media, Paper SPE 10979 presented at the 57th Annual Conf. of the SPE, New Orleans, LA, Sept 26-29, 1982.
6. Ergun, S. and Orning, A.A. : Fluid flow through simple fluids through porous materials, *Ind. Eng. Chem.* (1949) **41**(6), 1179-84.
7. Irmay, S. : On the theoretical derivation of Darcy and Forchheimer formulas, *Trans. Amer. Geophys. Union* (1958) **39**(4), 702-707.
8. Scheidegger, A.E. : *The Physics of Flow through Porous Media,* Toronto Univ. Press., Toronto, 2nd ed. (1960).
9. Bachmat, Y.: Basic transport coefficients as aquifer characteristics, IASH Symp. on Hydrology of Fractured Rocks, Dubrovnik (Oct. 1965) 63-75.
10. Blick, E.F. : Capillary orifice model for high speed flow through porous media, *Ind. Eng. Chem.* (1966) **5**(1), 90-94.
11. Rumer, R.R. and Drinker, P.A. : Resistance to laminar flow through porous media, *J. Hydraul.*, Proc. ASCE, HY5 (1966) **92**, 155-164.
12. Ahmed, N. and Sunada, D.K. : Nonlinear flow in porous media, *J. Hydrau.* Div. Proc. ASCE, HY6 (Nov. 1969) **95**, 1847-1857.
13. Ergun, S. : Fluid flow through packed columns, *Chem. Eng. Prog.,* (1952) **48**(2), 89.
14. Schneebeli, G. : Experiences sur la limite de validite de la loi de Darcy et l'apparition de la turbulence dans un ecoulement de filtration, *La Houille Blanche* (1955) **10**(2), 141.
15. Carman, P.C. : *Flow of Gases through Porous Media,* Butterworths Scientific Publish., London (1956).
16. Ward, J.C. : Turbulent flow in porous media, *J. Hydrau.*, Proc. ASCE, HY5 (1964) **90**, pp. 1-12.

NOMENCLATURE

[*Note* : Units given here are those which are commonly used in the existing literature. For conversion to the SI system of units, see *J. Pet. Tech.* (1985) pp.1415-1419 and 1801-1805].

Symbol		*Typical units*
a	coefficient in nonlinear equation of flow	cm^2
A	cross-sectional area	cm^2
A	Darcy coefficient in gas inflow equation	g/cm^3-s
A^f	surface bounding the macroscopic fluid region V^f	cm^2
A^{ff}	a part of A^f adjacent to the fluid	cm^2
A^{fs}	a part of A^f adjacent to the solid	cm^2
b	coefficient in nonlinear equation of flow	cm^{-1}
B	non-Darcy coefficient in gas inflow equation	g/cm^4
$B_o, B_1 \ldots$	partial regression coefficients	–
C, C_{kj}	inertial coefficient tensor in Chap.3	cm^{-1}
d	diameter	cm
$\mathbf{d}, d_{kj}$	rate of deformation tensor	sec^{-1}
da	microscopic infinitesimal surface area	cm^2
dv	microscopic infinitesimal volume element	cm^3
dV	a representative elementary volume (REV)	cm^3
dV^f	volume occupied by the fluid within the REV	cm^3
dV^s	volume occupied by the solid within the REV	cm^3
D	non-Darcy constant in rate dependent skin	–
e	unit vector in the direction of the microscopic velocity	–
	with components α_k	cm
e	equivalent to $\alpha_k \mathbf{i}^k$	–
$\mathbf{f}, f_k$	body force vector	N
g	gravitation acceleration	m/sec^2

G	gas gravity, (= M/29)	–
h	total formation thickness	ft
h_p	perforated interval thickness	ft
$\mathbf{i}^k$	unit vector in the direction of the coordinate axes	–
$\mathbf{J}, J_k$	driving force for fluid motion	N
k, k_f	permeability	md or cm^2
k_a	apparent permeability	md
	or permeability of the altered zone near wellbore	md
$\mathbf{k}^*, \mathbf{K}^*$	coefficient tensors defined in Chapter 3	md
L	length	cm
m(p)	real gas psudo pressure	$psia^2/cp$
M	molecular weight	gm/gm-mole
n	microscopic surface normal unit vector, directed from	
	the fluid to the solid phase	–
N	macroscopic surface unit normal vector	–
p, P	pressure	psi or atm.
q, Q	flow rate	cm^3 or ft^3
q	fluid mass flux	g/sec
r	radius (of pores or grains)	cm
r	microscopic position vector	cm
r_e	radius of external boundary	ft
r_w	radius of well bore	ft
R	universal gas constant	cm^3atm/g-mol K
$\mathbf{R}, R_{kj}$	resistivity coefficient tensor defined in Chapter 3	N/cm^2
$\mathbf{R}^*, R_{kj}^*$	coefficient defined in Chapter 3	N/cm^2
S	saturation	%
S	mechanical skin	–
S'	rate dependent skin	–
t	time	sec

$\mathbf{t}$, t_k	stress vector	N/cm^2
$\mathbf{t}$, t_{kj}	stress tensor	N/cm^2
$\mathbf{t}^*$, t_{kj}^*	stress tensor defined in Chapter 3	N/cm^2
T	temperature	^oC or K
$\mathbf{T}$, T_k	resistivity force defined in Chapter 3	N/cm^2
$\mathbf{v}$, v_k	fluid velocity vector	cm/s
$\mathbf{v}$	microscopic deviation velocity vector	cm/s
v	magnitude of the microscopic deviation velocity vector	cm/s
V	macroscopic portion of the porous region	cm^3
V^f	part of V occupied by the fluid	cm^3
V^s	part of V occupied by the solid	cm^3
W	mass flow rate	g/s
$\mathbf{x}$, x_k	macroscopic position vector	cm
Z	gas compressibility factor	_

Greek

α	coefficient of viscous flow resistance (1/k)	cm^{-2}
α_k	component of $\mathbf{e}$ in Chap.3	_
β	coefficient of inertial flow resistance	cm^{-1} or ft^{-1}
Δ	differential quantity	_
∇	vector gradient operator	1/cm
γ	specific gravity of gas (air = 1.0)	_
γ	distribution function defined in Chap.3	_
δ^k	angle between $\mathbf{i}^k$ and $\mathbf{e}$	_
δ_{jk}	Kronecker delta	_
κ, κ'	scalar quantites defined in Chap.3	_
λ	viscosity coefficient	Ns/m^2
Λ, Λ_{jk}	tensor defined in Chap.3	_

Π, Π_{jk}	coefficient tensor defined in Chap.3	_
ρ	fluid density	g/cm^3
σ	interfacial tension	dyne/cm
θ	angle	_
ϕ	porosity	%
μ	viscosity coefficient	cp or Ns/m^2
τ	stress vector	N/cm^2
ψ	an arbitrary quantity	_

Special Notation

ψ	deviating quantity
ψ	macroscopic quantity
$\psi_{,k}$ $\psi_{k,j}$	spatial derivative with respect to either **r** or **x**
< >	an averaging operator
i, j, k	components of Cartesian coordinates

BIBLIOGRAPHY

ADAMSON, J.F. (1950) *Nature*, **166**, 314.

AHMED, N. and SUNADA, D.K. (1969) *J. Hydraulics,* Proc. ASCE, **95**, 1847- 1857.

ALBERTA Energy Resource Conservation Board (1975) *Theory and Practice of the Testing of Gas Wells*, Alberta, Canada.

AMYX, J.W., BASS, D.M. and WHITING, R.L. (1960) *Petroleum Reservoir Engineering - Physical Properties,* McGraw Hill Book Co., New York.

ANVIR, D., FARIN, D. and PFEIFER, P. (1984) *Nature* , March 15, pp.308.

ANVIR, D., FARIN, D. and PFEIFER, P. (1985) *J. Coll. Interface Sci.*, **103**, 112.

ARCHER, J.S. (1986) *Developements in Petroleum Engineering,* (Ed.: R.A.Dawe & D.C. Wilson), Academic Press, London, Chap.2, p.11-41.

ARCHER, J.S. and WALL, C.G. (1986) *Petroleum Engineering - Principles and Practice,* Graham & Trotman, London .

ARCHER, J.S. (1984) Proc.11th World Petrol. Congress, J.Wiley & Sons, London, **3**, p.65.

ARCHER, J.S. and WONG, S.W. (1973) *Soc. Pet. Eng. J.,* Dec., 343-347.

ARIS, R. (1962) *Vectors, Tensors and the Basic Equations of Fluid Mechanics,* Prentice-Hall, Englewood Cliffs, N.J.

ATKIN, R.J. and CRANE, R.E. (1976) *Q. J. Mech. Appl. Math,* **29**, 209.

AZIZ, K. and SETTARI, A. (1975) *Petroleum Reservoir Simulation,* Applied Science, London

AZZAM, M.I.S. and DULLIEN, F.A.L. (1977) *Chem. Eng. Sci.*, **32**, 1445.

BACHMAT, Y. (1965) IASH Symp. on Hydrology of Fractured Rocks, Dubrovnik, 63-75.

BACHMAT, Y. (1972) *Israel J. Tech.*, 10, 391.

BAKHMETEFF, B.A. and FEODOROFF, N.V. (1937) *J. Appl. Mech.*, **4A**, 97.

BARAK, A.Z. and BEAR, J. (1981) *Adv. Water Resour.*, **4**, 54-66.

BAUDET, C., CHARLAIX, E., CLEMENT, E., GYRON, E., HULIN, F.P., LEROY, C. (1985) in *Scaling Phenomena in Disordered Systems,* (Eds.: P. Pynn & A. Skjeltorp) Plenum Press, N.Y., pp. 399-422.

BEAR, J. (1972) *Dynamics of Fluids in Porous Media,* Elsevier, New York.

BEAR, J. , ZASLAVSKY, D. and IRMAY, S. (1965) *Physical Principles of Water Percolation and Seepage,* UNESCO Arid Zone Research Publication, Vol XXIX, Paris

BEDFORD, A. and INGRAM, J.D. (1971) *J. Appl. Mech.*, **38**, 1-7.

BENTSEN, R.G. and ANLI, J. (1976) *J. Can. Pet. Tech.*, July, 75-79.

BIRD, R.B., STEWART, W.E. and LIGHTFOOT, E.B. (1960) *Transport Phenomena,* J. Wiley & Sons, New York.

BLICK, E.F. (1966) *Ind. Eng. Chem.*, **5**(1), 90-94.

BRINKMAN, H.C. (1947) *Appl. Sci. Res.*, **A1**, 27.

BROOKS, C.S. and PURCELL W.R. (1952) *Trans AIME*, **195**, 289.

BROWN, H.W. (1951) *Trans AIME*, **192**, 67-74.

BROWN, S.R. (1987) *J. Geophys. Res.*, **92** (B2) 1337-1347.

BROWNELL, L.E. and KATZ, D.L. (1947) *Chem. Eng. Prog.* **4**, 537.

BUELL, R.S. and CRAFTON, J.W. (1985) Paper SPE 14448, 60th Annual Conf. of the SPE, Las Vegas, NV, Sept. 22-25.

BURDINE, N.T., GOURNAY, L.S. and REICHERTZ, P.P. (1950)*Trans. AIME*, **189**, 195.

CARMAN, P.C. (1937) *Trans. Inst. Chem. Eng.* Lond. **15**, 150.

CARMAN, P.C. (1956) *Flow of Gases through Porous Media*, Butterworths Scientific, Lond.

CARNAHAN, B., LUTHER, H.A. and WILKES, J.O. (1969) *Applied Numerical Methods*, J. Wiley & Sons, N.Y.

CHILDS, E.C. and COLLIS-GEORGE, N. (1950) *Proc. Roy. Soc.*, A **210**, 392.

COLLINS, R.E. (1961) *Flow of Fluids through Porous Media*, Reinhold Publish Co., N.Y.

COOKE, C.E. (1973) *J. Pet. Tech.*, Sept. p.1101-1107.

CORE LABORATORIES : *Fundamentals of Core Analysis*, Published by Core Analysis Laboratories Inc., Dallas, Texas.

CORNELL, D. and KATZ, D.L. (1953) *Ind. Eng. Chem.*, **45**, 2145.

CRAWFORD, C.W. and PLUMB, O.A. (1987) *J. Fluids Eng.*, Trans ASME, **108**, 343-347.

CVETKOVIC, V.D. (1986)*Transport in Porous Media*, **1**, 63-97.

DAKE, L. P. (1978) *Fundamentals of Reservoir Engineering*, Elsevier Scientific, Amsterdam.

DARCY, H. (1856) *Les Fontaines Publiques de la Ville de Dijon*, Victor Dalmont, Paris .

DAVIS, J.C. (1973)*Statistics and Data Analysis in Geology*, J Wiley & Sons, New York.

DORN, W.S. and McCRAKIN, D.D. (1972) *Numerical Methods with Fortran IV Case Studies*, J. Wiley & Sons, New York, p.357.

DRANCHUK, P.M. and KOLADA, L.J. (1968) *J. Can. Pet. Tech.*, 36.

DRANCHUK, P.M. and SADIQ, S. (1965) *J. Can. Pet. Tech.*, 130.

DUDGEON, C.R. (1966) *La Houille Blanche*, **7**, 785-801.

DULLIEN, F.A.L. (1979) *Porous Media - Fluid Transport and Pore Structure*, Academic Press, New York.

DYBBS, A. and EDWARDS, R.V. (1984) in *Fundamentals of Transport Phenomena in Porous Media*, (Eds.: J. Bear and M.Y. Corapcioglu) Martinus Nijhoff Publishers, NATO-ASI, Series E, No.82, 201 -256.

ELATA, C. and TASKERMAN, U. (1976) *Israel J. Tech.*, **14**, 235-240.

ELENBASS, J.R. and KATZ, D.L. (1947) Trans. AIME **174**, 25.

ERGUN, S. (1952) *Chem. Eng. Prog.*, **48**(2), 89-94.

ERGUN, S. and ORNING, A.A. (1949) *Ind. Eng. Chem.*, **41**(6), 1179-1184.

EVANS, R.D., HUDSON, C.S. and GREENLEE, J.E. (1985) Paper 14206, 60th Annual Conf. of the SPE, Nevada, Sept. 22-25; also *SPE Prod. Eng. J.*, (Nov. 1987) p.331

EZUDEMBAH, A.S. and DRANCHUK, P.M. (1982) Paper SPE 10979, 57th Annual Conf. of the SPE, New Orleans, LA, Sept. 26-29.

FANCHER, G.H. and LEWIS, J.A. (1933) *Ind. Eng. Chem.*, **25**, 1139.

FAND, R.M., KIM, B.Y.K., LAM, A.C.C. and PHAN, R.T. (1987) *J. Fluids Eng.*, **109**, pp.268.

FIROOZABADI, A. and KATZ, D.L. (1979) *J.Pet.Tech.*, Feb., 211

FORCHHEIMER, P. (1901) *Z.Ver. deuts. Ing.*, **45**, 1782-1788.

FORCHHEIMER, P. (1914) *Hydraulik,* 2nd Ed., Teubner, Leipzig and Berlin (Sec. 116-118)

FOX, J.W. (1949) *Proc. Phys. Soc.*, B**62**, 829.

FREEMAN, D.L. and BUSH, D.C. (1983) *Soc. Pet. Engr. J.,* Dec., 928-936.

FUNG, Y.C. (1977) *A First Course in Continuum Mechanics,* Prentice Hall, Englewood Cliff

GEERTSMA, J. (1974) *Soc.Pet.Eng.J.*, Oct., 455.

GEERTSMA, J., CROES, G.A. and SCHWARTZ, N. (1956) Trans. AIME, **206**, 178.

GEWERS, C.W.W. and NICHOL, L.R. (1969) *J.Can.Pet.Tech.*, April, p.5.

GRAY, W.G. and LEE, P.C.Y. (1977) *Int. J. Multiphase Flow*, **3**, 333-340.

GRAY, W.G. and O'NEILL, K. (1976) *Water Resour. Res.*, **12**, 148-154.

GREEN, L. and DUWEZ, P.J. (1951) *J. Appl. Mech.*, **18**, 39.

GREENBERG, D.B. and WEGER, E. (1960) *Chem. Eng. Sci.*, **12**, 8.

HALDORSEN, H.H. (1986) in *Reservoir Characterization,* (Eds: L.W. Lake and H.B. Carroll), Academic Press, London, p. 293-340.

HANNOURA, A.A. and BARENDS, F.B.J. (1981) Proc. Euromech 143, Delft, pp. 37-51.

HAPPEL, J. and BRENNER, H. (1965) *Low Reynolds Number Hydrodynamics*, Prentice Hall, Englewood Cliffs, N.J.

HASSANIZADEH, M. and GRAY, W.G. (1979) *Adv. Water Resour.*, **2**, 131-144.

HASSANIZADEH, M. and GRAY, W.G. (1979) *Adv. Water Resour.*, **2**, 191-203.

HASSANIZADEH, M. and GRAY, W.G. (1980) *Adv. Water Resour.*, **3**, 25-40.

HASSLER, G.L. and BRUNNER, E. (1945) *Trans. AIME*, **160**, 114-123.

HAWKINS, M. F. (1956) *J.Pet. Tech.*, Dec., 65.

HEID, J.G., McMAHON, J.J., NEILSEN, R.F. and YUSTER, S.T. (1950) *Drill. Prod Prac.*, API, 230-246.

HIKOX, G.H. (1934) *Trans. Amer. Geophys. Un.*, **15**, 567.

HOUPERT, A. (1959) *Revue l'Inst Francaise Petrole,* **14**, 1468.

HUBBERT, M.K. (1940) *J. Geology*, **48**, 785-944.

HUBBERT, M.K. (1956) *Trans. AIME*, **207**, 222-239.

IRMAY, S. (1958) *Trans. Am. Geophys. Un.*, **39**(4), 702-707.

JAGAI, T. (1982) M.Phil. thesis (unpublished), Dept. of Chem. Eng., Univ. of West Indies.

JONES, S.C. (1972) *Soc. Pet. Engr. J.*, Oct., 383-397.

JONES, S.C. (1987) Paper SPE 16949, 62nd Annual Conf. of the SPE, Dallas, Sept 27-30.

KATZ, D.L. et al (1959) *Handbook of Natural Gas Engineering*, McGraw Hill Book Co., NY.

KEELAN, D.K. (1972) *J. Can. Pet. Tech.*, April, 42-55.

KLINKENBERG, L.J. (1941) *Drill. Prod. Prac.*, A.P.I. p.200.

KOZENY, J. (1927) S. Ber. Wiener Akad, Abt IIa, **136**, 271.

KOZENY, J. (1927) Wasserkr. U. Wasserw., **22**, 86.

KUTILEK, M. (1972) Trans. 1st IAHR *Symp. on Fundamentals of Transport Phenomena in Porous Media*, IAHR Elsevier, Amsterdam, pp.327.

LEVER, A. and DAWE, R.A. (1984) *J. Petrol. Geology,* **7**, 97-108.

LEVERETT, M. C. (1941)Trans AIME, **142**, 153.

LOMBOS, L. (1983) Robertson Research *Helium Gas Expansion Volume Meter : Instruction Manual,* supplied to Imperial College.

McFARLAND, J.D. and DRANCHUK, P.M. (1976) *J. Can. Pet. Tech.*, 71-78.

MACDONALD, I.F., EL-SAYED, M.S., MOW, K. and DULLIEN, F.A.L. (1979) *Ind. Eng. Chem. Fund.*, **18**, 199.

MALONEY, D.R., GALL, B.L. and RAIBLE, C.J. (1987) Paper SPE 16899, 62nd Annual Conf. of the SPE, Dallas, TX, Sept. 27-30.

MANDELBROT, B.B. (1982) *The Fractal Geometry of Nature*, Freeman, San Francisco.

MARSHALL, T.J. (1962) in *Symp. on Interaction between Fluids and Particles* (Ed.: P.A. Rottenburg) Inst. Chem. Eng., London.

MEYER, H.I. (1953) *J. Appl. Phys.*, **24**(5), 510-512.

MONICARD, R.P. (1980) *Properties of Reservoir Rocks : Core Analysis*, Edition Technip, Paris.

MORGAN, J.T. and GORDON, D.T. (1970) *J. Pet. Tech.*, Oct., 1199.

MORROW, N.R. (1970) *Ind. Eng. Chem.*, **62**(6), 33.

MORROW, N.R. (1972) *Am. Assoc. Pet. Geo. Bull.*, March, **55**, 514-522.

MUECKE, T.W. (1979) *J. Pet. Tech.,* Feb., pp.144.

MUSKAT, M. (1937) *The Flow of Homogeneous Fluids through Porous Media,* McGraw Hill Book Co., New York.

NEASHAM, J.W. (1977) Paper SPE 6858, 52nd Annual Fall Meeting of the SPE, Colorado, October 9-12.

NISSAN, A.H. (1942) *J. Inst. Pet.*, 28, 257.

NITTMANN, J., DACCORD, G. and STANLEY, H.E. (1985) *Nature*, **314**, 141-144.

NOMAN, R. (1985) Student paper, Offshore Europe '85 Conference, Aberdeen, Sept.10-13.

NOMAN, R., SHRIMANKER, N. and ARCHER J.S. (1985) Paper SPE 14207, 60th Annual Conf. of the SPE, Las Vegas, NV, 23-25 Sept.

NOMAN, R. and ARCHER, J.S. (1987) Paper SPE 16400, SPE/DOE Symp. on Low Permeability Gas Reservoirs, Denver, 18-19 May.

NOMAN, R. and ARCHER, J.S. (1988) *J. Can. Pet. Tech.*, (to appear).

NGUYEN, T.V. (1986) SPE 15473, 61st Annual Conf. of the SPE, New Orleans, Oct. 5-8.

PALLAT, N., WILSON, J. and McHARDY, W.J. (1984) *J. Pet. Tech.*, Dec., 2225.

PAYATAKES, A.C., TIEN, C. and TURIAN, R.M. (1973) *AIChE Jour.*, **19**, 67.

PERRY, J.H. and CHILTON, T.H. (Eds.) (1973) *Chemical Engineers Handbook*, 5th Ed., McGraw Hill Book Co., New York.

PHILIP, J.R. (1969) Trans. Ciba Foundation Symp. on Circulatory and Respiratory Mass Transport, (Eds.: G.E.W. Wolstenhome and J. Knight), p.25, Churchill Ltd., London.

PICKELL, J.J., SWANSON, B.F. and HICKMAN, W.B. (1966) *Soc. Pet. Eng. J.*, March, pp. 55.

PIRSON, S.J. (1958) *Oil Reservoir Enginering*, McGraw Hill Book Co., New York.

PLAIN, G.J. and MORRISON, H.L. (1954) *Amer. J. Phys.*, **22**, 143-146.

POLUBARINOVA-KOCHINA, P. Ya. (1962) *Theory of Groundwater Movement,* Princeton Univ Press., Princeton, N.J.

PULRABEK, W.W. and IBELE, W.E. (1987) *Int. J. Heat Mass Transfer,* **30**, 1103-1109.

PURCELL, W.R. (1949) *Trans AIME*, **186**, 39-48.

RALPH, M.E. (1987) *J. Fluids Eng.*, Trans. ASME, **109**, 255.

RAMEY, H. J. (1965) *J. Pet. Tech.*, Feb., 223

REYNOLDS, O. (1883) *Phil. Trans. Roy. Soc.*, A **174**, 935.

RITTER, L.C. and DRAKE, R.L. (1945) *Ind. Eng. Chem.*, **17**, 782.

ROOF, J.G. (1970) *Soc. Pet. Eng. J.*, **10**(1), 85.

ROSE, W. and BRUCE, W.A. (1949) *Trans AIME*, **186**, 127-142.

RUMER, R.R. and DRINKER, P.A. (1966) *J. Hydraul.*, Proc. ASCE, HY5, **92**, 155-164.

SCHEIDEGGER, A.E. (1954) *J. Appl. Phys.*, **25**, 994.

SCHEIDEGGER, A.E. (1974)*The Physics of Flow through Porous Media,* Univ. of Toronto Press, Toronto, 3rd ed.; also 2nd edition 1960.

SCHENEEBELI, G. (1955) *La Houille Blanche*, **10**(2), 141-149.

SCHMIDT, V., McDONALD, D.A. and PLATT, R.L. (1977) *Bull. Can. Pet. Geo.*, p.106.

SELLEY, R.C. (1975) *Proc. Geol. Assoc.*, London, **87**(4), 359-387

SHOUMATOFF, N. (1952) Amer. Soc. Mech. Eng., Paper 52, SA - 42.

SLATTERY, J.C. (1967) *A.I.Ch.E.J.*, **13**, 1066.

SLATTERY, J.C. (1969) *A.I.Ch.E.J.*, **15**, 866.

SLATTERY, J.C. (1972) *Momentum, Energy and Mass Transfer in Continua,* McGraw Hill Book Co., New York.

STARK, K.P. (1972) 1st Int. IAHR Symp. on Fundamentals of Transport Phenomena in Porous Media, IAHR Elsevier, Amsterdam, pp.86.

STEWART, C.R. and OWENS, W.W. (1958) Trans. AIME, **213**, 121.

STIEL, L.I. and THODOS, G. (1961) *A.I.Ch.E.Jour,* **7**, 611-615.

STOKES, J. (1983) PhD thesis, Dept. of Mechanics, Royal Inst. of Tech, Stockholm.

STUTZMAN L.F. and THODOS, G. (1956) Trans. AIME, **207**, 352-355.

SWANSON, B.F. (1981) *J. Pet. Tech.*, Dec., 2498-2504.

SZABO, M.T. (1972) *Soc. Pet. Eng. Jour.*, April, 85-88.

TARIQ, S.M. (1987) *SPE Prod Engr. Jour.*, May, 104-112.

TAYLOR, R.P. and WARDLAW, N.C. (1975) *J. Can Pet. Tech.*, April, 33-37.
TEK, M.R. (1957) Trans. AIME, **207**, 376.
TEK, M.R., COATS, K.H. and KATZ, D.L. (1962) *J. Pet. Tech.*, 799-806.
THOMEER, J.H.M. (1960) *Trans. AIME*, **219**, 354-358.
THOMEER, J.H.M. (1983) *J. Pet. Tech.*, April, 809-814.
WALL, C.G. (1965) *J. Inst. Petrol.*, Lond., **51**, 195.
WALLS, J.D., NUR, A.M., and BOURBIE, T. (1982) *J. Pet. Tech.*, April, 930-936.
WALLS, J.D. and AMAFULE, J.O. (1985) Paper SPE 13879, Joint SPE/DOE Symp. on Low Permeability Gas Reservoir, Denver, CO, May 19-22.
WALLICK, G.C. and ARONOFSKY, J.S. (1954) *Trans. AIME*, **201**, 322-324.
WARD, J.C. (1964) *J. Hydraulics*, Proc. ASCE, HY5, **90**, 1-12.
WARDLAW, N.C. and CASSAN, J.P. (1978) *Bull. Can. Pet. Geo.*, Dec., **26**, 572-585.
WARDLAW, N.C. and CASSAN, J.P. (1979) *Bull. Can. Pet. Geo.*, June, **27**, 117-138.
WARDLAW, N.C. and McKELLAR (1981) *Powder Tech.*, **29**, 127-143.
WARDLAW, N.C. and TAYLOR, R.P. (1976) *Bull. Can. Pet. Geo.*, June, **24**, 225-262.
WHITAKER, S. (1968) *Introduction to Fluid Mechanics*, Prentice-Hall, Englewood Cliff, N.J.
WHITAKER, S. (1969) *Ind. Eng. Chem.*, **61**(12), 14-28.
WHITAKER, S. (1973) *Chem. Eng. Sci.*, **28**, 139.
WILLIAMS, J.K. and DAWE, R.A. (1986) *Transport in Porous Media* **1**, 201-209.
WONG, S.W. (1970) *J.Can.Pet.Tech.*, Oct., 274.
WOODLAND, A.W. (ed.) (1975) *Petroleum and the Continental Shelf of the Northwest Europe*, Vol.1 Geology, Applied Science Publishers, London
WRIGHT, D.E. (1968) *J. Hydraulics*, Proc. Amer. Soc. Civil Eng. HY4, **94**, 851-872.
WRIGHT, R.J., WHEAT, M.R. and DAWE, R.A. (1987) *SPE Reservoir Engr. J.*, Feb., p.92
WYLLIE, M.R.J. and ROSE, W.D. (1950) *Nature*, **165**, 972.
YIH, C.S. (1969) *Fluid Mechanics : A Concise Introduction to the Theory*, McGraw Hill, NY.